Alfred-Wegener-Institut für Polar- und Meeresforschung
Universität Potsdam, Institut für Erd- und Umweltwissenschaften

Late Glacial to Holocene climate and vegetation changes on the Tibetan Plateau inferred from fossil pollen records in lacustrine sediments

Dissertation
zur Erlangung des akademischen Grades
"doctor rerum naturalium"
(Dr. rer. nat.)
in der Wissenschaftsdisziplin "Palaeoecology and Paleolimnology"

eingereicht an der
Mathematisch-Naturwissenschaftlichen Fakultät
der Universität Potsdam

von
Yongbo Wang

Potsdam,
Dezember 2011

Published online at the
Institutional Repository of the University of Potsdam:
URL http://opus.kobv.de/ubp/volltexte/2013/6315/
URN urn:nbn:de:kobv:517-opus-63155
http://nbn-resolving.de/urn:nbn:de:kobv:517-opus-63155

Table of Content

Acknowledgements

I would like to express my gratitude to all those who have provided me with the opportunity to complete this thesis: I could not have made it without you.

I am extremely grateful to my supervisor, Prof. Dr. Ulrike Herzschuh (AWI-Potsdam & Uni Potsdam), whose encouragement, guidance, and support from start to finish has enabled me to develop my understanding of the subject.

I am also grateful to Prof. Dr. Xingqi Liu (Nanjing Institute of Geography and Limnology, CAS), who is my former supervisor but continued to provide me with support for my Ph.D. projects throughout these three years.

I am also indebted to Prof. Dr. Steffen Mischke (Uni Potsdam & Freie Uni Berlin) for his kind encouragement, useful instructions, and for always providing a rapid response to my questions.

I would especially like to thank Prof. Dr. Hans-Wolfgang Hubberten, the head of the AWI-Potsdam research department, for accommodating my Ph.D. project and providing financial support for me to my attend international conferences.

I offer my sincere thanks to the administration and laboratory staff of AWI-Potsdam, especially for their understanding and patience with a non-German-speaking student: Christine Litz, Kathrin Klein, Sigrun Gräning, Antje Eulenburg, Ute Bastian, Heiko Gericke, Tobias Schmidt, and Gabriela Schlaffer.

This thesis would not have been possible without the support and assistance that I received from our cooperating parters: Prof. Dr. H J B Birks (Uni Bergen), Dr. habil. Bernhard Diekmann (AWI-Potsdam), Prof. Dr. Oliver Korup (Uni Potsdam) and Prof. Dr. Jürgen Böhner (Uni Hamburg).

It is my pleasure to thank our working group members at the AWI who provide me with a great deal of assistance: Dr. Annette Kramer, Dr. Bernhard Aichner, Dr. Jian Ni, Dr. Juliane Wischnewski, Juliane Klemm, Juliane Wolter, Liv Heinecke, Fang Tian, Xianyong Cao, Benjamin Bekeschus, Janina Stapel, Jannet Borkowski, Chrisiane Funk, and my roommate Dr. Sebastian Wetterich, as well as all the other AWI Ph.D.s.

I also would like to thank the China Scholarship Council, the Helmholtz Association, and AWI-Potsdam for providing my Ph.D. scholarship.

Finally, I am indebted to my family: to my wife, to my little son, and to my parents, who have selflessly supported me throughout the years. I love them more than I can say.

Yongbo Wang

Dec. 2011

Abstract

The past climate in central Asia, and especially on the Tibetan Plateau (TP), is of great importance for an understanding of global climate processes and for predicting the future climate. As a major influence on the climate in this region, the Asian Summer Monsoon (ASM) and its evolutionary history are of vital importance for accurate predictions. However, neither the evolutionary pattern of the summer monsoon nor the driving mechanisms behind it are yet clearly understood.

For this research, I first synthesized previously published Late Glacial to Holocene climatic records from monsoonal central Asia in order to extract the general climate signals and the associated summer monsoon intensities. New climate and vegetation sequences were then established using improved quantitative methods, focusing on fossil pollen records recovered from Tibetan lakes and also incorporating new modern datasets. The pollen-vegetation and vegetation-climate relationships on the TP were also evaluated in order to achieve a better understanding of fossil pollen records.

The synthesis of previously published moisture-related palaeoclimate records in monsoonal central Asia revealed generally different temporal patterns for the two monsoonal subsystems, i.e. the Indian Summer Monsoon (ISM) and East Asian Summer Monsoon (EASM). The ISM appears to have experienced maximum wet conditions during the early Holocene, while many records from the area affected by the EASM indicate relatively dry conditions at that time, particularly in north-central China where the maximum moisture levels occurred during the middle Holocene. A detailed consideration of possible driving factors affecting the summer monsoon, including summer solar insolation and sea surface temperatures, revealed that the ISM was primarily driven by variations in northern hemisphere solar insolation, and that the EASM may have been constrained by the ISM resulting in asynchronous patterns of evolution for these two subsystems. This hypothesis is further supported by modern monsoon indices estimated using the NCEP/NCAR Reanalysis data from the last 50 years, which indicate a significant negative correlation between the two summer monsoon subsystems. By analogy with the early Holocene, intensification of the ISM during coming decades could lead to increased aridification elsewhere as a result of the asynchronous nature of the monsoon subsystems, as can already be observed in the meteorological data from the last 15 years.

A quantitative climate reconstruction using fossil pollen records was achieved through analysis of sediment core recovered from Lake Donggi Cona (in the north-eastern part of the TP) which has been dated back to the Last Glacial Maximum (LGM). A new data-set of modern pollen collected from large lakes in arid to semi-arid regions of central Asia is also presented herein. The concept of "pollen source area" was introduced to modern climate calibration based on pollen from large lakes, and was applied to the fossil pollen sequence from Lake Donggi Cona. Extremely dry conditions were found to have dominated the LGM, and a subsequent gradually increasing trend in moisture during the Late Glacial period was terminated by an abrupt reversion to a dry phase that lasted for about 1000 years and coincided with the first Heinrich Event of the northern Atlantic region. Subsequent periods corresponding to the warm Bølling-Allerød period and the Younger Dryas cold event were

followed by moist conditions during the early Holocene, with annual precipitation of up to about 400 mm. A slightly drier trend after 9 cal ka BP was then followed by a second wet phase during the middle Holocene that lasted until 4.5 cal ka BP. Relatively steady conditions with only slight fluctuations then dominated the late Holocene, resulting in the present climatic conditions.

In order to investigate the relationship between vegetation and climate, temporal variations in the possible driving factors for vegetation change on the northern TP were examined using a high resolution late Holocene pollen record from Lake Kusai. Moving-window Redundancy Analyses (RDAs) were used to evaluate the correlations between pollen assemblages and individual sedimentary proxies. These analyses have revealed frequent fluctuations in the relative abundances of alpine steppe and alpine desert components, and in particular a decrease in the total vegetation cover at around 1500 cal a BP. The climate was found to have had an important influence on vegetation changes when conditions were relatively wet and stable. However, after the 1500 cal a BP threshold in vegetation cover was crossed the vegetation appears to have been affected more by extreme events such as dust storms or fluvial erosion than by the general climatic trends. In addition, pollen spectra over the last 600 years have been revealed by Procrustes analysis to be significantly different from those recovered from older samples, which is attributed to an increased human impact that resulted in unprecedented changes to the composition of the vegetation.

Theoretical models that have been developed and widely applied to the European area (i.e. the Extended R-Value (ERV) model and the Regional Estimates of Vegetation Abundance from Large Sites (REVEALS) model) have been applied to the high alpine TP ecosystems in order to investigate the pollen-vegetation relationships, as well as for quantitative reconstructions of vegetation abundance. The modern pollen–vegetation relationships for four common pollen species on the TP have been investigated using Poaceae as the reference taxa. The ERV Submodel 2 yielded relatively high PPEs for the steppe and desert taxa (*Artemisia* Chenopodiaceae), and low PPEs for the Cyperaceae that are characteristic of the alpine *Kobresia* meadows. The plant abundances on the central and north-eastern TP were quantified by applying these PPEs to four post-Late Glacial fossil pollen sequences. The reconstructed vegetation assemblages for the four pollen sequences always yielded smaller compositional species turnovers than suggested by the pollen spectra, indicating that the strength of the previously-reported vegetation changes may therefore have been overestimated.

In summary, the key findings of this thesis are that (a) **the two ASM subsystems show asynchronous patterns during both the Holocene and modern time periods,** (b) **fossil pollen records from large lakes reflect regional signals for which the pollen source areas need to be taken into account,** (c) **climate is not always the main driver for vegetation change,** and (d) **previously reported vegetation changes on the TP may have been overestimated because they ignored inter-species variations in pollen productivity.**

Zusammenfassung

Das Paläoklima in Zentralasien, besonders in der Hochebene von Tibet (HT), ist von großer Bedeutung um globale Klimaprozesse zu verstehen und mögliche Voraussagung für die zukunft zu treffen. Als wichtigstes Klimaphänomen nehmen der asiatische Sommermonsun (ASM) und seine Entwicklungsgeschichte eine Schlüsselposition ein. Dennoch sind derzeit weder das Entwicklungsschema noch der antreibende Vorgang ausreichend verstanden. Dies gilt insbesondere für das Holozän, für welches große Kimaschwankungen und regionale Diskrepanzen weithin belegt sind.

Deshalb habe ich zuerst holozäne Klimadaten zusammengefasst. Bereits veröffentlichte Publikationen aus den Monsungebieten Zentralasiens dienten als Grundlage, um die wichtigsten Klimasignale und die zugehörigen Intensitäten des Sommermonsuns heraus zu arbeiten. Anhand von Pollensequenzen aus tibetischen Seen erzeugte ich neue Klima- und Vegetationssequenzen, welche auf verbesserten quantitativen Methoden und rezenten Datensätzen beruhen. Außerdem wurden die Verhältnisse Pollen-Vegetation und Vegetation-Klima bewertet, um Schlussfolgerungen fossiler Pollensequenzen zu verbessern.

Die Zusammenfassung der zuvor veröffentlichten, niederschlagsbezogenen Paläoklimadaten im Monsungebiet Zentralasiens ergab generell unterschiedliche Muster für die zwei Teilsysteme des ASMs, den Indischen Sommermonsun (ISM) und den Ostasiatischen Sommermonsun (OASM). Der ISM weist maximale feuchte Bedingungen während des frühen Holozöns auf, während viele Datensätze aus dem Gebiet des OASMs einen relativ trockenen Zustand anzeigen, besonders im nördlichen Zentralchina, wo maximale Niederschläge während des mittleren Holozäns registriert wurden. Genaue Betrachtungen der Antriebsfaktoren des Sommermonsuns ergaben, dass der ISM hauptsächlich durch Veränderungen der Sonneneinstrahlung auf der Nordhemisphäre angetrieben wird, während der OASM potentiell durch den ISM beherrscht wird - dies führt zu asynchronen Entwicklungen. Diese Hypothese wird durch rezente Monsunindizes gestützt. Sie weisen eine signifikant negative Korrelation zwischen den beiden Sommermonsun-Teilsystemen auf.

Für die quantitative Klimarekonstruktion von Pollensequenzen wurde ein Sedimentkern aus dem See Donggi Cona im Nordosten der HT analysiert, der bis zum letzten glazialen Maximum (LGM) zurückdatiert wurde. Aufgrund der Tatsache, dass Donggi Cona ein relativ großer See ist, wird hiermit ein neuer Pollen-Klima-Kalibrierungsdatensatz auf Grundlage großer Seen in ariden und semiariden Regionen Zentralasiens vorgelegt. Das Konzept des Pollenherkunftsgebietes wurde in diese rezente, pollenbasierte Klimakalibrierung eingebracht und auf die Pollensequenz von Donggi Cona angewendet. Die Auswertung ergab, dass extrem trockene Bedingungen während des LGM (ca. 100 mm/yr) vorherrschten. Ein ansteigender Trend von Niederschlägen während des späten Glazials wurde durch einen abrupten Rückgang zu einer etwa 1000-jährigen Trockenphase beendet, welche mit Heinrich-Ereignis 1 in der Nordatlantik-Region übereinstimmt. Danach entsprechen die Klimaperioden dem warmen Bølling/Allerød und dem Kälteereignis der Jüngeren Dryas. Anschließend herrschten feuchte Bedingungen im frühen Holozän (bis zu 400 mm/yr). Ein etwas trockenerer Trend nach dem Holozänen Klimaoptimum wurde dann von einer zweiten Feuchtphase abgelöst,

welche bis 4,5 cal. ka vor heute andauerte. Relativ gleichmäßige Bedingungen dominierten das späte Holozän bis heute. Die Klimadynamik seit dem LGM wurde vor allem durch Entgletscherung und Intensitätsschwankungen des ASM bestimmt.

Bei der Betrachtung des Vegetation-Klima-Verhältnisses habe ich die zeitlichen Variationen der bestimmenden Faktoren hinsichtlich der Vegetationsdynamik auf der nördlichen HT untersucht. Dabei wurden hochauflösende holozäne Pollendaten des Kusai-Sees verwendet. Eine Redundanzanalyse (RDA) wurde angewendet um die Korrelation zwischen Pollenvergesellschaftungen und individuellen sedimentären Klimaanzeigern als auch die damit verbundene Signifikanz zu bewerten. Es stellte sich heraus, dass das Klima einen wichtigen Einfluss auf den Veränderungen in der Vegetation besaß, wenn die Bedingungen relativ warm und feucht waren. Trotzdem scheint es, dass, dass die Vegetation bei zu geringer Bedeckung stärker durch Extremereignisse wie Staubstürme oder fluviale Erosion beeinflusst wurde. Pollenspektren der vergangen 600 Jahre erwiesen sich als signifikant unterschiedlich verglichen mit den älterer Proben, was auf verstärkten anthropogenen Einfluss hindeutet. Dieser resultierte in einem beispiellosen Wandel in der Zusammensetzung der Vegetation.

In Hinsicht auf das Pollen-Vegetation-Verhältnis und der quantitativen Rekonstruktion der Vegetationshäufigkeit habe ich theoretische Modelle, welche für europäische Regionen entwickelt und weithin angewendet wurden, respektive die Modelle "Extended R-Value" (ERV) sowie "Regional Estimates of Vegetation Abundance from Large Sites" (REVEALS), auf die hochalpinen Ökosysteme der HT überführt. Dafür wurden rezente Pollen-Vegetations-Verhältnisse von vier weit verbreiteten Pollen-Arten der HT überprüft. Poaceae wurden als Referenztaxa verwendet. Bei der Anwendung dieser Verhältnisse auf vier Pollensequenzen, welche die Paläoumweltbedingungen seit dem letzten Glazial widerspiegeln, wurden die Häufigkeiten von Pflanzen auf der zentralen und nordöstlichen HT quantifiziert. Anteile von Artimisia und Chenopodiaceae waren dabei im Vergleich zu ihren ursprünglichen Pollenprozenten deutlich verringert. Cyperaceae hingegen wies eine relative Zunahme in dieser Vegetationsrekonstruktion auf. Die rekonstruierten Vegetationsvergesellschaftungen an den Standorten der vier Pollensequenzen ergaben stets geringere Umwälzungen in der Artenzusammensetzung, als durch die Pollenspektren zu vermuten gewesen wäre. Dies kann ein Hinweis darauf sein, dass die Intensität der bislang angenommenen Vegetationsveränderungen überschätzt worden ist.

Zusammengefasst sind die Hauptresultate dieser Dissertation, dass (a) **die zwei ASM Teilsysteme asynchrone Muster während des Holozäns und heute aufweisen**, dass (b) **fossile Pollensequenzen großer Seen regionale Klimasignale widerspiegeln sofern die Herkunftsgebiete der Pollen berücksichtigt werden**, dass (c) **Klima nicht immer der Haupteinflussfaktor für Vegetationswandel ist** und dass (d) **das Ausmaß von Vegetationsveränderungen in zuvor veröffentlichten Studien auf der Hochebene von Tibet überschätzt worden sein kann, weil Diskrepanzen der Pollenproduktivität zwischen den Arten nicht einbezogen wurden**.

List of figures

List of tables

List of abbreviations

A/C	*Artemisia*/Chenopodiaceae ratio
AMS	Accelerator Mass Spectrometry
AP	Arboreal Pollen content
ASM	Asian Summer Monsoon
BA	Bølling/Allerød warm period
CCA	Detrended correspondence analysis
C/N	Carbon/Nitrogen ratio
DCA	Detrended Correspondence Analysis
DCCA	Detrended Canonical Correspondence Analysis
EASM	East Asian Summer Monsoon
EC	Electrical Conductivity
EM	End-Member
EMMA	End-Member Modeling Algorithm
ERV	Extended R-Value model
IDW	Inverse Distance Weighting
ISM	Indian Summer Monsoon
LIA	Little Ice Age
LGM	Last Glacial Maximum
Mg/Ca	Magnesium/Calcium ratio
MH	Monsoon Hadley index
MRT	Multivariate Regression Trees
nMDS	non-metric Multidimensional Scaling
PCA	Principal Component Analysis
PPE	Pollen Productivity Estimate
PSA	Pollen Source Area
Rb/Sr	Rubidium / Strontium ratio
RDA	Redundancy Analysis
REVEALS	Regional Estimates of Vegetation Abundance from Large Sites model
RSAP	Relative Source Area of Pollen
SSI	Southly Shear Index
SST	Sea Surface Temperature
TIC	Total Inorganic Carbon content
TN	Total Nitrogen content
TOC	Total Organic Carbon content
TP	Tibetan Plateau
WA-PLS	Weighted Averaging – Partial Least Square
XRD	X-Ray Diffraction
XRF	X-Ray Fluorescence
YD	Younger Dryas

1 Introduction

Preface

Monsoons represent a seasonal reversal of low-level atmospheric circulation, especially of surface winds, with associated effects on precipitation (Wang, 2006). The Asian Summer Monsoon (ASM) system in particular, with a direct influence on one third of world's population, has become the focus of PAGES and was discussed in the IPCC 2007 report (Christensen et al., 2007). Abnormal behavior of the summer monsoon or abrupt variations in its intensity have the potential to cause severe natural hazards such as flooding, disease, or drought, and may even have influenced the evolution of Chinese society (Yancheva et al., 2007; Zhang et al., 2008). Predicting the behavior of monsoons is therefore an increasingly urgent task if potential human and economic losses are to be avoided, but will require a detailed understanding of the behavior of the summer monsoon system and its controlling mechanisms (Webster et al., 1998; 2010). An important key to achieving this understanding is the ability to learn from the past, for which valuable historical information can be acquired through palaeoclimatologic studies.

The Tibetan Plateau (TP) region, sometimes referred to as the "third polar region" of our planet, is a unique and extensive high altitude landform that has a significant influence on both regional and global atmospheric circulation (Prell and Kutzbach, 1992; Liu et al., 2003a). During the northern summer enhanced pressure and temperature gradients between the heated plateau and the Indian-Pacific Ocean accelerate the convective uplift of air-masses, producing an intensification of the ASM. Water vapor is then drawn inland from the ocean resulting in increased precipitation (Wang, 2006). In contrast, the influence of the TP on atmospheric circulation further inland in central Asia can lead to aridification by blocking moisture from the Indian-Pacific Ocean, resulting in the formation of sub-tropical deserts (Wu et al., 2009a). A number of studies during the last few decades have concentrated on the TP and adjacent regions, but they have failed to draw consistent conclusions.

The ecosystems on the TP, which consist of montane to alpine biomes, are assumed to be sensitive to climate change and their evolutionary history has therefore been widely considered to provide a reliable record of the palaeoclimate in this region. Various modern analogue methods have commonly been employed to infer past vegetation and climate changes from fossil pollen records (Seppä and Bennett, 2003). Changes in climate (precipitation and temperature) and vegetation (tree line shifts and biome replacements) have subsequently been investigated through pollen-based studies (e.g. Herzschuh et al., 2010; Kramer et al., 2010; Shen et al., 2008). In view of new developments in research methods and the increasing accumulation of data, fossil pollen records now need to be reinterpreted taking into account possible drivers for vegetation change other than climate.

1.1 Scientific background

1.1.1 Asian Summer Monsoon and its history during the Holocene

The Asian Summer Monsoon (ASM), which consists of two subsystems, the Indian Summer Monsoon (ISM) and the East Asian Summer Monsoon (EASM), exerts a major influence on the climate of central Asia. During the summer months the monsoon draws in water vapor from the Indian and Pacific Oceans to southern and eastern Asia, accounting for the main source of precipitation (Wang, 2006).

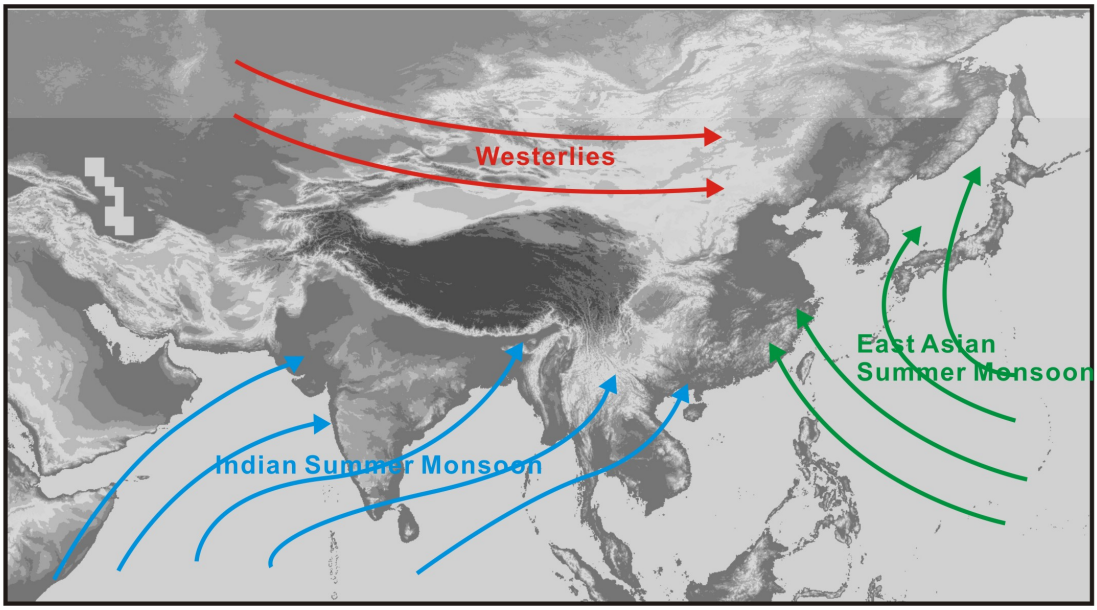

Figure 1-1 Map of monsoonal Asia, depicting the dominating circulation systems (Indian Summer Monsoon, East Asian Summer Monsoon and Westerlies). Wind directions are based on NCEP/NCAR 50-year reanalysis data.

The evolution of the ISM since the Last Glacial Maximum (LGM) has been interpreted from foraminifera in marine sediments from the Arabian Sea, which appear to indicate an intensification of the summer monsoon during the early Holocene followed by a gradual reduction in its intensity since the middle Holocene (Gupta et al., 2003; Overpeck et al., 1996; Sirocko et al., 1993). Records from the South China Sea appear to indicate a generally similar pattern for the EASM during the Holocene, despite the relatively low resolution of the fossil record and dating uncertainties (Wang et al., 1999).

Away from the oceans, many different types of archives have been investigated to trace the monsoonal history, of which isotope records from stalagmites have previously been considered to be a reliable indictor of monsoon intensity. Stalagmites from eastern China (Hulu Cave: Wang et al., 2001), central China (Sanbao Cave: Wang et al., 2008), south-western China (Dongge Cave: Dykoski et al., 2005; Wang et al., 2005; Yuan et al., 2004), and southern Oman (Qunf Cave: Fleitmann et al., 2003; 2007) have been analyzed and interpreted in terms of precipitation changes through the rainfall "amount effect", and subsequently in terms of variations in ASM intensity. Some doubt has, however, been cast on

these interpretations by recent modeling results (Pausata et al., 2011). The loess-paleosol sequences that are widely distributed across central and western China have been used to trace the monsoonal history on an orbital scale (An et al., 1991; Lu et al., 2004; Porter and An, 1995). A higher resolution is available in lacustrine sediments, from which various biological and geochemical proxies have been used to interpret summer monsoon intensities. The history of the EASM has, for example, been investigated using records from Lake Daihai in north-central China, and Lake Sihailongwan in north-eastern China (Schettler et al., 2006; Xiao et al., 2004; 2006). Further to the west, Lake Qinghai has been widely investigated and ISM signals extracted (Ji et al., 2005; Lister et al., 1991; Liu et al., 2002a; 2007; Shen et al., 2005). A long sequence of lacustrine sediments recently obtained from the Heqing Basin has made it possible to acquire information on an orbital scale (Zisheng et al., 2011). Monsoonal signals have also been reconstructed from peat sequences in north-eastern China and the eastern part of the Tibetan Plateau (Hong et al., 2003; 2005; Wang et al., 2004; Zhao et al., 2011; Zhou et al., 2002).

The different responses of individual proxies to monsoonal variations have, however, led to continuing debate concerning the onset and duration of the summer monsoon maximum during the Holocene, which has prompted various authors to publish syntheses of earlier results from recent decades. An et al. (2000) first reported an asynchronous Holocene Optimum in different regions of China, which appeared about 9000 years ago in north and north-eastern China, and as late as 3000 years ago in south and south-eastern China. In contrast, He et al. (2004) found a west-east trend for this optimum. By applying a consistent methodology to infer effective moisture levels from proxy records, Herzschuh (2006) found only minor differences between the temporal moisture patterns of the ISM, the EASM, and the Westerlies. The "out-of-phase" relationship between arid central Asia and eastern Asia observed by Chen et al. (2008) has been explained as being due to differences in moisture evolution between areas influenced by the mid-latitude Westerlies and areas dominated by the Asian Summer Monsoon. Maher (2008) argued that temporal differences between the Indian and the East Asian monsoonal moisture maxima may be due to differences in the seasonality of each of these monsoon systems.

The forcing mechanism behind the poorly understood history of the ASM is the key to understanding the monsoonal patterns, but remains a matter of debate. It is widely accepted that monsoonal changes on millennial or longer time-scales are predominantly forced by orbitally-induced changes in solar insolation and resulting shifts in the position of the Intertropical Convergence Zone (Fleitmann et al., 2003; 2007; Overpeck et al., 1996; Sirocko et al., 1993; Wang et al., 2001; 2005a; 2005b). Smaller monsoonal oscillations that are observed on decadal to annual timescales have been assumed to be a result of changes in solar activity through a “transfer effect” from the northern Atlantic Ocean (Wang et al., 2005b). Hypotheses concerning internal driving mechanisms have focused on the effects of the thermal contrast between the Eurasian continent and the surrounding oceans, influenced by changes in oceanic thermohaline circulation (Webster et al., 1998), sea surface temperatures (SST) (Bush, 2001,2005), teleconnections in atmospheric circulation (Wang, et al., 2005b) and/or high-latitude ice volumes (Overpeck et al., 1996). In addition, results from general climate models demonstrate that the position of the westerly jet stream relative to the Tibetan

Plateau probably also affected monsoonal evolution (Sato, 2009).

Further studies on high resolution palaeoclimate records, together with reliable chronology, are therefore still urgently required to uncover the history of the ASM. A synthesis of all available results on a sub-continental to continental scale is also required.

1.1.2 Inconsistent palaeoclimate results on the Tibetan Plateau

The Tibetan Plateau (TP) is a vast elevated plateau in central Asia, covering an area of approximately 2.5×106 km^2 between 25 and 40° N, and 75 and 105° E. The plateau is bordered to the north by the Kunlun Range which separates it from the Tarim Basin, and to the northeast by the Qilian Range which separates it from the Hexi Corridor and the Gobi Desert. To the east and southeast the plateau gives way to the forested gorge and ridge geography of the mountainous headwaters of the Salween, Mekong, and Yangtze rivers of western Sichuan (the Hengduan Mountains) and southwest Qinghai. The western limit of the plateau is marked by the Karakoram Range of northern Kashmir.

The uplift of the TP has been closely related to the development of monsoon and the Asian climate (An et al., 2000; Kutzbach et al., 1993). During the summer months the vast elevated plateau area absorbs heat from the solar insolation, resulting in the enhanced pressure and thermal gradients between the Eurasian Continent and the Indian-Pacific Ocean that trigger the summer monsoon (Wang, 2006). Meanwhile the continental circulation over the TP drives the sinking dry air masses further to the north and west, leading to the formation of a vast desert zone in central Asia (Wu et al., 2009a). These important climatic effects continue to attract ongoing research into the climate and environmental changes on the Tibetan Plateau.

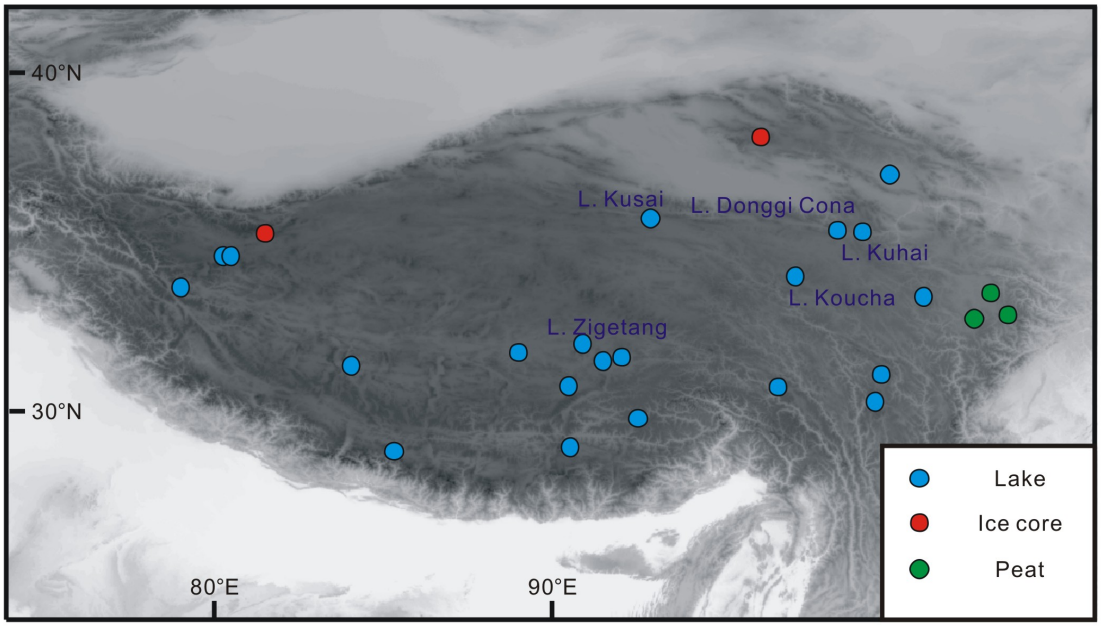

Figure 1-2 Current study sites on the Tibetan Plateau (sites that are employed in this thesis were named as, L. Kusai, L. Donggi Cona, L. Koucha and L. Zigetang)

The widely distributed lakes on the plateau provide abundant continuous records from which the late Quaternary climate can be reconstructed with a relatively high resolution. However, owing to the remoteness of the plateau most studies have focused on lakes in the marginal areas of the plateau, or in those central parts that are more readily accessible. Investigations have been carried out on lakes in the north-eastern and western parts of the plateau since the 1990s, e.g., at Lake Qinghai (Lister et al., 1991), Bangong Co (Fan et al., 1996; Fontes et al., 1996; Gasse et al., 1996; van Campo et al., 1996), Sumxi Co (Gasse et al., 1991; van Campo et al., 1993), and Siling Co (Kashiwaya and Yaskawa, 1991; Morinage et al., 1993). During the last decade various lakes have been investigated or reinvestigated using multi-proxy approaches. For example, Lake Qinghai is the largest lake in the northern part of TP, and has been studied using geophysical, geochemical, and biological approaches (Henderson et al., 2003; 2010; Ji et al., 2005; Liu et al., 2002; 2007; Shen et al., 2005; etc.). Studies in the southern and central parts of the TP have mainly focused on Ahung Co (Morril et al., 2006), Chen Co (Lu et al., 2011; Yang et al., 2004; Zhu et al., 2009), Co Ngion (Shen et al., 2008; Wu et al., 2006), Nam Co (Herrmann et al., 2010; Li et al., 2011; Lin et al., 2008; Zhu et al., 2008), Lake Hidden and Ren Co (Tang et al., 2009), Lake Naleng (Kramer et al., 2010a; 2010b), Lake Yidun (Shen et al., 2006), and Lake Zigetang (Herzschuh et al., 2006; Wu et al., 2007). Apart from Lake Qinghai, studies in the northern part of the TP have mainly concentrated on Lake Donggi Cona (Aichner et al., 2011; Mischke et al., 2010), Lake Koucha (Aichner et al., 2010; Herzschuh et al., 2009), Lake Kuhai (Mischke et al., 2009; Wischnewski et al.,2011), Lake Kusai (Liu et al., 2009) and Ximen Co (Mischke et al., 2010; Zhang and Mischke, 2010).

Ice cores collected from mountain glaciers on the plateau, mainly from the Dunde and Guliya Ice Caps, have also been used to trace past climate changes on both millennial and annual scales (Thompson et al., 1989; 1997; Liu et al., 1998; Yao et al., 1996; 1999). To the east of the TP peat deposits have been identified in the Zoige area and analyzed for indications relating to the Holocene climate and monsoonal history (Hong et al., 2003; 2005; Zhao et al., 2011).

Despite the abundance of results relating to past climatic and environmental changes on the TP, the reasons for the inconsistent temporal patterns and poor regional correlations are still being debated (Wischnewski et al., 2011). Their elucidation will require further high resolution records over long time scales, as well as consideration of the different responses of each individual proxy to climate change.

1.1.3 Fossil pollen records as indicators of climate and vegetation changes on Tibetan Plateau

Pollens are common fossils preserved in a wide variety of deposits and have been widely used for interpreting past changes in climate and vegetation (Birks, 1981; Birks and Seppä, 2004; Seppä and Bennett, 2003; Yu et al., 1998). Fossil pollen records have been identified and interpreted in terms of climate variations since the early 1990s, in conjunction with other investigations into Tibetan lakes and ice caps (Huang et al., 1996; Li et al., 1994; Liu et al.,

1998; Tang et al., 1999; van Campo et al., 1993). Despite the relatively low resolution of the pollen records and highly uncertain chronologies, these early studies were able to successfully outline past climate and vegetation changes on the plateau.

Modern pollen-climate calibration-sets have recently been developed and used in interpreting quantitative climatic variations on the TP (Shen et al., 2006; Herzschuh et al., 2010; Lu et al., 2011), resulting in a significant improvement in our understanding of the history and amplitude of past changes in climate. However, the pollen records preserved in sediments generally reflect regional-scale signals within the pollen-source area (Broström et al., 2008; Prentice, 1985; Sugita, 1993, 1994), and the inferred size of this source area can vary with the size of the basin as it is dependent on species-specific pollen grain morphology as well as dispersal and depositional characteristics (Prentice, 1985; Sugita, 1993). It has also been demonstrated that the inclusion of different types of present-day samples (e.g., moss samples, surface soil samples, or surface sediment samples from lakes) will influence the final climate reconstructions, probably as a result of the differences in their interpreted source areas (Goring et al., 2010; Xu et al., 2010; Zhao et al., 2009). Furthermore, since most of the fossil pollen records have been recovered from large or very large lakes, the application of a calibration dataset based on surface soils or small lakes is potentially problematic due to the dramatically different origins of the pollen grains.

Quantitative climate reconstructions are mainly based on the assumption that changes in vegetation are solely and directly driven by climate change, which is an assumption that warrants further consideration. Precipitation is commonly assumed to have a strong correlation with vegetation compositions on the TP due to the limited moisture supply available to this region, and variations in pollen spectra have mainly been quantitatively interpreted in terms of variations in precipitation (Herzschuh et al., 2010; Lu et al., 2011; Shen et al., 2006). However, by analyzing pollen records in peat deposits Zhao et al. (2011) revealed more complex responses of the ecosystem to climatic conditions, such as insolation-driven temperature acting in concert with monsoon-derived precipitation. Recent results from a transient global climate model covering the last 6000 years also demonstrate that the influence that temperature changes have had on Tibetan Plateau vegetation may have been underestimated (Dallmeyer et al., 2011). Changes in atmospheric CO_2 concentrations have also recently been suggested to be a major driver for mid-Holocene vegetation turnover on the Tibetan Plateau (Herzschuh et al., 2011). In contrast, Miehe et al. (2011) have suggested that Tibetan ecosystems remained ecological stable during the middle Holocene because of the dominance of climatically resilient species. In addition to the studies that have attributed ecological transitions to climatic variability, vegetation change has also been assumed to reflect the intensity of nomadic herding on the Tibetan Plateau (Miehe et al., 2009; Schlütz and Lehmkuhl, 2009). Clearly an improved understanding of the driving mechanisms behind vegetation changes and associated interactions with climate change during the Holocene remains a priority for research.

The interpretation of fossil pollen records in terms of vegetation/landscape changes may be less straightforward than has previously been considered. The relative percentages of pollen taxa in recovered pollen assemblages are biased by differences in the pollen productivities of different plant taxa and by species-specific dispersal and depositional processes (Prentice,

1985; Sugita, 1993). The development during recent decades of a theoretical framework and models for pollen–vegetation relationships, however, means that quantitative vegetation/ landscape reconstructions are now feasible (Andersen, 1970; Davis, 1963; Jackson et al., 1995; Jackson and Lyford, 1999; Parsons and Prentice, 1981; Prentice, 1985; Prentice and Parsons, 1983; Sugita, 1994). The Extended R-value (ERV) model has been used to produce pollen productivity estimates (PPEs) for key plant taxa and their corresponding "relevant source area of pollen" (RSAP) from Europe (e.g. Broström et al., 2008; Mazier et al., 2008; Nielsen and Sugita, 2005; Soepboer et al., 2008) and Africa (Duffin and Bunting, 2008). A "Regional Estimates of Vegetation Abundance from Large Sites" (REVEALS) model has been developed as a part of a "Landscape Reconstruction Algorithm" (LRA) approach to predicting regional vegetation abundances from pollen assemblages recorded in large lakes (Sugita, 2007a; 2007b); this approach has been applied and validated for Denmark (Nielsen and Odgaard, 2010), Sweden (Hellman et al., 2008, 2008b), the Swiss Plateau (Soepboer et al., 2010), and North America (Sugita et al., 2010). However, previously reported vegetation changes on the TP were deduced directly from the fossil pollen assemblages without taking into account variations in pollen productivity, thus potentially leading to serious misinterpretations. Using the pollen representation method introduced by Andersen (1970), Herzschuh et al. (2003, 2006) produced preliminary results for the pollen productivity of some desert plants on the Alashan Plateau. Zhao and Herzschuh (2009) and Wei et al. (2011) were able to draw general conclusions on over-representation (e.g. *Artemisia*, Chenopodiaceae and *Ephedra*), and under-representation (e.g. Cyperaceae), on the basis of investigations on modern pollen assemblages from the Tibetan Plateau and the Qaidam Basin. However, in these studies the pollen dispersal–deposition processes and the distance weighting for modern vegetation data were ignored when estimating pollen productivities. There remains an urgent need for a better understanding of the pollen–vegetation relationships in this region in order to better appreciate the vulnerability of Tibetan vegetation.

1.2 Aims and objectives

The principal aims of this thesis are directed towards improving both our understanding of the palaeoclimatology of central Asia and the methodologies employed in the associated investigations. One of the most important climatic developments during the Holocene was the evolution of the ASM, which has been widely investigated by means of proxy-reconstructions. These reconstructions have identified significant regional differences. One of the objectives of this thesis has been to identify the potential mechanisms behind these regional differences, requiring a detailed analysis of the Holocene climate variability within the ASM subsystems and of their interactions. Fossil pollen records have often been used for quantitative interpretations of past climate and vegetation, but the pollen records preserved in sediments are now known to have been greatly influenced by species-specific pollen productivities, as well as by dispersal-deposition processes. It is therefore important to reconsider the changes in climate and vegetation that have been previously interpreted from fossil pollen records, and to investigate the relationship between climate change and changes in vegetation. With this in mind four hypotheses (H) have been proposed and are set out below, together with scientific targets (*T*) and specific questions (Q) directed towards improved understanding [U] and

methodologies [M]:

Hypothesis H1 **That the regional climate differences in monsoonal central Asia during the Holocene were due to the different evolutionary patterns in the ASM subsystems, caused by their interactions with each other.**

T1 To track the climate and circulation changes in monsoonal central Asia on both millennial and inter-annual time scales covering the Holocene and the recent past.

Q1 What semi-quantitative moisture/temperature indices can be used to interpret Holocene pollen and non-pollen records? [U]

Q2 What are temporal and spatial patterns can be inferred from these moisture/temperature indices? [U]

Q3 Do the monsoonal subsystems show the same patterns during the Holocene as they do for the recent past? [U]

Q4 What are the possible driving mechanisms behind any differences in these patterns? [U]

Hypothesis H2 **That the quantitative climate inferences from the fossil pollen records preserved in large lakes reflect a regional signal within the pollen source area, rather than a local signal.**

T2 To quantitatively reconstruct past climate change using fossil pollen records preserved in a large lake (Lake Donggi Cona, north-eastern Tibetan Plateau) taking into account the concept of "pollen source area", and to compare the results inferred from pollen with those deduced from the sedimentary proxies.

Q5 How is the theoretical size of a pollen source area determined, and what are the constraining factors? [M]

Q6 To which climatic factors are fossil pollen records sensitive, and which of these factors can therefore be reconstructed? [U; M]

Q7 Do climate inferences from the pollen record in Lake Donggi Cona reflect a local or a regional signal? [U]

Q8 Are the interpreted changes to the Holocene climate on the north-eastern Tibetan Plateau consistent with the monsoon patterns? [U]

Hypothesis H3 **That changes in the Holocene vegetation on the northern Tibetan Plateau were multi-driven, i.e. that they were not driven solely by climate change, but also by sudden severe events and human impacts.**

T3 To evaluate the temporal variations between pollen and sedimentary proxies based on a high resolution record from Lake Kusai, northern Tibetan Plateau.

Q9 What are the signals preserved by individual proxies? [U]

Q10 How does the pollen record correlate with individual proxies? [U; M]

Q11 When did climate change exert a primary influence on vegetation change, and what were the climatic conditions at the time? [U]

Q12 When did the human impacts start to contribute to changes in vegetation? [U]

Hypothesis H4 **That the previously reported vegetation changes on the upper Tibetan Plateau were probably overestimated because of the lack of information on pollen productivity.**

T4 To derive relative pollen productivity estimates (PPEs) for common plant species on the

upper Tibetan Plateau (ERV model) and to reassess the Holocene vegetation changes (REVEALS model).

Q13 What are the relative productivities of common plant species on the upper Tibetan Plateau? [U; M]

Q14 What are the changes to vegetation reconstructions when the PPEs of pollen assemblages are taken into account? [U; M]

Q15 What is the corrected history of vegetation change on the upper Tibetan Plateau? [U]

Q16 Have there really been major compositional vegetation turnovers on the upper Tibetan Plateau, as previously reported? [U]

1.3 Structure of the thesis

1.3.1 Overview of the chapters

This thesis is an accumulative dissertation consisting of the introduction (Chapter 1), of which this sub-section as a part, and six individual manuscripts (Chapters 2-5, Appendix 1 and 2), followed by an overall synthesis and discussions (Chapter 6). Since the main topic of this thesis is the palaeoclimate and related inferences from pollen records, two manuscripts concerning mineral compositions (Manuscript 5) and lake formation processes (Manuscript 6) have been included in the Appendix, rather than in the main body of the text. The contents of the various chapters are outlined below.

- **Chapter 1 – Introduction:** Provides an overview of the study area, including the climatic background and some discussion on the application of fossil pollen records, as well as outlining the major objectives of the thesis.

- **Chapter 2 – Manuscript 1:** "Asynchronous evolution of the Indian and East Asian Summer Monsoon indicated by Holocene moisture patterns in monsoonal central Asia."
  Authors: Yongbo Wang, Xingqi Liu, Ulrike Herzschuh
  Status: Published in "Earth-Science Reviews" 2010, Vol. 103, Pages 135-153.
  Summary: In this manuscript previously published palaeoclimate records for the monsoonal areas of central Asia have been synthesized and climate indices used to estimate the moisture/temperature during the last 18 cal ka BP. Through numerical analyses we ascertained that the different moisture patterns may have been a result of the asynchronous nature of Asian Summer Monsoon sub-systems, which was further supported by estimates based on modern monsoon indices derived from the NCEP/NCAR Reanalysis data for the last 50 years. A detailed examination of the driving factors for summer monsoons revealed that the Indian Summer Monsoon was primarily driven by changes in northern hemisphere solar insolation, while the East Asian Summer Monsoon may have been constrained by the ISM, resulting in the asynchronous evolutionary patterns of these two sub-systems.

- **Chapter 3 – Manuscript 2:** "Quantitative reconstruction of precipitation changes on the NE Tibetan Plateau since the Last Glacial Maximum - extending the concept of pollen-source area to pollen-based climate reconstructions from large lakes."

Authors: Yongbo Wang, Lyudmila S Shumilovskikh, Steffen Mischke, H John B Birks, Juliane Wischnewski, Jürgen Böhner, Frank Schlütz, Frank Lehmkuhl, Bernhard Diekmann, Bernd Wünnemann, Chengjun Zhang, Ulrike Herzschuh
Status: Under review for the "Quaternary Science Reviews" journal.
Summary: In this research we made quantitative reconstructions of climate (precipitation) changes on the north-eastern Tibetan Plateau since the Last Glacial Maximum, using the fossil pollen record recovered from Lake Donggi Cona. In order to improve the climate reconstructions we introduced the concept of pollen source area into the modern calibration dataset, which derives from 26 large lakes in central Asia. Theoretical pollen source areas were estimated for each lake and modern meteorological parameters were distance-weighted within the individual source areas. Further uncertainties concerning the application of pollen records from large lakes (e.g., due to variations within lakes, and potential fluvial input of pollen) were also evaluated. Finally, we compared our pollen-based climate reconstruction with results based on ostracod assemblages from the same core and a pollen-based climate reconstruction from the nearby Lake Kuhai, which led to the conclusion that the fossil pollen records in large lakes reflect regional rather than local signals.

- **Chapter 4 – Manuscript 3:** "Temporally changing drivers for late Holocene vegetation changes on the northern Tibetan Plateau: moving-window-RDA of pollen record from Lake Kusai."
  Authors: Yongbo Wang, Xingqi Liu, Ulrike Herzschuh, Xiangdong Yang, Enlou Zhang, Guobang Tong
  Status: Submitted to the "Palaeogeography, Palaeoclimatology, Palaeoecology" journal.
  Summary: We recovered a high resolution (~15 year) late Holocene pollen record from Lake Kusai, northern Tibetan Plateau, as well as high resolution sedimentary proxies. In addition to the late Holocene climate and vegetation changes on the northern Tibetan Plateau, we paid special attention to the relationship between changes in vegetation and changes in climate, i.e. the driving factors behind vegetation changes. A moving-window-RDA was applied to determine the temporal variations between the fossil pollen assemblages and the climatic/environmental signals inferred from the sedimentary proxies. Our results showed that vegetation changes were mainly driven by climate during periods of climate stability. However, during periods of abrupt climate variations extreme events such as dust storms were also contributing factors resulting in vegetation changes. Human impacts could only be traced back for the last 600 years.

- **Chapter 5 – Manuscript 4:** "Reassessment of Holocene vegetation change on the upper Tibetan Plateau using the pollen-based REVEALS model."
  Authors: Yongbo Wang, Ulrike Herzschuh
  Status: Published in "Review of Palaeobotany and Palynology" 2011, Vol. 168 Pages 31-40.
  Summary: The pollen productivities of common plant species on the upper Tibetan Plateau were estimated and Holocene vegetation changes were reassessed in this manuscript. The modern pollen-vegetation relationship was determined using theoretical models (ERV model and REVEAL model) that have been widely validated in European

areas. In the alpine meadow/steppe communities, *Artemisia* and Chenopodiaceae were found to have relatively high productivities compared to Poaceae and Cyperaceae. Owing to such major differences in pollen productivity, the previously reported vegetation changes and turnovers on the Tibetan Plateau may well have been overestimated, which means that the results from previous vegetation studies in central Asia will now need to be re-evaluated.

- **Chapter 6 – Overall conclusions:** The general results and achievements of the manuscripts described above are summarized and discussed, together with outlooks for the future.

- **Appendix 1 – Manuscript 5:** "Environmental constraints on lake sediment mineral compositions from the Tibetan Plateau and implications for paleoenvironment reconstruction."
  Authors: Yongbo Wang, Xingqi Liu, Steffen Mischke, Ulrike Herzschuh
  Status: Published in "Journal of Paleolimnology" 2012, Vol. 47 Pages 71-85.
  Summary: This manuscript focuses on inorganic mineral compositions and their constraints in lacustrine sediments. The mineral compositions of modern lacustrine sediment samples were quantitatively identified using X-ray diffraction. The allogenic minerals were generally found to have originated from bedrock sources within the catchments. The electrical conductivity and Mg/Ca ratios of the water were found to be the most important factors controlling the precipitation of endogenic minerals. Using a Multivariate Regression Tree analysis and a Redundancy Analysis we were able to semi-quantitatively evaluate the correlation between endogenic minerals and these environmental or water geochemistry factors. Finally, our findings from modern sediment samples were applied to a sediment sequence from Chaka Salt Lake covering the period since Late Glacial. The lake's evolutionary history in terms of salinity variations was semi-quantitatively reconstructed, indicating it to have been a fresh water lake during the Late Glacial, turning into a saline lake during the middle Holocene.
- **Appendix 2 – Manuscript 6:** "High-resolution sedimentary archive from landslide-dammed Lake Mengda, north-eastern Tibetan Plateau."
  Authors: Yongbo Wang, Ulrike Herzschuh, Xingqi Liu, Oliver Korup, Bernhard Diekmann
  Status: In preparation.
  Summary: Sudden natural events such as earthquakes can have a significant effect on sedimentary sequences, especially in small lakes within in mountainous regions. This manuscript will focus on such topics, revealing the origins of Lake Mengda on the north-eastern Tibetan Plateau. The chronology and sedimentary proxies provide us with a hypothesis that the lake was dammed within the last century, which is further supported by the results of geomorphological investigations. Historical documents reveal that major earthquakes occurred in this region during the 1920s and these may possibly have triggered the landsides that dammed the former river valley and led to the lake's formation.

1.3.2 Author's contributions

As the first author of the above papers, I took part in the collection of samples, organized the laboratory analyses, processed the data analyses (except where otherwise specified), and prepared all the manuscripts. Ulrike Herzschuh, as my supervisor, provided guidance for all of the studies and helped with the organization of the manuscripts as well as with interpreting the results. Our Chinese cooperator, Xingqi Liu, also took part in field expeditions (Manuscripts 3, 5 and 6), as well as providing primary data (Manuscripts 3 and 5) and valuable suggestions (Manuscripts 1, 3, 5 and 6). Steffen Mischke contributed to the collection of modern surface samples and the sediment core from Lake Donggi Cona, as well as providing constructive comments (Manuscripts 2 and 5). H John B Birks offered valuable advice on quantitative climate reconstructions from pollen records (Manuscript 2). Juliane Wischnewski carried out the Procrustes analyses (Manuscript 2). Jürgen Böhner provided modeled modern climate information (Manuscript 2). Lyudmila S. Shumilovskikh counted the pollen in surface sediment samples from Lake Donggi Cona (Manuscript 2). Frank Schlütz, Frank Lehmkuhl, Bernhard Diekmann, Bernd Wünnemann, and Chengjun Zhang took part in the field expedition to Lake Donggi Cona (Manuscript 2). Xiangdong Yang, Enlou Zhang, and Guobang Tong took part in the field work at Lake Kusai (Manuscript 3). Oliver Korup introduced and guided the geomorphological analyses for the Lake Mengda region (Manuscript 6).

1.3.3 Methods

All the numerical analysis methods involved in the manuscripts are summarized in Table 1-1, and described in detail in the relevant manuscripts:

Table 1-1 Numerical analysis methods applied in the manuscripts and their purpose

Ms	Method	Purpose
1	PCA	To extract possible temporal and spatial climate patterns
	Procrustes	To evaluate the correlation between pollen and non-pollen records
2	RDA/MRT	To identify climate parameters and make quantitative reconstructions from fossil pollen data
	WA-PLS	To use climate parameters from fossil pollen data for quantitative reconstructions
	Procrustes	To evaluate the correlation between climatic interpretations from pollen and ostracod records
3	Moving-window-RDA	To evaluate temporal variations between pollen records and sedimentary proxies
	Time series	To identify possible periodicity in pollen records
	Procrustes	To compare pollen compositions from different core sections
	DCCA	To estimate compositional turnovers in pollen assemblages
4	ERV model	To estimate relative pollen productivities and pollen source areas
	REVEALS model	To quantitatively reconstruct vegetation abundances taking into

		account pollen productivities
	DCCA	To estimate compositional turnovers in both pollen assemblages and vegetation reconstructions
5	RDA/MRT	To identify and quantitatively reconstruct water geochemical / climatic parameters from authigenic mineral data
6	Spatial Analysis	To derive cross-sectional profiles for lake catchment areas
	End-Member	To extract information on possible sources for sediments

2 Manuscript 1: Asynchronous evolution of the Indian and East Asian Summer Monsoon indicated by Holocene moisture patterns in monsoonal central Asia

Yongbo Wang [a, b], Xingqi Liu [c], Ulrike Herzschuh [a, b]

[a] *Alfred Wegener Institute for Polar and Marine Research, Research Unit Potsdam, 14473 Potsdam, Germany*

[b] *Institute of Earth and Environment Science, University of Potsdam, 14476 Golm, Germany*

[c] *State Key Laboratory of Lake and Environmental Science, Nanjing Institute of Geography and Limnology, CAS, 210008 Nanjing, P.R.China*

Current Status: Published in "Earth-Science Reviews" 2010, Vol. 103, Pages 135-153.

Abstract

The numerical meta-analysis of 92 proxy records (72 sites) of moisture and/or temperature change confirms earlier findings that the dominant trends of climatic evolution in monsoonal central Asia since the Last Glacial roughly parallel changes in Northern Hemisphere summer insolation, i.e. the period following the Last Glacial Maximum was characterized by dry and cold conditions until 15 cal. kyr BP, followed by a warm, wet period coincident with the Bølling/Allerød warm period and terminated by a cold, dry reversal during the Younger Dryas period. After an abrupt increase at the start of the Holocene, warm and wet conditions prevailed until ca. 4 cal. kyr BP when moisture levels and temperatures started to decrease.

Ordination of moisture records reveals strong spatial heterogeneity in moisture evolution during the last 10 cal. kyr. The Indian Summer Monsoon (ISM) areas (northern India, Tibetan Plateau and southwest China) exhibit maximum wet conditions during the early Holocene, while many records from the area of the East Asian Summer Monsoon indicate relatively dry conditions, especially in north-central China where the maximum moisture levels occurred during the mid-Holocene. We assign such phenomena to strengthened Hadley Circulation centered over the Tibetan Plateau during the early Holocene which resulted in subsidence in the East Asian monsoonal regions leading to relatively dry conditions. Our observations of the asynchronous nature of the two Asian monsoon subsystems on millennial time scales have also been observed on annual time-scales as well as implied through the spatial analysis of vertical air motion patterns after strong ascending airflows over the Tibetan Plateau area that were calculated from NCEP/NCAR reanalysis data for the last 30 years. Analogous with the early Holocene, the enhancement of the ISM in a 'future warming world' will result in an increase in the asynchronous nature of the monsoon subsystems; this trend is already observed in the meteorological data from the last 15 years.

2.1 Introduction

The monsoonal regions of central Asia are assumed to be particularly vulnerable to past and present climatic change as they represent the transition zone between three circulation systems; the Indian Summer Monsoon (ISM), the East Asian Summer Monsoon (EASM) and the Westerlies (Figure 2-1) (Porter and An, 1995; Wang, et al., 2001b; Hong, et al., 2005; Wang, 2006, Clift and Plumb, 2008).

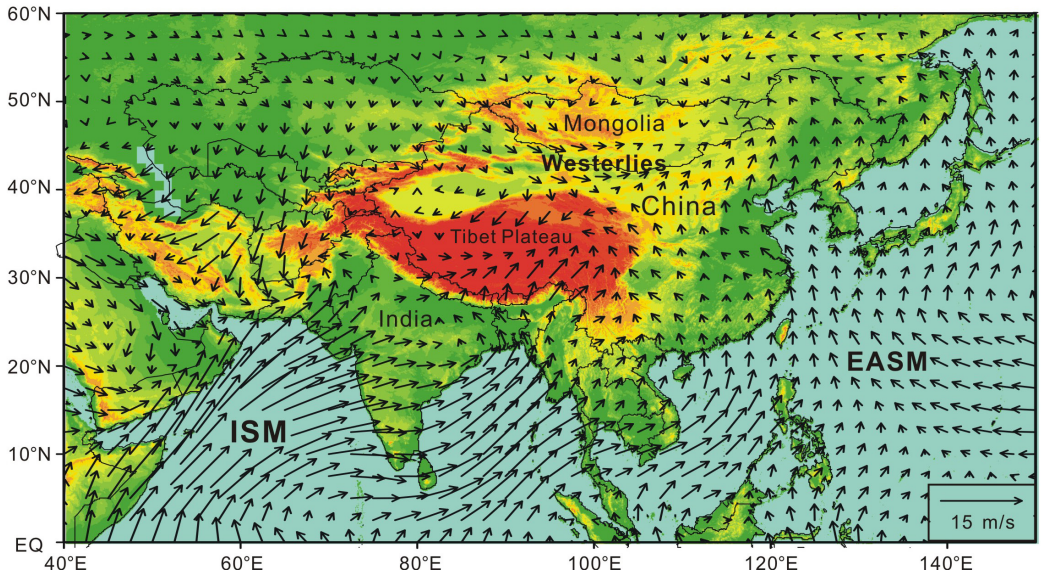

Figure 2-1 Overview map shows the study area and atmospheric circulation systems (ISM, Indian Summer Monsoon; EASM, East Asian Summer Monsoon; Westerlies). Arrows show 60-year mean summer (June, July, August) wind fields based on NCEP/NCAR reanalysis data (Level 1000 hPa) from Jan. 1948 to Dec. 2008.

In recent years, several studies have attempted to reconstruct late-Quaternary climatic histories by reviewing published proxy records in a descriptive manner; however, these have displayed inconsistent trends and contradictory explanations. An et al. (2000) first reported an asynchronous Holocene Optimum in different regions of China, which appeared ca. 9000 years ago in north and northeast China, and as late as 3000 years ago in south and southeast China. In contrast, He et al. (2004) found a west-east trend. By applying a consistent methodology to infer effective moisture from proxy records, Herzschuh (2006) found only slight differences in the temporal moisture patterns between the ISM, EASM and Westerlies. The 'out-of-phase' relationship between arid central Asia and eastern Asia observed by Chen et al. (2008) was explained by differences in the moisture evolution between areas influenced by the mid-latitude Westerlies and areas that are dominated by the Asian Summer Monsoon.

Furthermore differing opinions exist concerning the temporal relationship between insolation variations and monsoonal strength. Although most authors agree that the monsoonal maximum lags behind the insolation maximum, they have inferred different lag times (3000 yrs, Overpeck et al., 1996; 1500 yrs, Fleitmann et al., 2007); and two contrasting ideas exist concerning a gradual (Overpeck et al., 1996; Wang et al., 2005a; Fleitmann et al., 2007) versus an abrupt (Morrill et al., 2003) monsoon retreat pattern.

The external and internal forcing mechanisms of the Asian Summer Monsoon are key to understanding regional moisture patterns, however are still under debate. It is widely accepted that monsoonal changes on millennial or longer time-scales are predominantly forced by orbitally-induced changes in solar insolation and subsequent shifts in the position of the ITCZ (Sirocko et al., 1993; Overpeck et al., 1996; Wang et al., 2001a, 2005a; Fleitmann et al., 2003, 2007; Wang et al., 2005b). Smaller monsoonal oscillations that are observed on decadal to annual time-scales were assumed to be affected by the solar activity through the "transfer effect" of the northern Atlantic Ocean (Wang et al., 2005a). Hypotheses concerning internal driving mechanisms focus on the effects of the thermal contrast between the Eurasian continent and the surrounding oceans, exerted by changes in oceanic thermohaline circulation (Webster et al., 1998), sea surface temperatures (SST) (Bush, 2001,2005), teleconnections in atmospheric circulation (Wan et al., 2005a) and/or high-latitude ice volume (Overpeck et al., 1996). In addition, results from general climate models demonstrate that the relative position of the westerly jet to the Tibetan Plateau probably also affected monsoon evolution (Sato, 2009).

Using meteorological data available for the last 50 years, various monsoon indices were constructed to trace recent interannual variability in the monsoonal circulation and its subsystems (the ISM and the EASM) (Webster and Yang, 1992; Goswami et al., 1999; Wang et al., 2001b; Huang, 2004). Different interannual variations between the two subsystems are related to different convectional heat sources assumed to originate from either changing summer SSTs (Goswami et al., 1999; Zveryaev and Aleksandrova, 2004) or El Nino–Southern Oscillation (ENSO) (Chang et al., 2000; Wang et al., 2001b).

Numerous new records and further information based on previous work have been published in the last 3 years (Figure 2-2B), necessitating the development of a new synthetical review. Herewith, we provide a statistical meta-analysis of moisture patterns in monsoonal central Asia, as inferred from proxy records covering the last 18,000 years compared with spatial information concerning recent monsoonal development derived from NCEP/NCAR reanalysis data (National Centre for Environmental Prediction/National Centre for Atmospheric Research). We aim to: (1) synthesize the spatial and temporal patterns of moisture evolution in the monsoonal regions of central Asia, extending the data set by Herzschuh (2006); (2) investigate their relationships with extra-regional and global climate trends to identify potential forcing mechanisms, and (3) investigate the suppressant effect of the ISM on the EASM on both millennial and annual time-scales. From the comparison of vegetation and non-vegetation records, we (4) attempt to identify the point at which humans, rather than climate, became the dominant force driving regional vegetation composition.

2.2 Study Area

The monsoonal regions of central Asia covered in this study (70ºE-130ºE, 20ºN-50ºN) encompass most parts of China, Mongolia, northern India and Kyrgyzstan (Figure 2-1). Due to the large latitudinal and altitudinal extents, various climatic (from tropical to subpolar, and high-cold alpine zones) and vegetation zones (from tropical rain forest to boreal evergreen forest, together with desert and alpine tundra) are represented within the study area. Located

towards the eastern margin of the Eurasian continent, the climates of northern India, southwest China and eastern China are influenced by monsoon activity, having warm, humid summers coupled with cold, dry winters. Towards the west, there is a strengthening of continental conditions while the semi-arid and arid areas of northwestern China are dominated by westerly circulation.

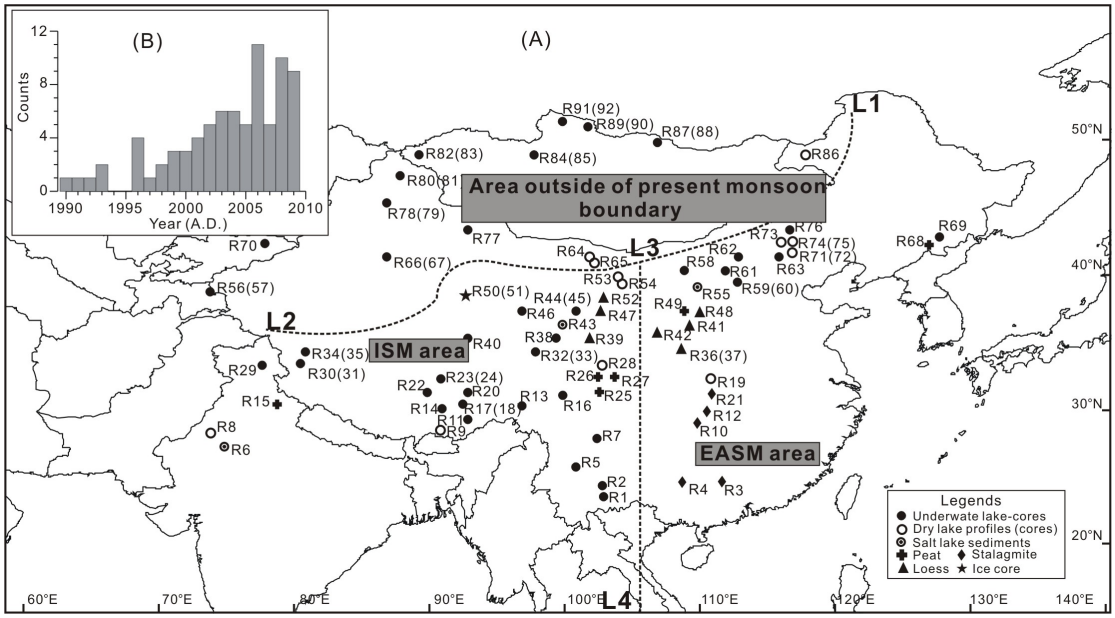

Figure 2-2 (A) Spatial distribution of palaeoclimatic records used in this study (numbers refer to the records in Table 1) and the extensions of three sub-regions. For sites with pollen and non-pollen based records, the numbers of pollen ones are shown in the brackets. (Line L1-L2, present monsoon boundary; Line L3-L4, 105° E longitude) (B) Number of published records during the last 20 years.

2.3 Materials and Methods

2.3.1 Selection of palaeoclimatic records

A large number of palaeoclimatic records from monsoonal central Asia have been published during the last two decades. However there is a large disparity in sample resolution and age control. To ensure sufficient data quality, all records included in our analyses were required to meet the following criteria:

1) Analyzed proxies should be indicative of moisture and/or temperature change.

2) Records should provide continuous information for at least 4000 years since 18 cal. kyr BP.

3) The sequences should be constructed using a reliable chronology, with at least four dating control points during the Holocene.

4) Sequences should have a sufficient resolution (< 200 years for the Holocene period).

Due to the low information density from Mongolia, Inner Mongolia and northwest China, ten

records with less dating control points or lower resolution were also included in our data set. 92 records (40 pollen records and 52 non-pollen records) from 72 sites were selected for this study (see detailed information and locations in Table 2-1 and Figure 2-2A). Non-pollen records are based on various proxies including geophysical (lithological description, color index, grain size, magnetic susceptibility etc.), geochemical (organic and inorganic carbon content, stable carbon and oxygen isotope ratios, elemental composition) and biological data (diatoms, ostracods and chironomidae). It is still debated whether isotopic records from ice cores reflect temperature change or local moisture evolution. As such, we didn't use these records for moisture reconstruction (e.g. Dunde, Thompson et al., 1990; Guliya, Thompson et al., 1997). Due to the differing nature of various climate archives, it is impossible to consistently translate each individual proxy into semi-quantitative climate signals at all sites. Therefore, after initially crosschecking the plausibility of their interpretations, we largely agreed with the original conclusions reached by the authors when classifying proxy-based climatic inferences from the records. Only ten records span the complete period between 18 and 0 cal. kyr BP. About 90 % (84 sites) of the records cover at least 7000 ^{14}C years. With the exception of 11 records from stalagmites, loess or ice cores that were dated by means of U/Th, OSL or TL, all sequences were dated using radiocarbon methods, mostly AMS ^{14}C dating. Most authors provided the original ^{14}C data, allowing us the opportunity to consistently re-establish age-depth relationships for all records. Following a correction for the 'reservoir effect' (necessary for 28 sites), all ^{14}C ages were computed to calendar ages using Calib 5.0.1 software and the 'IntCal04' database (Reimer et al., 2004). All ages in this text are given as calibrated ages with the notation 'cal. yr BP'. With the exception of 9 records from areas containing very few records, most sequences have a resolution of less than 200 years, which sometimes extends as far as decadal resolution (Table 2-1). In order to later evaluate the relationship between pollen and non-pollen records, sites with both pollen and non-pollen sequences were treated as two separate records. In cases where several records (both pollen and non-pollen) have been published from the same site (e.g. Qinghai Lake: two pollen records (Liu X.Q. et al., 2002; Shen et al., 2005) and more than five non-pollen records (Lister et al., 1991; Ji et al., 2005, 2009; Shen et al., 2005; Liu et al., 2007)), all individual records were evaluated during an initial screening step. Due to the consistency of the climatic inferences, we decided to include only the most recent record in our analyses.

In order to further examine sub-regional patterns in climate signals, we assigned our records to three sub-regions namely the area outside of the present monsoon boundary, the ISM area and the EASM area (Figure 2-2A). Owing to the fact that there is no definitive spatial boundary between the EASM and ISM, the definitions of sub-regions used here are based on the current understanding of monsoonal systems despite the fact that this is subject to change.

2.3.2 Inferences of moisture and warmth indices for palaeoclimatic records

We translated the moisture (temperature) signals from the separate studies into a moisture (warmth) index of a five-part scale (-2, -1, 0, +1, +2): the lowest value (-2) indicates the driest (coldest) intervals for each site since 18 cal. kyr BP while the maximum (+2) indicates the wettest (warmest) periods, (0) indicates that climatic conditions were similar to present. The

Table 2-1 Palaeoclimatic records from Central Asia arranged from south to north (Abbreviations see below)

No.	Section	N (°)	E (°)	Eleva. (m a.s.l.)	Archive	Time (cal. kyr BP)	Resol. (yr)	Dating* No.	method	A	B	C	D	E	Methods#	Reference
R1	Qilu Hu	24.18	102.75	1797	Lake	50.00	180	16	AMS ^{14}C	2	3	4	2	2	S O C dO G MS	Hodell et al.,1999
R2	Xingyun Hu	24.33	102.76	1723	Lake	25.00	~90	14	AMS ^{14}C	1	1	4	2	2	S O C dO G MS	Hodell et al.,1999
R3	Xiangshui Cave	25.15	110.55	400	Stalagmite	6.00	~75	4	Th/U	1	1	-	-	3	dO dC	Zhang et al.,2004
R4	Dongge Cave	25.32	108.09	680	Stalagmite	16.00	1~15	44	Th/U	1	1	-	-	1	dO	Dykoski et al.,2005
R5	Erhai	25.75	100.25	1974	Lake	12.90	~80	11	AMS ^{14}C	2	2	1	4	1	S MS P	Shen et al.,2006b
R6	Didwana Salt lake	27.33	74.58	n.d.	Salt Lake	>15.00	n.d.	6	^{14}C	2	2	4	3	3	S P	Singh et al.,1990
R7	Lake Shayema	28.50	102.00	2400	Lake	12.80	~100	5	^{14}C	2	2	4	2	3	S P O	Jarvis,1993
R8	Lunkaransar	28.50	73.75	n.d.	Dry Lake	10.70	~50	15	^{14}C	1	2	4	2	3	S X dC C G	Enzel et al.,1999
R9	Chen Co	28.95	90.55	4420	Lake Terrace	10-3.7	n.d.	8	AMS ^{14}C	1	1	3	4	2	S O C/N P G C E	Zhu et al.,2009
R10	Linhua Cave	29.48	109.54	455	Stalagmite	6.60	<10	10	U/Th	1	1	-	-	2	X dO dC	Cosford et al.,2008
R11	Hidden Lake	29.81	92.54	4980	Lake	13.450	~100	7	AMS ^{14}C	2	2	1	4	3	P	Tang et al.,2000
R12	Heshang Cave	30.45	110.42	294	Stalagmite	9.50	<10	21	Th/U	1	1	-	-	2	dO dC	Hu et al.,2008
R13	Ren Co	30.73	96.69	4450	Lake	19.60	~300	7	AMS ^{14}C	2	2	1	4	3	P	Tang et al.,2000
R14	Nam Co	30.75	90.50	4718	Lake	8.40	~25-250	12	AMS ^{14}C	1	1	3	4	2	G C M E X O B C/N	Zhu et al.,2008
R15	Gujjar Hut	30.90	78.80	~3500	Peat	7.80	~450	3	^{14}C	1	1	1	4	3	S MS P	Phadtare,2000
R16	Lake Naleng	31.10	99.75	4200	Lake	17.60	<100	11	AMS ^{14}C	2	3	3	1	2	S P	Kramer et al., 2010a,b
R17	Co Ngion	31.50	91.50	4515	Lake	5.80	~100	12	AMS ^{14}C	1	1	3	4	2	P O C M	Shen et al.,2008
R18	Cuoe Lake	31.50	91.50	4532	Lake	10.5-1.6	n.d.	13	AMS ^{14}C	1	1	3	3	1	S G O dC E C/N	Wu et al.2006
R19	Dajiu Lake	31.5	110	1700	Lake Basin	14.60	~80	7	^{14}C	1	2	4	4	3	S P	Liu et al.,2001
R20	Ahung Co	31.62	92.06	4575	Lake	9.5-4	<50	62	AMS ^{14}C	1	1	3	3	1	C O dC dO C/N M X S	Morrill et al.,2006
R21	Shanbao Cave	31.66	110.43	n.d.	Stalagmite	11.6-2.0	~40	14	U/Th	1	1	-	-	2	dO	Shao et al.,2006
R22	Siling Co	31.75	89.00	4500	Lake	15.50	~200	7	^{14}C	2	2	4	4	3	C dO dC	Morinaga et al.,1993
R23	Zigetang Lake	32.00	90.90	4560	Lake	10.60	n.d.	5	AMS ^{14}C	2	2	3	1	2	C O dC	Wu et al.,2007
R24	Zigetang Lake	32.00	90.90	4560	Lake	10.80	~170	5	^{14}C	2	2	3	1	2	P	Herzschuh et al.,2006
R25	Hongyuan	32.75	102.50	3466	Peat	13.00	15-30	17	AMS ^{14}C	1	1	1	2	2	C Co	Zhou et al.,2002
R26	Hongyuan No.1	32.75	102.50	3466	Peat	11.80	~30	15	AMS ^{14}C	1	1	1	4	3	O dC	Wang et al.,2004
R27	No.2 pit	32.85	103.60	3492	Peat	14.90	n.d.	9	^{14}C	1	2	1	4	3	P dC	Yan et al.,1999
R28	Waqie	33.08	102.75	n.d.	Profile	~30.00	n.d.	13	AMS ^{14}C	1	3	-	-	3	S	Zhou et al.,2001
R29	Tso Kar	33.16	78.00	4527	Lake	15.20	n.d.	32	AMS ^{14}C	1	1	3	1	2	S P	Demske et al., 2009
R30	Bangong Lake	33.67	79.00	4241	Lake	11.30	~100	35	^{14}C, U/Th	1	1	3	4	1	dC dO C X	Fontes et al.,1996
R31	Bangong Lake	33.67	79.00	4241	Lake	11.30	~100	35	^{14}C, U/Th	1	1	3	4	1	P	Campo et al.,1996
R32	Koucha Lake	34.00	97.20	4540	Lake	16.40	150-600	5	AMS ^{14}C	2	2	4	4	3	P	Herzschuh et al.,2009
R33	Koucha Lake	34.01	97.24	4530	Lake	16.30	80-200	5	AMS ^{14}C	2	2	4	4	3	S X O C dC dO Os M	Mischke et al.,2008
R34	Sumxi Co	34.60	80.25	5058	Lake	15.10	n.d.	6	^{14}C	2	2	1	4	3	M dC dO Os D O	Gasse et al.,1991
R35	Sumxi Co	34.60	80.25	5058	Lake	15.10	n.d.	6	^{14}C	2	2	1	4	3	P	Gasse et al.,1991
R36	Yaoxian	34.89	108.75	n.d.	Loess	>8.40	n.d.	19	OSL	1	1	-	-	3	S MS	Zhao H. et al.,2007
R37	Yaoxian	34.93	108.83	n.d.	Loess	12.00	~120	2	TL	2	2	-	-	3	S P	Li et al.,2003
R38	Lake Kuhai	35.30	99.20	4150	Lake	18.00	200	17	AMS ^{14}C	1	-	2	2	4	S P	Wischnewski et al., 2011
R39	Duowa	35.41	101.95	2000	Loess	12.5-0.8	~140	19	OSL	-	-	-	-	4	S MS G	Maher and Hu, 2006
R40	Kusai Lake	35.72	92.92	4475	Lake	3.90	~15	7	AMS ^{14}C	1	1	3	1	2	O G C/N	Wang et al.,2008
R41	Majiawan	36.00	108.16	1400	Loess	11.50	~100	3	OSL	2	2	-	-	3	G C O MS E S	Huang et al.,2004
R42	Xiaogou	36.00	105.00	~2000	Profile	~25.00	~300	18	AMS ^{14}C	2	2	4	4	3	S P	Wu et al.,2009
R43	Chaka Salt Lake	36.70	99.15	3200	Salt Lake	17.20	~350	10	AMS ^{14}C	1	2	3	2	2	S M O	Liu et al.,2008a
R44	Qinghai Lake	37.00	100.00	3200	Lake	18.00	n.d.	10	AMS ^{14}C	2	2	3	2	4	Os dO	Liu et al.,2007
R45	Qinghai Lake	37.00	100.00	3200	Lake	18.00	20-40	6	AMS ^{14}C	2	2	3	2	3	P	Liu et al.,2002
R46	Hurleg Lake	37.32	96.90	2817	Lake	14.00	~160	7	AMS ^{14}C	2	2	1	4	2	P C O	Zhao et al.,2007
R47	Haxi section	37.50	102.40	2450	Profile	10.90	70	5	^{14}C	2	2	4	4	3	S MS O C	Wu et al.,1998
R48	Jingbian	37.50	109.00	n.d.	Trench	10.00	~100	11	AMS ^{14}C	1	1	-	-	3	S G C	Xiao et al.,2002
R49	Midiwan	37.65	108.62	1400	Peat	15.40	~100	23	^{14}C	1	1	1	3	2	S P O dC	Zhou et al.,1996
R50	Dunde	38.10	92.40	5325	Ice Core	4.550	~100	-	ice counting	-	-	-	-	-	dO	Yao and Thompson, 1992

Table 2-1 (*continued*)

No.	Section	N (°)	E (°)	Eleva. (m a.s.l.)	Archive	Time (cal. kyr BP)	Resol. (yr)	Dating* No.	Dating* method	Dating* A	Dating* B	Dating* C	Dating* D	Dating* E	Methods#	Reference
R51	Dunde	38.10	92.40	5325	Ice Core	11.0-0	1~1000	-	-	-	-	-	-	-	P	Liu et al.,1998
R52	HongshuiRiver	38.16	102.76	1460	Profile	8.5-3.2	~50	9	AMS ^{14}C	-	-	-	-	4	S P	Ma et al.,2004
R53	Lake Zhuyeze	39.00	103.33	1320	Dry Lake	11.6-0	~50	12(8)	AMS ^{14}C	1	2	3	2	3	S O P	Chen et al.,2006
R54	Qingtu Lake	39.05	103.67	1309	Dry Lake	11.3-0	40	6	AMS ^{14}C	1	1	4	4	3	S G	Zhao et al.,2003
R55	Baahar Nuur	39.10	109.20	1450	Salt Lake	>13.80	~50	6	AMS ^{14}C	2	2	4	4	3	S MS G C	Feng et al.,2005
R56	Lake Kichikol	39.99	73.55	2541	Lake	6.3-0	~90	4(3)	AMS ^{14}C	2	2	1	4	2	S Ch O C	Beer et al.,2007
R57	Lake Kichikol	39.99	73.55	2541	Lake	6.3-0	~90	4(3)	AMS ^{14}C	2	2	1	4	2	P	Beer et al.,2007
R58	Lake Yanhaizi	40.15	108.45	1180	Lake	>15.00	~100	10	AMS ^{14}C	2	2	3	2	2	S C O C/N E M X MS	Chen et al.,2003
R59	Daihai Lake	40.55	112.75	1221	Lake	11.2-0	15-77	8	AMS ^{14}C	1	1	2	1	2	C O	Xiao et al.,2006
R60	Daihai Lake	40.55	112.75	1230	Lake	11.2-1	30-150	8	AMS ^{14}C	1	1	2	1	2	S P	Xiao et al.,2004
R61	Chasuqi	40.67	111.12	n.d.	Lake	10.2-0	~80	4	^{14}C	3	4	4	4	3	P	Wang et al.,1997
R62	Diaojiao Lake	41.30	112.35	1800	Lake	9.6-0	~100	4	AMS ^{14}C	2	2	4	4	3	P	Shi and Song, 2003
R63	Bayanchagan Lake	41.65	115.21	1355	Lake	12.5-0	<150	9	AMS ^{14}C	1	2	3	3	2	P	Jiang et al.,2006
R64	Lake Eastern Juyanze	41.83	101.63	n.d.	Profile	5.3-2.8	3-70	4	AMS ^{14}C	1	1	4	4	3	OS E dO dC X P S	Mischke et al.,2005
R65	Juyan palaeolake	41.89	101.85	892	Palaeolake	10.7-1.7	~150	5	AMS ^{14}C	1	1	-	4	3	S P	Herzschuh et al.,2004
R66	Bosten Lake	41.94	86.76	1048	Lake	8.6-0	~20	11	AMS ^{14}C	2	2	1	4	1	OS E dC dO	Mischke and Wünenmann, 2006
R67	Bosten Lake	42.00	87.00	1048	Lake	8.0-0	~100	5	AMS ^{14}C, OSL	2	2	3	3	2	S G P	Huang et al.,2009
R68	Hani Peat Bog	42.21	126.21	900	Peat	12.3-0	~20	10	AMS ^{14}C	1	1	1	4	3	dC	Hong et al.,2005
R69	Lake Sihailongwan	42.29	126.60	797	Lake	15.3-0	~1	36	AMS ^{14}C	1	1	1	1	2	O C E lam. P D	Schettler et al.,2006
R70	Lake IssykKul	42.50	77.00	1607	Lake	8.7-1.0	~180	16	AMS ^{14}C	1	1	3	4	2	S OS dO dC E	Ricketts et al.,2001
R71	Xiaoniuchang	42.62	116.83	1460	ancient lake	10.9-0	~250	3	AMS ^{14}C	2	2	-	4	3	S C G E	Liu et al.,2002a
R72	Xiaoniuchang	42.62	116.83	1460	ancient lake	10.9-0	~250	3	AMS ^{14}C	2	2	-	4	3	P	Liu et al.,2002a
R73	Liuzhouwan	42.71	116.67	1365	ancient lake	18.3-0	360	3	AMS ^{14}C	2	3	4	4	3	S G O C/N P M MS	Wang et al.,2001c
R74	Haoluku	42.96	116.75	1295	ancient lake	12.0-0	~220	3	AMS ^{14}C	2	3	4	4	3	S G O C/N M MS	Wang et al.,2001c
R75	Haoluku	42.96	116.75	1295	ancient lake	12.0-0	~220	3	AMS ^{14}C	2	3	4	4	3	P	Wang et al.,2001c
R76	Dali Lake	43.35	116.72	1226	Lake	12.7-0	~20	18	AMS ^{14}C	1	1	3	2	2	S C O	Xiao et al.,2008
R77	Barkol Lake	43.70	92.85	1580	Lake	9.4-0	38	7	^{14}C	1	2	3	1	2	S G	Xue et al.,2008
R78	Lake Manas	45.75	86.00	251	Lake	11.6-0	~150	8	AMS ^{14}C	2	2	4	4	3	S C M X G dO dC O D	Rhodes et al.,1996
R79	Lake Manas	45.75	86.00	251	Lake	11.6-0	~150	8	AMS ^{14}C	2	2	4	4	3	P	Rhodes et al.,1996
R80	Wulungu Lake	47.00	87.50	478.6	Lake	9.55-0	50-100	7	AMS ^{14}C	1	2	3	1	1	S G C C/N dC O	Liu et al.,2008b
R81	Wulungu Lake	47.00	87.50	478.6	Lake	9.55-0	50-100	7	AMS ^{14}C	1	2	3	1	1	P	Liu et al.,2008b
R82	HotonNur	48.66	88.30	2083	Lake	>11.5-0	~150	1+6	AMS ^{14}C	-	-	-	4	2	D S	Rudaya et al.,2009
R83	HotonNur	48.66	88.30	2083	Lake	>11.5-0	~150	1+6	AMS ^{14}C	-	-	-	4	2	P	Rudayaet al.,2009
R84	Lake Telmen	48.66	97.33	1789	Lake	7.1-0		8	AMS ^{14}C	1	1	1	1	2	S X D P lam.	Peck et al.,2002
R85	Lake Telmen	48.66	97.33	1789	Lake	7.0-0	~200	6	AMS ^{14}C	1	1	1	1	2	S P	Fowell et al.,2003
R86	Hulun Lake	49.00	117.00	545	Lake Profile	15.8-0	~150	10	^{14}C	1	1	1	4	3	S D	Xue et al.,2003
R87	Gun Nuur	50.25	106.60	600	Lake	12.2-0	300	7	^{14}C	1	2	4	4	3	S P	Dorofeyuk et al.,1998
R88	Gun Nuur	50.42	106.10	600	Lake	9.4-0	~30	9	AMS ^{14}C	1	1	3	4	3	S D C O dC MS	Feng et al.,2005
R89	Hovsgol Lake	50.54	101.16	1645	Lake	18.0-0		11	AMS ^{14}C	2	2	1	2	2	S E O C M	Murakami et al.,2009
R90	Hovsgol Lake	50.54	101.16	1645	Lake	7.1-0	450	2	^{14}C	2	2	4	4	3	S P	Dorofeyuk et al.,1998
R91	Dood Nuur	51.33	99.39	1538	Lake	14.4-0	~700	2	^{14}C	4	4	4	2	3	S D	Dorofeyuk et al.,1998
R92	Dood Nuur	51.33	99.39	1538	Lake	14.4-0	~700	2	^{14}C	4	4	4	2	3	S P	Dorofeyuk et al.,1998

Abbreviations (**Table 2-1**):

* Dating reliability,

A: Average frequency of dating (1-every 1500 yrs, 2-every 3000 yrs, 3-every 5000 yrs, 4-less often);

B: Maximum interval of dating (1-2000 yrs, 2-4000 yrs, 3-6000 yrs, 4-more);

C: Old carbon reservoir effect (1-no influence possible, 2-reservoir effect checked within 500 yrs, 3-reservoir effect checked, 4-reservoir effect not checked);

D: Continuality of the record (1-nor or only slight changes in the sediments, no interruptions, 2-sediment changes, no interruptions, 3-interruptions possible, covered by dating, 4-no attempt made to interruptions);

E: Presentation of chronology (1-presentation of detailed dating results, with extensive discussion, 2-presentation of original chronology with discussion, 3- presentation of original dating results, 4-no presentation of original chronology).

Methods:

Underlined methods are considered by the chronological resolution;

B-biomarkers; C-carbonate content; Ch-Chironomidae; Co-color; C/N-carbon/nitrogen ratios; D-diatoms; dC-carbon isotope; dO-oxygen isotope; E-elements; G-grain size; lam.-laminations; M-minerals; Mo-mollusks; MS-magnetic susceptibility; O-organic content; Os-Ostracod; P-pollen; S-sediment description; X-X ray diffraction.

justification for designating an ordinal moisture (warmth) scale is that each individual site may not be linearly comparable to others due to differences in geographic location, archives, proxies used and sensitivity. Moreover, owing to the qualitative nature of the palaeoclimatic records, it is impossible to translate this information on a finer climatic scale. The moisture (warmth) scales are relative, in a semi-quantitative sense and are only applicable to each individual site (Chen et al., 2008; Zhao et al., 2009a). Relative moisture (warmth) sequences were constructed for each 100-year interval during Holocene period (12-0 cal. kyr BP), and for each 200-year interval before the Holocene (18-12 cal. kyr BP).

Mean moisture index values for selected time slices were mapped using a Kriging interpolation model in the ArcGIS 9.2 program (Johnston et al., 2001).

2.3.3 Mapping and ordination of palaeomoisture index results

Ordination techniques are powerful tools to assess underlying patterns in large data sets. However, due to the low number of temperature records and the lack of sufficient moisture records before 10 cal. kyr BP, numerical analyses were performed only on 65 moisture sequences spanning the last 10 cal. kyrs, including 15 pollen and 50 non-pollen based records. Almost 25% of the records (19 counts) don't quite cover the whole period and contain gaps, usually of less than thousand years. To avoid subsequent biases, missing data was generally replaced with mean values from the nearest three sites when available; such mean values were also standardized to our five-part scale (e.g. Ahung Co, Morrill et al., 2006; Nam Co, Zhu et al., 2008).

To examine the underlying patterns of our synthesized climate indices, principal component analysis (PCA) using moisture indices from selected sites as variables and the time slices as observations (data were centered by species without transformation), was performed using

CANOCO 4.5 for ordination (ter Braak and Smilauer, 2002). Almost identical results were obtained by non-metric Multidimensional scaling (nmMDS; results not shown) that was processed through the Brodgar 2.5.7 program (Zuur et al., 2009).

To evaluate concordance between pollen and non-pollen based records, Procrustes analysis based on the results of four PCA axes from both pollen and non-pollen records, was performed using the R 2.9.0 Program (Mardia et al., 1979). The significance of the Procrustes fit was tested using 101 random permutations, which were modified to allow restricted permutations for time series data (pers. comm. Gavin Simpson). Correlation using symmetric Procrustes rotation was found to be 0.8399 combined with a significance of 0.009901 (meaning that the permutations failed only once during the calculation).This indicates significant concordance between pollen and non-pollen data sets (Peres-Neto and Jackson, 2001) implying synchronous signals between pollen and non-pollen records on centennial time-scales as reported by Seppa and Bennett (2003). This essentially means that Holocene pollen based records are not biased by anthropogenic activity, permitting us to use them together for ordination purposes.

PCA scores of the first two axes were mapped in order to extract regional moisture evolution pattern in Holocene using Kriging interpolation model in ArcGIS 9.2 program (Johnston et al., 2001).

2.3.4 Meteorology data of the Recent Past

Meteorological data used in this study are obtained from the NCEP/NCAR reanalysis project. Due to the fact that the reanalysis system and the model used remain unchanged throughout the period, the reanalyzed data provide a reliable database data for studying interannual circulation variability (Kalnay et al., 1996; Kistler et al., 2001). In this study, monthly mean winds (u-wind, v-wind and omega-wind) at standard pressure levels (totally 17 standard levels) from the reanalysis data for the period from January 1979 to December 2008 were used.

The Monsoonal Hadley Index (MH Index), a dynamical index for Indian Summer Monsoon variability defined by Goswami et al. (1999), is calculated as the meridional wind-shear anomaly (between 850 hPa and 200 hPa) averaged across the ISM dominated area (70ºE-110ºE, 10ºN-30ºN), expressed as:

$$MH_{ISM} = V^*_{850} - V^*_{200} \qquad (1)$$

Where V^*_{850} and V^*_{200} are the meridional wind anomalies at 850 hPa and 200 hPa respectively, averaged over the summer season (June to August) throughout the defined ISM region. All calculations and maps were computed using Grid Analysis and Display System (GrADS) Version 1.8 (Berman et al., 2001).

2.4 Results

2.4.1 Variations in the mean moisture and warmth indices

In total 40 pollen based and 52 non-pollen based records provide moisture indices from 72 sites, while 18 pollen based and 18 non-pollen based sequences are indicative of changes in warmth. The mean indices for both moisture and warmth during the last 18 cal. kyrs are shown in Figure 2-3. These show near-synchronous changes in pollen and non-pollen records, confirming the previous findings from Procrustes analyses and outlining the general trends for moisture and warmth evolution over the last 18 cal. kyrs.

Despite a scarcity of available data for periods prior to 15 cal. kyr BP, mostly dry and cold conditions prevailed. Thereafter, a relatively wet and warm period which lasted for ~2000 years (synchronous with the Bølling/Allerød period in the north Atlantic region) was followed by a 1500-yr dry, cold phase, probably reflecting the Younger Dryas event. At the beginning of Holocene, both moisture levels and temperatures increased abruptly reaching a maximum at around 10 cal. kyr BP. The Holocene Optimum lasted until 8 cal. kyr BP followed by a trend towards drier and colder conditions, which prevailed until the latter part of the Holocene.

Synthesized moisture indices from three sub-regions (see supplementary, Figure 2-10), confirm synchronous increase in moisture availability at the beginning of the Holocene (12-10 cal. kyr BP). However, different trends occurred following the period of maximum moisture. Moisture levels decreased first within the area outside of the present monsoon boundary around 7.5 cal. kyr BP (but with another wet period between 5 and 2 cal. kyr BP); by 6.5 cal. kyr BP moisture levels had also decreased in the ISM area and by ca. 4.5 cal. kyr BP in the EASM area.

2.4.2 Frequency of impacts of anthropogenic activity

In Figure 2-4, we summarize the previous studies within our data set that were judged by the authors to show evidence of anthropogenic impacts. The earliest human influences are described in studies from the Chinese Loess Plateau at 8 cal. kyr BP (Huang et al., 2004). After 6 cal. kyr BP, and especially from 4 cal. kyr BP onwards, evidence for anthropogenic impact increases and reaches a maximum during the last 1000 years (see also in Figure 2-6o). Spatial analysis shows that the records of anthropogenic impact centre around southern China and the Chinese Loess Plateau region and, are sparsely distributed throughout northern India, Mongolia, Kyrgyztan and Xinjiang (China) (Figure 2-6o).

2.4.3 Temporal and spatial analysis of PCA axes scores

The axes scores from PCA performed on the combined pollen and non-pollen data sets of the last 10 cal. kyrs are shown in Figure 2-4. The first axis (PC1), accounting for 46.3 % of the

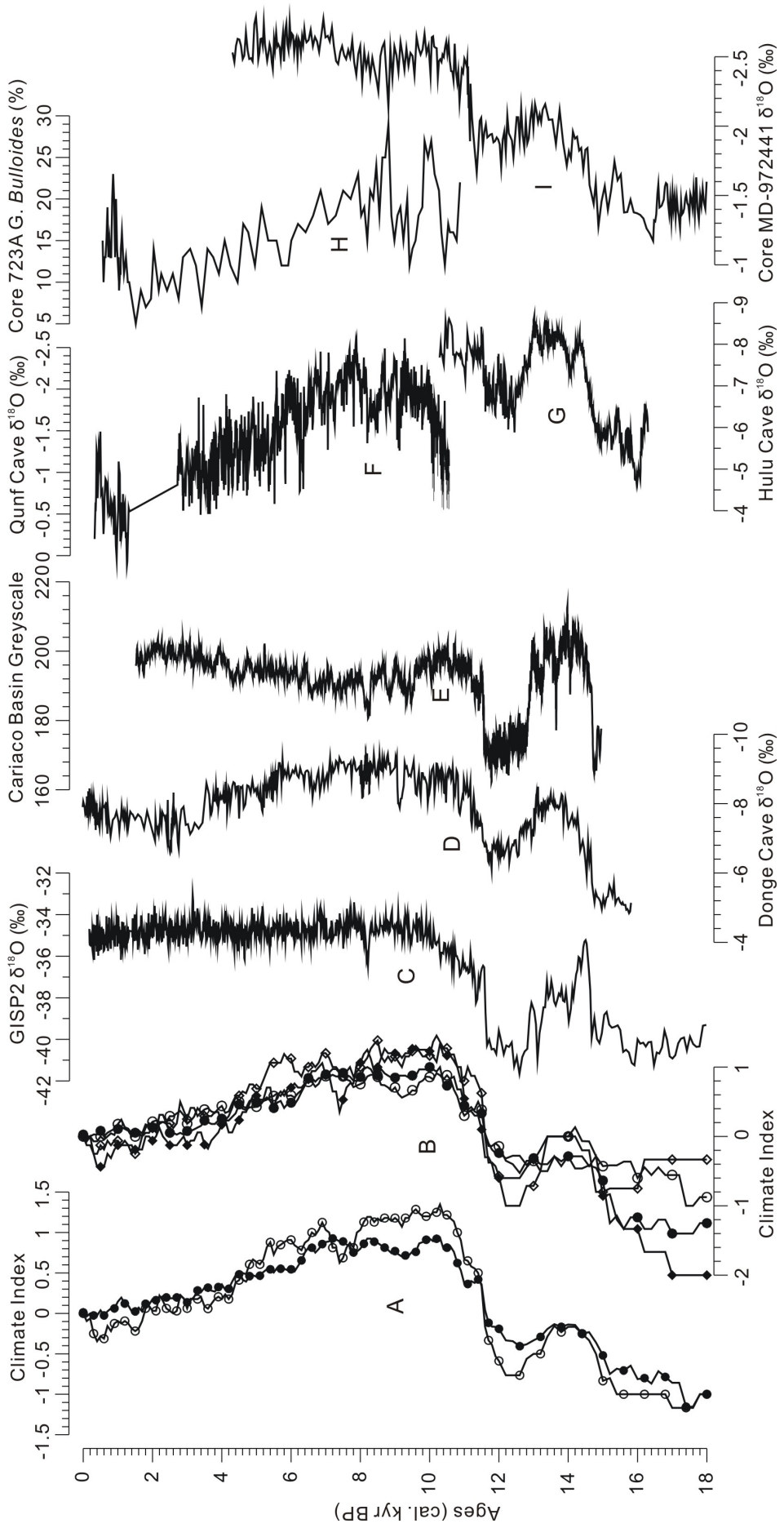
Ages (cal. kyr BP)
0
2
4
6
8
10
12
14
16
18
Climate Index
-1.5 -1 -0.5 0 0.5 1 1.5
GISP2 δ18O (‰)
-42 -40 -38 -36 -34 -32
Cariaco Basin Greyscale
160 180 200 2200
Qunf Cave δ18O (‰)
-0.5 -1 -1.5 -2 -2.5
Core 723A G. Bulloides (%)
5 10 15 20 25 30
Climate Index
-2 -1 0 1
Donge Cave δ18O (‰)
-4 -6 -8 -10
Hulu Cave δ18O (‰)
-4 -5 -6 -7 -8 -9
Core MD-972441 δ18O (‰)
-1 -1.5 -2 -2.5
A
B
C
D
E
F
G
H
I

Figure 2-3 Synthesized Holocene climate indices in Central Asia and comparison with selected palaeoclimatic proxy records. (A) Mean moisture (solid circles) and warmth (hollow circles) indices based on all synthesized records; (B) Mean climate indices based on pollen (moisture, solid circles; warmth, solid diamonds) and non-pollen records (moisture, hollow circles; warmth, hollow diamonds); (C) GISP2, Greenland, Grootes et al. 1993; (D) Dongge Cave D4, China, Dykoski et al., 2005; (E) Cariaco Basin, Venezuela, Hughen et al., 2000; (F) Qunf Cave, Oman, Fleitmann et al., 2007; (G) Hulu Cave, China, Wang et al., 2001a; (H) 723A-Core, Arabian Sea, Gupta et al., 2003; (I) MD972441-Core, Sulu Sea, Oppo et al., 2003.

total variance, shows relatively high values (ca. 1.5) until 7 cal. kyr BP, then decreases gradually over the following 3000 years to values of -1. After this, for the last 4000 years, values remain negative. Compared to the relatively steady PC1, the second axis (PC2, accounting for 13.4 %) shows more fluctuations. Following a gentle increase over 3500 years, PC2 reaches a maximum at about 5000 cal. yr BP which lasts for 2000 years, then decreases sharply to negative values of -0.5 in less than 1000 years. Values slightly fluctuated during the last period, illustrating a different temporal pattern from PC1.

The two PCA axes also show distinctive spatial patterns (Figure 2-5). PC1 decreases stepwise from south to north i.e. from the highest values in northern India and southwestern China, to the lowest values in Mongolia. PC2, in contrast, shows a more continuous decrease from southeast to northwest, except for two sites from the northeastern part of China which show negative values such as those found in northwestern China and western Mongolia. Additionally, roughly the same results were obtained for the warmth index (not shown), but they were not interpreted due to the low density of data points (only 26 sites available).

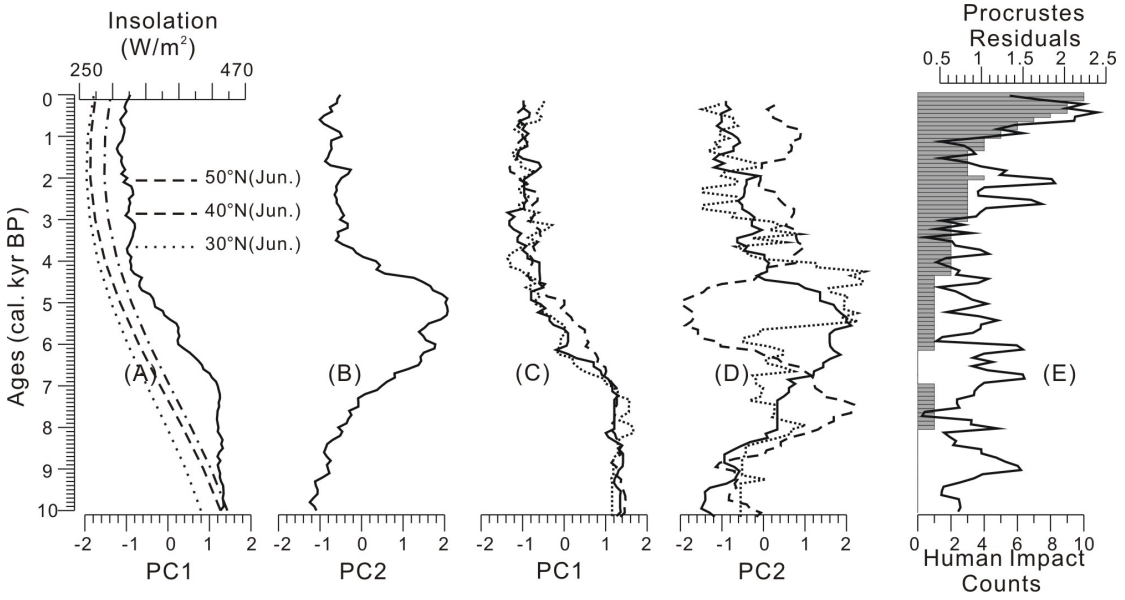

Figure 2-4 Temporal pattern of results after ordination analysis for the last 10 cal. kyr BP, as: (A) PC1 of all records (together with Northern Hemisphere solar insolation changes in June at 30°N, 40°N and 50°N, after Laskar et al., 2004), (B) PC2 of all records, (C) PC1 of records from each sub-region, (D) PC2 of records from each sub-region; (E) Residuals after Procrustes analysis (line), and records deemed to have been impacted by human activity within this study (columns). In (C) and (D), solid lines indicate EASM area, dash lines indicate ISM area and dot lines indicate the area outside of present monsoon boundary.

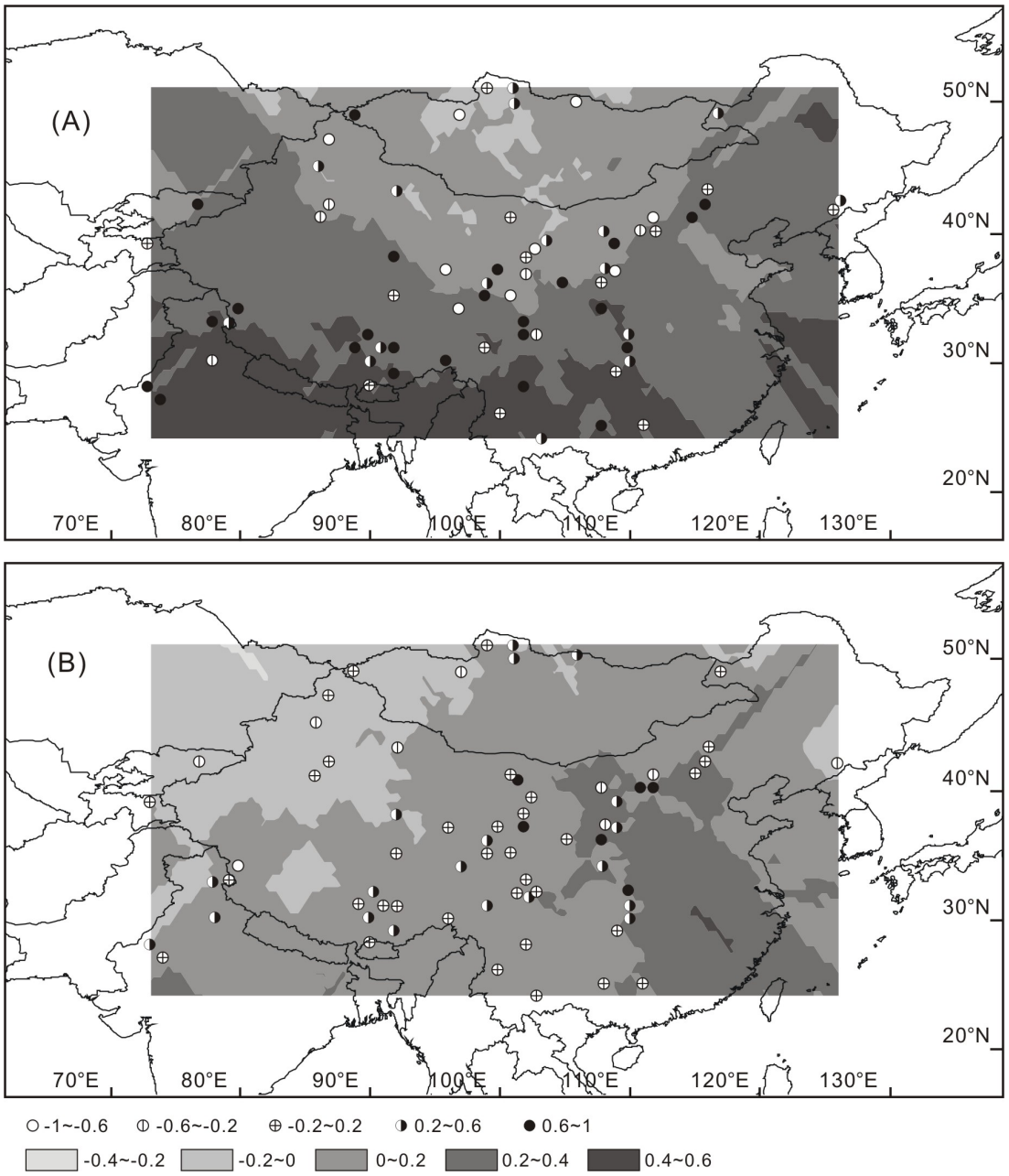

Figure 2-5 Spatial distribution of results after ordination analysis based on moisture indices from 72 sites as: (A) PC1, (B) PC2. Symbols indicate values for each site whilst colored bands represent interpolated zones through the Kriging model.

Independent PCA analyses of moisture indices since 10 cal. kyr BP for three sub-regions (Figure 2-4 C,D) present consistent first axis patterns with high values between 10 and 7 cal. kyr BP, and a gradual decrease to the present conditions until 4 cal. kyr BP. However for the second axis values, the region outside of present monsoon boundary, ISM and EASM areas show strongly differing signals with peaks at 5.5-4 cal. kyr BP, 8-7 cal. kyr BP and 7-4.5 cal. kyr BP respectively.

2.5 Discussion

2.5.1 Reliability of climate inferences from proxy records in monsoonal central Asia

Despite taking utmost care in both site selection and methodological approach, the climatic information that we obtained from our meta-analyses faced the following problems:

1). Temporal resolution and age-control of records differ. Generally, records derived from stalagmites have the highest resolution of decadal or even near-annual resolution. As the most common archive, lacustrine sediments from either underwater cores or dry sections vary in resolution from annual to centennial scales.

2). Spatial resolution of our data differs as archives are not evenly distributed across the study area. As shown in Figure 2-2, most of our records were obtained from central China, the eastern Tibetan Plateau and Inner Mongolia whilst information from remote areas in northern and western Tibet and from desert areas in northwestern China and Mongolia is sparse due to the lack of available archives.

3). Sensitivity to climate change differs in various proxies. On account of the nonlinear response to climate change, proxy-based moisture and temperature reconstructions all have individual signal-response relationships. Furthermore, warmth records are probably not as reliable since most proxies are dependent on moisture and encompass a mixture of precipitation and temperature signals (e.g. vegetation changes, lake level fluctuations, stable isotope records, etc.). In addition to this, our assumptions that associations exist between warm and wet conditions and between dry and cold conditions may have artificially biased the climatic inferences.

4). The reliability of climate inferences from glacial flora is limited due to formerly low CO_2 concentrations that supported the expansion of drought resistant vegetation which results in an underestimation of moisture levels from pollen records (Cowling and Sykes, 1999; Jackson and Williams, 2004; Wu et al., 2007).

5). Since the appearance of civilizations, anthropogenic activity has had an increasingly important impact on climate records and becomes more apparent in records dated since 6000 cal. yr BP, and especially since 1000 cal. yr BP (Figure 2-4). Furthermore the trend of records with an apparent human impact perfectly matches a significant increase in residuals following Procrustes analysis, meaning that the largest difference between pollen and non-pollen based records for the last 1000 years might be caused by the progressive importance of anthropogenic activity which is consistent with the results of Zhao et al. (2009). The main focus of our study has been on climate change whilst exploring the impact of humans was a secondary aim in order to assess the reliability of the climatic inferences. Even though no records in our data set support the transition between human- and climate-driven vegetation changes as suggested by Dearing et al. (2008) based on data from Erhai Lake, the level of continuous human activity has potentially biased the climatic significance of the proxies, especially in central China during the second half of the Holocene.

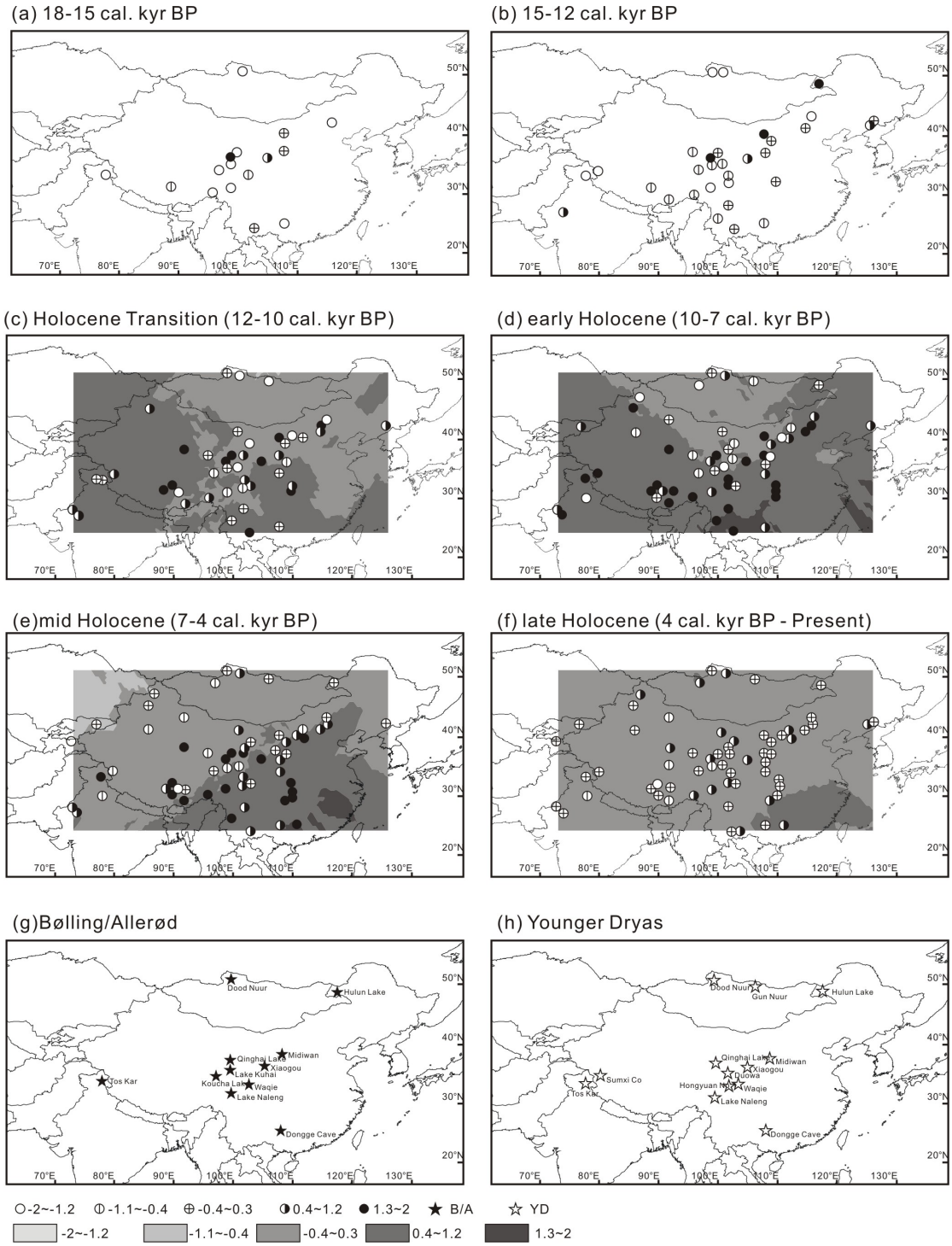

Figure 2-6 (a–f) Spatial distribution of moisture indices from Central Asia for defined time periods. (g, h) Distributions of records with the Bølling/Allerød warm period and Younger Dryas cold event. (i–n) Spatial patterns of warmth indices during the same periods as (a–f). (o) Temporal and spatial distribution of inferred human impact records in our dataset. For moisture and warmth indices, symbols indicate the values for each site during certain periods while the gray bands present the interpolated zones through Kriging model.

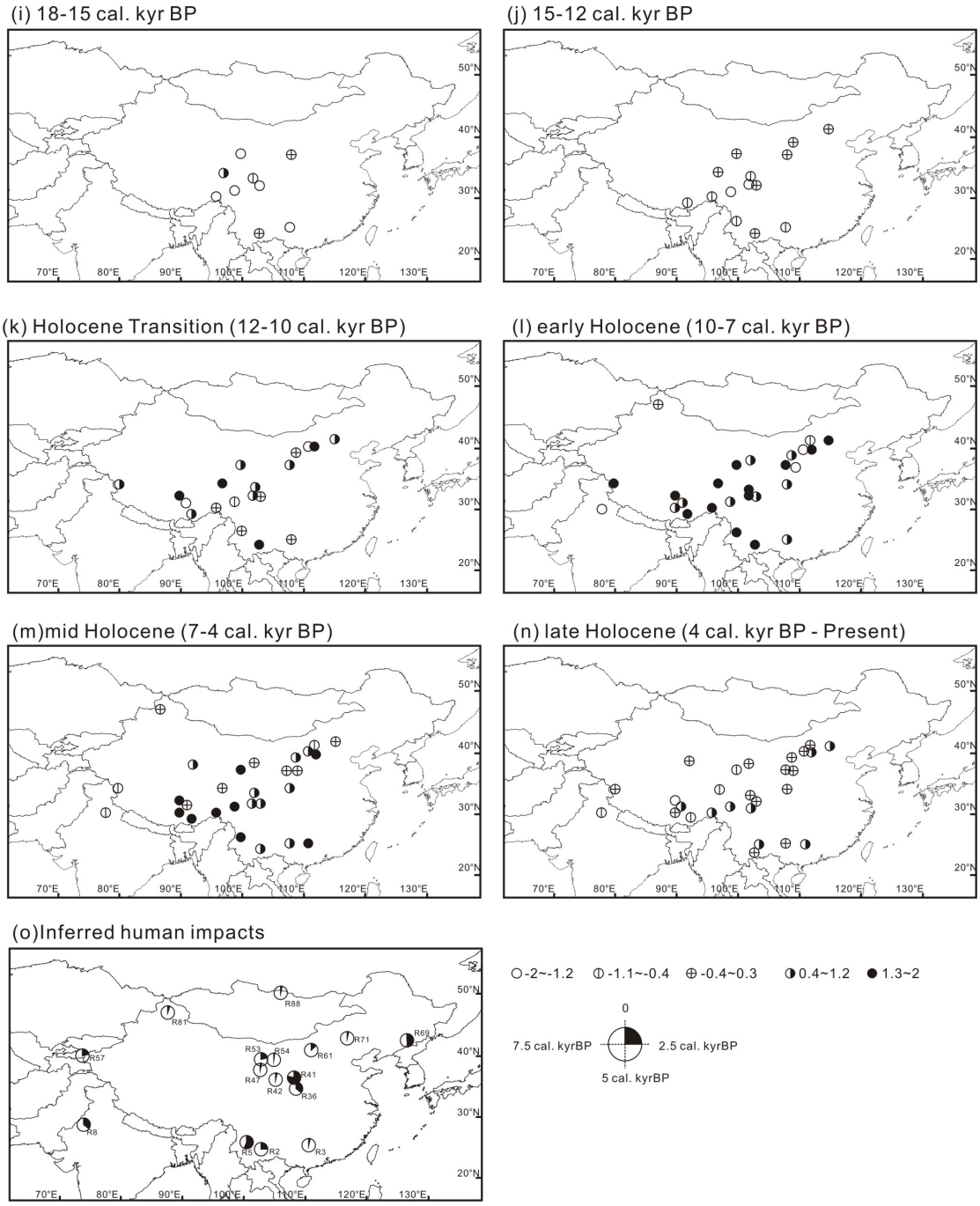

(**Figure 2-6** *continued*)

2.5.2 Spatial and temporal climate patterns in monsoonal central Asia since 18 cal. kyr BP

The main features of the climate history of monsoonal central Asian can be inferred from changes in the mean moisture (warmth) index values (Figure 2-3; Figure 2-10) and from maps showing spatially interpolated moisture (warmth) index values of selected time slices (Figure 2-6).

The majority of the 16 records that were available for the period from 18 to 15 cal. kyr BP reflect dry to moderately dry together with cold to moderately cold conditions throughout China (Figure 2-6a, i), yielding minimum mean values for the whole study interval (Figure 2-3), indicating that monsoonal central Asian climate in the time immediately after the LGM was characterized by dry and cold conditions. This is in agreement with inferences from high-latitude ice core records (GISP2, Grootes et al., 1993; Stuiver et al., 1995; Vostok, Sowers et al., 1993; Petit et al., 1999) and low-latitude marine records (Arabian Sea, Sonzogni et al., 1998; South China Sea, Wang et al., 1999; Steinke et al., 2001; Sulu Sea, Linsley, 1996; Oppo et al., 2003). However, two sites, namely Chaka salt lake (Qaidam Basin) and Xiaogou section (Chinese Loess Plateau), document abnormally wet conditions (Figure 2-6a). The authors inferred that these were related to the reduced evaporation rates during glacial times (Liu et al., 2008a; Wu et al., 2009b).

Moderate dry conditions were largely recorded between 15 and 12 cal. kyr BP (Figure 2-6b). However, two major climate events are clearly indicated by the mean values. Firstly a warm, wet period culminating at around 14 cal. kyr BP is consistent with findings of an initial increase in the Indian Summer Monsoon in the Arabian Sea area (Figure 2-3, Figure 2-6g, j) (Overpeck et al., 1996), which was synchronous with the Bølling/Allerød warm period recognized in European and North Atlantic climate records (Weaver et al., 2003). Secondly, a cold reversal immediately prior to the Holocene apparent in many records (Figure 2-3, Figure 2-6h) is probably related to the Younger Dryas cold event (Dansgaard et al., 1989). However, due to the low number of records available, it is difficult to define chronological control for these events. Using our available data it can only be stated that the Bølling/Allerød period was warm and wet and that the Younger Dryas was cold and dry, and that both events occurred in central China, on the western Tibetan Plateau and in northern Mongolia. Moisture and warmth increased abruptly and wet conditions prevailed in the western part of our study area at the beginning of the Holocene (Figure 2-3 and Figure 2-6c, k) representing a second enhancement of the summer monsoon after the LGM which is also documented in marine and stalagmite records from across the Asian monsoonal regions (Hodell et al., 1999; Dykoski et al., 2005; Shen et al., 2006a; Fleitmann et al., 2007).

When considering average moisture and warmth indices across the whole study area, the early Holocene (10-7 cal. kyr BP, Figure 2-3 and Figure 2-6d, j) represents the wettest and warmest phase since 18 cal. kyr BP. This period is also recognized as the Holocene Optimum period in reviews by An et al., (2000) and Herzschuh (2006), and is furthermore consistent with a maximum in the Asian Summer Monsoon recorded in ice core records from Tibetan Plateau (Guliya, Thompson et al., 1997; Dunde, Liu et al., 1998), marine records (Overpeck et al., 1996) and terrestrial monsoon records from outside our study area (Fleitmann et al., 2003, 2007). The mapping of moisture indices reveals regional differences. Whilst maximum moisture conditions are concentrated in southwest China, records from Mongolia, Inner Mongolia and Xinjiang indicate moderately dry conditions consistent with a period of low lake levels observed by Chen et al. (2008). However, newly published climatic data from two Mongolian lakes, Hoton Nur (Rudaya et al., 2009) and Lake Hovsgol (Murakami et al., 2009), imply that the early Holocene was characterised by a moisture optimum which is probably indicative of strong spatial differences in the moisture history of Mongolia during the early

Holocene.

The period between 7 and 4 cal. kyr BP (Figure 2-6e, m) is still warm and wet on average but is characterized by a clear southeast-northwest moisture gradient which is different from the early Holocene wet phase. Maximum moisture levels in southeast China were attained during the mid-Holocene which is explained by the 'southward moving Holocene Optimum Period' hypothesis outlined by An et al. (2000) despite the potential uncertainty raised from their low resolution records. However maximum moisture levels during the mid-Holocene were also recorded in Korea (Fujiki and Yasuda, 2004; Nahm et al., 2006), Japan (Schöne et al., 2004) and the East China Sea area (Li et al., 1997). In contrast, decreasing moisture levels were recorded in northern India, southwest China and in other terrestrial archives from the Indian Summer Monsoonal area such as the stalagmite records (Fleitmann et al., 2003, 2007; Dykoski et al., 2005; etc.) and marine records from Arabian Sea (Overpeck et al., 1996; Gupta et al., 2003), which are unanimously related to decreasing monsoonal activity.

For the last 4000 years, the environment has been more or less equal to the present day, apart from a number of weak moisture signals from southeast China. The overall conditions are slightly drier than those during the previous stage that was assigned to a further decrease in the Asian Summer Monsoon (Liu et al., 2001; Huang et al., 2004; Dykoski et al., 2005; Shao et al., 2006; Cosford et al., 2008; Hu et al., 2008).

In summary, climatic changes in monsoonal central Asia area follow a global pattern, with significant coherence with high-latitude ice core records and low-latitude marine sequences. However, our meta-analyses revealed marked spatial patterns in Asian moisture history that are not yet fully understood in terms of the driving mechanisms.

2.5.3 The asynchronous nature of the Asian monsoonal subsystems: past and present

The PCA analysis performed on the entire region reveals potential moisture evolution patterns. PC1 retains relative high values from 10 to 7 cal. kyr BP, followed by a gradual decrease towards present-day levels, exhibiting high values in northern India, Tibet and southwest China (Figure 2-4A, Figure 2-5). Similar patterns have also been reported from other areas influenced by the Indian Summer Monsoon such as the Arabian Sea (Overpeck et al., 1996; Gupta et al., 2003) and southern Oman (Fleitmann et al., 2003, 2007). This pattern, coherent with the PC1 values from the individual sub-regions (Figure 2-2A; Figure 2-4C), indicates the expanded influence of Asian Summer Monsoon during the early Holocene, accounting for the synchronous increases in moisture levels at the beginning of Holocene and the following moisture maximum, which is well recorded in each sub-region (see supplementary, Figure 2-10).

However, apart from this overall trend, regional differences in moisture evolution which originate from additional moisture sources or from moisture-suppressing mechanisms are indicated by the PC2 axis results from each sub-region (Figure 2-4D). PCA axis 2 of the ISM region exhibits an additional strong moisture signal during the early Holocene (8-7 cal. kyr BP), but starts to decrease after 7 cal. kyr BP. This is probably indicative of the retreat of the ISM (Figure 2-10). The PC2 scores from the EASM region account for as much as 21% of the

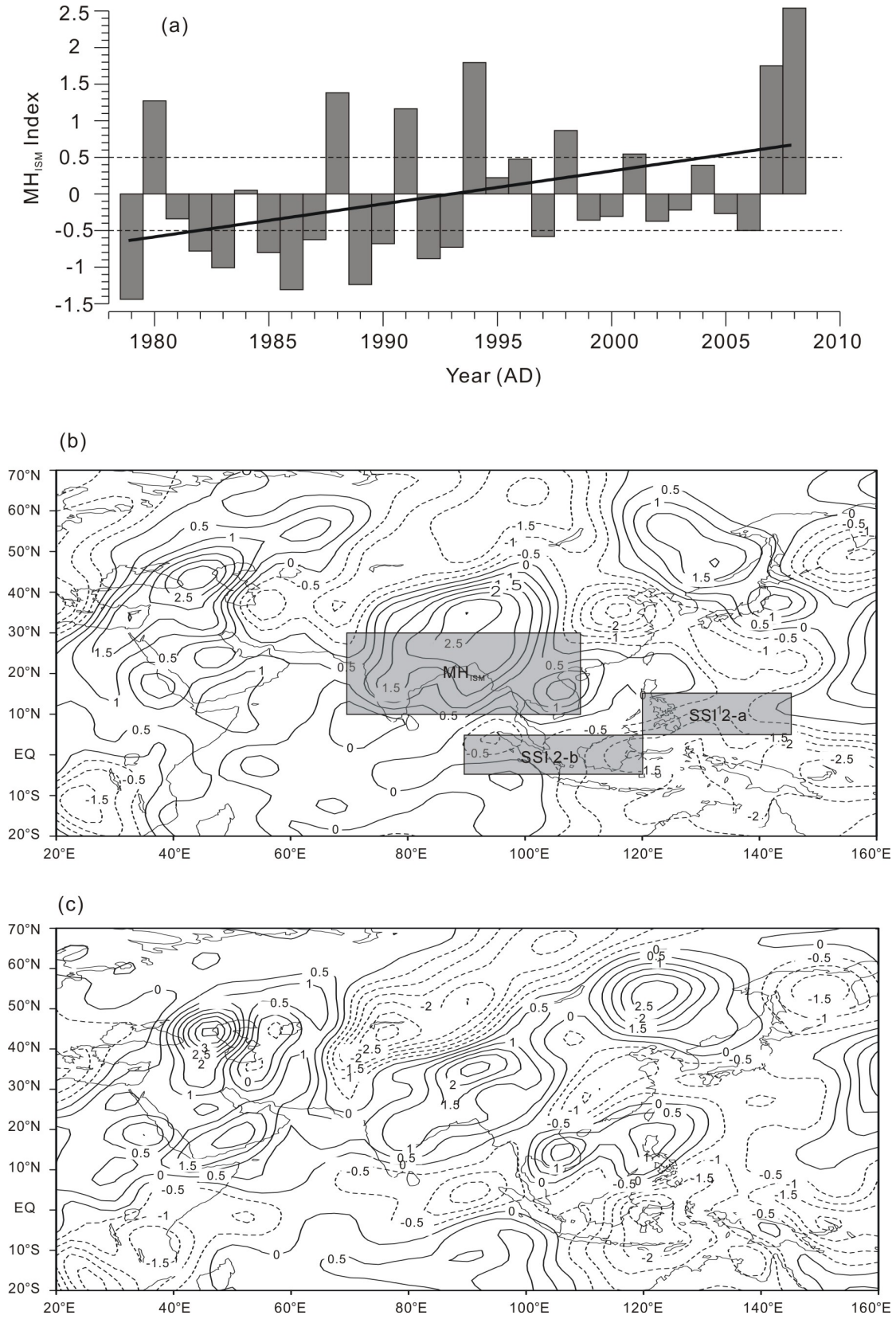

Figure 2-7 (a) Reconstructed Indian Summer Monsoon Hadley Circulation Index (MHISM Index) for the last 30 years based on NCEP/NCAR reanalysis data. (b) Hadley Circulation Index differences between strong and weak ISM years during the last 30 years, shadow regions indicate areas where monsoonal indices were defined. (c) Hadley Circulation Index differences between the second and the first half of the last 30 years.

total variance and reveal that many records, especially cave records from central eastern China (Liu et al., 2001; Shao et al., 2006; Cosford et al., 2008; Hu et al., 2008), were subject to a maximum moisture supply during the mid Holocene (7-4.5 cal. kyr BP) (Figure 2-4D, Figure 2-10). A similar pattern is seen in by records from the Korean peninsula (Fujiki and Yasuda, 2004; Nahm et al., 2006) and in marine records from the East China Sea (Li et al., 1997) and the Japan Sea (Jian et al., 2000; Schöne et al., 2004). Thus, after spatial-temporal analyses, the two primary signals revealed in PCA analysis over the whole region can be interpreted as indices of the Asian Summer Monsoon subsystems with PC1 indicating the Indian Summer Monsoon and PC2 the East Asian Summer Monsoon.

The PC2 scores from the region outside of the present monsoon boundary (Figure 2-4D) indicates that many records show a wet stage between 5 and 2 cal. kyr BP (Figure 2-10). Considering the transitional position of this region and the regression of Asian Summer Monsoon, these wet conditions during the late-Holocene probably reflect the influence of the Westerlies as was reported by Vandeberghe et al. (2006) and Chen et al. (2008). However, probably owing to the lack of continuous records, our study does not confirm an out-of-phase moisture evolution pattern during the mid and late Holocene in the arid central Asian area as reported by Chen et al. (2008) who described a dry early Holocene (12-8 cal. kyr BP) and relatively wet mid to late Holocene (since ca. 7 cal. kyr BP).

Hence, the regions influenced by the two Asian Summer Monsoon sub-systems evolved in notably different ways during the first half of the Holocene. The Indian Summer Monsoon (PC1) mirrored the path of Northern Hemisphere solar insolation, presenting a decreasing trend throughout the Holocene with maximum rates of change during the mid-Holocene. In contrast, the East Asian Summer Monsoon (PC2) shows a maximum moisture period between 7 and 4 cal. kyr BP which occurred immediately after the intense Indian Summer Monsoon period ended. Reassessing the main driving forces and mechanisms of Asian Summer Monsoon, namely insolation (1), sea surface temperature (2) and Hadley Circulation (3), may be the key to understand the different patterns of the two subsystems.

(1). The strength of the Indian Summer Monsoon is assumed to be largely driven by the summer ocean-continent temperature gradient that depends on insolation changes on the Tibetan Plateau at ~30°N (Ruddiman and Kutzbach, 1989; Sirocko et al., 1993; Overpeck et al., 1996; Wang et al., 2001a, 2005a, 2005b; Fleitmann et al., 2003, 2007; Yuan et al., 2004). The land-ocean contrast of the East Asian Summer Monsoon area reflects insolation changes in the low-elevation Asian interior between 30~50ºN. As the pattern of the insolation curves are approximately similar between 30 and 50°N, the asynchronous nature of the monsoonal subsystems is not forced by regional insolation differences on the Asian continent.

(2). Moreover, palaeo-SST records from marine areas surrounding southern and eastern Asia (MD77194, Arabian Sea, Sonzogni et al., 1998; 74KL, Arabian Sea, Sonzogni et al., 1998; GC18287-3, South China Sea, Steinke et al., 2001; Core 17940-1/2, South China Sea, Wang et al., 1999; Core-255, East China Sea, Li et al., 1997; Core-B3GC, middle Okinawa Trough, Jian et al., 2000; MD76, western tropical Pacific Ocean, Stott et al., 2004), show similar, relatively stable conditions during the Holocene, negating a potential Oceanic Thermal driven hypothesis.

(3). Hadley circulation, which is defined as global zonal-symmetric meridional circulation (Oort and Yienger, 1996), has been widely recognized as an important factor for the evolution of the Asian Summer Monsoon (Joseph, 1978; Tanaka et al., 2004; Mitas and Clement, 2006).

Based on meteorological data from the NCEP/NCAR reanalysis database, we reconstructed the Indian Summer Monsoonal Hadley (MHISM) Index for the ISM region (70ºE-110ºE, 10ºN-30ºN) since 1979 (Figure 2-7a), following the method described by Goswami et al. (1999), which was proven to be consistent with monsoonal precipitation indices (Indian Monsoon Rainfall and Extended Indian Monsoon Rainfall). Calculated as the anomalous meridional wind-shear, the broader scale Monsoonal Hadley (MH) Index is also suitable for describing the whole Asian Summer Monsoon system based on meteorological data from an extended area (20ºE - 160ºE, 20ºS - 70ºN) (Goswami et al., 1999). The difference in the MH index between strong ISM years (with MHISM index above +0.5) and weak ISM years (with MHISM index below -0.5) is shown in Figure 2-7b. Compared to the weak ISM years, relatively high values during strong ISM years were found in northern India, southwest China

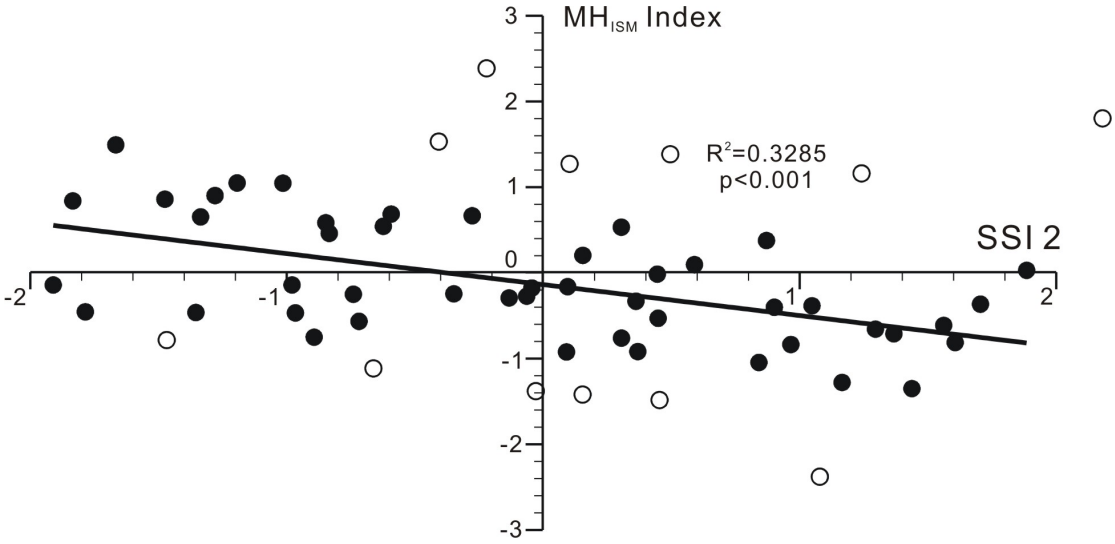

Figure 2-8 Correlation between two Asian monsoon indices, MHISM (Indian Summer Monsoon, Goswami et al., 1999), and Southerly Shear Index 2 (East Asian Summer Monsoon, Wang and Fan, 1999), during the last 60 years, based on NCEP/NCAR reanalysis data. Open circles indicate excluded data that were identified by twice standard deviation from the regression line. Most of the years excluded show extreme El Niño/La Niña events (eg. 1988, 1991 and 1994).

and some southern Asia areas, confirming the strong influences of the ISM system. Interestingly, areas surrounding this positive centre all showed negative values, indicating a weaker wind-shear that most probably hinders ascendance of even cause descending airflow in comparison with normal years. In particular, the north-central China region situated in the EASM region shows strong negative values. Considering a further dynamic index for EASM defined as Southerly Shear Index (SSI2) by Wang and Fan (1999), a generally negative correlation between modern ISM and EASM (R2=0.3285, p<0.001) is achieved for the last 60 years (Figure 2-8). The low R-value may be caused by further teleconnections which add variation to the monsoon systems such as the Southern Oscillation (SO) and El Niño that are supposed to influence the Asian Summer Monsoon (Meehl and Arblaster, 1998; Shukla and

Paolino, 1983), as well as Arctic Oscillation (AO), Northern Atlantic Oscillation (NAO) and Siberia High (SH) from the Northern Hemisphere (Wu and Wang, 2002a/b) that strongly influence the Asian Winter Monsoon.

Furthermore, we assume that a strong Hadley Circulation formed over Bengal Bay, northern India and southwest China, during the early Holocene (10-7 cal. kyr BP) following an

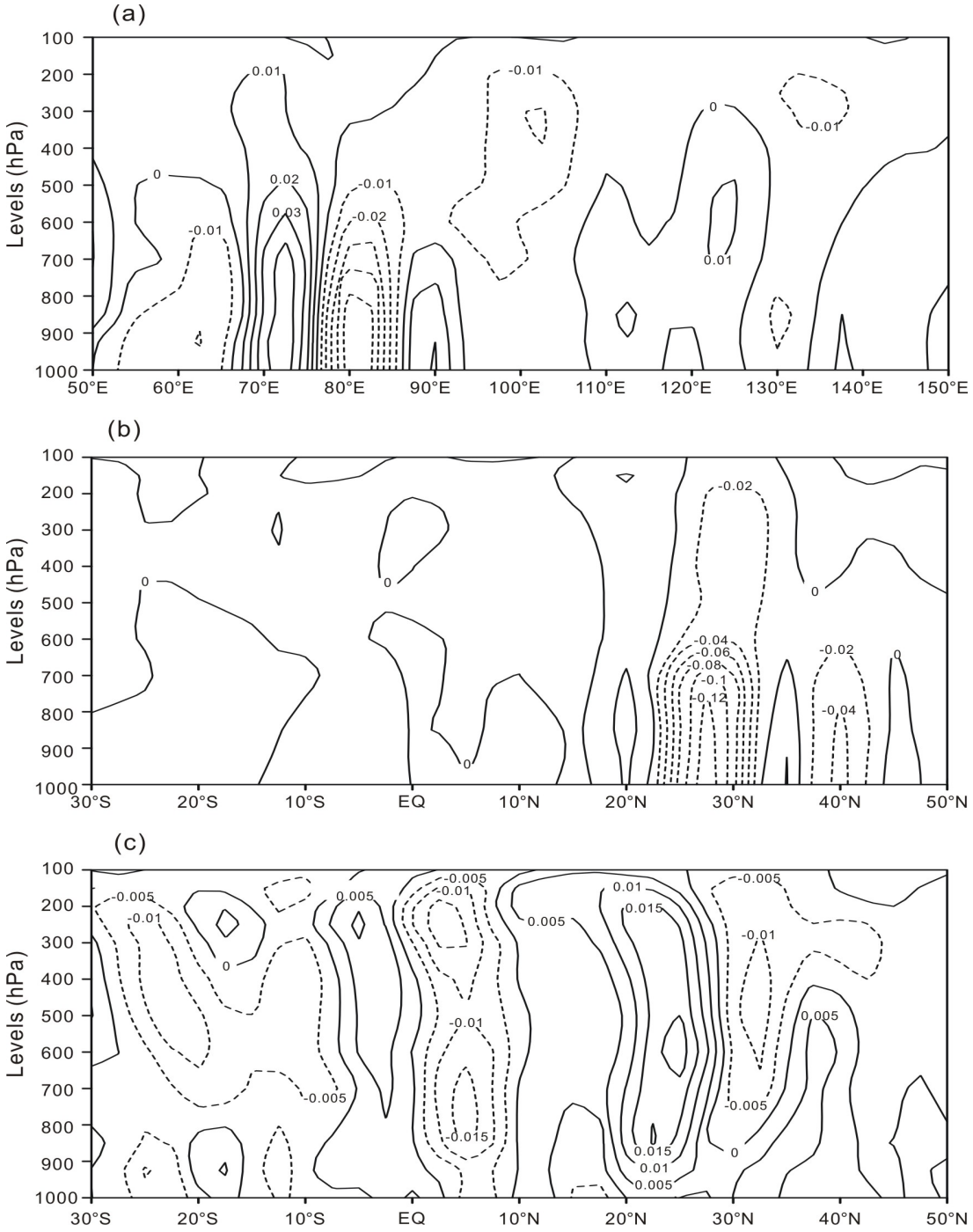

Figure 2-9 Vertical wind velocity differences between years with strong and weak Tibetan ascending airflows, for three sections: a, 35°N; b, 90°E and c, 115°E. Stronger ascending trends were indicated by negative values (dash lines), while relatively weaker ascending (or descending) airflows were expressed as positive values (solid lines).

increase in Northern Hemisphere solar insolation, resulting in intense Indian Summer Monsoon (see above). Subsequently, strong ascending currents over the heated Tibetan Plateau led to relatively weaker ascending (or even descending) airflows over north-central China area, which can confirmed by the modern vertical wind patterns (Figure 2-9). Figure 2-9 (a-c) show vertical wind velocity differences between years with strong and weak Tibetan ascending airflows, for three sections: a, 90ºE; b, 115ºE and c, 35ºN. Stronger ascending trends are indicated by negative values (dash lines), while relatively weaker ascending (or descending) airflows were expressed as positive values (solid lines). Obviously, when stronger ascending airflows happened over Tibetan Plateau area, relatively weaker ascending or even descending currents dominated the north-central China area (20ºN-50ºN, 110ºE-150ºE). By analogy to the modern data, restrained rising air currents in the north-central China region prevented a strengthening of the EASM, resulting a relatively dry phase during the early Holocene. During the mid-Holocene (7-4 cal. kyr BP), the ISM began to retreat due to a decrease in solar insolation, that resulted in a weakening of the suppressing effects over EASM areas allowing an enhancement of the EASM leading to a moisture maximum not only in north-central China (Liu et al., 2001; Shao et al., 2006; Cosford et al., 2008; Hu et al., 2008), but also in Korea, Japan and the East China Sea area (Li et al., 1997; Schöne et al., 2004; Fujiki and Yasuda, 2004; Nahm et al., 2006). Since this time, under the influence of a further decrease in Northern Hemisphere insolation, both ASM subsystems developed towards modern conditions.

In summary, during the Holocene, the evolution of the Asian Summer Monsoon was primarily controlled by Northern Hemisphere solar insolation changes in conjunction with internal interactions between the two subsystems.

2.6 Conclusions

Our synthesis of 92 palaeoclimatic proxy records (72 sites) indicates that the moisture and temperature history in monsoonal central Asia during the last 18.000 years has generally followed the patterns of the northern hemisphere described in other records. The synthesis curve indicates that monsoon strengthening since the LGM occurred in a rather stepwise fashion whilst the monsoonal retreat since the mid-Holocene has been gradual. The approximately synchronous environmental signals revealed by pollen and non-pollen records negated the potential of human-driven ecosystems except for the last 1000 years where we found significant biases. Our results also indicate that feedbacks between climate change and the human impact on ecosystems were of minor importance during most of the Holocene.

Despite the similar overall trend, we found significant regional differences in the moisture evolution patterns of the last 10.000 years. The ordination analyses revealed different moisture evolution patterns among EASM, ISM areas and the region outside of present monsoon boundary. The increasing moisture levels at many sites outside the present monsoon boundary during the late Holocene are possibly related to the influence of the Westerlies. Furthermore, whilst moisture evolution in the ISM area roughly follows Northern Hemisphere summer insolation reaching a maximum during the early Holocene, many sites in the EASM area stays relatively dry and reaches its maximum moisture levels between 7 and 4 cal. kyr BP.

We assume that enhanced Hadley Circulation leads to stronger upper-level air transport into the EASM monsoon region which regionally hinders ascending airflow motion and hence suppresses monsoonal circulation. Interpretation of a dynamic Monsoonal Hadley index (MHISM) that was calculated for the last 30 years using NCEP/NCAR data reveals the same pattern when comparing weak to strong ISM years confirming our mechanistic explanation of the asynchronous nature of the Asian monsoonal subsystems.

Moreover, the reconstructed MH_{ISM} Index (Figure 7a) increased during the last 30 years confirming observations of an increasing ISM in recent years (Gupta et al., 2003; Fleitmann et al., 2003, 2007; Yuan et al., 2004; Wang et al., 2005a; Dykoski et al., 2005). Consequently, when comparing the MH Index of 1979-1994 to last 15 years (1995-2008) a similar pattern was observed as when comparing weak to strong ISM years (Figure 7c). This implies that the stronger the ISM becomes in the future, the more the upward air motion in the EASM region will be suppressed which is probably related to drier conditions observed there. This implies that the arid desert-steppe areas of north-central China, being the dust source areas for e.g. Beijing dust storm events (Qian et al., 2002; Zhang et al., 2003; Wang et al., 2008a) might suffer from increasing dryness in the future. An early Holocene dust maximum observed in the Sihailongwan Maar Lake sediment record (Schettler et al., 2006), about 900 km east of Beijing, may be able to analogise to the future time in case that anthropogenically-driven strengthening of Hadley Circulation in Asia will persist. However, the further decreasing summer insolation will probably moderate this effect.

Acknowledgements

Special thanks to Hongli Wang (niglas) for her assistance in the analyses of modern meteorological data. We are grateful to Juliane Wischnewski (AWI-Potsdam) for her help in numerical analyses. Y. Wang's doctoral research is funded by "Helmholtz - China Scholarship Council (CSC) Young Scientist Fellowship" (No. 2008491101). The research was supported by German Science Foundation (DFG), the National Natural Science Foundation of China (Grant No. 40772108) and Nanjing Institute of Geography and Limnology, CAS (No. NIGLAS2010XK01). We appreciate the helpful comments of two anonymous reviewers.

Supplementary

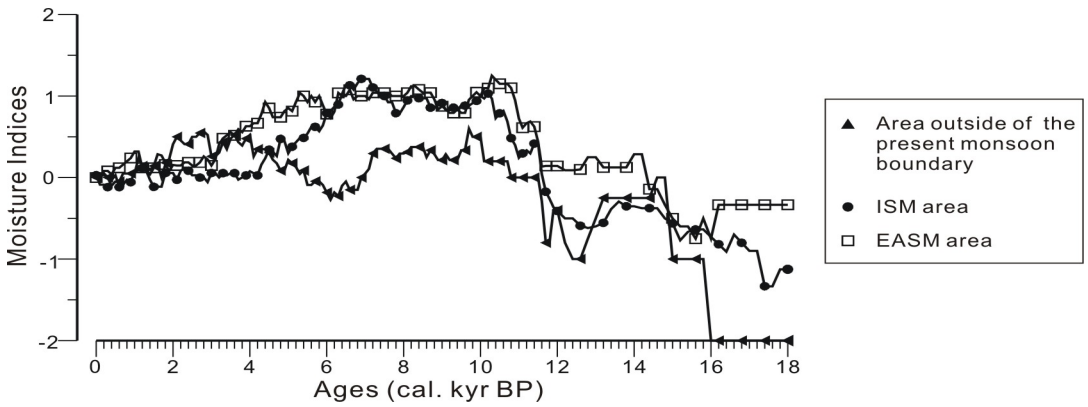

Figure 2-10 Mean moisture indices of all three sub-regions show relatively dry but fluctuant conditions prior to a synchronous increase of moisture levels at the beginning of the Holocene (from ca. 12 to 10 cal. kyr BP). However, different trends occurred following the maximum moisture period. With the shortest duration, the moisture decreased first within the area outside of the present monsoon boundary around 7.5 cal. kyr BP, followed by Indian Summer Monsoon area (ca. 6.5 cal. kyr BP) and East Asian Summer Monsoon area (ca. 4.5 cal. kyr BP). After a dry stage around 6.5 cal. kyr BP, the moisture in the region outside of the present monsoon boundary increased and another wet period followed from 5 to 2 cal. kyr BP.

3 Manuscript 2: Quantitative reconstruction of precipitation changes on the NE Tibetan Plateau since the Last Glacial Maximum - extending the concept of pollen-source area to pollen-based climate reconstructions from large lakes

Yongbo Wang [a, b], Lyudmila S. Shumilovskikh [c], Steffen Mischke [b, d], H John B Birks [e], Juliane Wischnewski [a, b], Jürgen Böhner [f], Frank Schlütz [c, g], Frank Lehmkuhl [h], Bernhard Diekmann [a], Bernd Wünnemann [i], Chengjun Zhang [j], Ulrike Herzschuh [a, b]

[a] *Alfred Wegener Institute for Polar and Marine Research, Research Unit Potsdam, Telegrafenberg A43, 14473 Potsdam, Germany*

[b] *Department of Earth and Environmental Science, University of Potsdam, Karl-Liebknecht-Str.24, 14476 Potsdam, Germany*

[c] *Department of Palynology and Climate Dynamics, Albrecht-von-Haller Institute for Plant Sciences, University of Göttingen, Untere Karspüle 2, 37073 Göttingen, Germany*

[d] *Institute of Geological Sciences, Free University Berlin, Malteserstr.74-100, 12249 Berlin, Germany*

[e] *Department of Biology, University of Bergen, Thormøhlensgate 53A, N-5006 Bergen, Norway; Bjerknes Centre for Climate Research, Allegaten 55, N-5007 Bergen, Norway; Environmental Change Research Centre, University College London, London, WC1E 6BT, UK; and School of Geography and the Environment, University of Oxford, Oxford, OX1 3QY, UK*

[f] *Institute for Geography, University Hamburg, Bundesstr. 55, 20145 Hamburg, Germany*

[g] *Institute of Geographical Sciences, Free University Berlin, Malteserstr. 74-100, 12249 Berlin, Germany*

[h] *Department of Geography, RWTH Aachen University, Templergraben 55, 52056 Aachen, Germany*

[i] *School of Geography and Oceanography, Nanjing University, Hanko Road 22, 210093 Nanjing, China*

[j] *Centre for Arid Environment and Paleoclimate Research, School of Resources and Environmental Sciences, Lanzhou University, 730000 Lanzhou, China*

Current Status: Under review for the "Quaternary Science Reviews" journal.

Abstract

Pollen records from large lakes have been used for quantitative palaeoclimate reconstruction but the influences that lake-size (as a result of species-specific variations in pollen dispersal patterns) and taphonomy have on these climatic signals have not previously been

systematically investigated. We introduce the concept of pollen-source area to pollen-based climate calibration using the climate history of the north-eastern Tibetan Plateau as our study area. We present a pollen data-set collected from large lakes in the arid to semi-arid region of Central Asia. The influences that lake size and the inferred pollen-source areas have on pollen compositions have been investigated through comparisons with pollen assemblages in neighbouring lakes of various sizes. In order to achieve this we have estimated the pollen-source area for each lake individually and used this information to infer modern climate data with which to then develop a modern calibration data-set, using both the Multivariate Regression Tree (MRT) and Weighted-Averaging Partial Least Square (WA-PLS) approaches. Modern pollen samples collected from different parts of Lake Donggi Cona (in the north-eastern part of the Tibetan Plateau) reveal variations in pollen assemblages within this large lake, which are interpreted in terms of the species-specific dispersal and depositional patterns for different types of pollen and in terms of fluvial input components. Fossil pollen data from Lake Donggi Cona have been used to reconstruct the climate history of the north-eastern part of the Tibetan Plateau since the Last Glacial Maximum (LGM). The mean annual precipitation was quantitatively reconstructed using WA-PLS: extremely dry conditions were found to have dominated the LGM, with annual precipitation figures of around 100 mm representing only 32% of present-day precipitation. A gradually increasing trend in moisture conditions during the late-glacial was terminated by an abrupt reversion to a dry phase that lasted for about 1000 years and coincided with “Heinrich Event 1” in the northern Atlantic region. Subsequently, periods corresponding to the warm Bølling/Allerød and the Younger Dryas cold event were followed by moist conditions in the early-Holocene, with annual precipitation of up to 400 mm. A slightly drier trend after the Holocene Climate Optimum, was then followed by a second wet phase in the mid-Holocene, lasting until 4.5 cal. ka BP. Relatively steady conditions with only slight fluctuations then dominated the late-Holocene, resulting in the present climatic conditions. The climate changes since the LGM have been primarily driven by deglaciation and fluctuations in the intensity of the Asian Summer Monsoon that resulted from changes in the Northern Hemisphere summer solar insolation, as well as by changes in the northern Atlantic climate through variations in the circulation patterns and intensity of the westerlies.

3.1 Introduction

The study of past natural climate change and its underlying driving mechanisms, especially during the late-glacial and the Holocene, provides an indispensable key to predicting future climatic conditions. Due to its global significance, the Tibetan Plateau has become a focus for several palaeoclimatological studies in recent years and over the last two decades a variety of records have been recovered from lake sediments (e.g. Gasse et al., 1991; Shen et al., 2005), ice cores (Thompson et al., 1997; Liu et al., 1998), and peat sections (Hong et al., 2005). It has been assumed that changes in the monsoon-derived moisture supply (An et al., 2000; Herzschuh, 2006; Wang et al., 2010) generally followed variations in the Northern Hemisphere summer insolation. The period following the Last Glacial Maximum (LGM) was characterised by cold, dry conditions, followed in turn by a warm, wet period corresponding to the Bølling/Allerød warm period, and was terminated by a cold, dry reversion during the

Younger Dryas period. Following an abrupt increase in moisture at the start of the Holocene, warm and wet conditions then prevailed until the mid-Holocene; after which moisture levels and temperatures gradually decreased (Wang et al., 2010). However, discrepancies exist not only between records from different climatic regions but also between records from the same region, owing to the very large size of the plateau, the complex geographic settings within the plateau, and the regional variations in the relative importance of single circulation systems such as the East Asian Summer Monsoon, the Indian Summer Monsoon, and the westerlies. Even individual proxies from the same site may indicate discrepancies in moisture evolution as they may reflect either local within-lake variations, or regional variations such as those inferred from changes in the surrounding vegetation (Wischnewski et al., 2011).

Pollen analyses from lacustrine sediments have been widely used to provide an indication of changes in palaeovegetation and/or palaeoclimate (Birks, 1981; Yu et al., 1998; Birks and Seppä, 2004; Zhao et al., 2009a; Birks et al., 2010; Xu, et al., 2010a). Recently, modern pollen-climate calibration-sets were developed and applied to the Tibetan Plateau (Shen et al., 2006a; Herzschuh et al., 2010a; Lu et al., 2011). The pollen records of lake sediments reflect regional-scale signals from within the pollen-source area (Prentice, 1985; Sugita, 1993, 1994; Broström et al., 2008). The inferred size of this source area, however, can vary with the size of the lake basin as it is dependent on species-specific pollen dispersal and depositional characteristics. A theoretical model to estimate the pollen-source area for an entire lake surface was developed by Sugita (1993), but its implications have rarely been taken into account in pollen-based climate calibration studies. It might, for example, be problematic to apply pollen-climate calibration functions that are based on samples of surface soil or surface-sediments from small lakes, to larger lakes (Birks, 2003; Zhao et al., 2009b; Birks et al., 2010; Goring et al., 2010; Xu et al., 2010b). Furthermore, there can clearly be large variations in pollen spectra within individual large lakes, mostly due to differences in grain-size, settling velocity, and related dispersal patterns in the atmosphere (Sun and Wu, 1987; Luly, 1997; Huang et al., 2004), to selective deposition controlled by within-lake hydrodynamics, or to fluvial input of pollen from the hydrological catchment (Debusk et al., 1997; Zhu et al., 2002; Xu et al., 2005).

Our objectives in this study are two-fold. First, we examine the influences that pollen-source area and within-lake pollen variations have on palaeoclimate reconstructions. For this purpose we have compiled a pollen-climate calibration data-set based solely on modern pollen spectra from large lakes in arid and semi-arid central Asian areas, together with a set of surface-sediment samples from Lake Donggi Cona, a large lake in the north-eastern part of the Tibetan Plateau. We apply these findings to quantitative interpretations of climate and vegetation from the Lake Donggi Cona fossil pollen record, covering the time interval from the LGM to the Holocene. We validate the pollen-based results through numerical comparisons with ostracod data from the same core and with other pollen records from nearby lakes. Second, we compare the resulting climatic reconstruction from Lake Donggi Cona to other quantitative records from the Tibetan Plateau in order to determine both the strength of the inferred changes in climate, and the drivers behind these changes.

3.2 Study area

Lake Donggi Cona (35.22-35.83°N, 98.33-98.75°E; 4090 m a.s.l.), covering an area of about 230 km^2, is located on the north-eastern Tibetan Plateau, to the north-west and east of the Anemaqin and Kunlun mountain ranges, respectively (Wang and Dou, 1998; Dietze et al., 2010). The catchment area of the lake encompasses 3174 km^2, including the foothills of the Anemaqin mountain range to the south-east with highest peaks around 5200 m, and a slightly lower mountain range to the north. The lake is fed from the east by a perennial river, the Dong Qu, and some episodic inflows from the north that form three major pro-grading arcuate delta systems (Dietze et al., 2010). The outflow from the lake is controlled by a gauge station set up during the 1970s and feeds into the Tuosu River, which flows into the Qaidam River and thence into the endorheic Qaidam Basin to the north-west (Figure 3-1B) (Wang and Dou, 1998; Dietze et al., 2010). For further details on the catchment characteristics, basin morphology, and limnology of Lake Donggi Cona, see Mischke et al. (2010a, 2010b) and Dietze et al. (2010).

The climate in this region, which is dominated by both the monsoon system and the extra-tropical westerlies, shows strong seasonal contrasts in precipitation and temperature. The mean annual temperature is -3.0°C, with mean January and July temperatures of -15.9°C and 7.8°C and maximum January and July temperatures of -7.6°C and 13.6°C, respectively. The mean annual precipitation is 311 mm, of which 76% falls during the monsoon season

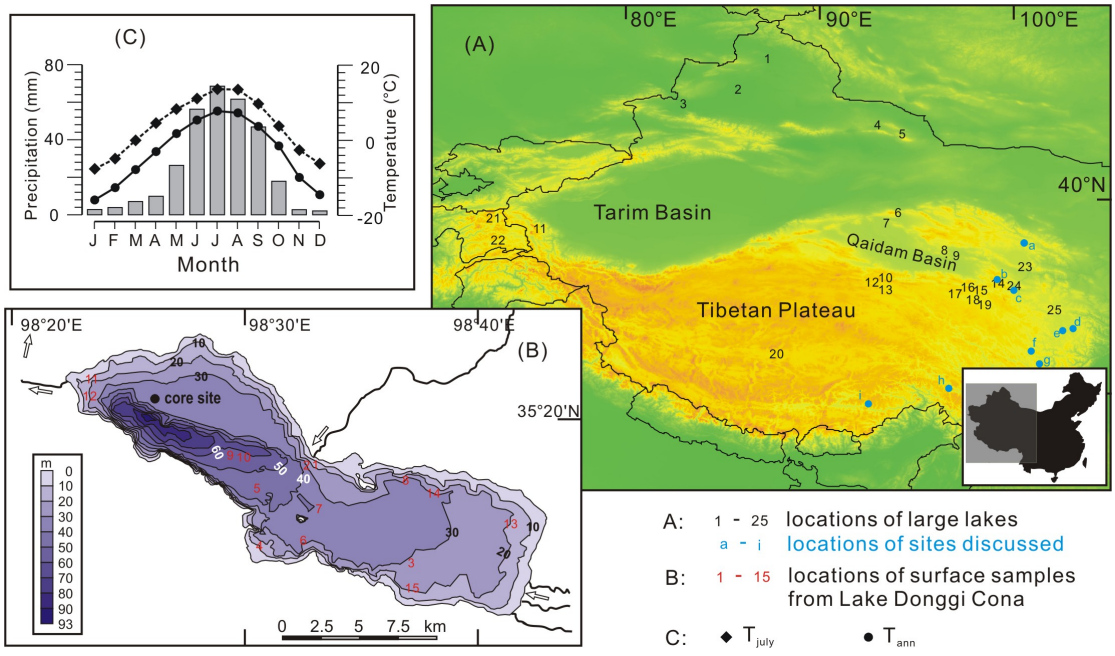

Figure 3-1 A: Overview of the study area and the locations of the large lakes sampled (1–25, see detailed information in Table 1), as well as study sites mentioned in the text: a, Lake Luanhaizi; b, Lake Donggi Cona; c, Kuhai Lake; d, No 2 pit; e, Lake Ximen Co; f, Naleng Lake; g, Yidun Lake; h, Ren Co; i, Hidden Lake. B: Bathymetric map of Lake Donggi Cona showing the surface-sediment sample locations (1–15) and the core site (PG1790), with arrows indicating the major inflows and outflows. C: Meteorological data between 1950 and 1990 A.D., from the Madoi station: mean annual precipitation (Pann, bars), mean annual temperature (Tann, points) and mean July temperature (TJuly, diamonds).

(June, July, August, and September) (Figure 3-1C). Cold and dry air and northerly winds prevail during the winter season as a result of the Asian Winter Monsoon, reflecting the

Table 3-1 Location, lake size, calculated pollen source area and corresponding climate data from sampled large and small lakes on the Tibetan Plateau.

No.	Lake name	Lat. (°)	Lon. (°)	Elev. (m asl.)	R. (m)	PSA (m)	P_{ann} (mm)	T_{July} (°C)	P^*_{ann} (mm)	T^*_{July} (°C)
LS-1	Wulungu Lake	47.07	87.26	475	12500	252647	76.1	25.1	106.5	23.4
LS-2	Manas Lake	45.75	85.71	235	4500	160140	57.3	27.4	72.0	26.4
LS-3	Aibi lake	45.07	82.81	181	10000	243387	83.7	26.6	157.9	23.8
LS-4	Balikun Lake	43.63	92.79	1574	4500	142693	108.3	21.0	129.5	20.1
LS-5	Tuoniekunie Lake	43.41	94.15	1890	1250	94690	67.1	18.5	94.2	17.4
LS-6	DaQaidam Lake	39.06	94.18	2821	1900	55512	54.5	16.2	60.8	15.4
LS-7	Sugan Lake	38.80	93.70	2772	3000	90162	49.0	12.8	55.1	13.5
LS-8	Hurleg lake	37.18	96.55	2850	3000	65170	57.9	15.9	62.9	15.9
LS-9	Toson Lake	37.08	97.00	2813	7500	119767	96.1	17.5	98.6	16.7
LS-10	Heihai	35.97	93.29	4437	2500	88615	153.9	7.1	167.5	6.6
LS-11	Karakuli Lake	38.44	75.06	3657	1250	97370	193.5	12.6	262.6	10.1
LS-12	Kusai Lake	35.65	92.98	4487	4500	97068	186.4	6.8	198.8	6.3
LS-13	Haiding Nur	35.61	93.18	4468	1900	48654	169.5	6.9	180.1	6.5
LS-14	Donggi Cona	35.28	98.64	4095	4500	94430	332.5	9.2	375.2	8.4
LS-15	*unknown*	35.04	97.90	4260	1250	76755	326.2	8.3	349.6	7.8
LS-16	*unknown*	35.02	97.63	4284	10000	84077	298.7	8.3	324.8	7.7
LS-17	E Ling Hu	34.93	97.27	4303	10000	91560	302.1	8.1	320.3	7.6
LS-18	*unknown*	34.86	98.10	4227	1900	42971	368.4	8.1	378.1	7.8
LS-19	Zhongxing Hai	34.80	98.21	4230	2500	59354	365.7	8.3	388.8	7.9
LS-20	Dasta Co	31.83	87.56	4478	7500	82346	262.1	12.1	352.0	10.9
LS-21	Karakul (Tajikstan)	39.02	73.51	3926	4500	182794	373.1	6.9	431.3	5.9
LS-22	Tuskul Lake	37.68	73.18	3678	1250	49722	372.6	10.4	424.1	8.6
LS-23	Qinghai Lake	36.61	100.57	3196	12500	243827	478.2	11.3	483.4	10.8
LS-24	Kuhai	35.31	99.18	4150	3000	70958	425.7	8.5	459.6	7.8
LS-25	Gahai	34.24	102.33	3485	3000	49310	686.2	10.3	720.8	9.8
SS-8	*unknown*	37.08	97.31	2848	175	-	125.4	16.3	-	-
SS-9	*unknown*	36.97	96.26	2734	10	-	31.5	19.6	-	-
SS-15	*unknown*	34.99	98.08	4256	20	-	330.4	8.5	-	-
SS-16	*unknown*	34.87	97.51	4290	30	-	314.1	7.9	-	-
SS-17	*unknown*	35.02	97.35	4310	20	-	257.4	8.3	-	-
SS-18	*unknown*	34.88	98.16	4244	95	-	372.9	8.1	-	-
SS-19	*unknown*	34.74	98.11	4241	100	-	391.9	8.1	-	-
SS-23	*unknown*	36.87	101.03	2965	190	-	414.4	11.9	-	-
SS-25	*unknown*	34.01	102.28	3430	30	-	694.1	10.6	-	-

P_{ann}, T_{July}, mean annual precipitation and mean July temperature at the lake site

P^*_{ann}, T^*_{July}, inverse distance weighted precipitation and temperature data within the pollen source area

influence of the Siberian-Mongolian High. Meteorological data since 1953 are available from the nearest climate station at Madoi, 50 km to the south-west of Lake Donggi Cona (WorldClimate: http://www.worldclimate.com).

The areas in the immediate vicinity of the lake have an alpine-steppe vegetation dominated by *Kobresia* (Cyperaceae), *Artemisia*, and Poaceae, while the relatively moist Anemaqin Mountain range supports alpine meadows (*Kobresia* spp.) and patches of alpine shrubs (*Salix*) with *Saussurea* spp. and *Potentilla* spp. (Kürschner et al., 2005; Wang et al., 2006).

3.3 Materials and methods

3.3.1 Surface-sediment sample collection, pollen-source area and climate estimations

In total, 25 surface-sediment samples from large lakes (with shortest radius greater than 1000 m) and 9 surface-sediment samples from small lakes (radius less than 200 m) situated close to a large lake, were collected from the Tibetan Plateau and the arid western China area (together with two sites from Tajikistan) during field expeditions from 2002 to 2009 (Figure 3-1A, Table 3-1). Surface-sediment samples (0-2 cm depth) were collected from the centre of each lake with a sediment grab or gravity corer, representing deposition during the last 20-30 years.

The pollen-source area for each large lake was estimated following Sugita's (1993) model for lake basins, which has the following inherent assumptions: (1) the sampling basin is a circular opening in the vegetation canopy, with the circular approximation of the basin shape for irregular shaped lakes being based on the shortest radius (Bunting and Middleton, 2005); (2) winds are uniform from all directions; and (3) the dominant components of pollen transport are wind above the canopy and gravity below the canopy. The pollen-source area (the area from which 50% of the pollen grains have derived) for four major pollen species (*Artemisia*, Chenopodiaceae, Poaceae, and Cyperaceae) was estimated using the lake radii (see details in Table 3-1), a wind speed of 3 m/s which is commonly used for pollen-vegetation modeling studies (e.g. Sugita 1993), and the pollen-fall speeds (Table 3-2) as model parameters. The pollen-source area for each lake was then adapted from the pollen-source areas of each species using their proportions within the total pollen assemblage.

Site-specific climate information on mean annual precipitation and mean July temperature was obtained from Böhner (2006). Climate estimates (precipitation, temperature, radiation, evapotranspiration) with a monthly resolution were derived on a regular grid network (3500 x 4000 grid cells) covering the Central and High Asian regions, with a grid-cell spacing of 1 km² (Böhner, 2006). The statistical down-scaling approach at the core of this geospatial climate modeling integrates gridded circulation variables (GCM data, re-analysis series), available station observations (climate records from more than 400 climate stations), and advanced terrain parameterisation methods (Böhner and Antonic, 2008) to account for the topoclimatic heterogeneity of Central Asia. A detailed description of the methods used is given in Böhner (2005). An inverse distance weighting (IDW) method was applied to estimate the climatic factors for each lake according to the data within its pollen-source area.

Table 3-2 Results of pollen grain size measurements and calculated fall speeds for four major pollen taxa.

Pollen species	Measured grains	Radius of pollen grain (μm)			Pollen fall speed [c] (m/s)
		Max.	Min.	Mean	
Artemisia	30	11.67	6.67	9.11	0.0101
Chenopodiaceae	30	13.33	6.67	9.75	0.0117
Poaceae	30	20.00	9.17	12.31	0.0185
Cyperaceae	30	25.00[a] 18.33[b]	15.00[a] 11.67[b]	17.69[a] 15.03[b]	0.0291

a, long axis; b, short axis; c, according to Stoke's Law (Gregory, 1973).

3.3.2 Coring, surface-sediment sampling of Lake Donggi Cona, and radiocarbon dating

A 4.84 m long sediment core (PG1790) was recovered at 98.436°E and 35.345°N using a UWITEC "Niederreiter 60" piston corer, from a water depth of 34.7 m (Figure 3-1A). X-ray fluorescence data were used to correlate and calibrate the overlaps between the four core segments. The sediments consist mainly of carbonate-rich laminated lake-mud. Light and dark laminae a few millimetres thick occur in the lower and upper sections of the core, while one millimetre thick couplets dominate between 2.3 and 3.6 m core depth. Sediments in the upper 1 m of the core have a mottled appearance, probably as a result of bioturbation by benthic invertebrates. In addition to the sediment core, 15 surface-sediment samples (0-2cm depth) were collected from different parts of Lake Donggi Cona using a sediment grab (Figure 3-1C).

Because of the absence of macrofossils, total organic carbon (TOC) was used for accelerator mass spectrometry (AMS) ^{14}C dating, carried out at the Poznan Radiocarbon Laboratory in Poland. As previously reported from the Tibetan Plateau area, the ^{14}C ages are commonly affected by the "Lake Reservoir Effect" (Morrill et al., 2006; Liu et al., 2009; Henderson et al., 2010). Sediments from the top 1 cm of core were used for radiocarbon-dating to estimate this effect which yields about 2000 years. In total, 17 ^{14}C ages from 13 depth layers were processed, corrected, and calibrated using the OxCal 4.1 program and the IntCal09 calibration data (Bronk Ramsey, 2009; Reimer et al., 2009). OxCal 4.1 was also used to establish an age-depth relationship using a Bayesian approach, which integrates the radiocarbon dates with their stratigraphical positions and lithological changes to develop the most plausible age-depth model given the available data (for a detailed description see Mischke et al., 2010b).

3.3.3 Pollen-sample treatment and analysis

Fossil pollen samples were taken at 4 cm intervals for the Holocene period and 8 cm intervals for the older stages. In total, 49 surface-sediment and 77 fossil pollen samples were treated and analysed following standard laboratory methods, including treatment with hydrogen chloride (HCl, 10%), potassium hydroxide (KOH, 10%), and hydrofluoric acid (HF, 50%), as well as acetolysis, fine sieving (with 7 μm mesh in an ultrasonic bath), and mounting in glycerine (Fægri and Iversen, 1989). Two tablets of *Lycopodium* spores were added to the

fossil samples for estimation of absolute pollen concentrations. The identification of pollen types was based on relevant published literature (Moore et al., 1991; Wang et al., 1997; Beug, 2004) and type collections. A minimum of 300 terrestrial pollen grains were counted apart from 23 samples from the Lake Donggi Cona core that were older than 13.5 cal. ka BP and had very low pollen concentrations (200-2000 grains/cm^3), for which only 50-150 pollen grains were counted.

3.3.4 Numerical analyses

Pollen percentages were calculated on the basis of the total pollen of arboreal and terrestrial non-arboreal pollen taxa. Only those pollen taxa that occurred with a frequency of 0.5% in at least three samples were included in the numerical analyses and in the compilation of the pollen diagrams. The diagrams were generated using the TGview (Version 2.0.2) software (Grimm, 2004), and the definition of local pollen-zone boundaries was based on the results of a Constrained Incremental Sum of Squares cluster analysis (CONISS), using the Edwards and Cavalli-Sforza's chord distance measure in TGview Version 2.0.2.

In order to minimise the effects of the long-distance transported pollen component on environmental interpretations, arboreal taxa were excluded from the numerical analyses. Furthermore, pollen percentages were square-root transformed for the numerical analyses in order to stabilize variances and to optimise the signal-to-noise ratio. Detrended correspondence analysis (DCA; Hill and Gauch, 1980) yielded turnover gradients of 1.78, 1.07, and 1.36 standard deviations for the pollen sample sets from large lakes surface-sediments, for the modern and fossil pollen samples from Lake Donggi Cona, respectively, indicating that linear-based methods such as Principal Component Analysis (PCA) and Redundancy Analysis (RDA), or non-metric methods such as non-metric Multidimensional Scaling (nMDS), are appropriate for these data-sets.

RDA was carried out using surface pollen data from large lakes as active samples, and the surface and fossil pollen data from Lake Donggi Cona as supplementary entries. Since we focused mainly on the inter-sample distances rather than on inter-species correlations, samples were centred. The forward selection option was used, together with a Monte Carlo permutation test (999 unrestricted permutations), to detect the relative weighting of environmental factors such as mean annual precipitation (P_{ann}) and mean July temperature (T_{July}). Partial RDAs were applied to 18 surface-sediment samples collected from 9 large lakes and 9 corresponding small lakes situated close to the large lakes, including P_{ann}, T_{July}, and square-root transformed lake radii as environmental variables, in order to assess the potential influence of lake size. All the ordination analyses were carried out using the CANOCO software (version 4.5) for ordination and the CanoDraw software for plotting (ter Braak and Šmilauer, 2002).

Weighted-Averaging Partial Least Squares models were developed for quantitative reconstructions based on modern pollen data collected from large lakes, associated with the inverse-distance weighted climate data, using the C2 program (Juggins, 2003). The numerical relationship between modern climate data and pollen values predicted by the calibration model (in leave-one-out cross-validation) was used to select the most appropriate

WA-PLS model and to help assess the performance of the calibration method.

Besides the commonly used WA-PLS approach, Multivariate Regression Tree (MRT) analysis, (De'ath, 2002) superimposed on an RDA (with modern data as active and fossil data as passive or supplementary samples) is another useful method for quantifying past environmental parameters (Davidson et al., 2010a, 2010b; Wang, et al., 2011a). In conjunction with the RDA approach, an MRT analysis was applied to the square-root transformed surface pollen data from large lakes and inverse-distance weighted climate data (P_{ann}, T_{July}), implemented using Brodgar 2.6.5 software (Zuur et al., 2009).

To evaluate the correlation of pollen data recovered from large and small lakes, as well as the underlying driven factor for vegetation changes, procrustes rotation (Peres-Neto and Jackson, 2001) was used to compare numerically pairs of multivariate data-sets (for application to palaeoecological data-sets see Wischnewski et al., 2011), i.e., (1) the pollen assemblages in surface-sediment samples from large lakes with those from corresponding small lakes, and (2) the Lake Donggi Cona fossil pollen assemblage with both ostracod assemblages (Mischke et al., 2010b) and fossil pollen assemblages from the near-by Lake Kuhai (Wischnewski et al., 2011). To allow statistical-based comparisons of comparable data-sets, the data-sets were interpolated and resampled at 250-year intervals using the AnalySeries 2.0.4.2 software (Paillard et al., 1996). Procrustes rotation analysis and the associated PROTEST permutation test were applied to the ordination (nMDS) results. The PROTEST function in R, which performs a random permutation test, was modified to allow restricted permutations for time-series data (Besag and Clifford, 1989, Wischnewski et al., 2011). The vegan package (Oksanen et al., 2008) in R (R Development Core Team, 2008) was used to carry out the nMDS ordinations, Procrustes analyses, and PROTEST (Peres-Neto and Jackson, 2001).

3.4 Results

3.4.1 Set-up and validation of modern pollen-climate calibration set from large lakes

In total, 55 pollen taxa were identified, of which 29 taxa were included in the pollen diagram (Figure 3-2A, B). Samples from the lowland desert or steppe areas consisted mainly of *Artemisia* and Chenopodiaceae pollen, which together generally constitute over 70% (and up to 90%) of the total pollen assemblage, as well as a relatively high *Ephedra* pollen component (*E. fragilis*-type and *E. distachya*-type). In contrast, Cyperaceae pollen made up higher percentages (20-40%) in samples from alpine *Kobresia* meadows on the eastern Tibetan Plateau. The contribution of arboreal pollen taxa (i.e. *Alnus*, *Pinus*, *Picea*, *Juniperus*, *Betula,* and *Quercus*) was generally less than 2%.

The Procrustes analysis between the 9 pairs of surface pollen data from large lakes and neighbouring small lakes yielded a statistically significant fit. Relatively high dissimilarities, as indicated by larger residuals, were identified for Poaceae, Cyperaceae, Brassicaceae, and *Potentilla*-type (see supplementary Figure 3-8). Furthermore, the partial RDA revealed that lake-size explains 7.9% of the total variance but this is not statistically significant ($p = 0.331$) when using lake radius as an environmental variable and P_{ann} and T_{July} as covariables.

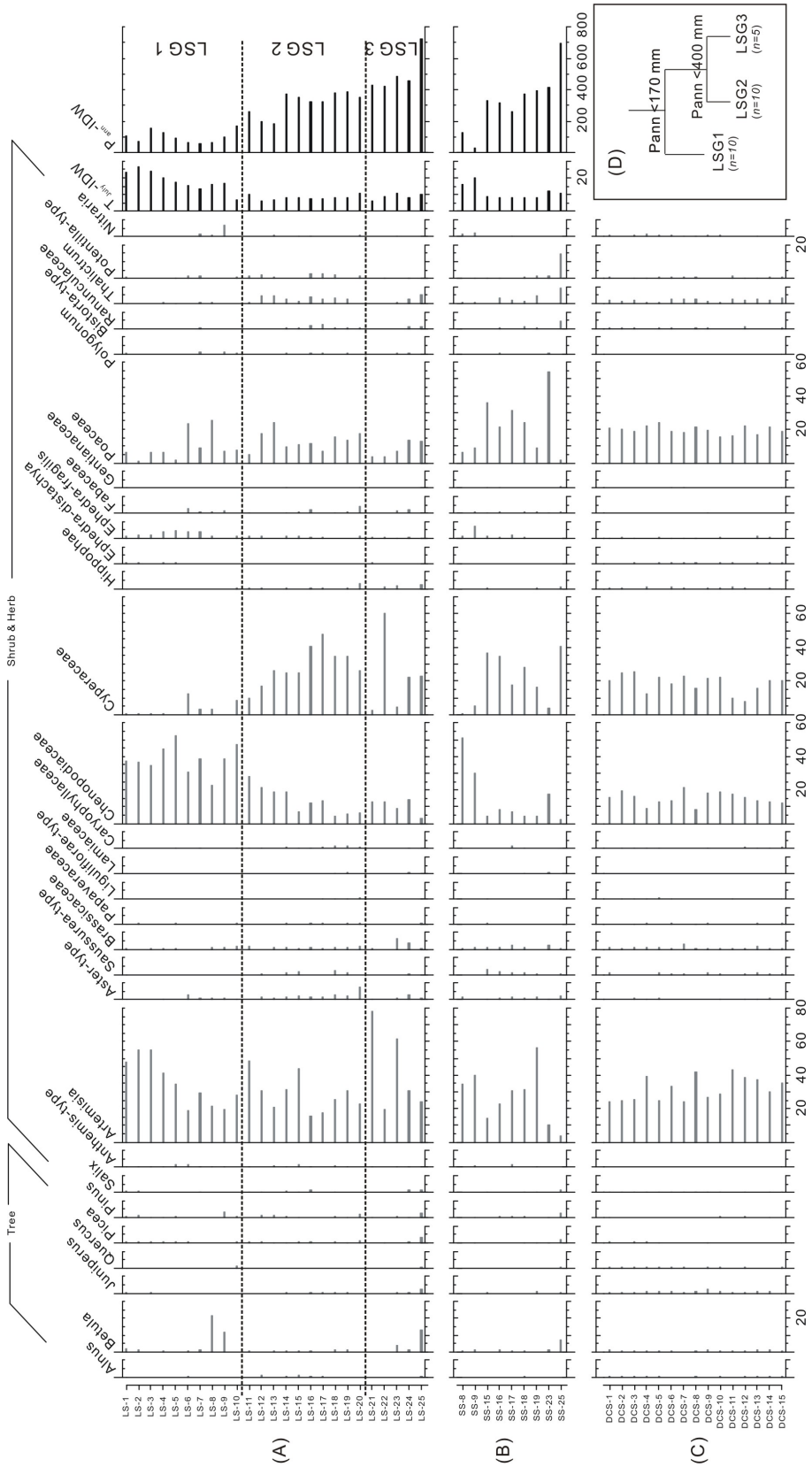

Figure 3-2 Pollen spectra from surface-sediment samples from large lakes (A), small lakes (B), and Lake Donggi Cona (C), together with the associated IDW climate data (P_{ann} and T_{July}, to the right of A, B). D: Multivariate Regression Tree plot for surface-sediment pollen data from the 25 large lakes, with the group classifications (LSG 1-3) shown in the pollen diagram (A).

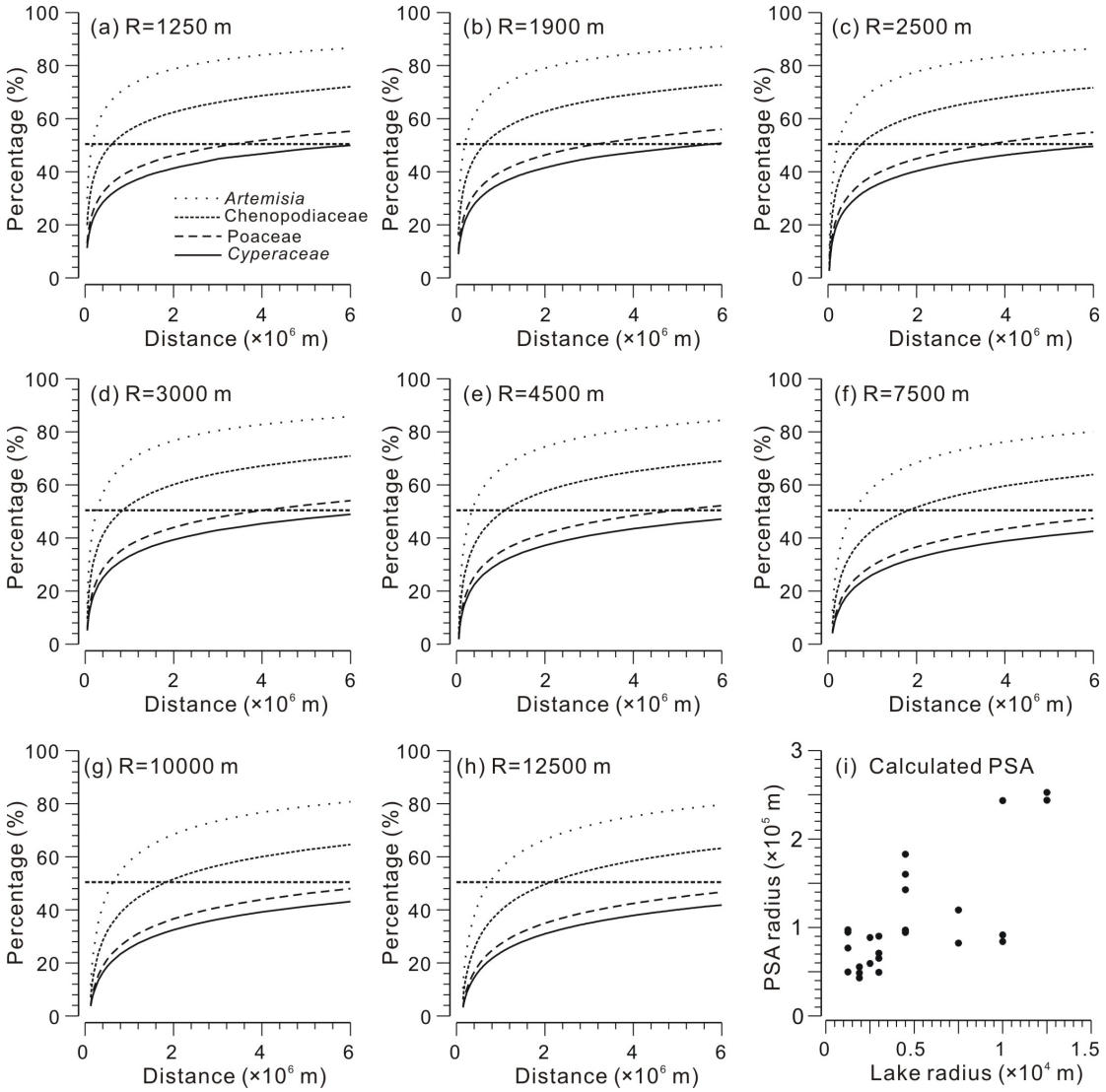

Figure 3-3 a–h: Establishment of pollen-source areas for the four major pollen types (*Artemisia*, Chenopodiaceae, Poaceae and Cyperaceae) using various lake sizes (radii ranging from 1250 to 12,500 m), showing the changes to the proportion of pollen loading in the lake (Y axes – percentages) with increasing distance from the lake (X axes – metres) (Horizontal lines indicate the 50% levels). i: Correlation of the calculated pollen-source area radius with the lake radius for 25 surface-sediment pollen samples from large lakes.

Alternatively, P_{ann} and T_{July} together significantly explain 46.1% of the total variance when lake-size is used as a covariable ($p < 0.001$).

As shown in Figure 3-3, relatively small pollen-source areas were estimated for the larger pollen grains for which distance 50% of pollen grains come from (Table 3-2), such as Cyperaceae and Poaceae. In contrast, small pollen grains such as *Artemisia* and Chenopodiaceae yielded relatively large source areas. Taking into account the relative proportions of the different pollen taxa, pollen-source areas covering distances ranging from 50 to 250 km from the lakes were estimated for the 25 large lakes (Figure 3-3i).

MRT analysis of surface pollen samples from the large lakes yielded a tree with 3 leaves, in which P_{ann} is responsible for all the divisions (Figure 3-2A, D). Large-lake Surface Group 1

(LSG 1), in which P_{ann} is below 170 mm, is characterised by high percentages of Chenopodiaceae pollen (>30%) and very low frequencies of Cyperaceae pollen. In contrast, LSG 3, which comprises sites with annual precipitation greater than 400 mm, is characterised by high proportions of Cyperaceae pollen and/or *Artemisia* pollen and a relatively low Chenopodiaceae pollen content, while LSG 2 is intermediate between the other two groups.

An RDA was performed to provide additional validation of the MRT results. Based on the surface pollen data from 25 large lakes, the first two RDA axes capture 41.9% of the total variance (axis 1, 36.3%; axis 2, 5.6%), suggesting that only a few underlying variables dominate the data structure. The forward selection option within RDA suggests that mean annual precipitation (P_{ann}) is the main factor determining the pollen assemblage, which significantly (p-value < 0.0010) explains 29% of the variance (Figure 3-4A). Following the

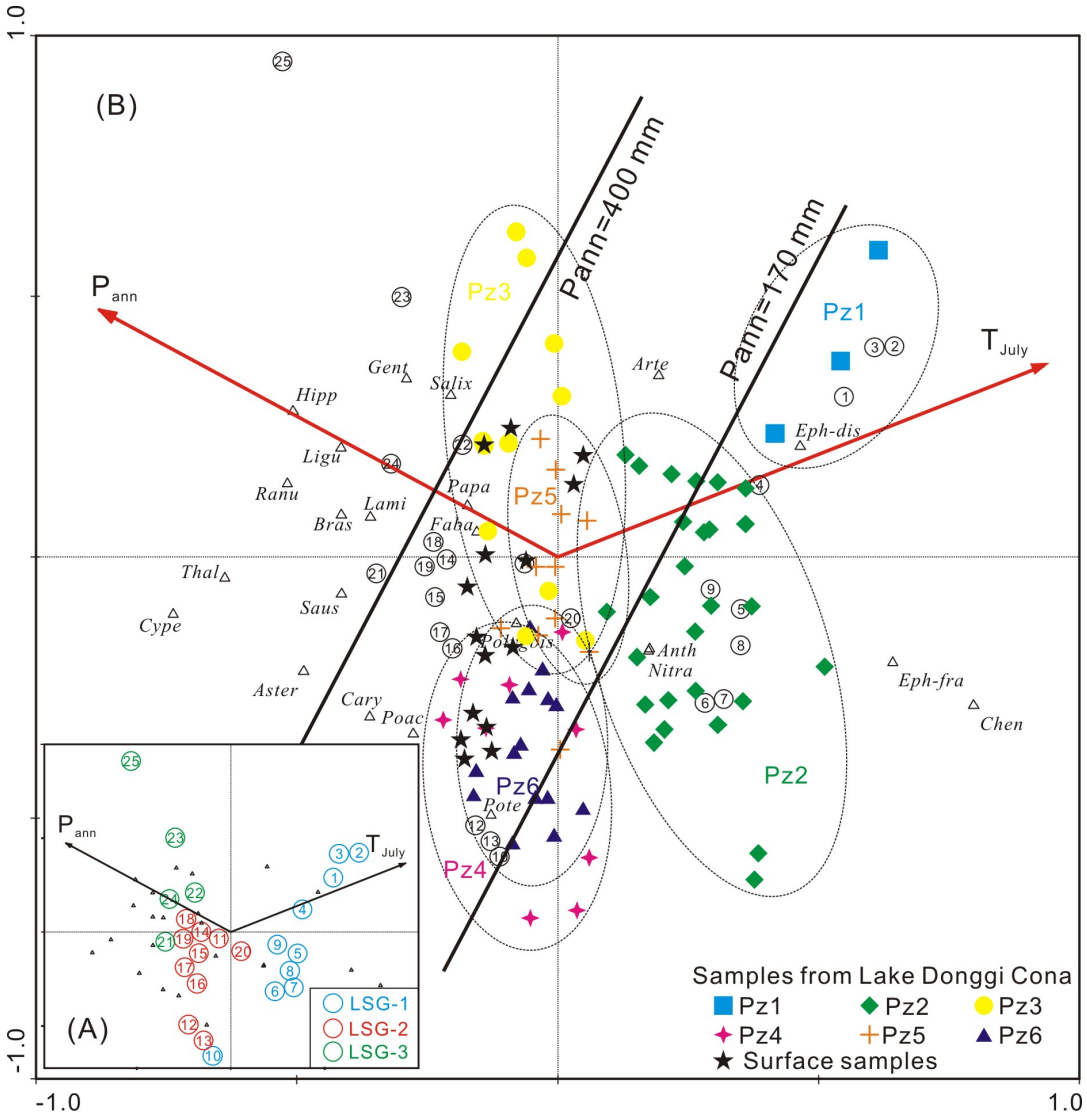

Figure 3-4(A) RDA tri-plot of surface pollen assemblages from 25 large lakes, constrained by mean annual precipitation (P_{ann}) and mean July temperature (T_{July}); samples have been classified using different colours while the numbers correspond to Figure 1A and Table 1. (B) Fossil and modern pollen samples from Lake Donggi Cona are supplementary objects on the RDA plot of (A): the bold black lines and associated precipitation results indicate the thresholds derived from the MRT analysis.

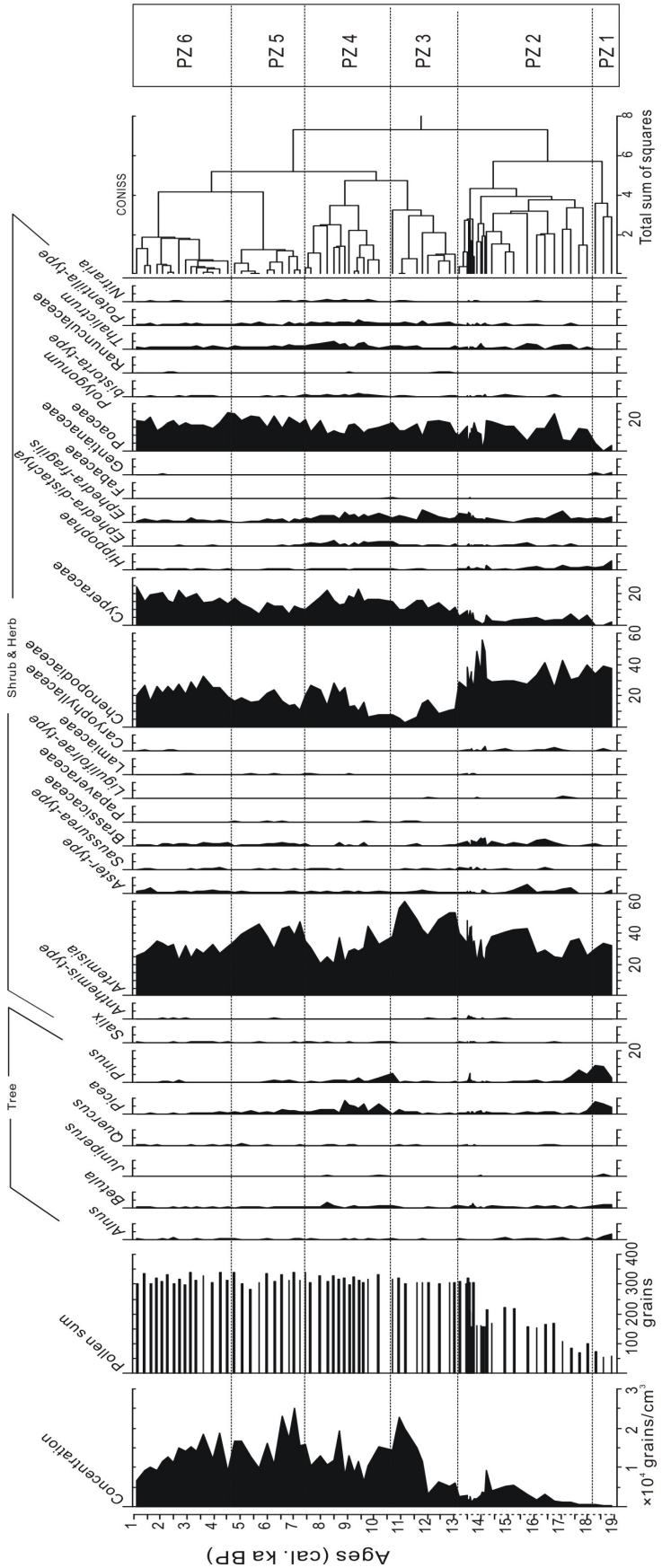

Figure 3-5 Stratigraphic diagram of fossil pollen results from Lake Donggi Cona, together with pollen-assemblage zones (PZ 1-6) defined by CONISS.

gradient of P_{ann}, the surface samples appear as three clusters in the sample plots, which is consistent with the MRT analysis.

Since both the RDA and MRT analyses reveal a strong correlation between P_{ann} and pollen compositions, WA-PLS models were developed to reconstruct mean annual precipitation. Finally, a two-component WA-PLS model was selected for P_{ann} reconstructions, taking into account the low root mean square error of prediction (RMSEP) of 95 mm and the high r^2 of 0.83.

3.4.2 Surface pollen samples from Lake Donggi Cona

In total, 79 pollen taxa were identified in the 15 surface-sediment samples from Lake Donggi Cona, of which 22 were used for numerical analysis (Figure 3-2C). The first two axes of the sample-centred PCA analysis captured 36.1% and 11.9% of the total variance, respectively. Three groups could be identified along the gradient of the first axis, correlating with the spatial distributions within the lake. Group DCS-I from the eastern part of the lake lies on the upper part of the second axis owing to the low amount of Chenopodiaceae pollen, while group DCS-II from the central part and group DCS-III at the western end of the lake lie at either end of the first axis due to their different Cyperaceae pollen contents (Figure 3-1, and supplementary Figure 3-9). When passively plotted on the RDA tri-plot based on the pollen data from 25 large lakes, all surface samples from Lake Donggi Cona are dispersed within the LSG 2 group (Figure 3-4B), representing a mean annual precipitation between 170 and 400

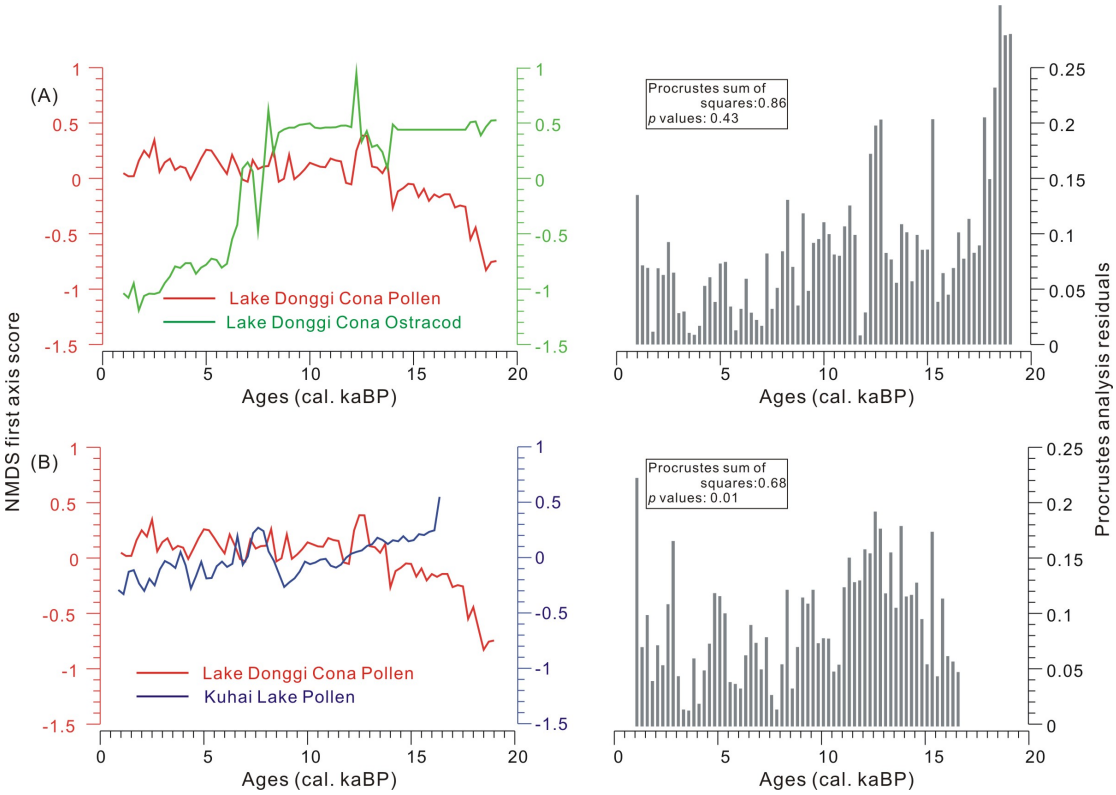

Figure 3-6 Non-metric multidimensional scaling (nMDS) axis 1 scores (left) and diagram of Procrustes analysis results (right) comparing pollen and ostracod data from Lake Donggi Cona (A), and comparing pollen data from Lake Donggi Cona with data from Lake Kuhai (B). The analyses were based on data-sets harmonised over 250 year intervals.

mm, and the WA-PLS derived annual precipitation results range from 257 to 346 mm, which fit well with the observed annual precipitation at meteorological station Madio (Figure 3-7D).

3.4.3 Core PG1790 from Lake Donggi Cona

Samples from core PG1790 consist mainly of four taxa of herbaceous pollen that are common in arid and semi-arid areas, i.e., *Artemisia*, Chenopodiaceae, Poaceae and Cyperaceae; these make up over 80% of the total pollen assemblage (Figure 3-5). *Aster*-type, *Thalictrum*, *Ephedra*, *Potentilla*-type and Brassicaceae pollen appear continuously in moderate quantities varying between 1 and 5%. The content of arboreal pollen taxa including *Pinus*, *Picea*, *Alnus*, *Betula* and *Quercus* is relatively low. The fossil pollen diagram is divided into six pollen-assemblage zones on the basis of the CONISS stratigraphically constrained cluster analysis, (PZ 1-6, Figs. 3-5 and 3-7). The characteristic pollen taxa, inferred vegetation, and inferred precipitation are shown in Table 3-3. Passively plotted on the RDA tri-plot, fossil samples mostly fall into LSG 1 and LSG 2, with the exception of three samples from PZ 3 that fall within the LSG 3 cluster (Figure 3-4B). Mean annual precipitations (P_{ann}) reconstructed using WA-PLS show variations ranging from about 100 mm during the late-glacial period to about 400 mm in the early Holocene (Figure 3-7).

The results of the Procrustes and PROTEST analyses are summarised in Figure 3-6 and Table 3-4. The low PROTEST correlation coefficient (0.36) together with the high *p*-value (0.43) indicate a non-fit between the pollen and ostracod data-sets from within Lake Donggi Cona, which could be further inferred from the high Procrustes residuals (Figure 3-6). In contrast, variations in pollen data from Lake Donggi Cona show a significant correlation with pollen data from Lake Kuhai, with a high PROTEST correlation coefficient (0.56) and low Procrustes rotation sum-of-squares (0.68).

3.5 Discussion

3.5.1. Reliability of pollen-based climate reconstructions from large lakes

We assume that the reliability of pollen-based climate reconstruction from large lakes will increase when the effects of (1) pollen-source area and (2) within-lake variations in pollen assemblage are taken into account, and when (3) pollen data are rigorously validated with other proxies and other sites.

(1) Pollen-source areas for sites in pollen-climate calibration sets. Pollen-source areas are assumed to depend mainly on the size of the lake basin and the species-specific dispersal and depositional characteristics of pollen grains (e.g. Prentice, 1985, 1987; Sugita, 1993; Broström et al., 2008). Our partial RDA, based on pollen data from 9 pairs of neighbouring large and small lakes, reveals an insignificant but consistent influence from lake size, explaining 7.9% of the total variance (48.1%) in the pollen-environment relationship. Furthermore, our numerical comparison of the inter-species relationships in small and large

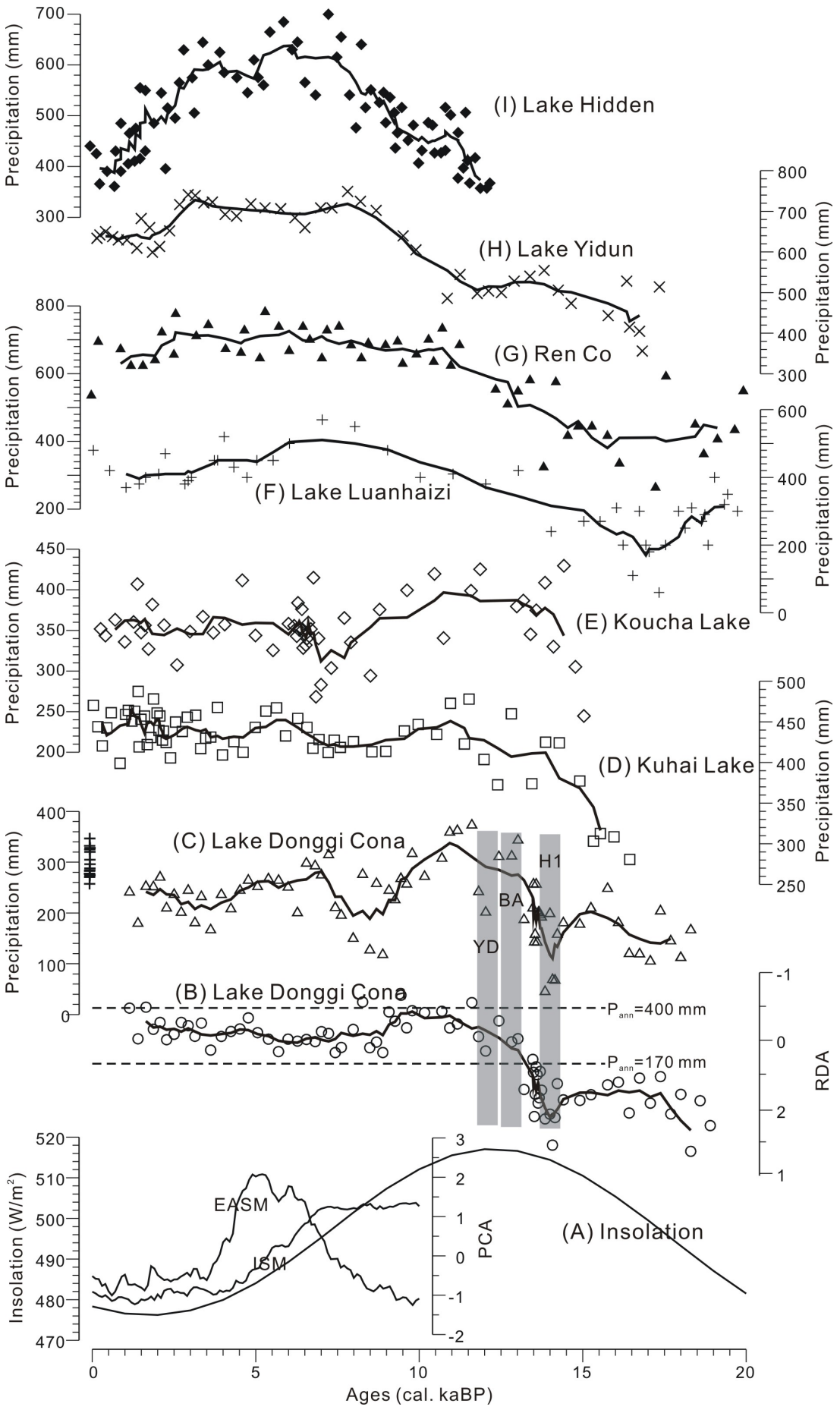
Precipitation (mm)
(I) Lake Hidden
(H) Lake Yidun
(G) Ren Co
(F) Lake Luanhaizi
(E) Koucha Lake
(D) Kuhai Lake
(C) Lake Donggi Cona
(B) Lake Donggi Cona
H1
BA
YD
P_{ann}=400 mm
P_{ann}=170 mm
RDA
Insolation (W/m^2)
EASM
ISM
PCA
(A) Insolation
Ages (cal. kaBP)

Figure 3-7 A: Summer (June) solar insolation at 35° N (after Laskar et al., 2004) and Asian Summer Monsoon indices (after Wang et al., 2010). B: First RDA axis scores from Lake Donggi Cona, together with the thresholds derived from the MRT analysis (dashed lines). C-E: WA-PLS reconstructed mean annual precipitation for Lake Donggi Cona (crosses indicate results from surface-sediment samples DCS1-15), Lake Koucha (after Herzschuh et al., 2009) and Lake Kuhai (after Wischnewski et al., 2011). F-I: Quantitatively reconstructed precipitation based on pollen data from Lake Luanhaizi (after Herzschuh et al., 2010a), Ren Co Lake (after Tang et al., 2004), Lake Yidun (after Shen et al., 2006a), and Lake Hidden (after Tang et al., 2004) on the eastern Tibetan Plateau. All fitting lines are based on LOESS smoothing; H1, BA, YD represent Heinrich Event 1, Bølling/Allerød and Younger Dryas respectively.

Table 3-3 Summary of the pollen assemblages and climate reconstructions from Lake Donggi Cona over the last >18.3 cal. ka BP

PZ	Depth (cm)	Ages (cal. ka BP)	Pollen assemblages	RDA group	WA-PLS based P_{ann}
1	475-455	>18.3	Dominated by herbaceous taxa *Artemisia* and Chenopodiaceae, characterized by extremely low pollen concentrations, and a high content of arboreal taxa (*Alnus*, *Pinus*, *Picea*, *Juniperus* and *Betula*), contributing up to about 20% of total terrestrial pollen.	LSG 1	Min 115 mm, max 169 mm, mean 144 mm
2	455-220	ca. 18.3-13.1	Dominated by *Artemisia* and Chenopodiaceae (up to 70%). Poaceae and Cyperaceae increased up to 20% and 10%, Caryophyllaceae, *Thalictrum*, *Aster*-type, Brassicaceae, and *Ephedra* started to appear, along with a reduction in arboreal taxa.	LSG 1&2	Min 48 mm, max 259 mm, mean 171 mm
3	220-153	13.1-9.5	Abrupt increase in the pollen concentrations, Chenopodiaceae decreased rapidly by 20-30% and was generally replaced by *Artemisia*. Cyperaceae increased steadily following the decrease of Brassicaceae and *Aster-typ*. Arboreal pollen reappeared at the end of this period.	LSG 2&3	Min 204 mm, max 375 mm, mean 307 mm
4	153-112	9.5-7.3	Characterized by a second high pulse of arboreal pollen frequencies, mainly resulting from an increasing content of *Picea*. *Artemisia* decreased gradually, synchronously with increasing frequencies of Chenopodiaceae.	LSG 1&2	Min 120 mm, max 278 mm, mean 209 mm
5	112-70	7.3-4.3	Chenopodiaceae and arboreal pollen decreased, together, with relatively high frequencies of *Artemisia*. *Ephedra, Thalictrum*, *Aster*-type and *Potentilla*-type still continuing, but to a lesser extent.	LSG 2	Min 203 mm, max 317 mm, mean 264 mm
6	70-16	4.3-1.1	Dominated by *Artemisia*, Chenopodiaceae, Poaceae and Cyperaceae, together with slightly higher frequencies of Brassicaceae and *Ephedra fragilis*-type.	LSG 1&2	Min 169 mm, max 273 mm, mean 225 mm

Table 3-4 Procrustes rotation and PROTEST diagnostics.

Data	Procrustes rotation sum of squares	RMSE	PROTEST (r)	p-values
Lake Dongi Cona pollen vs. Lake Donggi Cona Ostracod	0.86	0.11	0.363	0.43
Lake Dongi Cona pollen vs. Lake Kuhai pollen	0.68	0.10	0.56	0.01

lakes reveals higher residuals for taxa with large pollen grains (Cyperaceae, Poaceae) than for those with small grains (*Artemisia*, Chenopodiaceae). This confirms the modelling results for pollen-source areas, which indicated that the smaller the grain the larger the source area (pollen grain sizes, from large to small are Cyperaceae, Poaceae, Chenopodiaceae, and *Artemisia*; Figure 3-3a-h). Hence the relevant pollen-source area for a lake depends not only on the size of the lake but also on the species composition in the surrounding vegetation. This conclusion is supported by the results from our source-area estimations for the 25 surface-sediment samples presented in Figure 3-3i, where only a loose positive relationship can be inferred between lake size and source area. Both variations in lake size through time, and changes in the pollen composition, may therefore affect the pollen-source area of a lake, but these factors have rarely been considered when interpreting lake-pollen records.

Both RDA and MRT analysis applied to the calibration data-set reveal that precipitation is the major constraining variable for pollen spectra within the study region, which confirms the results of previous studies in Central Asia (Shen et al., 2006a, Herzschuh et al., 2010a). In order to take into account the concept of the pollen-source area when setting up the pollen-climate calibration model, we included only pollen spectra from large lakes and used distance weighted P_{ann} values as climate data (Table 3-1). The two-component WA-PLS model yields a slightly higher RMSEP as a percentage of the total gradient (14.3%, vs 7.2% in Shen et al., 2006a based on soil samples, and vs. 10.6% in Herzschuh et al., 2010a based predominantly on small lakes), which may originate from the generally higher noise-to-signal ratio in large lakes due to the higher long-distance component in such lakes. Thus, when applying pollen-climate correlations based on samples with much smaller pollen-source areas directly to pollen records recovered from large lakes, the RMSEP obtained from the modern calibration-set will underestimate the real error ranges of the reconstruction.

(2) Patterns of within-lake variability for pollen spectra. Pollen grains deposited in lakes are assumed to have originated mainly from the aerial pollen component. Large pollen grains are assumed to have a lower dispersability than small grains (Figure 3-3a-h) and hence to make up a higher proportion of the pollen in sediments that is derived from close to the lake margins than the pollen from the lake centre. This is supported by Luly (1997), who found an increasing proportion of Chenopodiaceae pollen in pollen traps towards the central part of Lake Tyrrell, in Australia. Concentric distribution patterns have also been reported for the herbaceous pollen proportions in Lake Dianchi, Yunnan Province, China (Sun and Wu, 1987). However, only the patterns have hitherto been described, while the influences that these within-lake variations have on pollen-based climate-calibrations have not previously been evaluated. WA-PLS derived precipitation figures for the surface-sediment samples from Lake Donggi Cona vary between 257 and 346 mm, showing a decreasing trend towards the lake centre (Figure 3-7D and supplementary Figure 3-10) that parallels a decrease in the *Artemisia* / Chenopodiaceae pollen ratio.

Fluvial input is another potential source of pollen in the sediments of large lakes. On the basis of pollen investigations in Lake Malawi and its catchment areas, Debusk (1997) concluded that fluvial supply of pollen is of the same order of magnitude as aerial input. Xu et al. (2005) reported variations in both pollen concentrations and pollen assemblages within Lake Daihai (Inner Mongolia, China). They found higher concentrations of pollen in sediments of alluvial

origin, and a good correlation between the pollen composition in the sediments and the composition of vegetation within the catchments of the inflows, from which they proposed that the pollen were primarily river transported. Investigations by Huang et al. (2004) of surface pollen samples from Bosten Lake in western China also revealed slight within-lake variations. Pollen grains from *Picea* and *Juniperus* were found to have been mainly river transported to lowland desert lakes in Inner Mongolia from the nearby Qilian Mountains (Zhu et al., 2002). Similarly, at Lake Donggi Cona we found the highest Cyperaceae pollen values at the inflows, which we assume originated from the *Kobresia* meadows in the mountains and from wetland vegetation drained by the river. Hence, fluctuations in lake water-level and the resulting changes in shoreline location, as well as the position and strength of discharges into the lake, are likely to influence the distribution of pollen within large lakes.

(3) Evaluation of climate reconstructions. We have aimed to differentiate the regional climate signal from local ecological/environmental noise by means of a rigorous proxy-to-proxy and site-to-site evaluation of the original proxy-data, as well as by applying two different calibration-methods. Aside from pollen, a variety of other proxies are commonly used for environmental reconstructions, among which ostracod assemblages on the Tibetan Plateau are assumed to primarily reflect limnological changes such as water depth and salinity (Mischke et al., 2007; Mischke et al., 2010 a, 2010b). We interpret the non-fit of the pollen data with the ostracod data obtained from the same core (thereby excluding the influence of age-depth-correlations) as indicating that the pollen data were not susceptible to within-lake changes or variations in the fluvial input but rather they reflected a terrestrial signal that was driven primarily by climate. That the pollen signal is regionally consistent is further confirmed by the significant fit between the pollen data from Lake Donggi Cona and pollen data from Lake Kuhai, 50 km away.

The quantitative precipitation reconstruction obtained by WA-PLS method was validated by the combined MRT/RDA calibration method (Davidson et al., 2010a, 2010b). The semi-quantitative results obtained varied between about 100 mm and 400 mm. Both the range and the pattern through time thus obtained are almost identical to the WA-PLS based reconstructions (Figure 3-7) despite the two different basic principles of the methods, WA-PLS assumes a unimodal pollen-climate response while RDA performs better with linear relationships (Birks et al., 2010). The fact that the reconstructions are independent of the calibration method used indicates the robustness of our approaches.

3.5.2 Late-Glacial and Holocene climate evolution of the Lake Donggi Cona area

To help decide whether the climate signals inferred from the Lake Donggi Cona pollen record are of local or of regional validity, we compared our results to other records from the eastern Tibetan Plateau (Figure 3-7) and attempted to identify the driving forces behind the reconstructed climate changes.

We have inferred a low vegetation cover in the Lake Donggi Cona area, as indicated by the high amount of pollen that may have undergone long-distance transport and by the extremely dry conditions (P_{ann} ~100 mm) from the basal sediments in our core, which accumulated during, or soon after, the LGM. These results are in agreement with previously reconstructed

precipitation results from the Luanhaizi (Herzschuh et al., 2010a) and Ren Co lakes (Tang et al., 2004) on the eastern Tibetan Plateau where precipitation was reconstructed to have been about half the present level. Additional lacustrine records from the eastern Tibetan Plateau, such as those from Ximen Co Lake and Lake Naleng on the eastern Tibetan Plateau (Zhang and Mischke, 2009; Kramer et al., 2010a) and Lake Shudu from Yunnan Province in south-western China (Cook et al., 2011), indicate that lake formation in many glacial basins started immediately after the LGM. As summarized in Herzschuh (2006), only few lakes existed continuously during the LGM in the present-day monsoonal areas of Central Asia due to the extremely low effective moisture, which resulted from the low temperatures of Northern Hemisphere (Dansgaard et al., 1993) and the shutdown of the Asian monsoonal system.

Thereafter, slightly wetter late glacial conditions (P_{ann} ~ 200 mm) are reconstructed, which were terminated by an abrupt reversion to extremely dry conditions. Generally increasing trends in precipitation after the LGM have also been reconstructed on the basis of pollen records from Lake Kuhai (Wischnewski et al., 2011), Lake Koucha (Herzschuh et al., 2009), Lake Yidun (Shen et al., 2006a), Lake Luanhaizi (Herzschuh et al., 2010a), and the Ren Co Lake (Tang et al., 2004), which are on the eastern Tibetan Plateau, and have been further confirmed by climate indices reviewed in Herzschuh (2006) and Wang et al. (2010). Following an increase in solar insolation, meltwater from glaciers and frozen ground probably contributed to an increase in the moisture available to vegetation. Taking into account the dating uncertainties, the reversion from the first wet period after the LGM may be stratigraphically consistent with “Heinrich Event 1” in the north Atlantic region (Broecker et al., 1992). This may indicate that the climate on the Tibetan Plateau during the early part of the Late-Glacial was influenced by cold and dry westerly air masses originating from the North Atlantic region, as has been previously suggested from a review of the loess records (Vandenberghe et al., 2006).

According to palynological studies from the nearby Lake Kuhai (Wischnewski et al., 2011) and Lake Koucha (Herzschuh et al., 2009), the abrupt decrease in Chenopodiaceae and increase in *Artemisia* pollen at about 14.5 cal. ka BP indicate the start of a period temporally consistent wtih the Bølling/Allerød event. Identical patterns were also found in the pollen sequences of Lake Donggi Cona, dated to about 13.5 cal. ka BP. We assume that the difference of about 1000 years results from local spatial and temporal variations in the “Lake Reservoir Effect”, and hence the radiocarbon ages from the bottom part of the core may be less reliable. Another reversion to dry conditions in the Lake Donggi Cona area at about 12 cal. ka BP is temporal correlated to the “Younger Dryas” cold event. Records from other nearby lakes, e.g. from Qinghai Lake (Shen et al., 2005), Lake Kuhai (Mischke et al., 2009), and Lake Koucha (Mischke et al., 2008), reveal identical wet Bølling/Allerød and dry Younger Dryas events, albeit with minor temporal inconsistencies.

The highest pollen derived annual precipitation (up to 400 mm) was reconstructed for the early-Holocene, which has also been reported from other sites on the Tibetan Plateau (see syntheses in Morrill et al., 2003; Herzschuh, 2006; Zhang and Mischke, 2009; Wang et al., 2010; Wischnewski et al., 2011). Although the reconstructed precipitation values for this period at Lake Yidun (Shen et al., 2006a), Lake Luanhaizi (Herzschuh et al., 2010a) and Ren

Co Lake (Tang et al., 2004) were not the maximum, they are consistently inferred to have been significantly higher (by ~50%) than in the Late-Glacial. The drivers behind this "Holocene optimum" were a further increase in solar insolation, increased meltwater from glaciers and the frozen ground, and enhanced precipitation due to an intensified Asian Summer Monsoon (ASM) (Wang et al., 2005a).

The annual precipitation inferred from the Lake Donggi Cona pollen record subsequently decreased to around 200 mm, resulting mainly from the increase in Chenopodiaceae pollen. Records from nearby lakes also indicate relatively low precipitation (Herzschuh et al., 2009; Wischnewski et al., 2011), but the signal is not as pronounced as at Lake Donggi Cona. This is probably due to the fact that the pollen loadings in the large Lake Donggi Cona derive from a larger source area at lower elevation, including a relatively high proportion of desert areas in the lowlands, e.g. the Qaidam Basin. Quantitative reconstructions from Lake Donggi Cona are consequently likely to overestimate the precipitation signal in the direct vicinity of the lake. The ASM (mainly the Indian Summer Monsoon) retreated after the early-Holocene following changes in Northern Hemisphere insolation, as revealed by marine records from the Arabian Sea (e.g. Overpeck et al., 1996), stalagmites (e.g., in the Dongge Cave in south-western China, Wang et al., 2005a and the Qunf Cave in southern Oman, Fleitmann et al., 2007), and synthetic moisture indices (Herzschuh, 2006; Wang et al., 2010), resulting in reduced monsoonal precipitation. Interestingly, the Lake Donggi Cona pollen record reveals a second wet period between about 7 and 4.5 cal. ka BP, with P_{ann} around 300 mm, which has also been found in various other climate reconstructions based on pollen records, e.g. at Lake Koucha (Herzschuh et al., 2009), Lake Kuhai (Wischnewski et al., 2011), Lake Naleng (Kramer et al., 2010b), and the No 2 Pit peat section (Yan et al., 1999). Over the same time period, maximum levels of precipitation were reconstructed from Lake Yidun (Shen et al., 2006a), Lake Luanhaizi (Herzschuh et al., 2010a), Lake Hidden, and Ren Co Lake (Tang et al., 2004). Other (non-pollen) studies from the eastern Tibetan Plateau and the Zoigê Plateau, e.g., stable carbon-isotope records from the Hongyuan Peat section (Hong et al., 2005), and multi-proxy results from Qinghai Lake (Shen et al., 2005), revealed identical patterns. Temporally, this second wet stage was synchronous with the intensification of the East Asian Summer Monsoon (EASM), revealed by a synthesis of moisture records from the monsoonal Central Asia region (Wang et al., 2010), which indicates that Holocene climate changes affecting the eastern Tibetan Plateau could also have, to some extent, been influenced by the EASM system.

The late-Holocene (4.5–0 cal. ka BP) shows relatively steady dry conditions that may have resulted from a further retreat of the ASM (Wang et al., 2010). Apart from reducing precipitation at Lake Hidden, a gradually increasing moisture trend after 3.5 cal. ka BP could be identified in the WA-PLS reconstructed precipitation results, reflecting the increasing Cyperaceae pollen component. An expansion of *Kobresia* meadows in the north-eastern Tibetan Plateau is described from the two neighbouring sites at Lake Kuhai (Wischnewski et al., 2011) and Lake Koucha (Herzschuh et al., 2009), as well as in pollen records from numerous peat sections near the Nianbaoyeze Mountains (Schlütz and Lehmkuhl, 2009), indicating either more effective moisture availability, a greater impact from grazing or, as favoured by Herzschuh et al. (2011), the promotion of *Kobresia* meadows as a result of higher atmospheric CO_2 levels than were present during the early-Holocene.

3.6 Conclusions

Through investigations and numerical analyses of various surface-sediment samples collected from large and small lakes, we have attempted to improve the current understanding of pollen-based climate reconstructions for large lakes, in particular with respect to pollen-source areas, within-lake variability in pollen assemblages, and vigorous validation of the reconstruction models.

The estimates of pollen-source areas show different patterns for individual pollen species depending on their various dispersal and depositional characteristics. A loose positive correlation can be identified between the pollen-source area and lake size.

Multivariate regression tree and redundancy analyses, together with WA-PLS, have been used to reconstruct precipitation in the Lake Donggi Cona area since the Last Glacial Maximum, revealing fluctuations in annual precipitation that range from about 100 mm during the Late Glacial Maximum to a peak of about 400 mm during the early-Holocene. Climate changes over the north-eastern Tibetan Plateau were triggered by variations in Northern Hemisphere insolation and primarily influenced by deglaciation and fluctuations in the intensity of the Asian Summer Monsoon, as well as by the westerlies derived from northern Atlantic Ocean.

Acknowledgements

We would like to thank Xiaolong Liu and Shupeng Yin for their assistance during fieldwork. Y. Wang's doctoral research is funded by the "Helmholtz - China Scholarship Council (CSC) Young Scientist Fellowship" (No. 2008491101). The research was supported by the German Research Foundation (Deutsche Forschungsgemeinschaft, DFG).

Supplementary

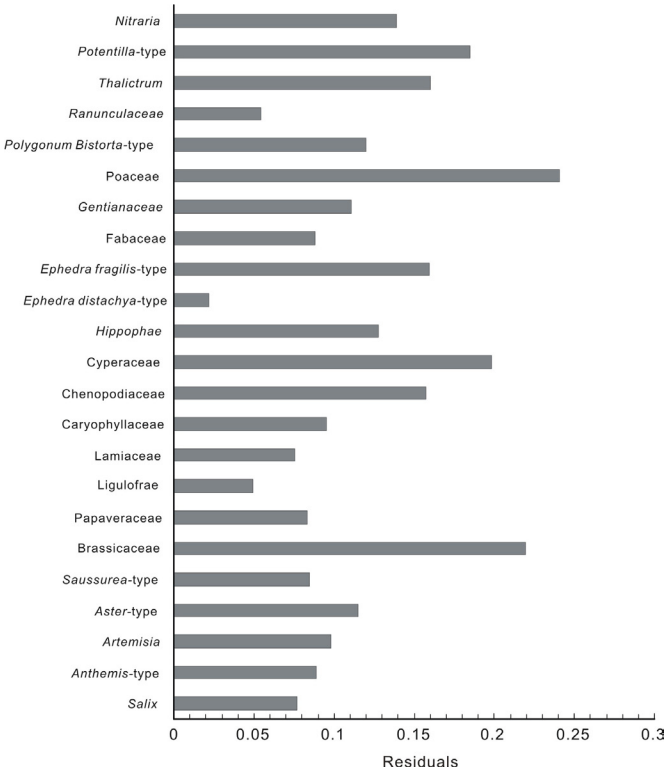

Figure 3-8 PROTEST residuals for pollen species after Procrustes analysis of surface pollen data from nine pairs of neighboring large and small lakes.

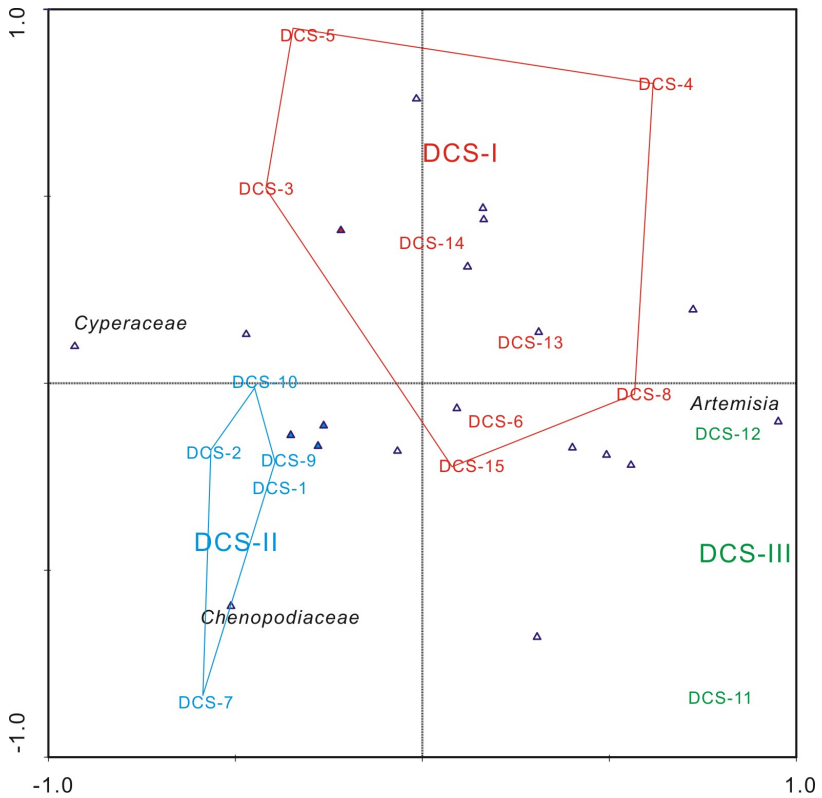

Figure 3-9 PCA bi-plot of surface sediment samples from Lake Donggi Cona, three groups (DCS-I, DCS-II and DCS-III) were identified according to the pollen assemblages.

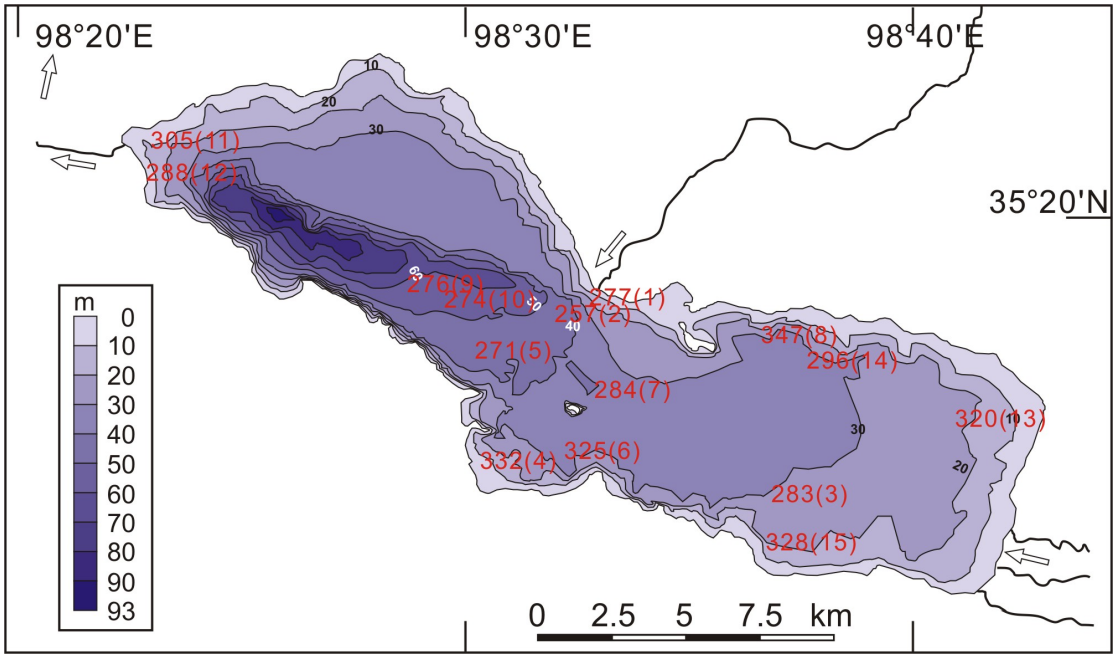

Figure 3-10 Within-lake variations in WA-PLS reconstructed mean annual precipitation for Lake Donggi Cona with red figures giving the sample number (numbers in brackets, see. Figure 3-9) and the amount of reconstructed precipitation in millimeters

4 Manuscript 3: Temporally changing drivers for late Holocene vegetation changes on the northern Tibetan Plateau: moving- window RDA of pollen record from Lake Kusai

Yongbo Wang [a, b, c], Xingqi Liu [a], Ulrike Herzschuh [b, c], Xiangdong Yang [a], Enlou Zhang [a], Guobang Tong [d]

[a] *State Key Laboratory of Lake Science and Environment, Nanjing Institute of Geography and Limnology, Chinese Academy of Sciences, 210008 Nanjing, P.R. China*

[b] *Alfred Wegener Institute for Polar and Marine Research, Research Unit Potsdam, 14473 Potsdam, Germany*

[c] *Institute of Earth and Environment Science, University of Potsdam, 14476 Potsdam, Germany*

[d] *Institute of Hydrological and Environmental Geology, Chinese Academy of Geological Sciences, 050803 Zhengding, P.R. China*

Current Status: Submitted to "Palaeogeography, Palaeoclimatology, Palaeoecology".

Abstract

Fossil pollen records have been widely used as indicators of past changes in vegetation and associated variations in climate. The driving mechanisms behind these vegetation changes have, however, remained unclear. In order to evaluate vegetation changes that have occurred in the northern part of the Tibetan Plateau and the possible drivers behind these changes, we have applied a moving-window Redundancy Analysis (RDA) to high resolution (10-15 yr) pollen and sedimentary data from Lake Kusai covering the last 3770 years. Our analyses have revealed frequent fluctuations in the relative abundances of alpine steppe and alpine desert components. The sedimentary proxies (which include the total organic carbon content, the total inorganic carbon content, and the "end-member" indices from grain size analyses) that explain the changes in the pollen assemblage vary significantly with time, most probably reflecting multiple underlying driving processes. The climate was found to have had an important influence on vegetation changes when conditions were relatively wet and stable. However, a gradual decrease in the vegetation cover was identified after 1500 cal a BP, from which time the vegetation appears to have been affected more by extreme events such as dust storms or fluvial erosion than by the general climatic trends. Furthermore, pollen spectra over the last 600 years have been revealed by Procrustes analysis to be significantly different from those recovered from older samples, which we attribute to an increased human impact that resulted in unprecedented changes to the composition of the vegetation. Overall, the changes in vegetation and associated changes in climate in the northern part of the Tibetan Plateau appear to have roughly followed the evolution of the Asian Summer Monsoon. After taking

into account the highly significant millennial (1512 yr) periodicity revealed by the time series analysis, the regional vegetation and climate changes also show variations that appear to match variations in the mid-latitude westerlies.

4.1 Introduction

Significant vegetation changes during the Holocene, deduced from fossil pollen data, have been reported from the Tibetan Plateau (Gasse et al., 1991; Shen et al., 2008; Tang et al., 2009; Herzschuh et al., 2010b; 2011) and have subsequently been interpreted in terms of climatic variations through the application of pollen-climate calibration functions (Herzschuh et al., 2010a; Lu et al., 2011; Shen et al., 2006a). However, the relationship between vegetation and climate is not straightforward because of the non-linear response of vegetation to the various climate parameters and related feedback mechanisms.

Precipitation is commonly assumed to be highly correlated with Tibetan vegetation compositions owing to the limited moisture supply available to this region, and variations in pollen spectra have mainly been interpreted in terms of variations in precipitation (Shen et al., 2006a; Herzschuh et al., 2010a; Lu et al., 2011). However, by analyzing pollen records in peat deposits Zhao et al. (2011) revealed more complex responses of the ecosystem to climatic conditions, such as insolation-driven temperature changes that act in concert with variations in monsoon-derived precipitation. Recent results from a transient global climate model covering the last 6000 years also demonstrate that the influence that temperature changes have had on Tibetan Plateau vegetation may have been underestimated (Dallmeyer et al., 2011). Changes in atmospheric CO_2 concentrations have also recently been suggested to be the major driver for mid-Holocene vegetation turnover on the Tibetan Plateau (Herzschuh et al., 2011). In contrast, Miehe et al. (2011) suggested that Tibetan ecosystems remained ecological stable during the mid-Holocene, due to the dominance of climatically resilient species. In addition to these studies that have attributed ecological transitions to climatic variability, vegetation change has also been assumed to reflect the intensity of nomadic herding on the Tibetan Plateau (Miehe et al., 2009; Schlütz and Lehmkuhl, 2009).

An improved understanding of the driving mechanisms behind vegetation changes and associated interactions during the Holocene is urgently required if the future impacts of climate and humans on the unique Tibetan ecosystems are to be predicted, and would also allow the use of pollen sequences as a climate proxy to be more reliably exploited. Such information is of particular interest for the central-northern parts of the Tibetan Plateau, where the vegetation may be more sensitive to climatic change owing to the interactions between the Asian Summer Monsoon (ASM) and the westerly winds (Wang et al., 2005a; Vanderberghe et al., 2006; Liu, et al., 2009). However, because of its remoteness palaeoenvironmental studies from that part of Tibetan Plateau are scarce and no information is available on the drivers behind vegetation changes (Wang et al., 2010).

In this study we present a high resolution late Holocene pollen sequence recovered from Lake Kusai, in the northern part of the Tibetan Plateau. Our main objectives were (1) to reconstruct the late Holocene vegetation and climate changes for the northern part of the Tibetan Plateau,

(2) to identify the underlying driving mechanisms for vegetation changes by evaluating the correlations between vegetation changes and environmental changes on the basis of pollen and sedimentary proxies from the same core (Liu et al., 2009), for which a moving-window constrained ordination analysis (Redundancy Analysis - RDA) was applied, and (3) to assess the possible influences that human impacts have had on the northern part of the Tibetan Plateau, which are little known at present.

4.2 Study area

Lake Kusai (approximately 35.62-35.83° N and 92.63-93.25° E) is a closed basin lake situated about 4475 m a.s.l. in the northern part of the Tibetan Plateau (Figure 4-1). It covers an area of about 255 km^2 and has a catchment area of approximately 3700 km^2. The lake is fed mainly from the southwest by the Kusai River, which originates to the west of the lake on the Daxue Mountain. The lake is rather shallow in the southeast where the mean water depth is about 10 m, and much deeper in the northwest, with depths of up to about 50 m in the center of the sub-basin (Li, 1996; Wang and Dou, 1998). The 30-year records available from the nearest meteorological station at Wudaoliang (35.22° N, 93.08° E), which is about 50 km from Lake Kusai, indicate a mean annual temperature of about -5.4 °C, a mean annual precipitation of 275 mm, and a potential annual; evaporation of about 1300 mm (China Meteorological Administration, unpublished data).

As a result of the limited precipitation and high elevation, alpine steppe plant communities dominate the present-day vegetation surrounding Lake Kusai (Hou, 2001). The immediate vicinity of the lake is covered by *Carex moorcroftii* alpine steppe to the west and *Stipa*

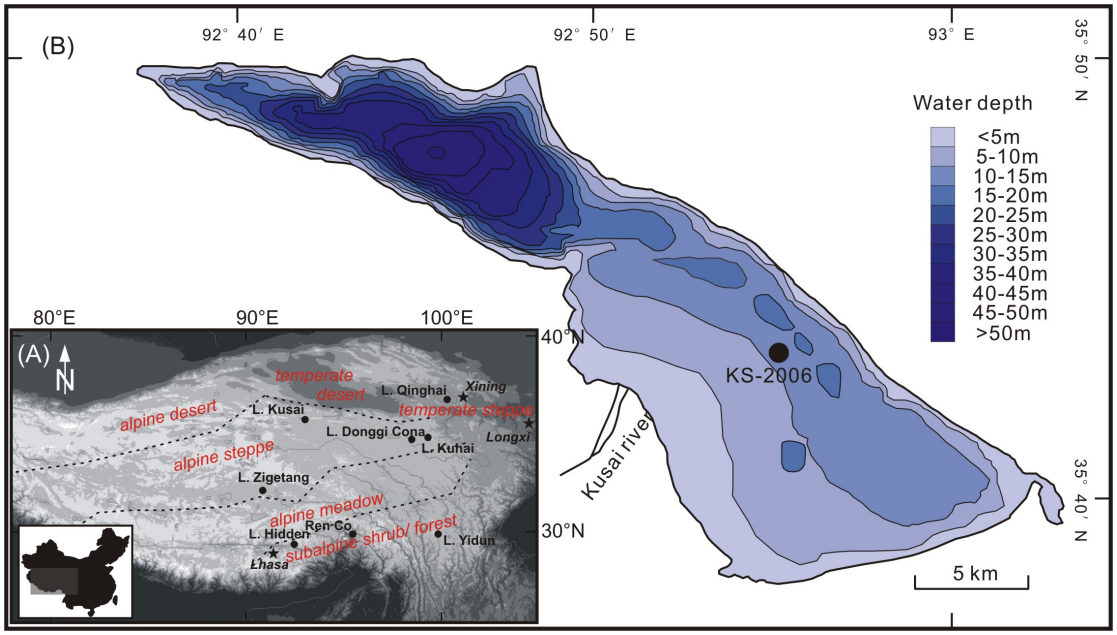

Figure 4-1 Location of Lake Kusai and the study sites mentioned in the text, as well as the distribution of vegetation communities on the Tibetan Plateau and adjacent areas (after Hou, 2001); B: bathymetry of Lake Kusai and the location of KS-2006 core.

purpuren alpine steppe to the east. The western sections of the high elevation Kulun Mountains are dominated by *Saussurea medusa*, *Saussurea spp.* sparse vegetation, while *Arenaria musciformis*, *Androsace tapete* cushion vegetation is distributed on the eastern sections. Alpine steppe (*Carex moorcroftii*, *Stipa purpuren*) vegetation is present on the northern slopes of the Kunlun Mountains. Patches of alpine meadow (mainly *Kobresia pygmaea*) can also be found in the mountainous areas, where there is a greater availability of moisture, and patches of alpine shrubs (*Salix orithrepha*, *Saussurea spp*. and *Potentilla-type*) occur in restricted areas (Hou, 2001).

4.3 Material and methods

4.3.1 Coring, chronology, and sedimentary proxy analyses

Two long sediment cores (637 cm and 592 cm long, measured in field) were collected during an expedition in 2006 from a water depth of 14.5 m in the southeastern part of Lake Kusai, using UWITEC coring equipment (Figure 4-1). A short core of 17 cm length was also recovered in the vicinity of the long cores using a gravity corer. Overlaps between the long cores were identified using scanned magnetic susceptibility data, resulting in a 606 cm continuous sediment record. Sub-samples at 1 cm intervals were taken in the laboratory for further analyses.

Table 4-1 AMS dating results and corresponding calibrated ages used to construct the age-depth model for the KS-2006 core.

Sample No.	Laboratory Code	Depth (cm)	Dated material	14C ages (a BP)	Ages corrected by 3400yr (a BP)	Calendar ages (cal a BP) by 2σ
Ks1-1-82	TKa-14104	82-83	TOC	3670 ± 35	270 ± 30	281-335 (308)
Ks1-1-102	TKa-14105	102-103	TOC	3855 ± 30	455 ± 35	478-536 (530)
Ks1-2-26	TKa-14107	184-185	TOC	4580 ± 35	1180 ± 45	1047-1180 (1100)
Ks1-2-126	TKa-14109	284-285	TOC	5235 ± 35	1835 ± 35	1698-1868 (1850)
Ks1-3d-66	TKa-14234	470-471	TOC	6257 ± 45	2875 ± 50	2871-3084 (2900)
Ks1-4-70	TKa-14112	573-574	TOC	6630 ± 40	3230 ± 65	3377-3557 (3550)
Ks1-4-100	TKa-14113	603-604	TOC	6955 ± 40	3555 ± 50	3718-3930 (3750)

In view of the absence of plant macrofossils and the low pollen concentrations, ^{14}C dating of total organic carbon samples was carried out using accelerator mass spectrometry (AMS). Samples from seven different levels were processed and dated at the Radiocarbon Laboratory of the University of Tokyo, in Japan (Table 4-1). In addition, ^{210}Pb and ^{137}Cs radiometric dating results from the short core were used to determine the "Carbon Reservoir Effect", which has been commonly reported from lake sediments on the Tibetan Plateau (Fontes et al., 1996; Shen et al., 2005; Morrill et al., 2006; Henderson et al., 2010), yielding a Carbon Reservoir Effect of about 3400 years. All the ^{14}C ages were then corrected for this effect calibrated using the Calib 5.1 program (Reimer et al., 2004), and then interpolated and extrapolated to obtain ages for each horizon. The age obtained for the bottom of the

investigated core was 3770 cal a BP.

Measurements of the sedimentary proxies, i.e. the total organic carbon (TOC) content, total inorganic carbon (TIC) content, and grain sizes, were performed at 2 cm intervals, representing a 10 to 15 year resolution. The End-Member Modeling Algorithm (EMMA) developed by Weltje (1997), which can convert measured grain-size distributions into proportional contributions of an optimal set of end-members (Weltje and Prins, 2003; 2007), was used to determine the end-members (EMs) from the total set of grain size measurements. Detailed descriptions and discussions concerning the measurements and the chronology can be found in Liu et al. (2009).

4.3.2 Pollen analyses

Pollen samples collected at 2 cm intervals (303 samples in total) were treated and analyzed following standard laboratory procedures that included treatment with hydrogen chloride (HCl, 10%), potassium hydroxide (KOH, 10%), and hydrofluoric acid (HF, 50%), as well as acetolysis, fine sieving (with 7 μm mesh in an ultrasonic bath), and mounting in glycerin (Fægri and Iversen, 1989). Two tablets of Lycopodium spores were added to the fossil samples in order to estimate absolute pollen concentrations. A minimum of 300 terrestrial pollen grains were counted from each sample and the pollen content calculated as a percentage of the total pollen from both arboreal and terrestrial non-arboreal pollen taxa.

4.3.3 Numerical analyses

Only those pollen taxa that occurred with a frequency greater than 0.5% in at least five samples were included in the numerical analyses and in the compilation of the pollen diagrams. These diagrams were generated using the TGView (version 2.0.2) software (Grimm, 2004), and the pollen assemblage zone boundaries were defined on the basis of the results from a Constrained Incremental Sum of Squares (CONISS) cluster analysis, using the Edwards and Cavalli-Sforza's chord distance in TGView (version 2.0.2).

To evaluate the potential noise in our high resolution pollen data, a spectra analysis was applied to the *Artemisia* content (in percentages) using the REDFIT 3.8 program, which was designed to estimate red-noise spectra directly from unevenly spaced palaeoclimatic time series (Schulz and Mudelsee, 2002). Strong multi-decadal scale noise (ca. 30 years) was identified (Figure 4-2A), which, in view of our sampling resolution of about 15 years, was thought to represent inter-sample variations. Since we were mainly focusing on long term trends, all the data (both pollen and sedimentary proxies) were then interpolated and re-sampled at 15 year intervals in order to reduce such multi-decadal scale noise (Figure 4-2B), this being achieved using AnalySeries 2.0.4.2 software (Paillard et al., 1996). All numerical analyses were thereafter performed using the re-sampled data.

Pollen percentages were square-root transformed for the numerical analyses in order to stabilize variances and to optimize the signal-to-noise ratio. Detrended correspondence

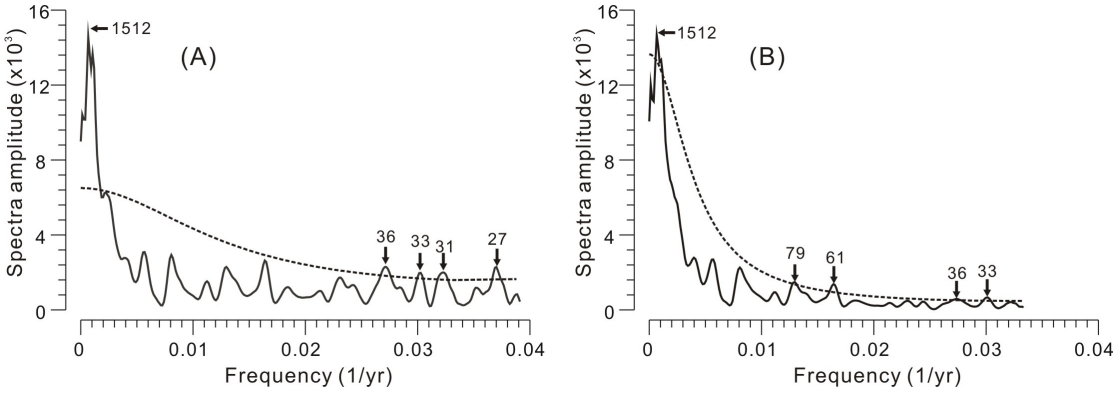

Figure 4-2 Results of spectra analyses using the original *Artemisia* percentages (A) and re-sampled data (B). The dashed lines indicate 90% confidence levels.

analysis (DCA; Hill and Gauch, 1980) yielded turnover gradients of 0.99 standard deviations, indicating that linear-based methods such as Principal Component Analysis (PCA) and Redundancy Analysis (RDA) are appropriate for the dataset.

We used the pollen assemblages and parallel sedimentary proxies (TOC, TIC, and end-members from grain size analyses) from the same core in order to avoid any potential chronological uncertainties. Using pollen data as variables and sedimentary proxies as environmental factors, an RDA was carried out to assess the temporal variations in their correlations in terms of weighting and significance for each proxy. In general, every 40 stratigraphically-continuous samples were grouped and analyzed together. The forward selection option in RDA was used, together with a Monte Carlo permutation test (999 unrestricted permutations), to determine the relative weight and significance of sedimentary proxies for each group. The *p*-values were not corrected for multiple comparisons.

In order to estimate the amount of compositional species turnover along gradients in time, a Detrended Canonical Correspondence Analysis (DCCA) was also applied using the transformed pollen percentage data. All the ordination analyses were carried out using the CANOCO software, version 4.5 (ter Braak and Šmilauer, 2002).

A Procrustean Randomization Test (PROTEST) was applied to examine the correlation along the core between pollen assemblages and their environments (Jackson, 1995). The pollen sequence was classified into six continuous sections (KSH 1-6) with 40 samples in each. Using the species scores for each section after PCA, PROTEST analysis was then used to compare the similarities in species compositions between any pair of sections. All the analyses were performed using a Protest program (Peres-Neto and Jackson, 2001).

4.4 Results

4.4.1 Late Holocene pollen record from Lake Kusai

A total of 77 terrestrial pollen types were identified in the samples and 38 taxa included in the pollen diagram and numerical analyses. The pollen assemblages consist mainly of four taxa of

herbaceous or shrub pollen that commonly appear in arid and semi-arid parts of China, i.e. *Artemisia*, Chenopodiaceae, Poaceae, and Cyperaceae, which together make up over 80%of the total pollen in all samples (Figure 4-3). *Ephedra*, Asterceae p.p., Ranuculaceae, Caryophyllaceae (*Arenaira*-type), and Brassicaceae pollen also appear continuously in all samples, but in more moderate quantities that vary between 1 and 5% of the total pollen. The contribution of arboreal pollen taxa, including *Pinus*, *Picea*, *Juniperus*, *Betula*, and *Ulmus*, is also relatively low, with a similar range between 1 and 5%, and is dominated by *Pinus*.

In general, the fossil pollen sequence is characterized by a decrease in both *Artemisia*/Chenopodiaceae (A/C) ratios and total pollen concentrations from bottom to top, together with an increase in the arboreal pollen proportion (Figure 4-4). The fossil pollen diagram was divided into three pollen assemblage zones (PAZ 1-3) on the basis of the stratigraphically-constrained CONISS cluster analysis (Figure 4-3), mainly reflecting variations in the relative abundances of *Artemisia*, Chenopodiaceae, and *Pinus*. The first assemblage zone (PAZ 1: 3770-2400 cal a BP) is characterized by a Chenopodiaceae content trend that first decreases and then increases, resulting in the opposite trend for the A/C ratio. The content of *Ephedra* pollen shows a gradually decreasing trend, while the total pollen concentration and arboreal pollen content are both low (Figure 4-4b, d). The second assemblage zone (PAZ 2: 2400-900 cal a BP) shows fluctuations in *Artemisia* and Chenopodiaceae content. The Chenopodiaceae content shows an abrupt increase at about 1700 cal a BP, lasting around 100 years. The arboreal pollen content increases in parallel with a decreasing total pollen concentration (Figure 4-4d). The PAZ 3 assemblage is characterized by the general replacement of *Artemisia* by Chenopodiaceae after 900 cal a BP, resulting in a continuing decrease in the A/C ratio, while the *Arenaira*-type and the arboreal pollen content (especially of *Pinus*), reach their maxima (Figure 4-3; Figure 4-4d).

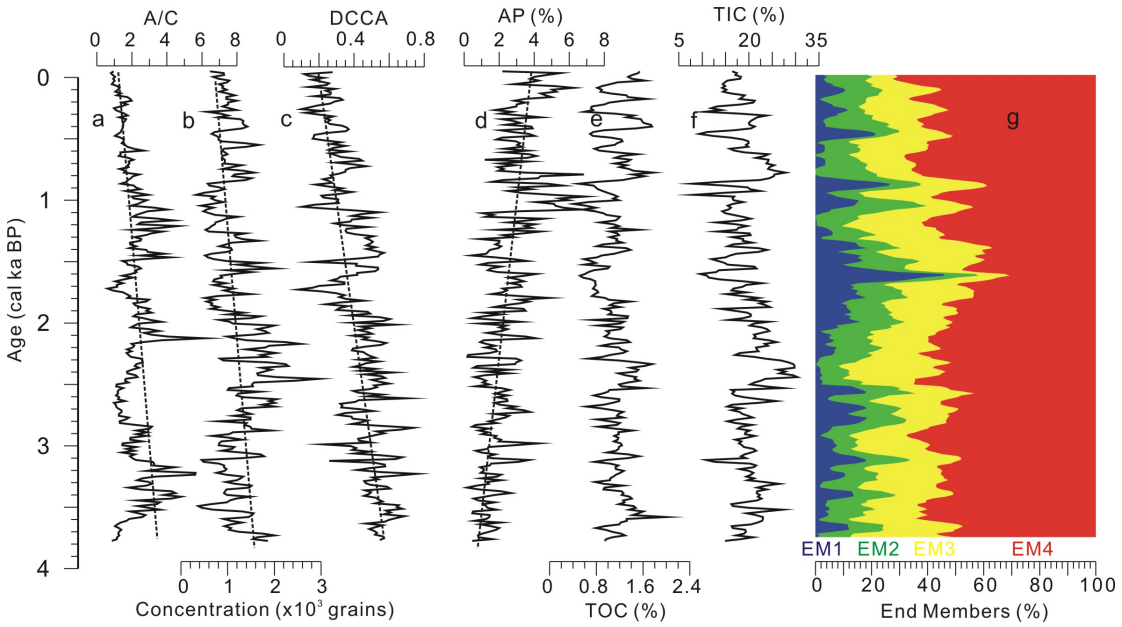

Figure 4-3 Pollen and sedimentary indices: **a** *Artemisia*/Chenopodiaceae (A/C) ratio; **b** pollen concentration; **c** DCCA first axis scores; **d** arboreal pollen content (AP); **e** total organic carbon (TOC) content; **f** total inorganic carbon (TIC) content; **g** proportions of four end members (EM1–4). The dashed lines indicate the general trends for individual indices.

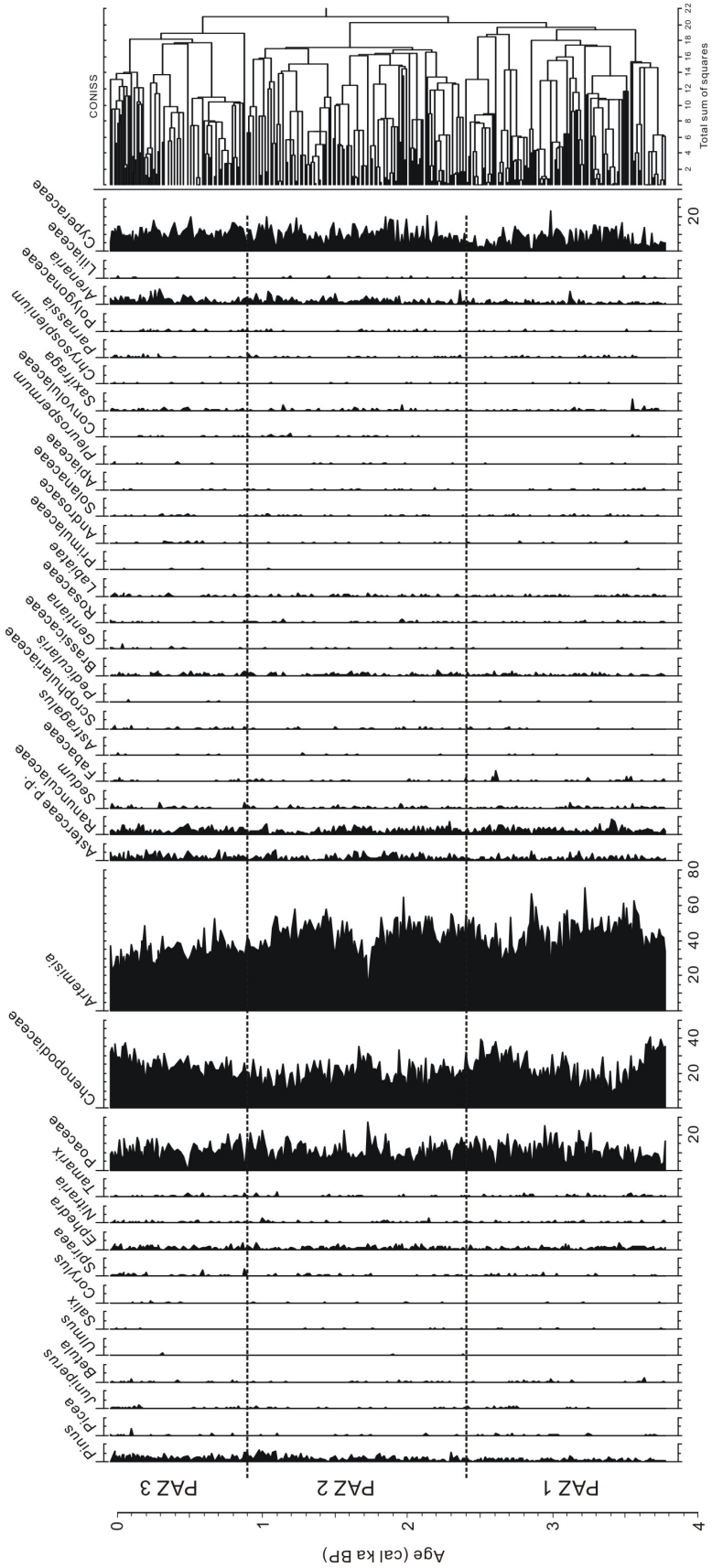

Figure 4-4 Stratigraphic diagrams representing the results of palynological analysis of the KS-2006 sediment core. The dashed lines indicate the pollen assemblage zones, which are classified according to the CONISS results.

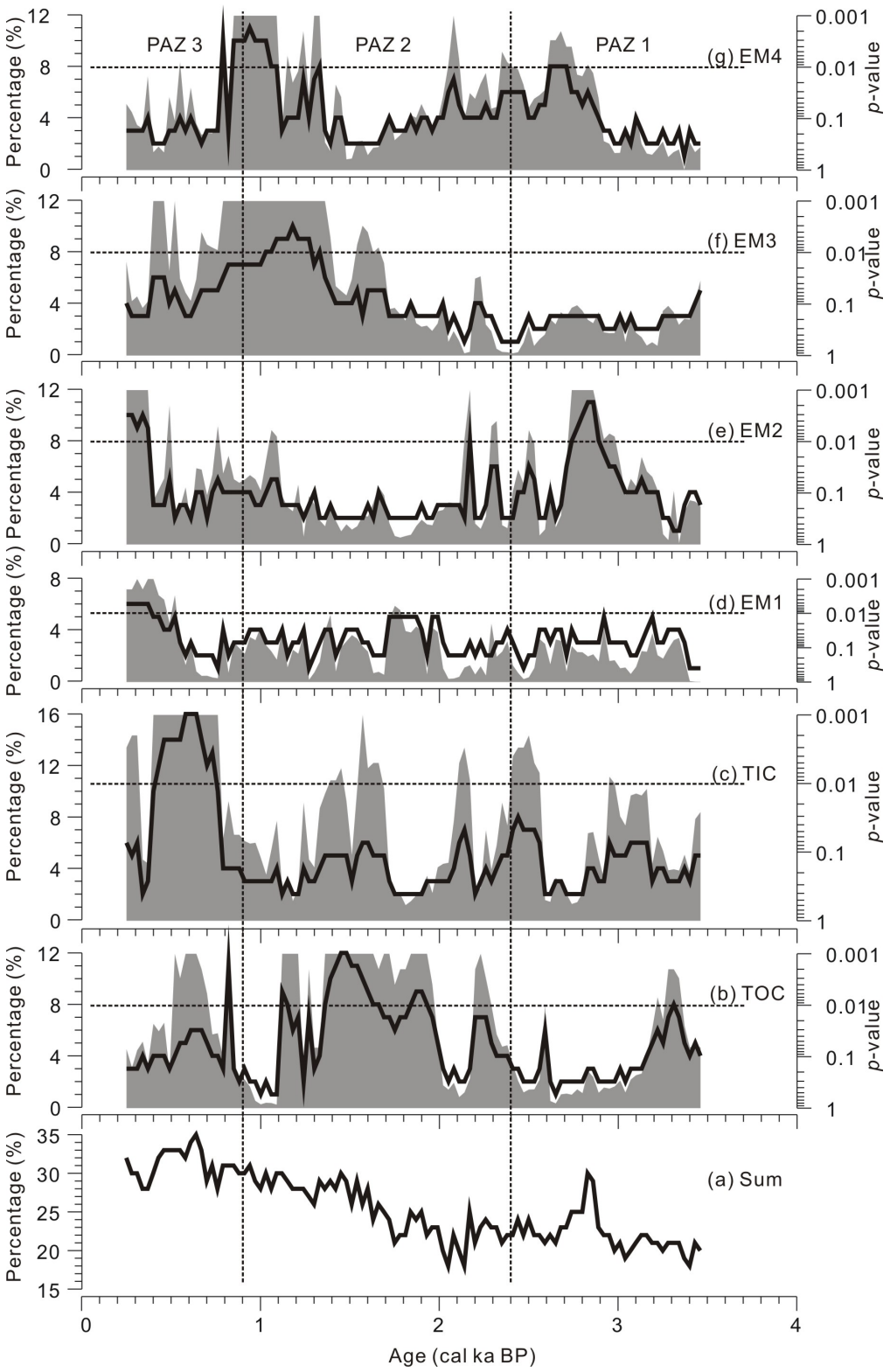

Figure 4–5 Results of moving–window RDA: **a** total correlation between pollen assemblages and all sedimentary proxies; **b–g** correlation between pollen assemblages and individual proxies, namely TOC (total organic carbon) content, TIC (total inorganic carbon) content, and EM 1–4 (end members from grain size data). The black curves indicate the correlations, while the gray backgrounds represent the significance levels with the horizontal dashed lines at the p=0.01 (significance) level. The vertical dashed lines indicate the boundaries between pollen assemblage zones.

4.4.2 Pollen-environment correlations

The apparent gradually increasing total amount of variance in the pollen assemblages from bottom to top is explained by the sedimentary proxies as environmental factors in a moving-window RDA (Figure 4-5a). Except the first few centuries after 3000 cal a BP, PAZ 1 is characterized by a relatively low correlation of around 20% between pollen assemblages and the constrained environmental factors, while PAZ 2 is dominated by a continuously increasing trend in the total correlation from about 20% to 30%. The highest correlations were detected during PAZ 3, reaching up to 35%.

The TOC content in the sediment is generally low, varying between 0.6% and 2.4% (Figure 4-4e), which explains a significantly part of the variance in the pollen assemblages during PAZ 2, as well as at the beginning of PAZ 1 and PAZ 3, generally contributing around 8% to total variances (Figure 4-5b). Rather high contents of between 5% and 35% were determined for TIC (Figure 4-4f). In addition, particularly high values for explained variance, along with marked fluctuations, were detected for TIC, particularly in PAZ 3 where extremely high explained variance values (up to 16%) were identified (Figure 4-5c).

Four end-members (EMs) were deduced from the EMMA analysis on the grain size data (Figure 4-4g, Liu et al., 2009), with EM1 having the coarsest grain size fraction, generally over 100 μm. The EM2 and EM3 end-members consist mainly of the intermediate fractions, with predominant modal grain sizes of 40 μm and 10 μm respectively which are consistent with the grain size distributions for present-day aeolian samples. The EM4 end-member is characterized by the finest fraction (ca. 4 μm). The correlation between pollen assemblages and EM1 is generally low (below 4%), and is insignificant except for during the last few centuries (Figure 4-5d). Variations in correlation in EM2 could, to a large extent, explain the variations in pollen assemblages during parts of PAZ 1, as well as during the last few centuries (Figure 4-5e). The EM3, on the other hand, shows a highly significant correlation of around 8% between 1500 and 800 cal a BP (Figure 4-5f). Two significant pulses are determined for EM4, both during the transitional periods from PAZ 1 to PAZ 2, and from PAZ 2 to PAZ 3 (Figure 4-5g).

4.4.3 PROTEST analyses

As shown in Table 4-2, the PROTEST analyses between the youngest section (KSH 6) and the older sections (KSH 1-5) reveal relatively high residuals (1.52, 1.41, 1.47, 1.31, 1.32, respectively), together with high probabilities of rejection (0.737, 0.291, 0.532, 0.071, 0.094, respectively), which both indicate that the pollen species composition in section KSH 6 is different from that in the other sections. In contrast, low residuals (1.05-1.27) and probability of rejection (0.001-0.05) between pairs of older sections indicate generally consistent pollen species compositions during these older periods of time, with only minor fluctuations.

4.4.4 Artemisia time-series analysis

The spectra analysis on the original *Artemisia* percentages reveals statistically significant multi-decadal periodicities with intervals of 27, 31, 33, and 36 years with a greater than 90% confidence level, as well as a millennial scale periodicity of 1512 yr (Figure 4-2A). However, using the data that had been re-sampled at 15 year intervals, the signals of multi-decadal periodicities tended to disappear (Figure 4-2B) leaving only the millennial signal consistent with the results from the original data.

Table 4-2 Summary of PROTEST analysis residuals between each pair of groups, and the probability of rejection (in brackets). Higher residuals and probability of rejection indicate higher levels of dissimilarity.

	KSH 6	KSH 5	KSH 4	KSH 3	KSH 2	KSH 1	KSH 6
KSH 6	/	1.32 (*0.094*)	1.31 (*0.071*)	1.47 (*0.532*)	1.41 (*0.291*)	1.52 (*0.737*)	/
KSH 5	/	/	1.05 (*0.001*)	1.23 (*0.014*)	1.29 (*0.050*)	1.18 (*0.004*)	/
KSH 4	/	/	/	1.09 (*0.001*)	1.07 (*0.001*)	1.23 (*0.018*)	/
KSH 3	/	/	/	/	1.11 (*0.002*)	1.27 (*0.025*)	/
KSH 2	/	/	/	/	/	1.22 (*0.012*)	/
KSH 1	/	/	/	/	/	/	/

4.5 Discussion

4.5.1 Environmental indicator value of individual sedimentary proxies

In view of the low organic carbon to nitrogen (C/N) ratios (below 10; Liu et al., 2009), the TOC content recovered from our sediment samples can generally be taken to be representative of the primary productivity within the lake system (Meyers and Lallier-Verges, 1999). Furthermore, the variations in TOC content show patterns that are consistent with precipitation reconstructions based on tree-rings from Delingha, in the northern part of the Tibetan Plateau (Shao et al., 2005), indicating that the TOC-related primary productivity in Lake Kusai is largely controlled by changes in precipitation, as has also been widely reported from the arid and semiarid regions in central Asia (Xiao et al., 2002; 2006; Shen et al., 2005; Mischke et al., 2010b). The productivity in the lake increased during periods of higher precipitation resulting in a higher TOC content in the sediments, and conversely during drier periods.

X-ray diffraction (XRD) analysis has revealed that the carbonate minerals in the sediments from Lake Kusai consist mainly of aragonite, which is commonly reported to be an autogenic mineral on the Tibetan Plateau (Wang et al., 2012), and which has also been considered to be of biogenic because of the high ostracod content in the sediments (Wang, unpublished data; Yao et al., 2011). The distribution of ostracods has been shown to be sensitive to lake water

salinity (Mischke et al. 2007; 2010). Since the Lake Kusai is currently a brackish water lake, any variations in salinity are likely to have a considerable influence on the subsistence of ostracods and the corresponding TIC content in the sediments.

The EMMA analysis has been widely applied to identify possible sources of sediments in ocean and lakes (Weltje and Prins, 2003; 2007; Liu et al., 2009). The first end-member, the sand-size fraction, has been considered by Liu et al. (2009) to represent glacially supplied material. However, the northern Tibetan Plateau has been recognized as an area that is greatly influenced by dust storm events (Wang et al., 2004a), and analyses on modern dust samples collected at Lenghu Meteorological Station have revealed that, in the Qinghai-Tibet area, the coarse grain-size fraction (>63 μm) is an indicator of dust storm events (Qiang et al., 2007a; 2007b). We therefore interpret EM1 to represent coarse sands derived during dust storm events (Wang et al., 2009). In contrast, the intermediate fractions, EM2 and EM3, represent grain size distributions matching those of modern aeolian dust samples that were collected from Lake Kusai during an expedition in the winter of 2009, and so could be used to indicate the intensity of regular aeolian activities (Liu et al., 2009). Considering the fact that, in arid regions, rivers with low discharge rates are usually incapable of transporting coarse particles into the central part of a lake, EM4 was interpreted to represent non-aeolian mud associated with fluvial processes (Liu et al., 2009). For such arid regions, both the aeolian dust and the fluvial sediments are highly dependent on the regional vegetation coverage, which can significantly influence the erosion and transport of soils. Reduced vegetation coverage is likely to enhance the intensities of both aeolian activities (during winter and spring) and fluvial transport (in summer) (Wolfe and Nickling, 1993; Ludwig et al., 2005).

Our analysis of pollen from Lake Kusai has revealed that the northern part of the Tibetan Plateau was characterized by high components of *Artemisia* and Chenopodiaceae during the late Holocene, which is generally consistent with results obtained by other investigators from nearby sites such as Lake Qinghai (Liu et al., 2002b; Shen et al., 2005), Lake Hurleg (Zhao et al., 2007), Lake Kuhai (Wischnewski et al., 2011), and Lake Donggi Cona (Wang et al., 2011). For pollen records from the arid and semi-arid areas, the A/C ratio has been shown to be a reliable indicator for changes in moisture levels owing to the different ecological habits of *Artemisia* and Chenopodiaceae (Campo et al., 1996; Cour et al., 1999; Herzschuh et al., 2003, 2004; Herzschuh, 2007). In contrast, the arboreal pollen grains in samples from arid steppe or desert regions, and especially those pollen grains with air bags (i.e. *Pinus*), are commonly considered to represent long transport distances (Lu et al., 2010), with a high content of such grains indicating limited local pollen productivity as a result of relatively dry conditions or reduced vegetation coverage. Variations in pollen concentrations have traditionally been interpreted in terms of changes in vegetation and/or climate, but such interpretations should be treated with caution because of variations in species-specific pollen productivities. For instance, when the climate becomes drier, the slight increase in Chenopodiaceae in the vegetation is accompanied by a marked decrease in *Artemisia*, but could still lead to an increase in pollen concentration owing its high productivity despite opening up of the vegetation cover (Wang and Herzschuh, 2011). Furthermore, since our study area is located close to the arid, low elevation Qaidam Basin, which is dominated by desert plants (Zhao et al., 2007; 2010), this may have affected the pollen assemblages recovered due to the high

transportability of Chenopodiaceae pollen grains, as has previously been discussed for the northeastern part of the Tibetan Plateau at Lake Donggi Cona (Wang et al., 2011) and Lake Kuhai (Wischnewski et al., 2011).

4.5.2 Vegetation changes during the late Holocene and possible drivers

(1) From 3770 to 2400 cal a BP: vegetation fluctuations under abrupt climate changes

The gradual expansion of alpine desert over the extensive alpine steppe that we observed at the beginning of the late Holocene has also been reported from Lake Zigetang (Herzschuh et al., 2006a), Lake Kuhai (Wischnewski et al., 2011), Lake Donggi Cona (Wang et al., 2011) and Lake Hurleg (Zhao et al., 2007) (Figure 4-3). The correlations between pollen and the individual sedimentary proxies show marked fluctuations at low significance levels (Figure 4-5), which explains the rather low total variance compared to the later periods. Significant correlation phases could be identified for the lake system (TOC and TIC), the aeolian transportation (EM2), and the fluvial process (EM4), but none of these were persistent.

High A/C ratios together with low arboreal pollen content during this period are suggestive of relatively wet a condition, which is consistent with the results of previous investigations into the evolution of the Asian Summer Monsoon (ASM) (Dykoski et al., 2005; Wang et al, 2005a; Wang et al., 2010). During this period, the ASM was still undergoing an obvious retreat process. Such rapid climate change possibly caused strong fluctuations in regional vegetation compositions, reflected in the high compositional turnovers indicated by the DCCA (Figure 4-4c). The terrestrial and aquatic environments can exhibit different time-lags in their responses to these oscillations and periods of disequilibrium between climate and the ecosystems may then predominate, resulting in low correlations between pollen assemblages and the sedimentary proxies. Such an effect has been previously reported from a multi-proxy study on Lake Kuhai, in the northeastern part of the Tibetan Plateau, (Wischnewski et al., 2011).

(2) From 2400 to 900 cal a BP: gradual decrease in vegetation coverage

Minor fluctuations between alpine steppe and alpine desert are still obvious during this period, but they are characterized by lower amplitudes, which are also indicated by the lower compositional turnovers indicated by DCCA (Figure 4-4c). Rather stable environmental conditions have also been reported from nearby lakes on the basis of their pollen assemblage records (Liu et al., 2002b; Shen et al., 2005; Zhao et al., 2007; Wang et al., 2011; Wischnewski et al., 2011) and geochemical proxies (Ji et al., 2005; Mischke et al., 2009; Henderson et al., 2010).

Highly significant correlations between pollen assemblages and TOC characterize the period between 2400 and 1700 cal a BP, which has been assumed from the stalagmite record to have been a period with a relatively stable ASM (Dykoski et al., 2005; Wang et al., 2005a). Such stable conditions with relatively high effective moisture favored both the development of alpine steppe vegetation and primary productivity in the lake, resulting in the high concordance observed between the pollen assemblage and the TOC content. However,

following the sudden decrease in the strength of the ASM after 1700 cal a BP (Dykoski et al., 2005) the pollen assemblages show significant correlations with aeolian activity (EM3) and fluvial erosion (EM4). This suggests that changes in the moisture levels are only critical for vegetation change during times of generally high and stable moisture levels, such as during the periods of highly significant correlation between pollen assemblages and TOC that occurred from 3200 to 3400 cal a BP and 2000 to 1400 cal a BP (Figure 4-5b), when high A/C ratios were also determined (Figure 4-4a). In contrast, during periods with rather low moisture levels (such as after 1400 cal a BP) the vegetation became more sensitive to the extreme events and instabilities indicated by aeolian dust and fluvial input, rather than to the general climatic trends.

This argument is further supported by the variations in total pollen concentration. It has been previously established that, on the Tibetan Plateau, Chenopodiaceae has the highest pollen productivity (representation ability) of the common alpine taxa (Wang and Herzschuh, 2011). Thus, at the time of the switch from *Artemisia* to Chenopodiaceae which occurred at around 2800 cal a BP, the total pollen concentration also increased. Although the drier climatic conditions indicated by the expansion of alpine desert may have constrained the productivity of regional vegetation, the overall pollen productivity increased as a result of the appearance of the highly productive Chenopodiaceae plants. However, when another switch from *Artemisia* to Chenopodiaceae occurred at around 1500 cal a BP, the total pollen concentration decreased, which possibly indicates that even the growth of Chenopodiaceae plants was restricted due to extremely limited moisture availability. This theory may also be supported by the high content of arboreal pollen at this time, and in particular of pollen from *Pinus*, which is indicative of long-distance transport and is well represented during times of low local and regional pollen productivity. A reduced coverage of regional vegetation was probably responsible for the intensification of surface erosion by both the wind and surface runoff, producing the high levels of correlation observed between pollen assemblages and the EM3 and EM4 grain-size populations (Figure 4-5g, h). A critical threshold in the vegetation coverage may have been crossed, beyond which vegetation compositions were driven by sudden, severe climatic events rather than by general climatic changes.

(3) From 900 cal a BP to present: introduction of human impact as a main driver of vegetation change

The last 900 years have been characterized by a gradual expansion of alpine desert, replacing alpine steppes; this is indicative of a further decrease in effective moisture and is consistent with pollen results from the Qaidam Basin (Zhao et al., 2010), the stalagmite record (Wanxiang Cave, Zhang et al., 2008), and the precipitation index from Longxi (Tan et al., 2008). The lake's internal environmental factors, such as the TIC content, showed the highest levels of correlation with pollen assemblages. Since aragonite dominates the carbonate minerals of Lake Kusai and possibly has a biogenic origin (e.g., from ostracod shells) (Wang, 2008; Yao et al., 2011), the decreasing TIC content may relate to unfavorable living conditions for ostracods such as high salinity levels in the lake water, as has been reported for Lake Ulungur in northern China since 1200 cal a BP (Jiang et al., 2008; Mischke and Zhang, 2011).

The lowest total pollen concentration and the highest content of long-distance transported arboreal pollen (*Pinus*) were both recorded during this period, indicating a further decrease in regional vegetation coverage. Meanwhile, the lake's external environmental factors changed to coarser grain-size fractions as indicated by EM1 and EM2, particularly after 500 cal a BP (Figure 4-5d, e), indicating intensified aeolian activity and even dust storm events as a result of the reduced vegetation coverage, such as commonly occur in this region (Qiang et al., 2007a; Wang et al., 2009). Furthermore, modern ecosystem studies have shown that the introduction of human impacts would have reduced the climatic resilience of the alpine vegetation communities, leading to high correlations between vegetation changes and non-climatic severe events (Wang et al., 2004b).

Interestingly, the PROTEST analysis reveals different taxa interrelationships for the pollen records after 600 cal a BP from those for the earlier periods (Table 4-2). Given the low vegetation diversity in this part of the plateau, it is rather unlikely that an extensive plant species exchange (that is not visible in genus and family levels of pollen analyses) would be the cause of these changes in the interrelationships between pollen taxa. Human impacts on the vegetation are more likely to have altered the former inter-species relationships. Human impacts on marginal areas of the plateau have been inferred to extend back as far as 8800 cal a BP (Guo et al., 2006; Dearing et al., 2008; Meyer et al., 2009; Miehe et al., 2009). However, only one Neolithic archaeological site (at Chugong, 5 km from Lhasa), dated to around 3700 cal a BP, has been reported to date (Aldenderfer, 2007). Pollen records from lakes and peat in the eastern part of the plateau have, however, revealed increased grazing activities during the late Holocene, dating from about 3400 cal a BP in the Hengduan Mountains (Kramer et al., 2010b) and from about 2200 cal a BP in the Nianbaoyeze Mountains (Schlütz and Lehmkuhl, 2009). In addition, by synthesizing both pollen and non-pollen records from central Asia, Wang et al. (2010) reported that the pollen records have possibly been affected by human impacts during the last 1000 years. Humans appear to have only reached the northern parts of the Tibetan Plateau around 600 cal a BP, probably because of its remoteness and the extremes of weather (e.g., dust storms), leading to sustained changes in vegetation.

4.5.3 Underlying climatic mechanisms

As discussed above, the gradually decreasing A/C ratio and total pollen concentration, together with the increasing arboreal pollen content, indicate a gradual decrease in effective moisture during the late Holocene, which is generally consistent with previously reported results from the Tibetan Plateau and adjacent regions, e.g., Lake Zigetang (Herzschuh et al., 2006a), Lake Qinghai (Shen, et al., 2005), Lake Luanhaizi (Herzschuh et al., 2010a), Lake Yidun (Shen et al., 2006a), Lake Hidden and Lake Renco (Tang et al., 2000). In addition, synthesized moisture evolution for the monsoonal regions shows identical patterns during the late Holocene, illustrating a gradually decline in the ASM (Herzschuh, 2006; Wang et al., 2010), which is also recorded in Asian stalagmites (Dykoski et al., 2005; Wang et al, 2005a; Fleitmann et al., 2007) and in marine sediments from the Arabian Sea (Overpeck et al., 1996; Gupta et al., 2003). Changes in the climate on the northern Tibetan Plateau during the late Holocene were therefore probably a response to changes in the ASM system (Liu et al., 2009).

There is, however, no evidence in our pollen record for the increase in ASM intensity during the last few centuries that has been interpreted several times from stalagmites (Dykoski et al., 2005; Wang et al, 2005a; Fleitmann et al., 2007). Such signals might have become blurred by the parallel appearance of major human impacts on the vegetation. However, the A/C ratio yielded higher values at about 300 cal a BP, indicating a relatively wet phase that is temporally consistent with the Little Ice Age (LIA) (Figure 4-4) and which has also been detected in the pollen record from the Dunde ice core (Liu et al., 1998). An increase in effective moisture during the cool LIA has also been deduced from carbonate oxygen isotopes from Lake Qinghai, and was considered to be due to a reduction in evaporation caused by colder air temperatures and an increase in the relative importance of moisture-bearing westerlies (Henderson et al., 2010). In addition, our *Artemisia*–based time series analysis revealed a significant periodicity over 1512 years which is consistent with the 1500 year "Bond Cycle" from the North Atlantic (Bond et al., 2001). Despite the relatively short record that we have used, the obvious periodicities in both the A/C ratio and the pollen assemblages may indicate possible teleconnections between climate changes in central Asia and the North Atlantic, through the mid-latitude westerlies jet (Vandenberghe et al., 2006).

4.6 Conclusion

In summary, the susceptibility of late Holocene vegetation in the northern part of the Tibetan Plateau to various environmental triggers has changed over the course of time. Identical responses to climate changes have been identified in regional vegetation for periods under generally wet and stable conditions. Following a threshold for vegetation cover at around 1500 cal a BP, the vegetation response became more sensitive to severe events, which led to increases in the correlation with both aeolian and fluvial transportation. The extensive and large-scale impacts of humans on the natural ecosystems of the northern Tibetan Plateau appear not to have started until about 600 cal a BP. Our results therefore generally indicate that a variety of factors may have acted as drivers for the changes to former vegetation compositions, and that each of these various possibilities needs be taken into account when interpreting fossil pollen records.

Acknowledgements

The authors would like to thank Bo Yang (Institute of Salt Lakes, CAS) and Rong Wang (Nanjing Institute of Geography and Limnology, CAS) for their help during the field work. Janett Borkowski (University of Potsdam) is also acknowledged for her assistance in data handling. The research was supported by the Strategic Priority Research Program of the Chinese Academy of Sciences (Grant No. XDA05080403), the China Global Change Research Program (Grant No. 2010CB950101), the German Research Foundation (DFG), and the "Helmholtz - China Scholarship Council Young Scientist Fellowship".

5 Manuscript 4: Reassessment of Holocene vegetation change on the upper Tibetan Plateau using the pollen-based REVEALS model

Yongbo Wang[a, b], Ulrike Herzschuh[a, b]

[a] *Alfred Wegener Institute for Polar and Marine Research, Research Unit Potsdam, Telegrafenberg A43, 14473 Potsdam, Germany*

[b] *Institute of Earth and Environment Science, University of Potsdam, Karl-Liebknecht-Str.24, 14476 Potsdam, Germany*

Current Status: Published in "Review of Palaeobotany and Palynology" 2011, Vol. 168 Pages 31-40.

Abstract

Previous studies based on fossil pollen data have reported significant changes in vegetation on the alpine Tibetan Plateau during the Holocene. However, since the relative proportions of fossil pollen taxa are largely influenced by individual pollen productivities and the dispersal characteristics, such inferences on vegetation have the potential to be considerably biased. We therefore examined the modern pollen-vegetation relationships for four common pollen species on the Tibetan Plateau, using Extended R-value (ERV) models. Assuming an average radius of 100 m for the sampled lakes, we estimated the relevant source area of pollen (RSAP) to be 2200 m (which represents the distance from the lake). Using Poaceae as the reference taxa (Pollen Productivity Estimate, PPE = 1), ERV Submodel 2 derived relative high PPEs for the steppe and desert taxa: 2.079 ± 0.432 for *Artemisia* and 5.379 ± 1.077 for Chenopodiaceae. Low PPEs were estimated for the Cyperaceae (1.036 ± 0.012), whose plants are characteristic of the alpine *Kobresia* meadows. Applying these PPEs to four fossil pollen sequences since the Late Glacial, the plant abundances on the central and north-eastern Tibetan Plateau were quantified using the "Regional Estimates of Vegetation Abundance from Large Sites" (REVEALS) model. The proportions of *Artemisia* and Chenopodiaceae were greatly reduced compared to their original pollen percentages in the reconstructed vegetation, owing to their high productivities and their dispersal characteristics, while Cyperaceae showed a relative increase in the vegetation reconstruction. The reconstructed vegetation assemblages of the four pollen sequence sites always yielded smaller compositional species turnovers than suggested by the pollen spectra, as revealed by Detrended Canonical Correspondence Analyses (DCCA) of the Holocene sections. The strength of the previously reported vegetation changes may therefore have been overestimated, which indicates the importance of taking into account pollen-vegetation relationships when discussing the potential drivers (such as climate, land use, atmospheric CO_2 concentrations) and implications (such as for land surface-climate feedbacks, carbon storage, and biodiversity) of vegetation change.

5.1 Introduction

Changes in vegetation (or land cover) have been widely interpreted from fossil pollen data in the high alpine region of the Tibetan Plateau, in terms of response to, and feedback with, climate change (e.g. Yasunari, 2006; Shen et al., 2008; Herzschuh et al., 2010b, 2011). Sun and Chen (1991) reported vegetation fluctuations during the mid Holocene through a synthesis of ten pollen sequences from the Tibetan Plateau. More recently, Zhao et al. (2009) argued that vegetation in the highland meadow/steppe region of the Tibetan Plateau had changed from steppe forest/meadow to meadow/steppe, following a review of several pollen records from lacustrine sediments and wetlands. In particular, the replacement of *Artemisia*-dominated alpine steppe by *Kobresia* -dominated high alpine meadow during the mid-Holocene has been indicated by various long term lacustrine pollen records (Shen et al., 2003, 2008; Herzschuh et al. 2009, 2011; Tang et al., 2009). However, the reason for this apparent mid-Holocene expansion of *Kobresia* meadows remains a matter of debate: apart from climatic forcing (Shen et al., 2008; Herzschuh et al., 2009) it has also been interpreted as being a response to nomadic herding on the Tibetan Plateau (Miehe et al., 2009; Schlütz and Lehmkuhl, 2009), and a recent hypothesis has pointed out the possibility of changes in atmospheric CO_2 concentration acting as a driving force for changes in vegetation composition (Herzschuh et al., 2011). However, the real strength of vegetation change (rather than using pollen as a proxy) has not been quantified to date.

The relationship between pollen and vegetation is not straightforward. The relative percentages of pollen taxa in the recovered pollen assemblages are biased by differences in pollen productivities between different plant taxa and species-specific dispersal-deposition processes (Prentice, 1985; Sugita, 1993). The development of a theoretical framework and models of pollen-vegetation relationships over recent decades, however, means that quantitative vegetation/landscape reconstructions are now feasible (Davis, 1963; Andersen, 1970; Parsons and Prentice, 1981; Prentice and Parsons, 1983; Prentice 1985; Sugita, 1994; Jackson et al., 1995; Jackson and Lyford, 1999). The Extended R-value (ERV) model has been used to produce pollen productivity estimates (PPEs) for key plant taxa and corresponding relevant source areas of pollen (RSAP) from Europe (e.g. Nielsen and Sugita, 2005; Broström et al., 2008; Mazier et al., 2008; Soepboer et al., 2008) and Africa (Duffin and Bunting, 2008).

As a part of the “Landscape Reconstruction Algorithm” (LRA) approach proposed by Sugita (Sugita et al., 1999; Sugita, 2007a, 2007b), the “Regional Estimates of VEgetation Abundance from Large Sites” (REVEALS) model was developed to predict regional vegetation abundance from pollen assemblages recorded in large lakes (Sugita, 2007a). As a new method to quantitatively reconstruct the past vegetation composition, the REVEALS model has been applied and validated in Denmark (Nielsen and Odgaard, 2010), in Sweden (Hellman et al., 2008a, 2008b), on the Swiss Plateau (Soepboer et al., 2010), and in North America (Sugita et al., 2010).

In contrast to the well investigated European area there is a paucity of information on pollen-vegetation relationships on the vast Asian continent, except for results from northern

China published recently by Li et al., (2011). Using the pollen representation method introduced by Andersen (1970), Herzschuh et al. (2003, 2006a) produced preliminary results concerning pollen productivity for some desert plants on the Alashan Plateau. Based on investigations of modern pollen assemblages from the Tibetan Plateau and the Qaidam Basin, Zhao and Herzschuh (2009) and Wei et al. (2011) drew general conclusions on over-representation (e.g. *Artemisia*, Chenopodiaceae and *Ephedra*), and under-representation (e.g. Cyperaceae). However, for estimating pollen productivities the pollen dispersal-deposition process and the distance weighting for modern vegetation data were ignored in these studies. An urgent need remains for a better understanding of the pollen-vegetation relationships in this region in order to better understand the vulnerability of Tibetan vegetation to past and future changes in climate, land-use, and atmospheric CO_2 concentrations.

In this study we introduce the REVEALS model to High and Central Asia, presenting a modern pollen-vegetation calibration dataset from the alpine meadow/steppe dominated region on the north-eastern Tibetan Plateau as well as its application to four pollen records recovered from lacustrine sediments in Lake Donggi Cona, Lake Kuhai, Lake Koucha and Lake Zigetang. Our objectives were (1) to obtain the pollen productivities of key plant taxa in the alpine steppe and alpine meadow dominated Tibetan Plateau, and (2) to quantitatively evaluate the vegetation changes that occurred on the Tibetan Plateau area during the Holocene.

5.2 Study area

The Tibetan Plateau covers an area of 2.3 million km^2 in the south-western part of China between 80-105°E and 27-37°N, and is mostly over 4000 m above sea level (a.s.l.). Influenced by the Asian Summer Monsoon systems, both temperature and precipitation generally decrease from south-east to north-west (Sun, 1999).

Owing to its high elevation the plateau is mainly covered by high alpine vegetation, except for the coniferous forests distributed along its south-eastern margin (Hou, 2001) (Figure 5-1A). The north-eastern part of the plateau is covered by subalpine scrub (e.g. *Salix*, *Potentilla*, *Rhododendron*, *Lonicera*, *Caragana* and *Berberis*) and alpine meadows consisting of various *Kobresia* species, such as *K. pygmaea*, *K. humilis*, and *K. capillifolia*, which generally make up over 50% of the local vegetation; Poaceae plants (mainly *Stipa purpurea*) commonly make up a further 5-10% and *Artemisia* (e.g. *A. gmelinii*, *A. argyi*) and Chenopodiaceae (e.g. *Chenopodium hybridum*) have abundances below 1% (Table 5-2). The central part of Tibetan Plateau comprises temperate steppe dominated by a mixture of Cyperaceae (ca. 10%), Poaceae (ca. 20-30%) and *Artemisia* (ca. 3%). Only a limited amount of moisture reaches the north-western part of the plateau resulting in the development of temperate desert, dominated by Chenopodiaceae species accompanied by *Artemisia*, Poaceae, *Ephedra* and *Nitraria* (Wu, 1995; Kürschner et al., 2005; Wang et al., 2006).

Four lakes have been investigated in this study, one (Lake Koucha) from the alpine meadow zone and three (Lake Kuhai, Lake Donggi Cona and Lake Zigetang) from the transitional

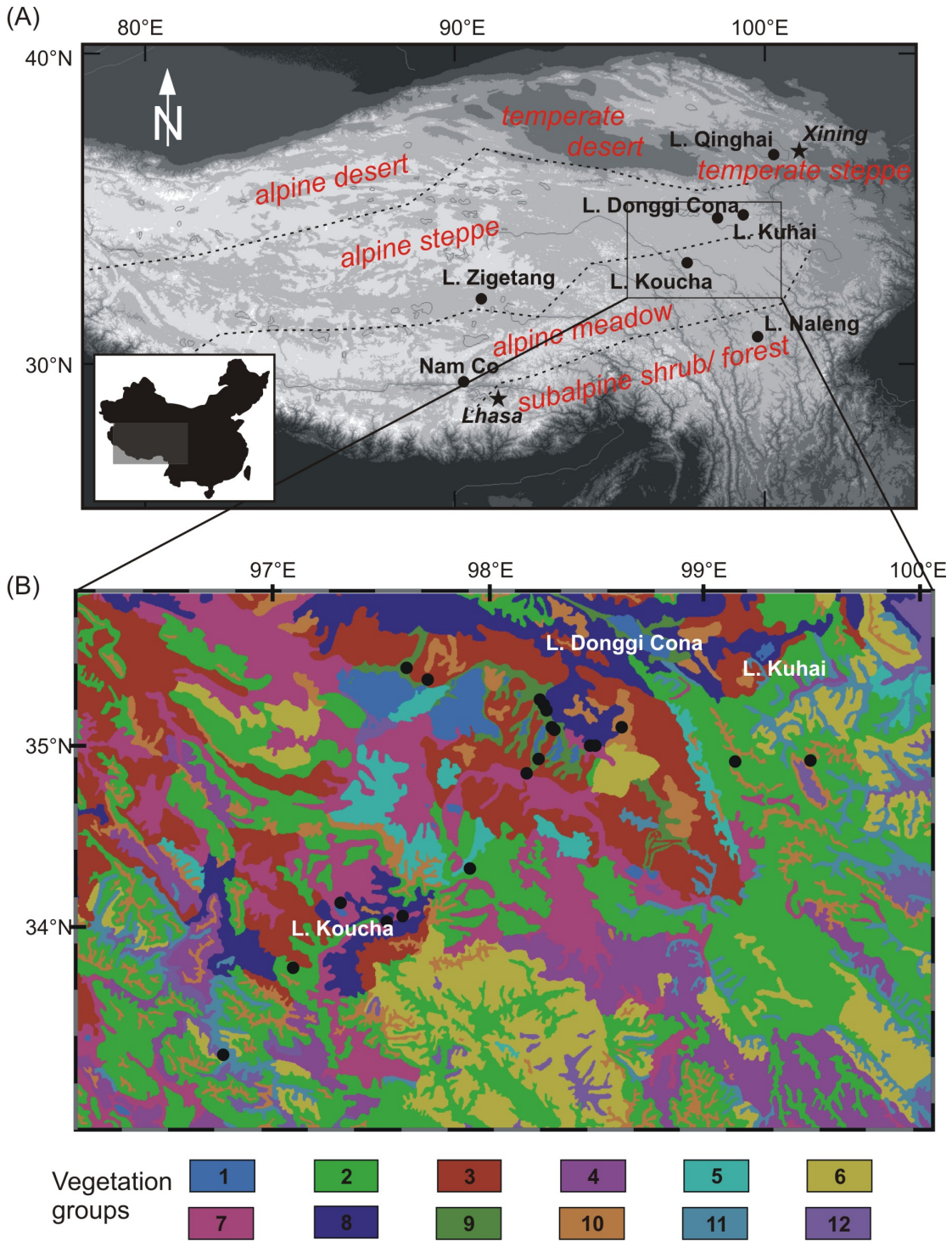

Figure 5-1 A: Distribution of the main vegetation types on the Tibetan Plateau (modified from Hou et al., 2001) together with the locations of the lakes mentioned in the text. B: Reclassified vegetation groups on the north-eastern Tibetan Plateau and the locations of modern pollen samples used for estimating pollen-vegetation relationships. Vegetation groups: 1, Water bodies; 2, Kobresia pygmaea meadow; 3, Kobresia pygmaea, Stipa purpurea meadow; 4, Kobresia pygmaea, Polygunum sphaerastachyum meadow; 5, Kobresia humilis meadow; 6, Kobresia capillifolia meadow; 7, Kobresia spp. Carex spp. Meadow; 8, Stipa purpurea steppe; 9, Poa spp. Meadow; 10, Sparse vegetation; 11, Scrub; 12, others (detailed compositions of each vegetation group are listed in Table 5-2).

Table 5-1 Information on fossil pollen records (Lake Koucha, after Herzschuh et al., 2009; Lake Kuhai, after Wischnewski et al., 2011; Lake Donggi Cona, after Wang et al., 2011; Lake Zigetang, after Herzschuh et al., 2006a).

Lake	Location	Elev.	Area (km^2)	Region	Vegetation	Dating[c]	Pollen[d]
Lake Koucha	34.0°N, 97.2°E	4540	20	NETP[a]	alpine meadow	5	66
Lake Kuhai	35.3°N, 99.2°E	4150	41	NETP	alpine meadow / alpine steppe	17	60
Lake Dongi Cona	35.22-35.83°N, 98.33-98.75°E	4090	230	NETP	alpine meadow / alpine steppe	17	77
Lake Zigetang	32.0°N, 90.9°E	4560	190	CTP[b]	alpine meadow / alpine steppe	5	69

NETP[a]: north-eastern Tibetan Plateau CTP[b]: central Tibetan Plateau

Dating[c]: number of samples dated Pollen[d]: number of pollen samples counted

zone between alpine meadow and alpine steppe (see details in Figure 5-1A and Table 5-1).

Lake Koucha (34.0°N, 97.2°E; 4540 m a.s.l.) is a freshwater lake on the eastern Tibetan Plateau, with a maximum depth of about 6 m and covering an area of ca. 20 km^2. The mean annual precipitation is 469 mm and the mean annual temperature 4.4 °C, according to records from the nearest meteorological station at Chengduo. The immediate vicinity of Koucha Lake to the south and east is covered by various types of *Kobresia* meadows, which consist mainly of Cyperaceae, Poaceae and sparse *Artemisia*. To the north, *Stipa purpurea* steppes dominate, containing higher proportions of Poaceae and *Artemisia* (Herzschuh et al., 2009).

Lake Kuhai (35.3°N, 99.2°E; 4150 m a.s.l.) is a closed basin saline lake situated to the north of the Anemaqin Mountain and covering about 41 km^2, with a maximum depth of 20.6 m. The closest climate station is Madoi (4272 m a.s.l.), 100 km south-west of Lake Kuhai, which has a mean July temperature of 7.8 °C, a mean January temperature of -15.9 °C, and a mean annual temperature of -3.1 °C. The mean annual precipitation, which is primarily restricted to the summer months, is about. 310 mm. The dominant vegetation surrounding the lake today comprises mainly taxa of *Kobresia pygmaea* and *Stipa purpurea* forming high-alpine meadows, with patches of alpine shrubs (*Salix orithrepha*, *Saussurea spp*. and *Potentilla-type*) to the south-east (Wischnewski et al., 2011).

Lake Donggi Cona (35.22-35.83°N, 98.33-98.75°E; 4090 m a.s.l.), which covers an area of about 230 km^2, is located on the north-eastern part of Tibetan Plateau, to the north-west and east of the Anemaqin and Kunlun mountain ranges, respectively. The mean annual temperature is -3.0 °C, with mean January and July temperatures -15.9 °C and 7.8 °C respectively. Mean annual precipitation is 311 mm, of which 76% occurs during the monsoon season (June, July, August and September). The vegetation consists mainly of alpine meadows and steppes dominated by *Kobresia (*Cyperaceae*)*, *Artemisia*, and Poaceae, together with patches of alpine shrubs (*Salix*, *Caragana* and *Potentilla*) (Wang et al., 2011).

Lake Zigetang (32.0°N, 90.9°E; 4560 m a.s.l.) is located in a closed basin on the central Tibetan Plateau and has a salinity of 266 g/l. The lake has a surface area of about 190 km^2 and

a maximum depth of about 40 m. Mean annual precipitation and temperature at the nearby Bange meteorological station (4700 m a.s.l.) are 320 mm and 0.3 °C, respectively. The region is covered by alpine steppe vegetation on the plains and high-alpine *Kobresia* meadows in the nearby Tanggula Mountains (Herzschuh et al., 2006a).

5.3 Data and model settings

5.3.1 Pollen data

A modern pollen dataset originally presented in Herzschuh et al. (2010b) was used to estimate the modern pollen-vegetation relationship for the alpine meadow/steppe of the north-eastern Tibetan Plateau area. In total, 19 lakes with radii of around 100 m were selected on the north-eastern Tibetan Plateau, keeping the distance between any two lakes to greater than 2 km (Figure 5-1B) in order to avoid an "auto-correction effect" between samples.

Pollen samples were treated and analysed following standard laboratory methods, including treatment with hydrogen chloride (HCl, 10%), potassium hydroxide (KOH, 10%), and hydrofluoric acid (HF, 50%), as well as acetolysis, fine sieving (with 7 µm mesh in an ultrasonic bath), and mounting in glycerine (Fægri and Iversen, 1989). Two tablets of Lycopodium spores were added to the fossil samples for estimation of absolute pollen concentrations. The identification of pollen types was based on relevant published literature (Moore et al., 1991; Wang et al., 1997; Beug, 2004).

To access the Holocene vegetation history of the Tibetan Plateau four fossil pollen sequences, from the alpine meadow zone and the transitional zone between alpine meadow and alpine steppe, were selected covering the Late Glacial and Holocene periods (ranging between ca. 12,000 and 20,000 cal yrs BP). These sequences have been previously analyzed and discussed mainly in terms of climatic changes: Lake Koucha by Herzschuh et al. (2009), Lake Kuhai by Wischnewski et al. (2011), Lake Donggi Cona by Wang et al. (2011b), and Lake Zigetang by Herzschuh et al. (2006b).

5.3.2 Present day vegetation

The distribution and composition of modern vegetation types are fundamental variables in the establishment of pollen-vegetation relationships. The classification and distribution of modern vegetation types were derived from the vegetation atlas of China (1:1,000,000) (Hou, 2001), assisted by the "Spatial Analyses Tools" in the ArcMap 9.2 program (Johnston et al., 2001). Owing to the regional moisture gradient and local elevation differences, the relevant area on the north-eastern Tibetan Plateau contained a complex of 43 vegetation types that were assigned to 12 higher vegetation type groups according to their ecological similarities (Figure 5-1B, Table 5-2). The abundances of the target taxa in each vegetation type grouping were inferred from field measurements (by Herzschuh U., presented in Kürschner et al., 2005) and previously published results from vegetation surveys (Zhou et al., 1986; Wu et al., 1995; Wang et al., 2006; Miehe et al., 2008).

Table 5-2 Reclassified vegetation groups and the corresponding compositions for the north-eastern Tibetan Plateau area (see distributions in Figure 5-1B).

No	Name	Vegetation code[a]	Perc.[b]	Cove.[c]	A[d]	Ch[e]	P[f]	Cy[g]	References
0	Bare	bd	0	0	-	-	-	-	-
1	Water bodies	hl	1.7	0	-	-	-	-	-
2	*Kobresia pygmaea* meadow	486a, 486a+487	28.4	100	1	0.5	8.1	63.3	Wu et al., 1995; Kürschner et al., 2005; Wang et al., 2006; Miehe et al., 2008
3	*Kobresia pygmaea, Stipa purpurea* meadow	486b, 486c	14.2	100	1	0.5	7.0	63.6	Wu et al., 1995; Kürschner et al., 2005; Wang et al., 2006
4	*Kobresia pygmaea, Polygunum sphaerastachyum* meadow	486d	7.3	100	1	0.5	5.9	53.7	Kürschner et al., 2005; Wang et al., 2006
5	*Kobresia humilis* meadow	487	2.7	90	1	0.5	5	50	Wu et al., 1995; Kürschner et al., 2005
6	*Kobresia capillifolia* meadow	488a,488b,488c	10.8	100	1	0.5	7	65	Zhou et al., 1986; Kürschner et al., 2005
7	*Kobresia* spp. meadow	493, 493a, 493a+486a	12.6	100	1	0.5	5.4	43.8	Kürschner et al., 2005; Wang et al., 2006
8	*Stipa purpurea* steppe	405a, 405a+486a	6.9	47	2.8	0.5	32.5	0	Zhou et al., 1986; Kürschner et al., 2005; Wang et al., 2006
9	*Poa* spp. meadow	497a	1.6	73	2.5	0.5	19.5	12.37	Kürschner et al., 2005; Wang et al., 2006
10	Sparse vegetation	536, 543, 544	6.2	40	1	0.5	5	5	Wu et al., 1995; Kürschner et al., 2005
11	Scrub	233, 233a, 234, 238	4.9	100	1	0.5	5	2 5	Wu et al., 1995; Kürschner et al., 2005
12	others	*20 types*	2.7	100	1	0.5	5	1 5	Wu et al., 1995; Kürschner et al., 2005

a: vegetation codes are according to Hou, 2001 b: percentage of each vegetation group in the regional vegetation; c: coverage of each vegetation group;
d: Artemisia e: Chenopodiaceae; f: Poaceae; g: Cyperaceae.

5.3.3 Model settings

Four major taxa that reached sufficiently high abundances in both the vegetation and the pollen assemblages were selected for investigation of their pollen-vegetation relationships, these being Chenopodiaceae, *Artemisia*, Poaceae and Cyperaceae, which together generally make up over 80% of both the modern and the fossil pollen assemblages. For modeling purposes, the percentages were recalculated including only these four species in the pollen sum. The grain size was measured on 30 randomly selected pollen grains from each taxon and the mean values used for the calculations of fall speed following Stoke's Law (Gregory, 1973) (Table 5-3). Poaceae was chosen as the reference taxon because of its common appearance in modern vegetation and in both modern and fossil pollen spectra, as well as its well-defined morphology and its utilization in previous studies (e.g. Herzschuh et al., 2003; Broström et al., 2008; Mazier et al., 2008; Zhao and Herzschuh, 2009).

The ERV model with three submodels was developed to estimate pollen productivity for individual taxa (Parsons and Prentice, 1981; Prentice and Parsons, 1983; Sugita, 1994). One taxon is set to unity and the PPE of the other taxa are calculated relative to this reference taxon. The submodels differ in their assumptions about the background pollen component. ERV Submodels 1 and 2 (Parsons and Prentice, 1981; Prentice and Parsons, 1983) are designed for datasets in which both pollen and vegetation data are expressed as percentages. ERV Submodel 1 assumes that the background pollen percentage is constant for individual taxa, whereas ERV Submodel 2 assumes that the ratio of background pollen loading to the total plant abundance within the survey area is constant for individual taxa. ERV Submodel 3 (Sugita, 1994) is used when the pollen data are expressed in percentages but the vegetation data in absolute values; the model assumes constant background pollen loading. All three submodels can be used for any dataset and should give comparable results provided the background pollen loading is low compared to the total pollen loading.

The size of the pollen source area reflected in pollen assemblages from similarly-sized lakes varies from region to region, depending mainly on the spatial distributions (local and regional) and sizes of vegetation patches (Sugita, 1994; Bunting et al., 2004; Broström et al., 2005; Nielsen and Sugita 2005; Mazier et al., 2008). Sugita (1994) proposed the ‘‘relevant source area of pollen’’ (RSAP) as a sound theoretical definition of the spatial scale of vegetation represented by pollen assemblages. The RSAP can be defined as the distance at which the goodness-of-fit of the pollen-vegetation relationship to the model (e.g. ERV submodels) no

Table 5-3 Grain size and corresponding fall speed for four pollen species.

Pollen species	No.	Pollen Radius (μm)			FS[c]	Pollen Productivity Estimate			
		Max.	Min.	Mean	(m/s)	mod-1	S.D.	mod-2	S.D.
Artemisia	30	11.67	6.67	9.11	0.0101	2.079	0.432	3.267	0.628
Chenopodiaceae	30	13.33	6.67	9.75	0.0117	5.442	1.225	5.379	1.077
Poaceae	30	20.00	9.17	12.31	0.0185	1	0	1	0
Cyperaceae	30	25.00[a] 18.33[b]	15.00[a] 11.67[b]	17.69[a] 15.03[b]	0.0291	1.036	0.012	0.66	0.021

a: long axis; b: short axis; c: pollen fall speed, according to Stoke's Law (Gregory, 1973).

longer improves (Sugita, 1994). This also means that the differences in pollen abundance between similarly-sized sites represent differences in plant abundance within the RSAP, superimposed on a constant pollen background coming from beyond the RSAP (Sugita, 1994, 2007b). The RSAP has been estimated in previous studies for various basin sizes and vegetation types, using both empirical and simulated pollen-vegetation datasets (Sugita, 1994; Calcote, 1995; Sugita et al., 1999; Bunting et al., 2004; Broström et al., 2005; Nielsen and Sugita, 2005; Mazier et al., 2008).

For calculation of PPEs and RSAP the vegetation data for each taxon was distance-weighted for each distance increment. The vegetation map was processed using PolFlow in the HUMPOL software package (Bunting and Middleton, 2005) and vegetation data for 25 m wide rings around each sampling point was extracted up to a distance of 5000 m. Cumulative distance-weighted plant abundances were calculated for each site using different methods: d^{-1}, d^{-2}, Prentice's model (Prentice, 1985), and the Ring Source model (Sugita, 1993). Extended R-value (ERV) analysis was carried out using Submodels 1 and 2 in the ERV-V7.2 program (Sugita, unpublished), together with other parameters such as pollen fall speed (see above), a wind speed of 3 m/s (5 m/s was also used to test the potential influence of wind speed on the model results), and a lake basin radius of 100 m. ERV Submodel 3 was not processed because of its requirement for absolute vegetation abundance data.

The key assumption of the REVEALS model is that the regional vegetation composition for each taxon is expressed as the ratio of the pollen counts for each taxon weighted by its pollen productivity and dispersal characteristics, to the total sum for all taxa. Simulations suggest that the distance representing the regional vegetation can be set to between 50 and 400 km away from the lake (Sugita, 2007a). When sites are more than 100 ha in size the site-to-site variation in pollen assemblages is small, even when the vegetation is very patchy and heterogeneous (Sugita, 2007a; Hellman et al., 2008). We refer to Sugita (2007a) for more detailed descriptions of the model.

The PPEs and corresponding "variance and covariance matrix" derived from the ERV models were subsequently applied to the vegetation reconstructions based on fossil pollen sequences recovered from the four large lakes. Using the original pollen counts for the four pollen taxa, together with corresponding calibrated ^{14}C ages (cal a BP), the former regional vegetation abundances up to 400 km away from the sampling sites were calculated with the REVEALS V4.2.2 program (Sugita, unpublished), using the lake model (Sugita, 1993).

5.3.4 Ordination analysis

As a constrained or canonical form of Detrended Correspondence Analysis (Hill and Gauch, 1980), Detrended Canonical Correspondence Analysis (DCCA) (ter Braak, 1986) has been widely used to estimate compositional changes of ecological data (Birks, 2007). DCCA was able to directly scale the sample scores on the ordination axes in standard deviation unit of composition change or turnover as the beta diversity (Birks, 2007; McCune and Grace, 2002; Velland, 2001). In order to estimate the amount of compositional species turnover along gradients in time, DCCA was applied to both the fossil pollen and corresponding

reconstructed vegetation data from the four sites, always including percentages of the four target taxa. The DCCA was implemented using CANOCO 4.5 software (ter Braak and Smilauer, 2002). We restricted our investigation to the Holocene period (the last ~12 cal ka BP) in order to allow comparisons to be made between all four lakes.

5.4 Results

5.4.1 Pollen fall speed, Relevant Source Area of Pollen, and Pollen Productivity Estimates

The calculated fall speeds for the four selected pollen species were found to vary with the pollen grain size: the fall speeds for *Artemisia* (0.0101 m/s) and Chenopodiaceae (0.0117 m/s) were almost identically low owing to the small size of their pollen grains (9.11 μm and 9.75 μm respectively), Poaceae had moderate values for both fall speed (0.0185 m/s) and pollen grain size (12.31 μm), and Cyperaceae, which is the species with the largest pollen grains (15.03-17.69 μm), showed the highest fall speed of 0.0291 m/s (Table 5-3).

As shown in Figure 5-2A, the likelihood scores obtained using four distance weighting methods show slightly different patterns in which the d^{-2} based results reach the asymptote at distance about 2200 m from the lakes. Despite variations in the absolute values, results from the other three methods (d^{-1}, Prentice's model and Sugita's model) all show the lowest values at a distance of approximately 2200 m, even though they never reach an asymptote. Thus 2200 m was subsequently determined to define the relevant source area of pollen and was used for further modeling in combination with the d^{-2} distance weighting method. In addition, results based on 5 m/s wind speed parameter, show similar patterns and yield identical RSAP estimates (Supplementary, Figure 5-5).

Based on the ERV Submodels 1 and 2, comparable PPEs were estimated for the RSAP of 2200 m (Figure 5-2B, Table 5-3). Chenopodiaceae shows the highest productivities of the four pollen species for the both submodels (5.442±1.225 and 5.379±1.007, respectively). Moderate

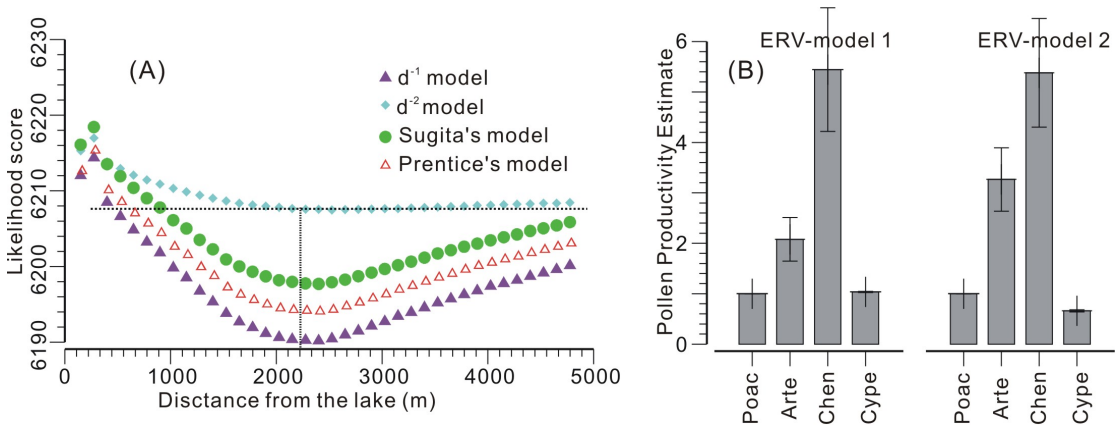

Figure 5-2 A: Likelihood scores and distance from lakes derived using four distance weighting methods. B: ERV model deduced PPEs for four major pollen taxa (left, ERV Submodel 1; right, ERV Submodel 2).

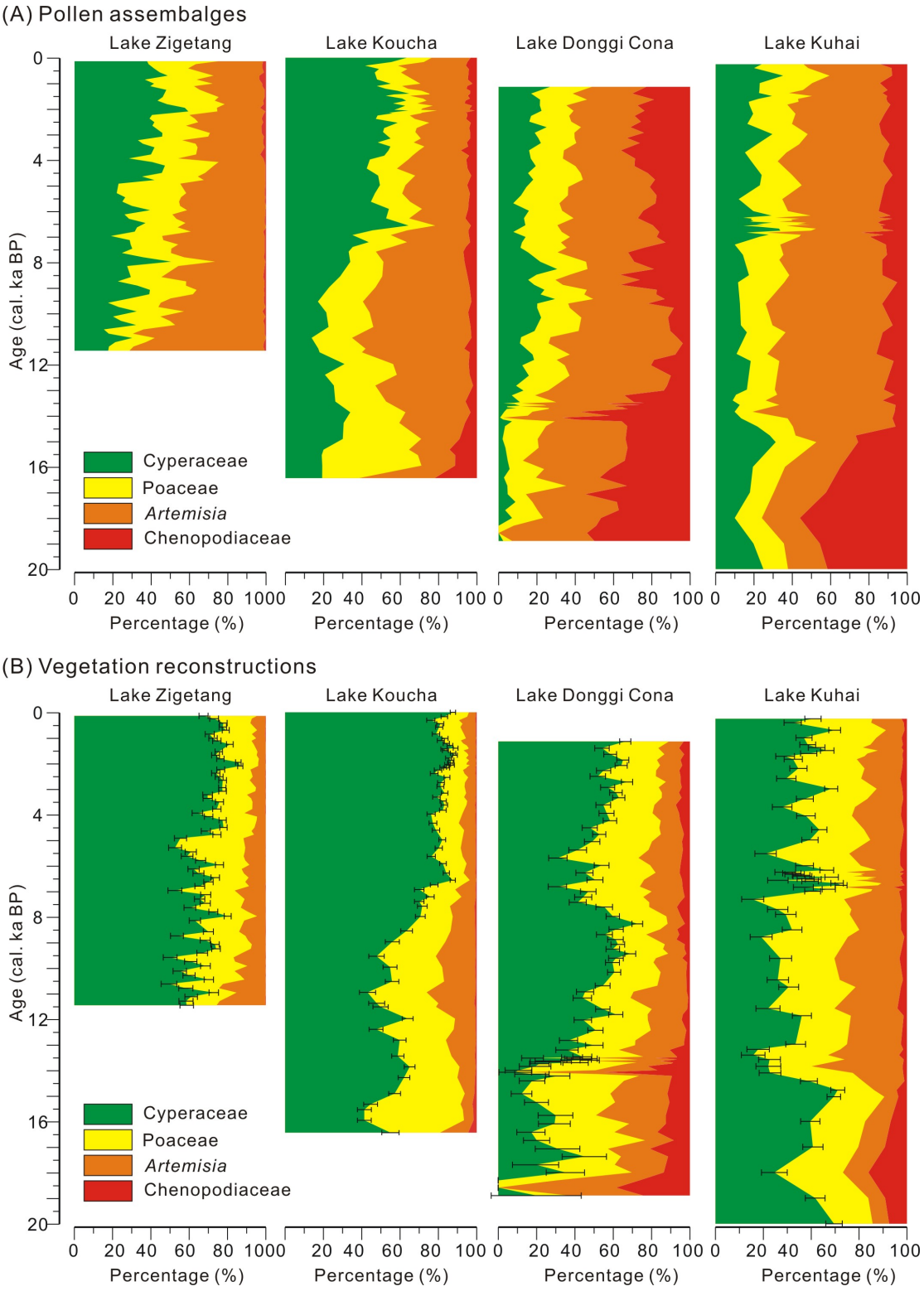

Figure 5-3 A: Percentages of the four most common pollen taxa (Cyperaceae, Poaceae, *Artemisia*, and Chenopodiaceae) from Lake Zigetang (after Herzschuh et al., 2006a), Lake Koucha (after Herzschuh et al., 2009), Lake Donggi Cona (Wang et al., 2011) and Lake Kuhai (Wischnewski et al., 2011). B: REVEALS model based vegetation reconstructions using PPEs from ERV Submodel 2, where horizontal error bars indicate the standard errors of Cyperaceae reconstructions.The other three taxa show similar standard errors to Cyperaceae, which are not shown here.

PPE values were estimated for *Artemisia* (3.267±0.628 and 2.079±0.432, respectively), while Cyperaceae (0.66±0.021 and 1.036±0.012 respectively) had productivities slightly lower than, or similar to, Poaceae.

5.4.2 Vegetation reconstructions

The reconstructed vegetation composition based on the REVEALS model, shows identical trends to the pollen assemblages (Figure 5-3 for ERV Submodel 1 derived PPEs and supplementary Figure 5-6 for ERV Submodel 2 based PPEs). Poaceae represents similar proportions in both the pollen and vegetation data, ranging between 20% and 40%. Because of its low pollen productivity the dominant taxon for the alpine *Kobresia*-meadows, Cyperaceae, is far better represented in the reconstructed vegetation than in the pollen assemblages. In contrast, the alpine steppe/desert components, i.e. *Artemisia* and Chenopodiaceae, have reconstructed contributions to vegetation that are substantially lower than in the original pollen assemblages due to their high productivities (Figure 5-3).

Extremely high proportions of desert pollen (Chenopodiaceae, up to 40%) in the Late Glacial period (before 12 cal ka BP) have been identified from the two northern lakes (Kuhai and Donggi Cona), but the proportions appear to have been much lower (about 10%) in the reconstructed vegetation (Figure 5-3). In contrast, the abundance of Cyperaceae was 20% in the pollen assemblages from the Koucha and Kuhai lakes compared to around 60% in the reconstructed vegetation surrounding them. Slightly lower proportions of alpine meadow were inferred for the Lake Donggi Cona area because of its lower Cyperaceae pollen component. Furthermore, relatively high standard errors were also estimated for the Late Glacial period, especially for Lake Donggi Cona and Lake Kuhai (Figure 5-3B).

More accurate reconstructions were estimated for the Holocene period, as indicated by the lower standard errors (Figure 3B). With the advent of the Holocene the proportion of Chenopodiaceae pollen in the pollen spectra decreased and the desert component in the vegetation reconstructions fell to 5-10% for the northern lakes (Lake Kuhai and Lake Donggi Cona) and have only low coverage in the vegetation reconstructions for the Lake Koucha and Lake Zigetang regions. Alpine *Kobresia*-meadow dominated the regional vegetation, making up about 50% of the total in the Lake Kuhai and Lake Donggi regions, 80% in the Lake Zigetang region, and up to 90% in the Lake Koucha region (Figs. 5-3 and 5-4). Slight expansions in alpine *Kobresia*-meadow since the early mid-Holocene were also indicated on the extensive alpine steppes, in all the records.

5.4.3 Compositional species turnovers in pollen assemblages and vegetation reconstructions

The results of the DCCA analyses for both the pollen and vegetation data during the Holocene are summarized in Table 5-4 in terms of the length of gradient on the first axis (in Standard Deviation, S.D. units), the total inertia (= variance) of each sequence, and the estimated species turnover (in S.D. units). The estimated species turnover is a measure of the total

amount of change in the pollen or vegetation datasets along the time gradient. For the Holocene records, compositional species turnovers were all below 1 S.D. in both the pollen and vegetation data, although these may have been underestimated because we restricted our research on the four common taxa. Nevertheless, higher values were always estimated for the

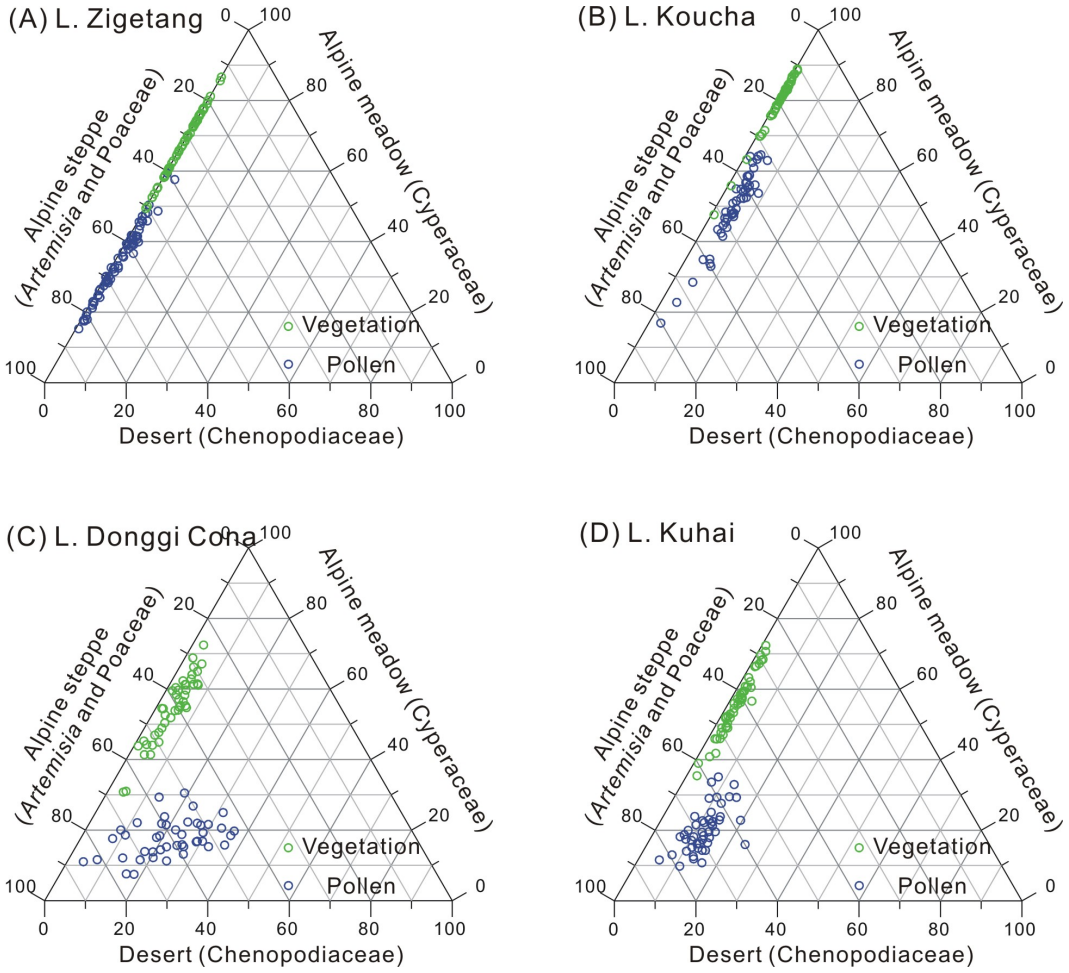

Figure 5-4 Holocene vegetation compositions deduced from the original pollen percentages and the REVEALS reconstructions (all values in percentage). The scattered distributions of pollen data indicate rather stronger compositional turnovers than those in the vegetation reconstructions.

Table 5-4 Results of species turnover calculations based on Detrended Canonical Correspondence Analyses for the four Holocene pollen records using both the pollen and vegetation data.

Lake	Duration	Data	Turnover (S.D.)	Inertia	Turnover per ka (10^{-2} S.D.)
Lake Koucha	0 - 11522	Pollen	0.672	0.086	5.832
		Vegetation	0.507	0.078	4.400
Lake Kuhai	0 - 11863	Pollen	0.476	0.126	4.012
		Vegetation	0.231	0.073	1.947
Lake Donggi Cona	1034 - 11815	Pollen	0.387	0.077	3.590
		Vegetation	0.198	0.054	1.837
Lake Zigetang	0 - 11442	Pollen	0.528	0.082	4.615
		Vegetation	0.321	0.053	2.805

pollen assemblages (0.672, 0.476, 0.387 and 0.528) than for the reconstructed vegetation data (0.507, 0.231, 0.198 and 0.231), as well as high inertia, indicating rather stronger species turnovers among pollen assemblages. Among the four lakes, species turnover rate was the highest for Lake Koucha (5.832, 4.400 10^{-2} S.D. per ka), intermediate for Lake Zigetang (4.615, 2.805 10^{-2} S.D. per ka) and relatively low for Lake Kuhai (4.012, 1.947 10^{-2} S.D. per ka) and Lake Donggi Cona (3.590, 1.837 10^{-2} S.D. per ka). In addition, the pollen assemblage data show rather scattered patterns compared to the vegetation reconstructions (as shown in Figure 5-4), which also indicates higher compositional turnovers.

5.5 Discussion

5.5.1 Critical assessment of the data

When designing and applying the pollen-vegetation models we were aware of the following limitations that had the potential to reduce the robustness of our vegetation reconstructions:

a) *Modern vegetation data*: The distribution and composition of modern vegetation are fundamental information used in deriving the PPEs and RSAP (Bunting and Hjelle, 2010), but owing to the remoteness of most of the Tibetan Plateau rather few detailed regional vegetation studies are available. However, using vegetation maps instead has been shown to produce reliable results in previous studies (e.g. Nielsen and Sugita, 2005).

b) *Site selections*: Ideally the modern pollen sample sites used for estimating the pollen-vegetation relationships should be randomly selected within the study area which, due to geographic constraints, is impossible when using pollen assemblages derived from lake sediments. To avoid potential influences on the RSAP estimates (Broström et al., 2005) samples sites were selected with over 2 km separation. Furthermore, since our samples were collected from the transitional zone between alpine steppe and alpine desert, the variations in vegetation composition may also lead to potential uncertainties for the PPE and RSAP estimates, which may also be possible the reason why the distance weighting methods (except for the d^{-2} model) do not reach the typical asymptotes.

c) *Variations in PPEs*: The REVEALS modeling approach assumes that PPEs of the pollen taxa show no spatial or temporal variances, and that the pollen productivity of single taxon is unaffected by environmental changes (Broström et al., 2008) such as changes in climate, atmospheric CO_2 concentration, or soil development. However, since we used pollen taxa representing the species-rich genus *Artemisia* or whole plant families, the species composition in modern vegetation varies between the different vegetation types and most probably also varied in the past. Applying the REVEALS model, however, we assume constant PPEs through time which has the potential to introduce errors in the vegetation reconstructions. The application of the model to pre-Holocene pollen assemblages is particularly questionable given that no analogous situation exists in the modern vegetation of the Tibetan Plateau.

d) *Variations of pollen spectra within large lakes*: It is assumed that the pollen loadings are of aerial origin (Parsons and Prentice, 1981; Prentice and Parsons, 1983; Sugita, 2007a). However, evidence has been observed in large lakes of variations in pollen spectra that are possibly due to fluvial pollen loadings and/or selective deposition of pollen species as a result of water dynamics (e.g. Xu, et al., 2005; Wang et al., 2011). For example, the pollen assemblages recovered from surface sediment samples in Lake Donggi Cona revealed a higher Cyperaceae content where inflows enter the lake (Wang et al., 2011). Furthermore, various studies have demonstrated that up to 90% of the total pollen in some lakes could have been washed in by inflows (e.g. Bonny, 1978; Pennington, 1979).

5.5.2 Pollen fall speed, PPEs, RSAP and the pollen-vegetation relationship

Considering the potential regional differences, the estimated pollen fall speeds in our study are generally consistent with the previously reported results from inner Mongolia (Li et al., 2011b) and southern Africa (Duffin and Bunting, 2008). Chenopodiaceae (0.0117 m/s, this study; 0.0090 m/s, inner Mongolia) and *Artemisia* (0.0101 m/s, this study; 0.0096 m/s inner Mongolia) show relatively low fall speeds, while Poaceae (0.0185 m/s, this study; 0.0231 m/s, inner Mongolia; and 0.019 m/s, southern Africa) and Cyperaceae (0.0291 m/s, this study; 0.020 m/s, southern Africa) are a little higher.

One of the key challenges in applying ERV models is the choice of appropriate ways to measure vegetation composition when developing calibration data sets for parameter estimation, such as the PPE and the RSAP (Mazier et al., 2008). Of the four distance-weighting methods employed and considering the similar ranges of likelihood scores, the d^{-2} method appears to be the best method for handling long distance vegetation components, reaching an asymptote at 2200 m which is determined to be the RSAP for our modern sample site. Similar RSAPs have also been derived for small lakes in Europe (e.g. 2360 m in Denmark: Nielsen and Sugita, 2005). On the other hand, when other distance weighting methods were applied (d^{-1}, Prentice's model and Sugita's Ring model) the likelihood scores did not approach asymptotes but instead reached minimums at distances of 2200 m from the lake shore.

The two ERV Submodels 1 and 2 present comparable pollen productivity estimates (Figure 5-2B, Table 5-3), with slight variations due to the different assumptions used for the background pollen component (Parsons and Prentice, 1981; Prentice and Parsons, 1983). In both submodels the highest productivities (5.442, 5.379) were estimated for Chenopodiaceae, which is consistent with the over-representation according to the pollen representation factor (*R*-value) previously reported by Herzschuh et al. (2003, 2006). Another dominant species in the pollen spectra commonly recovered from arid and semi-arid regions, *Artemisia*, also shows evidence of over-representation, with intermediate PPEs (2.079, 3.267). Our data confirm the previous findings from northern and north-western China (Li et al., 2011b; Wei et al.; 2011) that Chenopodiaceae and *Artermisia* are strongly over-represented relative to Poaceae and Cyperaceae, but in contrast to our results these studies revealed higher productivity for *Artermisia* relative to Chenopodiaceae. The relative productivity difference

between Chenopodiaceae and *Artermisia* is still a matter of debate, probably due to spatial variations, which indicates the need for further pollen productivity studies in typical desert areas, both warm and cold. Cyperaceae consistently shows low PPEs (Herzschuh et al., 2003, 2006; Broström et al., 2008, Zhao and Herzschuh, 2009; Wei et al., 2011) which is consistent with studies from Europe despite the different ecologies reflected by the pollen taxon Cyperaceae.

Applying the PPEs to the vegetation reconstructions, the contributions of plant taxa with higher PPEs (*Artemisia* and Chenopodiaceae in this study) are generally lower than in the pollen spectra, and conversely (Figure 5-3; Figure 5-4), the abundance of low PPE taxa (Cyperaceae) is higher, a pattern that is inherent to this approach (Figure 5-3; Figure 5-4) (see also Nielsen and Odgaard, 2010; Soepboer et al., 2010). Furthermore, surface pollen data collected from the typical alpine meadow regions (*Kobresia* spp. dominant) always contain plenty of *Artemisia* pollen, ranging between 10% and 20% in the pollen spectra (Herzschuh et al., 2010b; Lu et al., 2011; Wei et al., 2011), which also confirms the high productivity of *Artemisia*. Reconstructions using the REVEALS model consistently yielded results that were more similar to observed modern vegetation compositions, based on pollen percentages on the Swiss Plateau (Soepboer et al., 2010), as well as results from Sweden (Hellmann et al., 2008b) and Denmark (Nielsen and Odgaard, 2010). Thus, the pollen-based landscape reconstruction algorithm method is a new and effective way of reconstructing regional vegetation composition, introducing a more straightforward way of interpreting the pollen assemblages in terms of landscape changes (Sugita, 2007a; Nielsen and Odgaard, 2010; Soepboer et al., 2010).

5.5.3 Vegetation evolution on the Tibetan Plateau

Vegetation changes across the Tibetan Plateau have been investigated in terms of tree line shifts in the marginal regions (Liu et al., 2002b; Kramer et al., 2010b) and biome replacements (or ecotone shifts) in the central parts (e.g. Shen et al., 2008; Tang et al., 2009; Herzschuh et al., 2010b;), which have generally been deduced from percentage changes in fossil pollen assemblages. However, as we have shown above, the relationship between pollen and vegetation is not straightforward, but on the contrary, the relative proportions of pollen taxa are strongly biased by pollen productivities and transportation characteristics.

Desert landscapes have previously been deduced for the Late Glacial period because of the high Chenopodiaceae pollen content in fossil pollen spectra (Figure 5-3) (Wischnewschki et al., 2011; Wang et al., 2011). However, alpine *Kobresia*-meadow made up about 30-50% of the regional vegetation during this period (Figure 5-3), which indicates a patchy existence of alpine meadow on the north-eastern Tibetan Plateau at this time, although less than at present. The high desert pollen component (Chenopodiaceae) in Lake Kuhai and Lake Donggi Cona may possibly have derived from the low elevation arid Qaidam Basin during the Late Glacial period (Zhao et al., 2007, 2010).

Marked vegetation fluctuations during the Holocene have been reported from the central and north-eastern Tibetan Plateau. However, contrary to what might have been inferred from the

pollen percentages, Cyperaceae always constitutes more than 50% (up to 90%) of the regional vegetation, which indicates a dominance of alpine *Kobresia*-meadows on the northeastern Tibetan Plateau throughout the Holocene. Our results therefore indicate that the reconstructions of steppe as the dominant biome for the early to mid-Holocene using pollen-based biomization methods (Herzschuh et al., 2010b for Lake Zigetang and Lake Koucha; Li et al., 2011a for Lake Nam Co) now need to be reconsidered.

Furthermore, DCCA analyses have revealed much higher compositional species turnovers in the Holocene fossil pollen assemblages than in the vegetation reconstructions (Table 5-4), which means that the signal produced by past vegetation changes may have been magnified by the pollen spectra as a result of different pollen productivities (Birks 2007). The reconstructed vegetation composition also shows more concentrated patterns for each lake and between the four investigated lakes than the original pollen assemblages, as can be seen in Figure 5-4. In other words, the strength of the previously reported vegetation changes and regional differences on the Tibetan Plateau, based on original pollen percentages, was probably over-estimated, which indicates the need for appropriate considerations of pollen-vegetation relations to be included in any future discussion of past vegetation changes, their drivers, and their implications.

5.6 Conclusions

By introducing theoretical models to the upper Tibetan Plateau area, we have been able to estimate the modern pollen-vegetation relationship, revealing distinct differences in pollen productivities between pollen taxa commonly distributed in alpine meadow and alpine steppe. Such variations in pollen productivities have possibly led to the overestimations of the real vegetation changes since the Late Glacial, which have been previously reported from the upper Tibetan Plateau. A better understanding of the pollen-vegetation relationship is therefore shown to be essential when fossil pollen data are interpreted in terms of vegetation and/or climate changes.

Acknowledgements

We would like to thank Anne Birgitte Nielsen and Thomas Gisecke for introducing us to the pollen-vegetation models during a course in University of Göttingen. We are grateful to Shinya Sugita for providing us with the computing programs (ERV V7.2 and REVEALS V4.2.2) and helpful suggestions. Juliane Wischnewski is acknowledged for providing the pollen data from Kuhai Lake. Y. Wang's doctoral research is funded by the "Helmholtz - China Scholarship Council (CSC) Young Scientist Fellowship" (No. 2008491101). The research was supported by the German Research Foundation (Deutsche Forschungsgemeinschaft, DFG). We thank Dr. A.F. Lotter and two anonymous reviewers for their helpful suggestions regarding improvements to our manuscript.

Supplementary

Figure 5–5 Likelihood scores and distance from lakes derived using four distance weighting methods under different wind speed conditions: A, 3 m/s and B, 5 m/s.

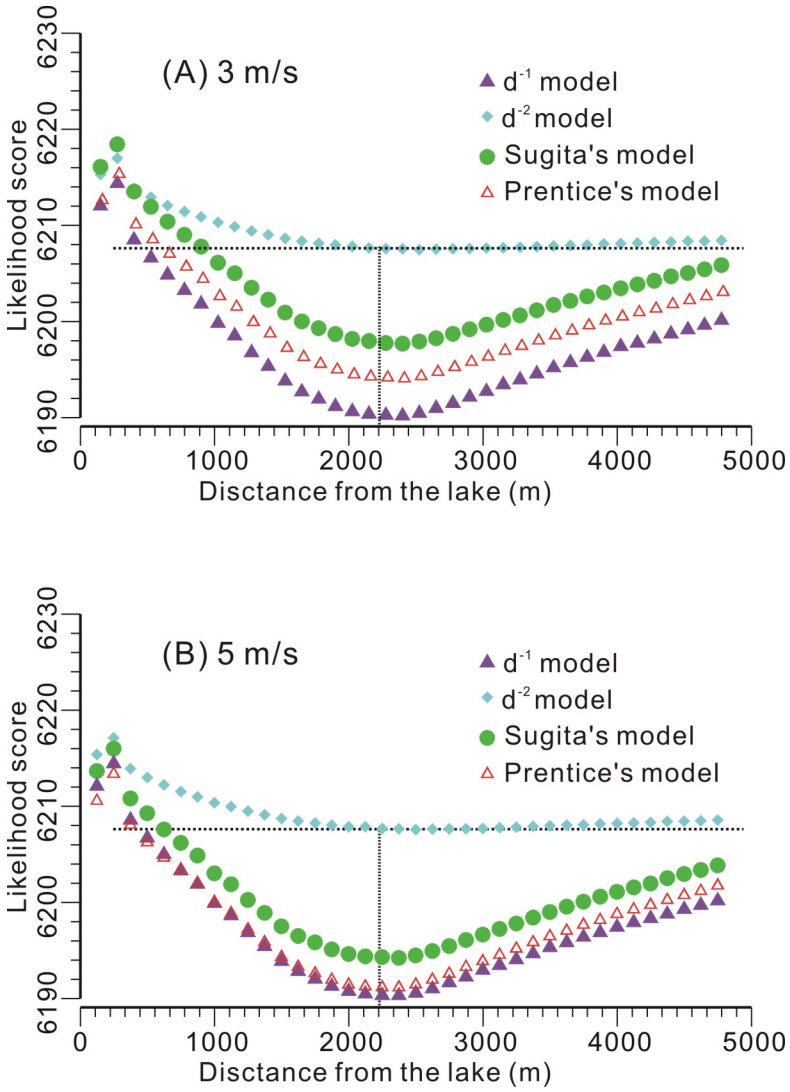

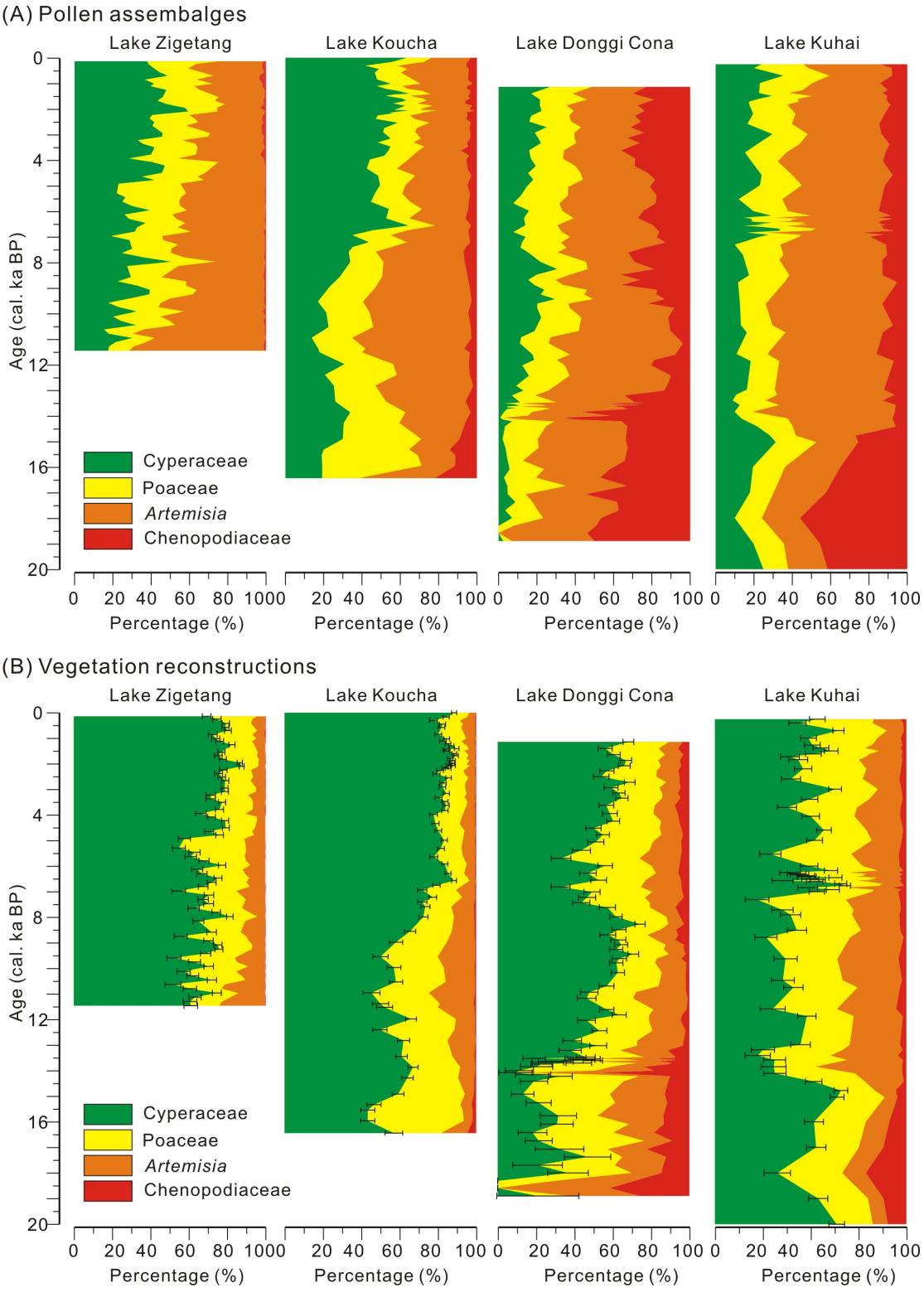

Figure 5-6 REVEALS model based vegetation reconstructions using PPEs after ERV Submodel 1, for comparison with the reconstructions showed in Figure 5-3, where PPEs after ERV Submodel 2 are used.

6 Overall conclusions

6.1 Improved understanding of climate and vegetation variations in central Asia

6.1.1 Evolution of Asian Summer Monsoon during the Holocene

Because of its importance to the climate and to the environment, a large number of investigations have been carried out into the evolution of the ASM. These investigations have, however, resulted in significant discrepancies between the interpreted climate signals. In order to overcome such problems and to gain further insight into the evolutionary patterns of the monsoon, previously published palaeoclimatic records since 18 cal ka BP for central Asia have been collated and synthesized (**Manuscript 1**).

The semi-quantitative climate (moisture and temperature) interpretations show generally consistent patterns during the Holocene for both the pollen and non-pollen proxies, providing an opportunity to combine all of the records together for numerical analysis (**Q1**, scientific questions 1 in Section 1.2). The overall trends from our reconstructed climate indices show identical patterns to the classic climate sequences in the northern hemisphere, indicating a global-scale signal. Slightly different moisture patterns were recognized for the ISM region, the EASM region, and the region beyond the present range of either monsoon, indicating the existence of regional variations. Numerical ordination analysis (PCA) of the Holocene records revealed different moisture signals for the regions influcenced by different monsoon subsystems, especially with regard to the moisture maximum periods. The ISM areas exhibited maximum wet conditions during the early Holocene, while many of the records from EASM areas indicated relatively dry conditions, especially in north-central China where the maximum moisture levels occurred during the middle Holocene (**Q2**). Furthermore, the modern monsoonal indices were derived from the NCEP/NCAR Reanalysis dataset, resulting in generally negative correlations between the ISM and EASM intensities which is consistent with the millennial-scale patterns during the Holocene (**Q3**).

The summer monsoon has been assumed to be due to the land-ocean thermal gradient, and to be driven by internal (sea surface temperature, SST) or external (summer solar insolation) forcing mechanisms (Sirocko et al., 1993;Overpeck et al., 1996; Bush, 2001, 2005; Wang et al., 2001; Fleitmann et al., 2003; 2007). However, according to Laskar et al. (2004), the northern hemisphere summer solar insolation shows identical variations in the low and mid-latitudes during the Holocene. The SST results deduced from marine sediments also show generally stable evolution over the Arabian Sea and South China Sea during the Holocene (Li et al., 1997; Sonzogni et al., 1998; Wang et al., 1999; Jian et al., 2000; Steinke et al., 2001; Stott et al., 2004). However, neither the SST-driven hypothesis nor the insolation-driven hypothesis is able to explain the asynchronous patterns of the ISM and

EASM sub-systems. With the aid of modern meteorological data it now appears that these temporal differences may have been caused by interactions between the monsoon sub-systems themselves. During strong ISM years an enhanced Hadley Circulation is centered over the Tibetan Plateau area, which results in subsiding air streams in the east Asian monsoonal regions that acts as a constraint preventing intensification of EASM. By analogy, the existence of an over-heated Tibetan Plateau during the early Holocene accelerated the intensification of the ISM with a strengthened Hadley Circulation, which further suppressed the EASM system. During the middle Holocene, the weakening of the Hadley Circulation over the Tibetan Plateau and subsequent reduction in intensity of the ISM allowed the EASM to intensify and reach its maximum. The evolution of the ASM during the Holocene therefore followed a change in northern hemisphere solar insolation, and the asynchronous patterns of the ISM and EASM were due to interactions between these monsoon sub-systems (**Q4**).

6.1.2 Climate change on the northeastern Tibetan Plateau since the LGM

Fossil pollen records covering the last 20 ka from Lake Donggi Cona were analyzed in order to further understanding of the monsoonal evolution and climate change on the north-eastern Tibetan Plateau (**Manuscript 2)**.

The pollen assemblage, which is dominated by *Artemisia*, Chenopodiaceae, and Cyperaceae, indicates that the landscape during that time over the north-eastern part of the Tibetan Plateau consisted mainly of alpine steppe, together with alpine meadow and alpine desert components. The annual mean precipitation was quantitatively reconstructed. Extremely dry conditions were interpreted for the LGM period, with an annual precipitation of around 100 mm which is only 32% of present-day precipitation. A subsequent gradually increasing trend in moisture conditions during the Late Glacial was terminated by an abrupt reversion to a dry phase, which lasted for about 1000 years and coincided with “Heinrich Event 1” in the northern Atlantic region. Subsequent periods corresponding to the warm Bølling/Allerød period and the Younger Dryas cold event were followed by moist conditions during the early Holocene, with annual precipitation of up to 400 mm. A slightly drier trend after the Holocene Climate Optimum was then followed by a second wet phase during the middle Holocene that lasted until 4.5 cal ka BP. Relatively steady conditions with only slight fluctuations then dominated the late Holocene, resulting in the present climatic conditions (**Q6)**.

Procrustes analyses indicate a non-fit between the pollen and ostracod assemblages (Mischke et al., 2010b) from Lake Donggi Cona, but a significant fit between pollen assemblages from Lake Donggi Cona and Lake Kuhai (Wischnewski et al., 2011), which is about 50 km from Lake Donggi Cona. The ostracod assemblages on the Tibetan Plateau are assumed to primarily reflect limnological changes such as water depth and salinity (Mischke et al., 2007, 2010 a, 2010b). The non-fit of the pollen data with the ostracod data from the same core (thus excluding any possibility of errors due to age-depth correlations) therefore indicates that the pollen data were not susceptible to within-lake changes or variations in the fluvial input, but reflected a regional terrestrial signal that was driven primarily by climate, a theory supported by the significant fit between the pollen records from the two lakes (**Q7**).

The pollen-based precipitation reconstructions from Lake Donggi Cona and two nearby lakes (Lake Kuhai and Lake Koucha) all show rather high values during the early Holocene that reach over 400 mm per annum, consistent with the maximum period of the ISM (Herzschuh et al., 2009; Wischnewski et al., 2011). Furthermore, the wet mid-Holocene phase revealed in the Lake Donggi Cona pollen record has also been found in various other climate reconstructions based on pollen records from the Tibetan Plateau and the adjacent areas, e.g., at Lake Koucha (Herzschuh et al., 2009), Lake Kuhai (Wischnewski et al., 2011), Lake Naleng (Kramer et al., 2010b), the No 2 Pit peat section (Yan et al., 1999), Lake Yidun (Shen et al., 2006), Lake Luanhaizi (Herzschuh et al., 2010), Lake Hidden, and Ren Co Lake (Tang et al., 2004), and has also been reported from non-pollen studies such as stable carbon-isotope records from the Hongyuan Peat section (Hong et al., 2005), and multi-proxy results from Lake Qinghai (Shen et al., 2005). This second wet stage was synchronous with the intensification of the EASM, indicating that the Holocene climate changes affecting the eastern Tibetan Plateau could also have been to some extent influenced by the EASM system (**Q8**).

6.1.3 Driving factors of vegetation change on the Tibetan Plateau

Climate reconstructions from fossil pollen records are generally based on the assumption that past changes in vegetation were primarily driven by changes in climate, but this assumption remains a matter of debate. In **Manuscript 3**, we have attempted to identify possible variations in the driving factors behind vegetation changes.

A late Holocene (3770 years old) sediment sequence from Lake Kusai in the northern part of the Tibetan Plateau was used for both pollen and sedimentology analyses. The C/N ratios were always below 10, indicating that the total organic carbon (TOC) content generally reflects the primary productivity within the lake system, which was further confirmed to be closely related to the regional moisture variations (Liu et al., 2009). The total inorganic carbon content (TIC) was interpreted in terms of lake water salinity since it consists mainly of autogenic calcite, which mostly derives from ostracod shells. The different signals in the grain size results were extracted using the End-Member modeling method to obtain relative proportions of fluvial and aeolian transported material (**Q9**). Both the correlation and the significance between pollen assemblages and individual sedimentary proxies vary considerably through time. Before 2.4 cal ka BP all proxies show rather low and insignificant correlations with pollen assemblages. TOC contributes around 12% to the total variations in pollen assemblages during the period from 2 to 1.2 cal ka BP, while the TIC is significant between 0.9 and 0.2 cal ka BP. The proportions of fluvial and fine aeolian transported materials only show a significant correlation with pollen between 1.4 and 0.8 cal ka BP. Furthermore, the coarsest grain size fraction, which represents possible dust storm events, showed significant correlation with pollen after 0.6 cal ka BP, which is assumed to relate to human activity (Wang et al., 2009) (**Q10**). The ASM has been shown to have generally reduced in intensity during the middle to late Holocene, but the period before 2.4 cal ka BP may have experienced significant climatic variations resulting in the generally low correlations between sedimentary proxies and pollen assemblages (Herzschuh, 2006; Wang et

al., 2005, 2010). Highly significant correlations between TOC and pollen assemblages indicate that the regional climate was wetter than it is at present and that the vegetation changes were mainly climate driven. Thereafter, and probably as a result of the reduction in intensity of the ASM, the limited moisture available caused a decrease in vegetation coverage and subsequent fluvial and aeolian erosion, reflected by the high level of correlations between fluvial ro aeolian sediments and the pollen assemblage. During this period vegetation change may therefore have been more influenced by the extreme events than by the general climate trends. The lake system indicator (the TIC) subsequently again showed dominant contributions to the pollen assemblage, revealing a climate driven mechanism (**Q11**). A Procrustes analysis revealed that the species compositions during the last 600 years are significantly different from those before that time, suggesting the possibility of human influence on the landscape, which may also be supported by the dramatic increase in regional dust storm events (**Q12**).

6.1.4 Holocene vegetation change on the Tibetan Plateau

Reconstruction of past vegetation changes appears to be more straightforward than climate reconstruction, despite still being constrained by a lack of information concerning pollen productivities. Vegetation changes across the Tibetan Plateau have previously been deduced directly from fossil pollen percentages (Liu et al., 2002; Shen et al., 2008; Tang et al., 2009; Herzschuh et al., 2010, 2011; Kramer et al., 2010), which may have concealed the true picture of vegetation evolution. In **Manuscript 4** we evaluated the vegetation-pollen correlation using modern pollen and vegetation data from the north-eastern Tibetan Plateau, and reassessed the Holocene vegetation changes on the basis of these new findings.

The modern pollen assemblage from 19 small lakes, each with a radius of about 100 m, together with the corresponding distance-weighted regional vegetation compositions, were employed to run the ERV models in order to evaluate the relative pollen productivity estimates (PPEs, relative to Poaceae) of four common plant species, i.e. Chenopodiaceae, *Artemisia*, Poaceae, and Cyperaceae. Relatively high PPEs were deduced for the alpine steppe and desert taxa: 2.079±0.432 for *Artemisia* and 5.379±1.077 for Chenopodiaceae. Lower PPEs were estimated for the alpine meadow plant, Cyperaceae (1.036±0.012). The PPEs obtained for the alpine meadow and alpine steppe species are generally consistent with previously reported results from Inner Mongolia and South Africa (Duffin and Bunting, 2008; Li et al., 2011) (***Q13***). By applying the PPEs to the REVEALS model (Sugita, 2007a), the Holocene vegetation changes in the north-eastern and central parts of Tibetan Plateau have been quantitatively reconstructed based on fossil pollen records from Lake Koucha (Herzschuh et al., 2009), Lake Zigetang (Herzschuh et al., 2006), Lake Kuhai (Wischnewski et al., 2011) and Lake Donggi Cona (Wang et al., 2011). The vegetation reconstructions for the Holocene period are generally more reliable than for the Late Glacial, despite the potential biases due to the variations in the PPEs through time. In the vegetation reconstructions the proportions of *Artemisia* and Chenopodiaceae are largely reduced compared to the pollen assemblages, owing to their high PPEs, while the contributions of Cyperaceae in regional landscapes increase, possibly indicating a wider distribution of alpine meadow than

previously reported (**Q14 & Q 15**). Furthermore, the DCCA results reveal somewhat higher compositional turnovers in the pollen assemblages than in the vegetation reconstructions, which suggest that the previously reported large vegetation changes or turnovers during the Holocene may have been overestimated as a result of ignoring variations in species-specific pollen productivities (**Q16**). It is therefore of great important to take pollen–vegetation relationships into account when discussing the potential drivers of vegetation change (such as climate, land use, atmospheric CO_2 concentrations) and its implications (for example, for land surface–climate feedbacks, carbon storage, and biodiversity).

6.2 Methods for improving current climate and vegetation interpretations from fossil pollen records

6.2.1 Estimating pollen source area for large lakes

Fossil pollen records preserved in lacustrine sediments have been widely applied as a common proxy in quantitative climate and vegetation reconstructions (Birks et al., 2010; Seppä and Bennett, 2003). However, the pollen record represents a regional signal for the source area of the pollen grains, the "pollen source area", rather than for the specific location from which the samples were recovered (Prentice, 1985; Sugita, 1993, 1994; Broström et al., 2008). An indispensable precondition for interpreting pollen records is therefore to identify the pollen source area, but this has rarely been considered to date. The size of a source area can vary with the size of the lake basin, as it is dependent on species-specific pollen dispersal and depositional characteristics. A theoretical model to estimate the pollen-source area for an entire lake surface has been developed by Sugita (1993), taking into account variations in basin size, wind speed, and pollen fall speed. Applying Sugita's model to the large lakes in central Asia ranging from 1 km to 15 km in radius, the theoretical radius of the pollen source area was estimated to range from 50 km to 250 km from the lake. The size of the pollen source area depends mainly on the size of lake basin, but is also influence by pollen compositions and the landscape due to pollen grain size constraints on dispersal-deposition characteristics (**Q5**).

6.2.2 Multivariate Regression Tree analysis

Multivariate Regression Tree (MRT) analysis is a statistical technique that can be used to explore, describe, and predict the relationships between multi-species data and environmental characteristics (De'ath, 2002); it has also been employed to identify constraints on fresh water biology or mineral compositions (Davidson et al., 2010a, 2010b; Wang, et al., 2011). By repeated splitting of the sample data the MRT analysis creates clusters corresponding to environmental factors which can then be used to analyze complex ecological data. These factors may include imbalance, missing values, nonlinear relationships between variables, and high-order interactions. The MRT method has been applied to our modern pollen dataset from the large lakes in central Asia, together with modern meteorological data that includes the mean annual precipitation, mean annual temperature, mean July temperature, and the potential water balance. Three clusters resulted from the MRT analysis, all of which are distinguished

by the mean annual precipitation indicating that the pollen assemblage and the underlying vegetation compositions are more sensitive to annual moisture changes than to other parameters such as temperature or water balance (**Q6**).

6.2.3 Moving-window RDA

Redundancy Analysis (RDA) has traditionally been used to explore the correlation between response variables and explanatory variables, especially in ecological studies (ter Braak and Smilauer, 2002). A moving-window RDA has recently been used to examine temporal variations in such correlations in order to identify the controls on plant communities in Alaska (Carlson et al., 2010). Interpreting fossil pollen records in terms of climate assumes that the primary driving factor for vegetation change is the climate which, however, remains a matter of debate. A detailed examination of correlations between pollen and climate is required as a matter of considerable priority. It is, however, impossible to obtain a definitive climate sequence as a reference for the entire Holocene period and chronological uncertainties could seriously bias multi-site correlations. A moving-window RDA was therefore performed on the high resolution sediment record from Lake Kusai, for which both pollen and sedimentological results are available. Variations in the correlations, together with fluctuations in the significance levels, were thus able to provide information on the driving factors behind changes in vegetation (**Q10**).

6.2.4 ERV model and REVEALS model

The relationship between a pollen assemblage and the abundance of the vegetation is of great importance if past changes in vegetation are to be inferred from fossil pollen records. Theoretical pollen-vegetation models (the ERV model and the REVEALS model) have been developed and been applied to European forest regions, leading to progress in both the estimation of pollen productivities and quantitative vegetation reconstructions (e.g. Nielsen and Sugita, 2005; Broström et al., 2008; Mazier et al., 2008; Soepboer et al., 2008). However, because of the shortage of information on modern pollen and vegetation abundance on the remote Tibetan Plateau, the pollen-vegetation relationships for this area remain largely unknown. With the assistant of vegetation atlas and field vegetation surveys, the general compositions of plant communities in the alpine ecosystems have been estimated and these theoretical models applied to determine the modern pollen-vegetation relationships. Despite the uncertainties and regional variations, our results are in line with those previously reported from northern China and Africa (**Q13& Q14**).

6.3 Outlooks

6.3.1 Global Monsoon

The summer monsoon is an important conveyor of energy that affects the climate on a global, rather than just a regional scale; it has therefore been termed a "global monsoon" (Clift and

Plumb, 2008). Recent studies have asserted that the northern hemisphere monsoon systems could be driven by processes in the southern hemisphere (Zisheng et al., 2011). A thorough understanding of the interconnections between monsoon systems would greatly improve our understanding of monsoon dynamics, and consequently of climate change. Six summer monsoon systems are recognized in the modern world, i.e. the African, Indian, East Asian, Australian, North American, and South American monsoons (Wang and Ding, 2006, 2008), although the latter two do not show seasonal wind reversals (Webster et al., 1998). As shown in Figure 6-1, the four summer monsoon systems in the eastern hemisphere show potential teleconnections, especially between the Australian and East Asian monsoons and between the east African and Indian monsoons (Beaufort et al., 2010; Trenberth et al., 2000). It would therefore be of great interest and importance to extend our palaeoclimate index dataset for central Asia so that it includes Australia and eastern Africa, in order to reveal the global monsoon processes.

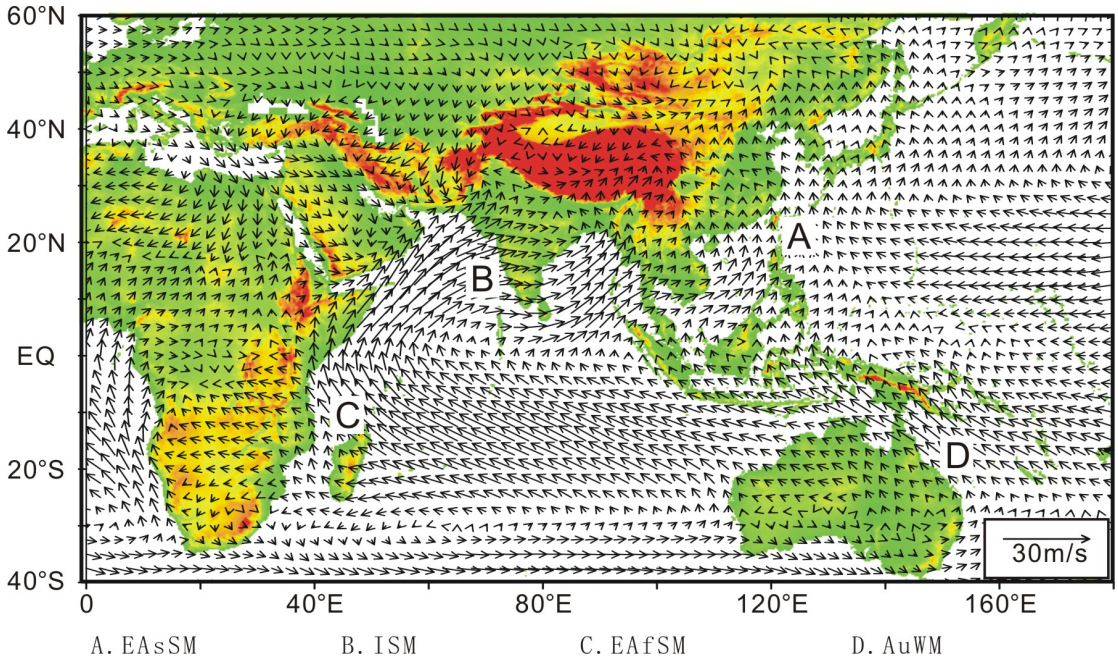

Figure 6-1 Atmospheric circulation systems over the eastern Hemisphere. A: East Asian Summer Monsoon, B: Indian Summer Monsoon, C: East African Summer Monsoon, D: Australian Winter Monsoon. Arrows show 60-year mean boreal summer (June, July, August) wind fields based on NCEP/NCAR Reanalysis data (Level 1000 hPa) from Jan. 1948 to Dec. 2008.

6.3.2 Response to, and feedback between, vegetation and non-climate factors

Traditionally, past vegetation changes recorded by fossil pollen assemblages have simply been interpreted in terms of variations in the climate. However, the results from Lake Kusai (**Manuscript 3**) indicate that climate is not always the driving factor behind vegetation evolution, and that some severe events (such as dust storms, or river floods) that correlated with land erosion processes could have been both an influence on, and a response to, changes in vegetation. However, time restrictions have meant that, to date, such information is only

available for a single site in the northern Tibetan Plateau area. It would be necessary to examine such issues on a broader scale and extend the study area to the whole of the Tibetan Plateau, and even into the arid and semi-arid areas of western China, to better evaluate the driving factors behind vegetation change.

6.3.3 Past vegetation reconstructions in central Asia

In **Manuscript 4** Holocene changes in vegetation on the Tibetan Plateau were reassessed, yielding results that were generally different from those previously interpreted on the basis of pollen percentages. Past changes in vegetation over the whole of central Asia may also have been overestimated in the same way as in the Tibetan Plateau area, and therefore now need to be reinterpreted. Together with additional fossil pollen data and reliable chronologies, pollen productivity estimates are therefore required as a matter of priority. Such information is, however, largely constrained by the complexity of vegetation distributions and by spatial variations in pollen productivities. A fossil pollen dataset for central Asia since the Late Glacial period will shortly become available, and with a better understanding of pollen productivities the actual changes in vegetation across the whole of central Asia could therefore be reassessed.

7 Appendix-1 Manuscript 5: Environmental constraints on lake sediment mineral compositions from the Tibetan Plateau and implications for paleoenvironment reconstruction

Yongbo Wang [a,b,c] , Xingqi Liu [c], Steffen Mischke [b,d], Ulrike Herzschuh [a,b]

[a] *Alfred Wegener Institute for Polar and Marine Research, Research Unit Potsdam, 14473 Potsdam, Germany*

[b] *Institute for Earth and Environmental Sciences, University of Potsdam, Karl-Liebknecht-Str. 24, 14476 Golm, Germany*

[c] *State Key Laboratory of Lake Science and Environment, Nanjing Institute of Geography and Limnology, CAS, East Beijing Road 73, 210008 Nanjing, P.R.China*

[d] *Institute of Geological Science, Freie Universität Berlin, Malteserstrasse 74-100, 12249, Berlin, Germany*

Current Status: Published in "Journal of Paleolimnology" 2012, Vol. 47 Pages 71-85.

Abstract

Inorganic minerals form a major component of lacustrine sediments and have the potential to reveal detailed information on previous climatic and hydrological conditions. The ability to extract such information however, has been restricted by a limited understanding of the relationships between minerals and the environment. In an attempt to fill in this gap in our knowledge, 146 surface sediment samples have been investigated from 146 lakes on the Tibetan Plateau. The mineral compositions derived from these samples by X-Ray Diffraction (XRD) were used to examine the relationships between mineral compositions and the environmental variables determined for each site.

Statistical techniques including Multivariate Regression Trees (MRT) and Redundancy Analysis (RDA), based on the mineral spectra and environmental variables, reveal that the electrical conductivity (EC) and Mg/Ca ratios of lake water are the most important controls on the composition of endogenic minerals. No endogenic minerals precipitate under hyper-fresh water conditions (EC lower than 0.13 mS/cm), with calcite commonly forming in water with EC values above 0.13 mS/cm. Between EC values of 0.13 and 26 mS/cm the mineral composition of lake sediments can be explained in terms of variations in the Mg/Ca ratio: calcite dominates at Mg/Ca ratios of less than 33, whereas aragonite commonly forms when the ratio is greater than 33. Where EC values are between 26 and 39 mS/cm, monohydrocalcite precipitates together with calcite and aragonite; above 39 mS/cm, gypsum and halite commonly form. Information on the local geological strata indicates that allogenic (detrital) mineral compositions are primarily influenced by the bedrock compositions within

the catchment area.

By applying these relationships to the late glacial and Holocene mineral record from Chaka Salt Lake, five lake stages have been identified and their associated EC conditions inferred. The lake evolved from a freshwater lake during the late glacial (before 11.4 cal. ka BP) represented by the lowest EC values (<0.13 mS/Cm), to a saline lake with EC values slightly higher than 39 mS/cm during the early and mid Holocene (ca. 11.4-5.3 cal. ka BP), and finally to a salt lake (after 5.3 cal. ka BP). These results illustrate the utility of our mineral-environmental model for the quantitative reconstruction of past environmental conditions from lake sediment records.

7.1 Introduction

Because of its global significance with regard to climate evolution, the Tibetan Plateau has, in recent years, become the target of palaeoclimatological studies and the broad distribution of lakes on the plateau has resulted in their lacustrine sediments being widely investigated and interpreted.

As the major component of lacustrine sediments, the inorganic minerals have potentially preserved abundant hydrological and climatic information that is unfortunately not yet fully understood owing to a lack of knowledge about mineral-environmental relationships. Mineral data have been reported from many sites (e.g., Sumxi Co [where Co = lake], Gasse et al. 1991; Lake Qinghai, Yu and Kelts 2002; Lake Siling, Goto et al. 2003; Ahong Co, Morrill et al. 2006; Nam Co, Zhu et al. 2008; Lake Koucha, Mischke et al. 2008; Lake Kuhai, Mischke et al. 2010), but have unfortunately never been interpreted as indicators of past salinity in Tibetan lakes, but only as supplements to the well-studied biological, geochemical or geophysical indices, demonstrating the urgent need for a better understanding of the relationship between mineral composition and environmental conditions.

From the origins, three types of minerals can be distinguished: allogenic (detrital), endogenic (primary autogenic), and authigenic (secondary autogenic) minerals (Last 2001). In general, the composition of the allogenic fraction reflects variations in sediment sources, and in the weathering and transportation processes. Evidence concerning the former environmental conditions in a lake can be gained from the endogenic mineral fraction because it provides a snapshot of the water chemistry at the time of mineral formation (Last 2001).

Traditionally, water-quality variables within lakes, such as electrical conductivity (or salinity), ionic composition, pH value, and temperature, as well as external climatic variables (e.g. temperature, precipitation), have been widely considered to be the determinants of endogenic mineral composition. Carbonate is among the most common endogenic constituents in fresh to slightly brackish lakes, whereas more complex mineral assemblages, including compounds such as gypsum and halite, appear in brackish or saline lakes. According to a study of 25 lakes by Müller et al. (1972), the Mg/Ca ratio is particularly important for determining the nature of carbonate precipitation, with Mg/Ca ratios of < 2 commonly result in the precipitation of low-Mg calcite, followed by high-Mg calcite at ratios between 2 and 12, and finally, the precipitation of aragonite where Mg/Ca > 12. However, apart from the multi-site

investigations of Müller et al., most information on the relationships between mineral assemblages and the properties of lake water has been gained either from laboratory studies and modeling using seawater (Garrels and Thompson 1962; Hardie and Eugster 1980; Millero and Pierrot 1998), or from single-site reconstructions (Last 1982; Mullins 1998). In addition, the study by Müller et al. (1972) was restricted to carbonate minerals because they only investigated freshwater lakes.

In this paper, we present mineral composition data for surface sediment samples collected from 146 lakes on the Tibetan Plateau. We use the findings from this modern study to interpret the mineral composition of a sediment core from Chaka Salt Lake (northern Qinghai-Tibetan Plateau), where changes in salinity have been reported in a previous study by Liu et al. (2008). We attempt to (1) trace the potential patterns of allogenic mineral compositions and their regional constraints, (2) reveal the main variables controlling the formation of endogenic minerals and the corresponding thresholds, and (3) quantify past environmental changes at Chaka Salt Lake from the sedimentary mineral record.

7.2 Study Area

This study encompasses a large area on the eastern Tibetan Plateau (25°30′N to 39°30′N, 87°E to 102º30′E) including the Qaidam Basin, the Qilian Mountains, and the Yunnan-Sichuan mountainous region (Figure 7-1a). With the exception of the low-lying Qaidam Basin, the area has an elevation greater than 4,000 m above sea level (a.s.l.). The TibetanPlateau landmass is dominated by magmatic rocks such as granite, diorite, and gabbro, with sporadic outcrops of limestone on the south-central Tibetan Plateau and in the Qaidam Basin (IGSNRR 1990; Zhang 2000). In areas above 4,000 m the soils are characterized by permafrost conditions (Large et al. 2009).

Climate gradients exist across the study area, from high summer temperatures (T_{July} up to 19°C) and annual precipitation (over 700 mm) in the south-east to low summer temperatures (T_{July} ca. 6°C) and annual precipitation (below 100 mm) in the north-west (Sun 1999). Most of the precipitation falls during the Asian summer monsoon which produces a typical summer precipitation maximum. In addition to the large range of precipitation/evaporation (P/E) ratios, the various geological and geomorphological conditions result in the lakes having different chemical characters (i.e. pH values, ionic compositions, and water conductivities), and salinities that range from freshwater to brackish and even saline. A description of the climatic and limnological conditions of the sample sites is provided in Table 7-1.

Chaka Salt Lake (36.63-36.75°N, 99.00-99.20°E; 3,200 m a.s.l.) is located in the northern Qinghai-Tibetan Plateau (Figure 7-1a). The lake, which has no outflow, is fed by fresh water from the Mo River in the north-west, the Hei River in the south-west, and by some glaciers to the north and north-west (Liu et al. 2008a). The mean annual temperature is 3.5°C, with a lowest monthly mean of -12.4°C in January and a highest monthly mean of 14.4°C in July. The annual precipitation (198 mm) is well below the potential mean annual evaporation (2,075 mm) (Wang and Dou 1998).

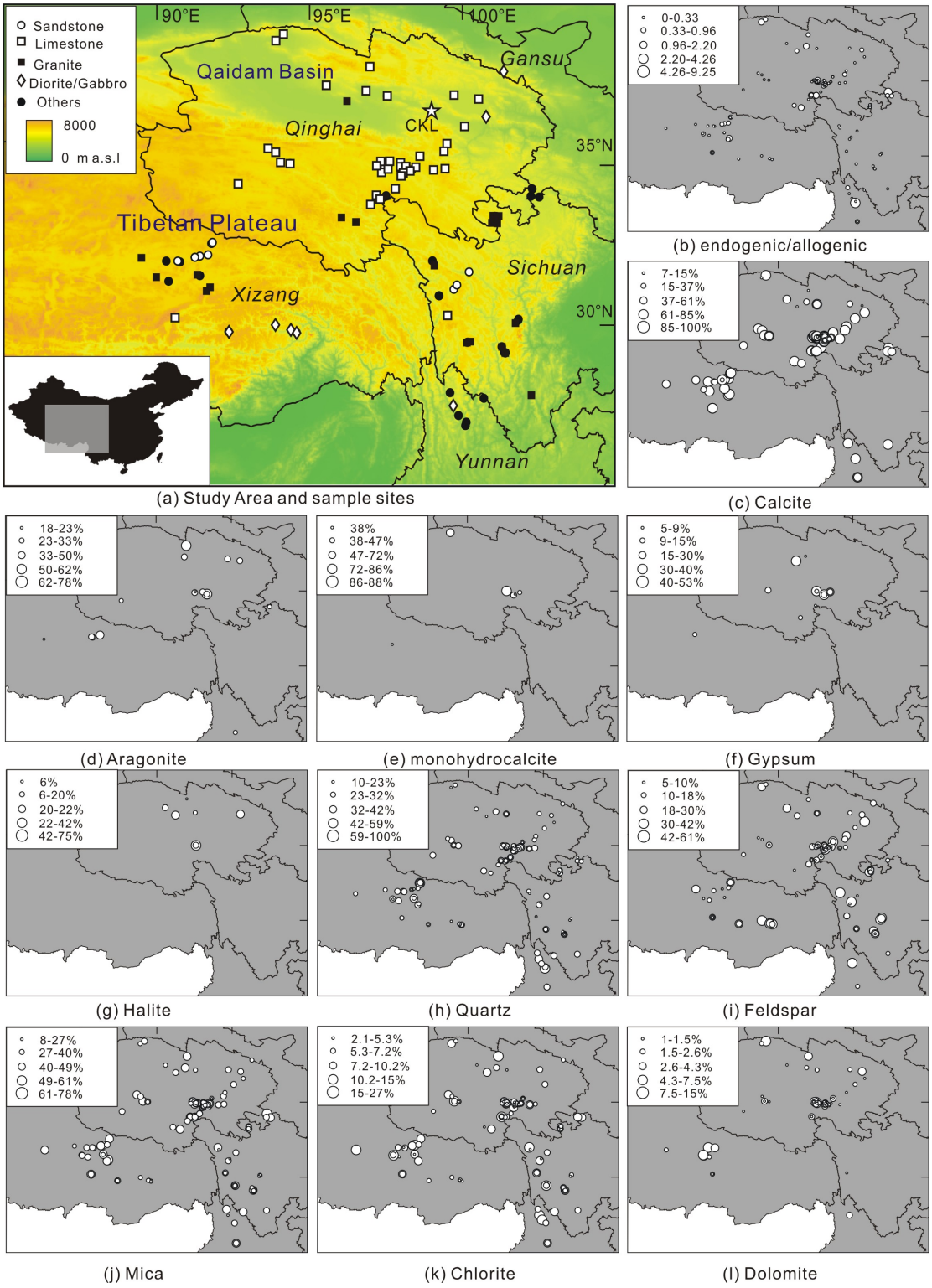

Figure 7-1 Maps showing (a) the study area, sample sites, and corresponding geological strata within catchments summarized from the geological map of the Tibetan Plateau (IGSNRR 1990): the background is the Digital Elevation Model (DEM) obtained from the Shuttle Radar Topography Mission (SRTM); the star (CKL) indicates Chaka Salt Lake; *italic letters* stand for the names of Chinese provinces; (b) the distribution of the ratios between endogenic and allogenic minerals; (c–l) mineral compositions detected within the surface samples (percentages are calculated separately for autogenic and allogenic minerals).

Table 7-1 Environmental variables used in this study; those numbered were included in the numerical analyses

No	Variable	Min.	Max.	Mean	Trans.	Or. RDA	Eigen.	*p*
1	Lat. (°N)	25.64	39.35	33.01	No	-	-	-
2	Lon. (°E)	87.56	102.55	97.44	No	-	-	-
	Elev. (m a.s.l.)	1500	5133	4055				
3	Depth (m)	0.05	46.1	5.85	Log(X+1)	4	0.02	0.041
4	EC (mS cm^{-1})	0.005	133.7	7.14	Log(X+1)	2	0.04	0.001
5	pH	4.7	10.83	8.85	No	-	-	-
6	Alk (meq l^{-1})	0	1204.1	14.60	Log(X+1)	-	-	-
7	T_{July*} (℃)	4.30	23.79	9.36	Log(X+1)	-	-	-
8	P_{ann*} (mm)	30.77	1779.37	590.94	Log(X+1)	-	-	-
	T_{water} (℃)	3.1	29.7	13.54				
	Na (meq l^{-1})	0	3632.01	101.41				
	Mg (meq l^{-1})	0.01	2056.60	47.51				
	Ca (meq l^{-1})	0.02	22.45	1.92				
	K (meq l^{-1})	0	52.17	1.64				
	Cl (meq l^{-1})	0.03	5641.75	107.37				
	SO_4 (meq l^{-1})	0	761.99	24.42				
	NO_3 (meq l^{-1})	0	7.85	0.13				
9	Mg/Ca	0	142.1	13.1	Log(X+1)	1	0.14	0.001
10	NaK/CaMg	0	87.4	4.5	Log(X+1)	3	0.03	0.007
11	Alk/Cl	0	288	25.9	Log(X+1)	-	-	-
12	Alk/SO4	0	320	24.9	Log(X+1)	5	0.02	0.113

Trans.: transformation of the data Or. RDA: the order of variable after forward selection

Eigen.: Eigenvalues after forwards selection *P*: p-value after 999 permutations

7.3 Materials and Methods

7.3.1 Field work

Surface sediment samples were collected from 146 lakes (one sample per lake) on the eastern Tibetan Plateau and in adjacent regions during the summers of 2002 to 2005 for mineralogical analyses (Figure 7-1a). Ostracod, pollen and biomarker data have already been published (Mischke et al. 2007; Herzschuh et al. 2010; Aichner et al. 2010a, 2010b).

Surface sediment samples (0-2 cm) were collected from the center of each lake using a benthic dredge or gravity corer. These samples represent the last 20-30 years of sedimentation, as inferred from unpublished $^{210}Pb/^{137}Cs$ dating results from short cores. Water depths at the sampling sites were measured with a portable echo-sounder and water samples for chemical analysis were collected from 0.3 m below the surface immediately prior to sediment sampling. Electrical conductivity (EC), pH, and water temperature were measured at 0.3 m water depth using a portable (WTW Multi 340i) measuring instrument. Alkalinity was measured in the field using a Macherey-Nagel Alkalinity AL 7 titration test kit.

A 9-m-long sediment core (CKL-2004) was collected at a water depth of 2 cm from the south-eastern part of Chaka Salt Lake during the autumn expedition in 2004, using a strengthened corer (chamber length 1 m, inner diameter 7 cm). The sediment sequence consisted largely of halite for the upper 565 cm, followed by a mixture of soluble and sparingly soluble sulfate salts in dark silicic clay from 565 to 693 cm, and then dark silicic clay layers to the bottom of the core (Figure 7-2). The sediment core was split into 590 sub-samples by 1 – 2 cm intervals for dating and laboratory analysis. A further 161 samples were selected from the CKL-2004 core for mineralogical analysis, representing a resolution of between 5 and 7 cm in depth or about 100 years. For further details see Liu et al. (2008).

7.3.2 Laboratory analyses

Modern and fossil sediment samples for mineralogical analysis were freeze-dried and ground with a pestle and mortar. The measurements for surface sediment samples and samples from the CKL-2004 core were performed at the Institute of Salt Lakes, Chinese Academy of Sciences, using a Phillips X'Pert Pro X-ray diffraction system with Cu Kα radiation (λ=1.5406 Å) at a scanning rate of 2° min-1 for 2θ ranging from 10° to 80°. Mineral identifications and concentrations were inferred from the bulk mineral diffractograms using the intensity of the strongest peak for each mineral (Schultz 1964; Chung 1974; Last 2001) aided by the use of an automated search-match computer program (X'Pert HighScore Plus - RIR value calibration) with an approximate error of ±5% after double checking (Liu et al. 2008a).

The carbonate content of surface sediment samples was analyzed at the Nanjing Institute of Geography and Limnology, Chinese Academy of Sciences, using a chemical method as following. The carbonate content is calculated by the volume of gas collected following acidification of the sediment samples with hydrochloric acid (HCl, 10%), and calibrated against standard carbonate samples (calcite, 99% purity). The error after repetitious measurements was found to be less than ±1%.

Major ion concentration analyses of water samples were performed at the Institute of Geological Sciences of the Freie Universitaet Berlin (see details in Mischke et al. 2007).

7.3.3 Numerical analyses

Site-specific information on annual precipitation and the mean July temperature was obtained from Böhner (2006). Climatic estimates (precipitation, temperature, radiation, evapotranspiration) at a monthly resolution were made on a regular grid network (3,500 x 4,000 grid cells), covering the Central and High Asian regions with a grid-cell spacing of 1 km² (Böhner 2006). The statistical downscaling approach at the core of geospatial climate modelling integrates gridded circulation variables (GCM data, reanalysis series), available station observations (climate records from more than 400 climate stations), and advanced terrain parameterization methods (Böhner and Antonic 2008) to account for the topoclimatic heterogeneity of Central Asia. A detailed description of the methods used is given in Böhner (2005).

Several numerical analyses were performed in order to assess the relationships between mineral composition and selected environmental variables. Through data exploration we identified significant colinearities between several environmental variables, such as between July mean temperature (T_{July*}) and water temperature (T_{water}), T_{July*} and elevation, EC and the various ion concentrations. As a result, T_{water} and elevation data were excluded from ordination while the ion concentrations were replaced by EC and molar ratios used to classify the hydrochemical variables (Table 7-1).

In order to stabilize variances and to optimize the signal-to-noise ratio, mineral percentages were square-root transformed, and all environmental variables were transformed using either square-root or $\log_{10}(x+1)$ methods. Detrended correspondence analysis (DCA; Hill and Gauch 1980) yielded a gradient of 1.90 standard deviations for endogenic mineral data, indicating that linear-based methods (Principle Component Analysis, PCA; Redundancy Analysis, RDA) are appropriate for this data set. Unimodal-based constrained ordination (c, CCA) was also performed to assess the robustness of the results. The forward selection option of Redundancy analysis (RDA) was used to identify a minimum environmental data set that could explain the variation in endogenic mineral distributions, with surface data treated as active samples and the Chaka Salt Lake data included as supplementary samples. The statistical significance of each forward selected variable was tested by a Monte Carlo permutation test (999 unrestricted permutations). All ordination analyses were carried out using version 4.5 of CANOCO software (ter Braak and Smilauer 2002).

Multivariate regression trees (MRT) analysis was applied as a useful method to explore the relationships between multi-species data and environmental characteristics (De'ath 2002), using the same environmental variables as in ordination analyses. The original data were used without any transformations or normalizations, while the similarities were measured by the Bray-Cutis method. MRT analysis was implemented using Brodgar 2.6.5 (Zuur et al. 2009).

7.4 Results

7.4.1 Chronology of the CKL-2004 core

Owing to the lack of organic remains, ten bulk organic samples were processed for accelerated mass spectrometry (AMS) ^{14}C dating in order to construct an age-depth model for the CKL-2004 core. Six of these samples were pretreated for carbonates, combusted, and cryogenically purified at Miami University and then analyzed at the University of Arizona's NSF-AMS Laboratory, while another four samples from a parallel core were analyzed at the University of Tokyo's Radiocarbon Laboratory. Assuming a constant "carbon reservoir effect" of 1,700 years derived from the asynchronous starting point of Younger Dryas (YD) event with well dated northern hemisphere records, all dating results (except the last two dates which are obviously biased from the age-depth sequence) were corrected, calibrated to calendar ages using Calib 4.4 program (Stuiver et al. 1998) (Table 7-2, Figure 7-2). Considering that the core was taken under the present lake water and the consistent lithology for the upper 450 cm of the core, we assume a continuous sedimentation process and the age

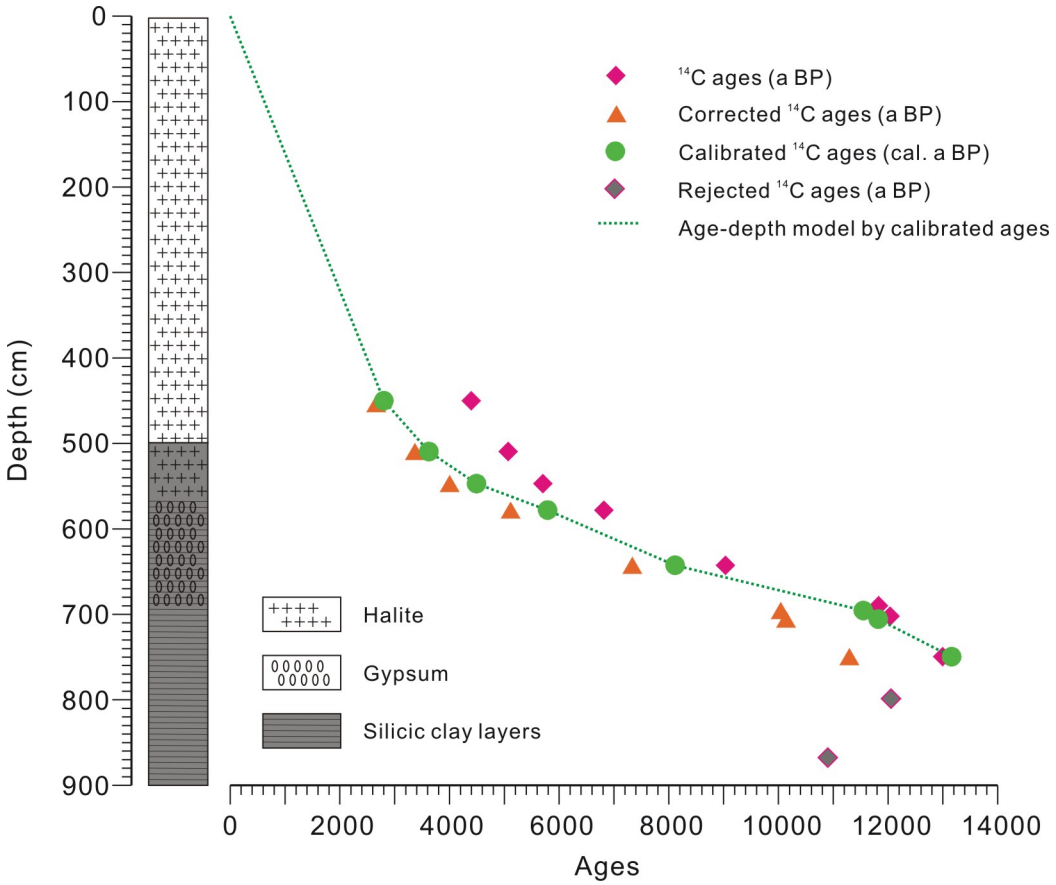

Figure 7–2 Lithology and chronology results for the CKL–2004 core

Table 7–2 AMS dating results and corresponding calibrated ages used to construct the age–depth model for the CKL–2004 core

Sample No.	Laboratory Code	Depth (cm)	Dated material	14C ages (a BP)	Ages corrected by 1700yr (a BP)	Calendar agesf (cal. aBP) by 2σ
CKL326[a]	TKa-14017[d]	447-453	TOC	4395 ± 30	2695 ± 30	2754-2851 (2802)
CKL340[a]	TKa-14018[d]	508-511	TOC	5070 ± 35	3370 ± 35	3554-3694 (3624)
CK308[b]	AA67512[e]	546-548	TOC	5705 ± 45	4705 ± 45	4401-4586 (4493)
CKL378[a]	TKa-14019[d]	577-579	TOC	6815 ± 35	5115 ± 35	5749-5830 (5789)
CK395[b]	AA67514[e]	642-643	TOC	9035 ± 50	7335 ± 50	8021-8208 (8114)
CK435[b]	AA67515[e]	695-696	TOC	11,740 ± 65	10,040 ± 65	11,270-11,824 (11,547)
CKL577[a]	TKa-14020[d]	705-706	TOC	11,840 ± 50	10,140 ± 50	11,601-12,041 (11,820)
CK480[b]	AA67516[e]	749-750	TOC	12,995 ± 85	11,295 ± 85	12,997-13,321 (13,159)
CK519[b,c]	AA67517[e]	798-799	TOC	12,054 ± 65	10,354 ± 65	11,979-12,401 (12,190)
CK568[b,c]	AA67518[e]	867-868	TOC	10,900 ± 120	9,200 ± 120	10,168-10,707 (10,437)

[a] Samples from the core parallel to the CKL–2004 core

[b] Samples from the CKL–2004 core

[c] Rejected ages

[d] Samples dated at Univerity of Tokyo's Radiocarbon Laboratory

[e] Samples prepared at Miami University and dated at University of Arizona's ASF–AMS Laboratory

[f] Ages in brackets were used for interpolations

of surface sediment is 0 cal. ka BP. All the calibrated ages were subsequently interpolated and extrapolated, in order to construct an age-depth model for the whole sequence. For further information about the chronology and more detailed discussions on this subject the reader is referred to Liu et al. (2008).

7.4.2 Mineral composition of surface samples

Chlorite and nine non-clay minerals were detected in our 146 surface samples. In order to take into account the fact that the surface samples were collected over a large area and were likely to be affected by variations in allogenic mineral influx, mineral composition percentages were calculated separately for endogenic and allogenic groups, according to Last (2001). As the dominant component of endogenic minerals, calcite was detected in all areas, with typical abundances greater than 50% and even up to 100% in some samples (Figure 7-1c). In contrast to calcite, the distribution of other endogenic minerals (aragonite, monohydrocalcite, gypsum and halite) was almost entirely restricted to the Qaidam Basin and the north-eastern Tibetan Plateau, with the exception of aragonite detected in three samples from the central Tibetan Plateau (Figure 7-1 d-g).

The allogenic mineral fraction is dominated by quartz, feldspar, mica and chlorite, but no obvious regional pattern was identified (Figure 7-1 h-k). The highest percentages of quartz occur in the central areas of the Tibetan Plateau and in the Yunnan area, while feldspar dominates the allogenic mineral spectra from the Qilian Mountains and Sichuan-Yunnan mountainous region. Dolomite is classified with the allogenic group, following the classification by Last (2001). It shows high abundances in the Qaidam Basin and central Tibetan Plateau and appears sporadically on the north-eastern Tibetan Plateau (Figure 7-1 l).

7.4.3 Carbonate content of surface sediment samples

In order to further verify the mineral compositions measured by XRD, the total carbonate content of surface sediment samples was analyzed by chemical methods. The carbonate contents derived from both of these methods, i.e. the total carbonate content from the chemical methods and the carbonate minerals determined by XRD (including calcite, aragonite, monohydrocalcite and dolomite), show a highly consistent correlation (Figure 7-3), which further confirms the reliability of our identifications and calculations for minerals using XRD methods.

7.4.4 Ordination of modern endogenic mineral spectra and environmental variables

Of the 146 surface samples, 39 were excluded from ordination analyses as no endogenic minerals were detected in them. The first two PCA axes capture 70.9% of the total variance (axis 1, 45.5%; axis 2, 25.4%), suggesting that the data structure is dominated by just a few underlying variables. The forward selection option within RDA analysis (including all the environmental variables listed in Table 7-1) identified three variables (the Mg/Ca ratio, the EC, and the Na+K/Ca+Mg ratio) that explained the variation in the endogenic mineral data

almost as well as the complete environmental data set (Figure 7-4; Table 7-1). This was also confirmed by the unimodal-based CCA analysis (results not shown). Partial RDA analysis was carried out for each of the three selected environmental variables. The variables capture 14% (Mg/Ca ratio), 13% (EC) and 4% (Na+K/Ca+Mg ratio) of the variance in the mineral dataset which is considered to be highly significant, suggesting that the Mg/Ca ratio and the EC have the greatest influence on the composition of endogenic minerals.

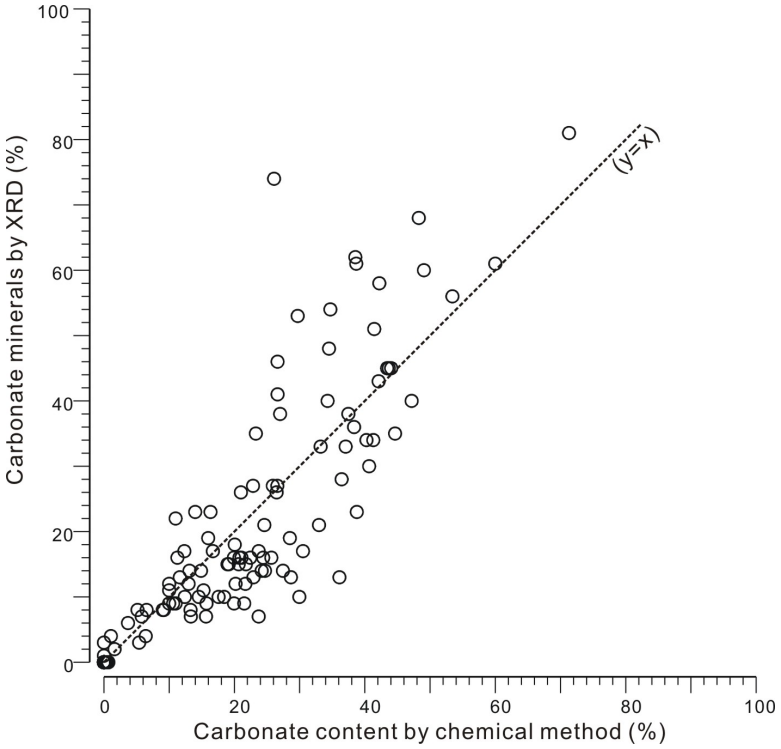

Figure 7-3 Scatter plot of carbonate mineral composition detected by XRD (percentages in bulk sediments) against the total carbonate content from chemical measurement.

7.4.5 MRT clustering of modern mineral spectra and environmental variables

The recursive partitioning procedure within MRT analysis, including all 12 environmental variables, resulted in a tree with 5 leaves (Figure 7-5), in which the EC and the Mg/Ca ratio were responsible for the first three levels of tree bifurcation and were able to explain 58% of total species variations. Endogenic minerals do not form when the EC is lower than 0.13 mS/cm (Group 1), which may explain the rejection by RDA analysis. The Mg/Ca ratio plays an important role in the mineral composition of lake sediments with EC values between 0.13 and 26 mS/cm: calcite dominates under low Mg/Ca ratio conditions (<33, Group 2) while aragonite is more common when the Mg/Ca ratio is above 33 (Group 3). EC values between 26 and 39 mS/cm also support the precipitation of monohydrocalcite, together with calcite and aragonite (Group 4), while values above 39 mS/cm result in the formation of gypsum and halite (Group 5).

7.4.6 Mineral composition of the Chaka Salt Lake sediment record

The samples from the CKL-2004 core consist mainly of three types of endogenic mineral

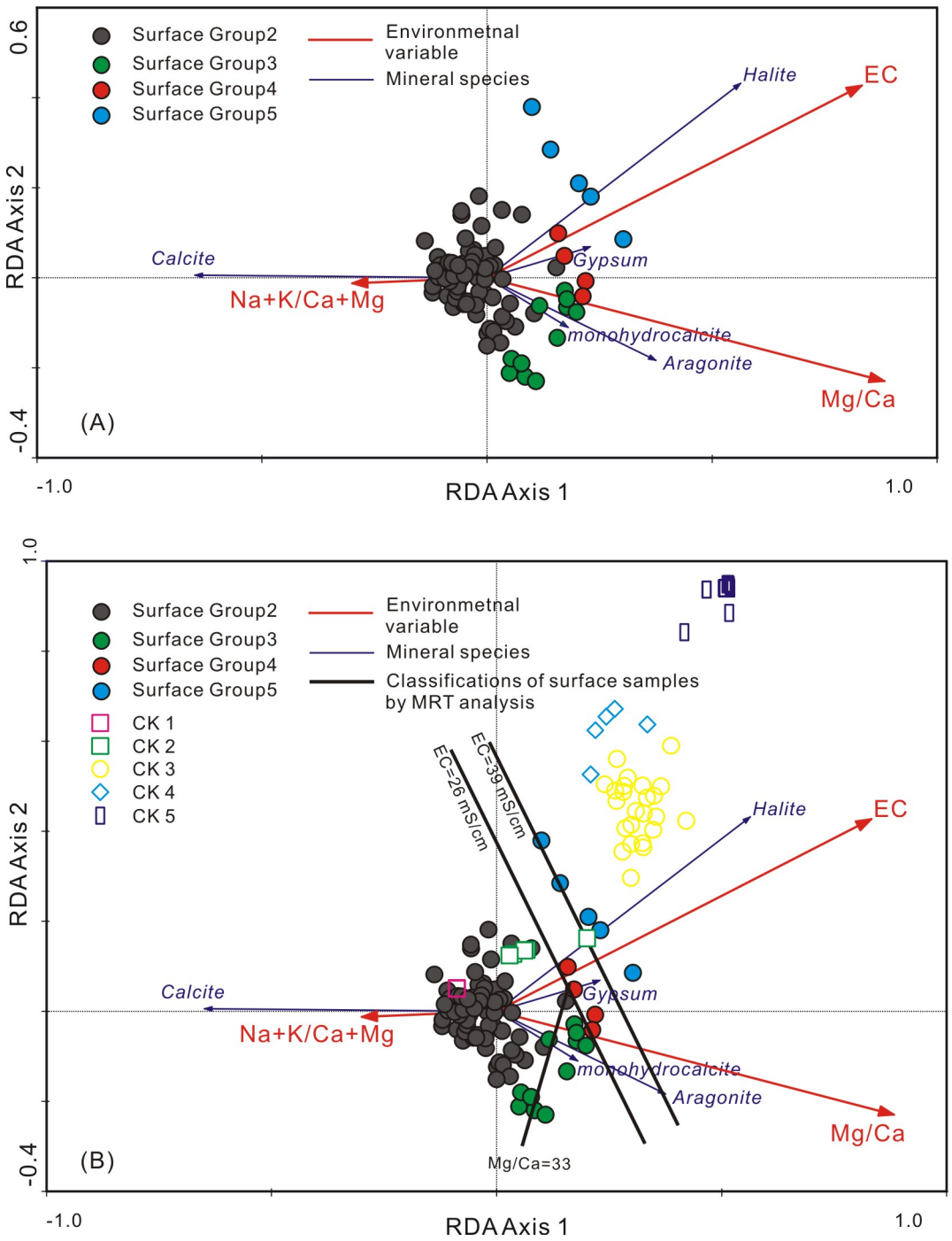

Figure 7-4 (A) Redundancy analysis (RDA) bi-plot of endogenic mineral assemblage of surface samples constrained by electrical conductivity (EC), Mg/Ca and Na+K/Ca+Mg ratios; the groups (solid dots) were identified by different colors. (B) RDA bi-plot, as in (A), and passively projected samples from the CKL-2004 core (empty symbols), together with the boundaries and associated threshold values derived from Multivariate Regression Trees (MRT) analysis (bold black lines, with the values near by).

(calcite, gypsum and halite) which make contributions to the bulk sediment composition that vary from 10% at the base of the core up to 100% in the upper part, and are accompanied by small amounts of several other evaporite minerals (glauberite, mirabilite, polyhalite and bloedite - not shown here; Liu et al. 2008a). From the variations in mineral compositions and

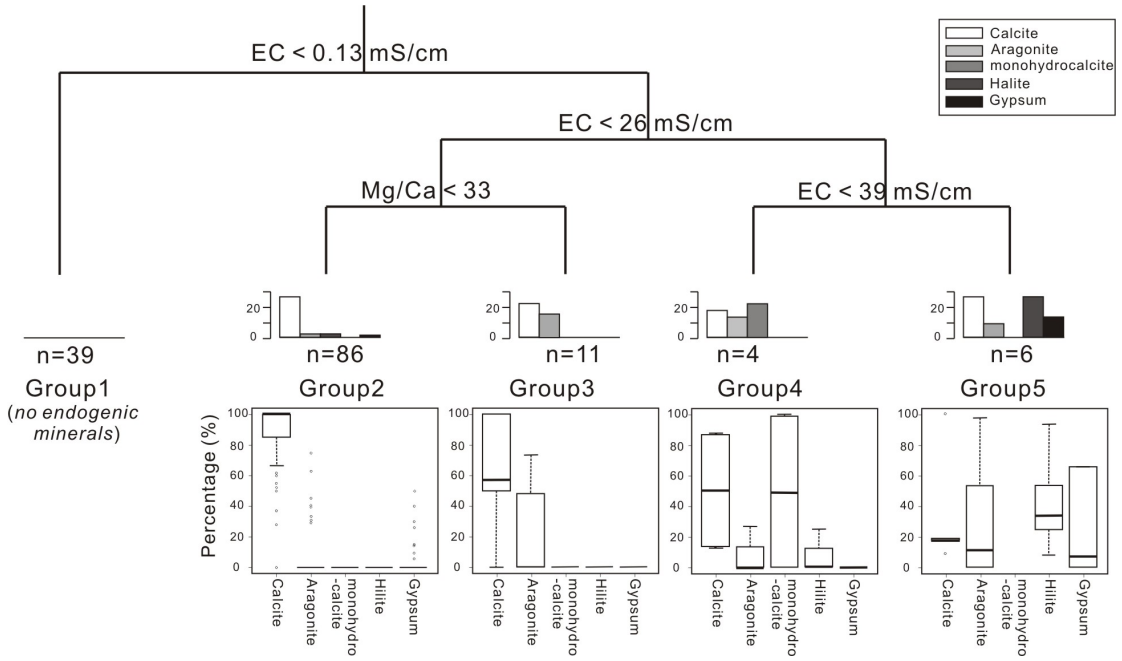

Figure 7-5 Multivariate Regression Tree (MRT) plot for endogenic minerals from 146 surface samples: histograms indicate the indicator values of mineral species in each group; box-plots show the mineral compositions of each group.

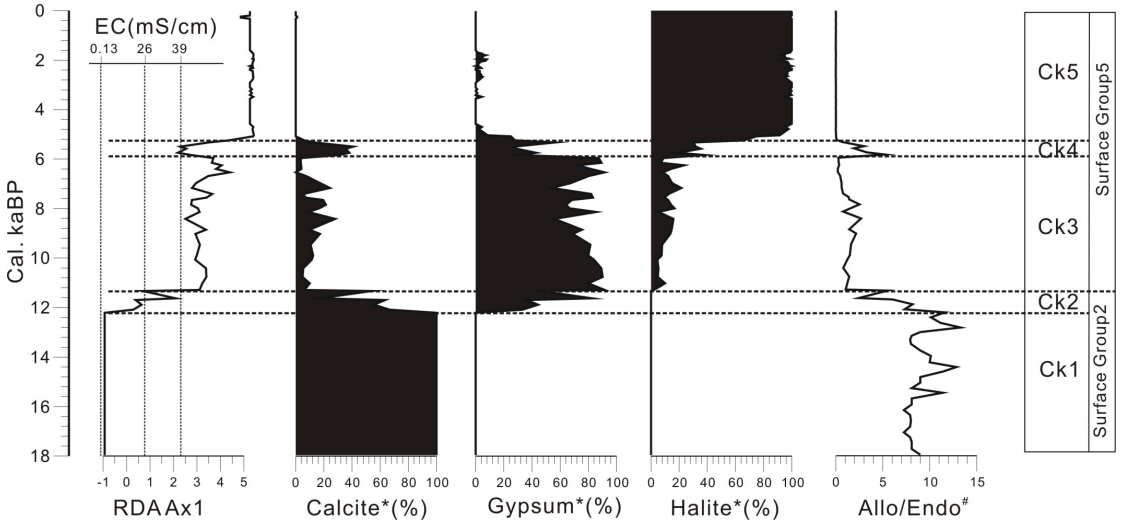

Figure 7-6 Mineral compositions for Chaka Salt Lake (after Liu et al. 2008a), and first axis scores from the RDA analysis. The stages of lake evolution and their associated groups are shown on the right (* percentages are calculated for endogenic minerals # Allo/Endo indicates the ratio of allogenic to endogenic minerals)

.the first axis score after RDA analysis, five sedimentary stages (from CK1 to CK5) could be identified between the bottom and the top of the core (Figure 7-6), which could be further classified into surface mineral Group 2 and Group 5 when passively plotted in the RDA biplot, due to the absence of aragonite and monohydrocalcite (Figure 7-4). The RDA first axis scores indicate a stepwise lake evolution; the scores were low before 12.4 cal. ka BP when the samples consist mainly of allogenic and a minor component of calcite, and then increase from -1 to 3 between 12.4 and 11.4 cal. ka BP in association with a decrease in the proportion of

allogenic minerals and the appearance of gypsum. A predominantly stable period then continued until 6 cal. ka BP when there was a sudden return to lower values, again characterized by a relatively high allogenic mineral component and calcite instead of gypsum as an endogenic mineral. After 5.3 cal. ka BP, the axis scores increase once again, reaching 4.5 and remaining consistently high until the present, correlating with the almost pure halite crystal section.

7.5 Discussion

7.5.1 Spatial distribution of modern mineral spectra from lake surface sediments

The allogenic minerals in lake sediments are probably transported into the lakes via surface streams, shoreline erosion, mass movement, or aeolian activity. Allogenic mineral spectra are therefore strongly affected by the hydrological conditions and geological settings of the lake's catchments. We used the geological map of the Tibetan Plateau (IGSNRR 1990) to summarize the geological strata in our study area into five rock types, namely limestone, granite, sandstone, diorite/gabbro, and all other rock types (Figure 7-1a). Despite its wide distribution, the above-average values of quartz in the mineral spectra from the central Tibetan Plateau are consistent with exposures of sandstones. The high quartz content at the Yunnan sites, however, probably derives from the quartz-granite dominated region to the east of these sites (Figure 7-1h). Exposures of diorite and gabbro are likely to be responsible for the high feldspar levels in mineral spectra from the south-eastern Tibetan Plateau, the Qilian Mountains, and the Yunnan and Sichuan provinces (Figure 7-1i). The geological map's description of limestone is rather imprecise and its distribution can therefore not be regarded as accurate information for use in the identification of mineral sources. In samples from the central Tibetan Plateau, the Qaidam Basin and some parts of the north-north-eastern Tibetan Plateau, more than 10% of the allogenic minerals derive from dolomite (Figure 7-1l). This is consistent with the observations of Zhang (2000), who indicated that limestone was the predominant rock type on the south-western Tibetan Plateau and in the Qaidam Basin. Furthermore, several lacustrine studies (Ahung Co: Morrill et al. 2006; Lake Erhai: Shen et al. 2006) have also confirmed the occurrence of limestone strata on the Tibetan Plateau and in the Yunnan area.

The only clay mineral detected in our study was chlorite, which made up between 0 and 27%, with an average abundance of around 10% (Figure 7-1k). Although chlorite has been used as an indicator of the primary source lithologies (Gibbs 1967) or the degree of weathering (Potter et al. 1975), no obvious distribution patterns could be identified from our surface samples, probably reflecting the coherent nature of the bedrock and the relative absence of chemical weathering processes under alpine climatic conditions.

Calcite constitutes the main endogenic mineral component across the entire study area, with a median abundance ~70%, as most of the lakes sampled are fresh or only slightly saline. Aragonite, monohydrocalcite, gypsum and halite are restricted to lakes on the northern Tibetan Plateau and in the Qaidam Basin due to the low precipitation levels and high ion concentrations in those areas (Figure 7-1 c-g). However, no pattern was discerned in the ratios

between endogenic and allogenic minerals (Figure 7-1b).

7.5.2 Water chemistry constraints on endogenic mineral formation

Endogenic minerals are indicative of lake water chemistry at the time of mineral formation. Endogenic mineral spectra consequently have been interpreted in terms of past changes in the geochemistry of the lake water, including the salinity (or EC), pH values, and/or Mg/Ca ratios (Campbell et al. 2000; Last 2001). Water temperature is also considered to influence the formation of endogenic minerals (Last 2001) with higher temperatures favoring the precipitation of carbonates.

The forward selection option within RDA analysis indicates that the Mg/Ca ratio and the EC are the two most important variables controlling the formation of endogenic minerals (Figure 7-4). This is also confirmed by the MRT results (Figure 7-5), as the Mg/Ca ratio and EC are responsible for the first three levels of tree bifurcation. No relationship was found between endogenic mineral compositions and meteorological factors such as temperature and precipitation.

Our analyses confirm the results obtained from a study of sediments in 25 European lakes by Müller et al. (1972), who found a relationship between Mg/Ca ratios and carbonate composition, i.e. that calcite precipitates at lower Mg/Ca ratios than aragonite. Although the threshold value of 33 inferred from our dataset is much higher than that of 12 suggested by Müller et al. (1972), this lower value remains a reasonable estimate since it relates only to the first appearance of aragonite, whereas the higher threshold value from our study relates to sites in which aragonite constitutes a major part of the mineral composition.

The pH value is an important geochemical factor in lake water and exerts a significant constraint on the precipitation of endogenic carbonate minerals by controlling the solubility of bicarbonate anions (HCO_3^-) (Canfield and Raiswell 1991). However, since most of our samples were collected from alkaline lakes (92% of the total lakes sampled - 134 lakes in total - had a pH above 7.5, and 82% - 120 lakes - had a pH above 8.0), neither the ordination (RDA) nor the MRT analyses detected any influence from the pH value.

The EC (or salinity) of lake water is generally considered to be a major factor influencing mineral precipitation, with carbonates dominating in fresh or brackish conditions and evaporites forming in saline to hypersaline lakes (Campbell et al. 2000; Last 2001). However, traditional descriptions of lake salinity status using terms such as “fresh”, “brackish”, “saline" and "hypersaline” are too vague, and EC values provide a more precise perspect. Our MRT results indicate that an EC value of 0.13 mS/cm is the minimum for mineral formation, which is also confirmed by the rejections in RDA analysis which indicate that no mineral precipitation occurs in “hyper-fresh conditions” owing to the absence of the necessary ions. Values up to 39 mS/cm correspond to fresh and brackish conditions, in which carbonates (calcite, aragonite and monohydrocalcite) predominate. In saline lakes where the EC value is greater than 39 mS/cm, gypsum and halite precipitate. However, owing to the lack of samples from saline and hypersaline lakes, no other evaporites were detected in our study, making it difficult to define any further EC thresholds.

7.5.3 Evolution history of Chaka Salt Lake based on mineral composition

Samples from Chaka Salt Lake, which were passively included in the RDA analysis, are aligned along the EC axis indicating that changes in this environmental variable are of primary importance for mineral formation. The general absence of aragonite indicates that the Mg/Ca ratios for the lake water never reached as high as 33, or even below 12. Five development stages have been identified for Chaka Salt Lake, based on the first axis scores and the compositions of endogenic minerals (Figs. 4 and 6). Using the Pitzer simulation model (Pitzer 1973), Liu et al. (2004, 2008) qualitatively reconstructed the salinity history of Chaka Salt Lake, with results that are broadly consistent with our own study.

The samples from the CK1 and CK2 stages fell into Group 2 of the surface samples after MRT analysis, implying a fresh to saline lake with EC values ranging from 0.13 mS/cm to less than 26 mS/cm. The sediment is mainly composed of allogenic materials with minor calcite before 12.4 cal. ka BP (Stage CK1) reflecting the prevalence of freshwater lake under relatively wet conditions. Evidences of wet phases during the late glacial were also reported from the Qinghai-Tibetan Plateau, such as the lake overflow in Zabuye Salt Lake (Wang et al. 2002), the climate amelioration in Qinghai Lake (Shen et al. 2005), which probably resulted from the input of glacial melt water into the lakes, and/or increased precipitation following the onset of Asian Summer Monsoon (ASM).

The decreasing ratio of allogenic to autogenic minerals and the increasing gypsum content during the subsequent thousand years (Stage CK2) indicate a transition from a freshwater to a slightly saline lake. Such decreasing regional effective moisture reflected by the increase in salinity is, however, conflicting with the widely reported intensification of ASM in the early Holocene (Shen et al. 2005; Mischke et al. 2008), in the other hand, might be explained by the potential increase of summer temperature and subsequent evaporation which exceeded the precipitation brought by the ASM.

The allogenic mineral content decreases markedly after 11.4 cal. ka BP (Stage CK3), and gypsum replaces calcite as the main endogenic mineral. In addition, the first appearance of halite indicates that the lake's salinity had increased to conditions with EC over 39 mS/cm, which held the first half of the Holocene. Following the further intensification of the ASM (Wang et al. 2005a), enhanced precipitation probably balanced the local evaporation, resulting in a stable saline lake during this period.

However, after a brief period between 6.0 and 5.3 cal. ka BP (Stage CK4), where high allogenic mineral and calcite existed, indicative for a slight decrease in the EC, the sediment is dominated by nearly pure halite, indicating the development of hypersaline conditions (Stage CK5). Owing to retreat of ASM after mid-Holocene, decrease in precipitation and corresponding water balance caused the further increase in EC of lake water, which reached conditions much higher that 39 mS/cm. However, our data set does not contain enough information from high salinity lakes to allow quantification of the changes within these last three stages.

In summary, applying the first axis scores from the RDA ordination, in combination with the

EC thresholds obtained from the MRT analysis, indicates that changes in the EC of the lake water exerted a major influence over the mineral composition in Chaka Salt Lake, while changes in the Mg/Ca ratio were of minor importance. Reconstructed EC conditions represent the evolution of Chaka Salt Lake from a freshwater at the late glacial, to the present hypersaline lake, which is primarily driven by the summer solar insolation, and the corresponding fluctuations of Asian Summer Monsoon.

7.5.4 Implications for paleolimnological studies

Our study indicates that the mineral composition of sediments is of great value in the interpretation of paleolimnological records. Challenges still remain with these interpretations, however, due to the complexities of mineral formation and deposition.

Identification of the mineral source is the most difficult aspect of interpreting mineral composition from the Tibetan Plateau. Most minerals can derive from multiple possible origins: carbonate minerals, for example, could be allogenic, authigenic or endogenic. Especially for dolomite, it could dominate the weathered sediments owing to its higher residence to weathering compared with calcite. Where such investigations are performed at sites with restricted catchment areas and a low aeolian sediment contribution, the analysis of soil and bedrock samples from the vicinity of the lake may help to identify allogenic mineral sources.

The development of X-ray diffraction techniques provides us with the opportunity to make semi-quantitative estimates of mineral composition. However, no definitive method has yet been developed for the precise quantification of mineral composition, although various methods have been proposed, such as using added minerals (e.g., corundum) as comparable species (Liu et al. 2003), monomineral sample calibrated peak intensities (Mischke et al. 2008), and RIR-value calibration. Furthermore, some trace minerals that constitute less than 5% of bulk samples, are difficult to detect by common XRD methods.

Our study indicates that further investigations into the mineral compositions of lacustrine sediment samples, together with environmental variables or even environmental monitoring, would yield significant advances in our understanding of the relationships between mineral formation and the environment. With regard to the Tibetan Plateau, additional samples from saline and hyper-saline lakes would further strengthen our data set and allow environmental thresholds in the upper EC range to be determined.

7.6 Conclusions

By relating the mineral compositions of 146 surface sediment samples from lakes on the Tibetan Plateau to their geographic location and local environmental variables, we have been able to infer that

(1) the compositions of common allogenic minerals, i.e. quartz, feldspar and mica, are similar across the Tibetan Plateau, and regional maxima in quartz and feldspar abundances can be reasonably explained by the local geological settings; the contributions of dolomite, on

the other hand, need to be regarded cautiously owing to its complicated origins,

(2) electrical conductivities and Mg/Ca ratios in lake water are the main environmental variables controlling the composition of endogenic minerals, and

(3) the evolution history of Chaka Salt Lake over the last 18,000 years can be quantified from the sedimentary mineral record in terms of electrical conductivity variations.

Acknowledgements

Special thanks to Bo Yang (Institute of Salt Lakes, CAS) for his assistance with XRD measurement and quantitative identification. Y. Wang's doctoral research is funded by the "Helmholtz - China Scholarship Council (CSC) Young Scientist Fellowship" (No. 2008491101). The research was funded by China Global Change Research Program (Grant No. 2010CB950101), the German Research Foundation (DFG) and the National Natural Science Foundation of China (Grant No. 41072131). We gratefully acknowledge the assistance provided by Chengjun Zhang (Lanzhou University) during the field work. We appreciate the helpful comments of Dr. Thomas J Whitmore (chef editor), Dr. Jonathan Holmes (associate editor) and two anonymous reviewers.

8 Appendix-2 Manuscript 6: High-resolution sedimentary archive from landslide-dammed Lake Mengda, north-eastern Tibetan Plateau.

Yongbo Wang [a, b, c], Ulrike Herzschuh [a, b], Xingqi Liu [c], Oliver Korup [b], Bernhard Diekmann [a]

[a] *Alfred Wegener Institute for Polar and Marine Research, Research Unit Potsdam, Telegrafenberg A43, 14473 Potsdam, Germany*

[b] *Institute of Earth and Environment Science, University of Potsdam, Karl-Liebknecht-Str.24, 14476 Potsdam, Germany*

[c] *State Key Laboratory of Lake Science and Environment, Nanjing Institute of Geography and Limnology, Chinese Academy of Sciences, 210008 Nanjing, P.R. China*

Current Status: In preparation.

Abstract

Lacustrine sediments have been widely used to investigate past climatic and environmental changes over millennial to seasonal time scales. However, the sedimentary archives of lakes in mountainous regions may also record non-climatic events such as earthquakes or catastrophic sediment pulses. We argue herein that a set of 64 annual laminations sufficiently reconciles a stratigraphically inconsistent accelerator mass spectrometry (AMS) 14C chronology in a ~4-m long core from Lake Mengda, in the north-eastern part of the Tibetan Plateau. These laminations indicate that the lake was most likely formed by a large landslide triggered by the 1927 Gulang earthquake (M=8.0). The lake sediment sequence can be separated into three units based on lithologic, sedimentary, and isotopic characteristics. Starting from the bottom of the sequence these are: (1) unweathered coarse sandy valley-floor deposits that pre-date the lake, (2) landslide deposits capped by fine-grained soil with a high organic content, and (3) lacustrine sediments with a low organic content and typical laminations. These laminations provide a high-resolution record of anthropogenic and environmental changes during the 20th century, recording sediment input associated with two phases of construction activities. At the same time, the high mean sedimentation rates of up to 4.8 mm yr–1 underscore the potential for distinct sediment pulses, even in remote, forested, and seemingly undisturbed mountain catchments.

8.1 Introduction

Lake sediments have been commonly used to trace past climatic and environmental changes because of the relatively stable and continuous deposition processes that are assumed for most large, stable lake basins (Last and Smol, 2001). However, a number of lakes formed by

tectonic, glacial, volcanic, or other natural damming processes may be of a more transient nature (Lerman, 1978). Dams formed by ice, moraine, and landslides in particular may be short-lived and can give rise to large floods during sudden events, resulting in substantial loss of life and damage to property (e.g. O'Connor and Costa, 2004). Systematic studies on the stability of such lakes are therefore of great importance for mitigation of future losses.

Hundreds of naturally dammed lakes occur in the mountainous regions of central and western China, especially along the upper tributaries of the Yangtze River and the Yellow River. How many of these lakes have the potential to develop into future hazards remains unknown (Chai et al., 2000; Ma et al., 2004b). The history of most of these dammed lakes has not been investigated, indicating a large gap in our knowledge of the geomorphology of these mountainous regions. Most of the studies that have been completed on naturally dammed lakes have tended to focus on ice-dammed lakes that formed over long-term glacial-interglacial time scales (Huss et al., 2007; Mangerud et al., 2001). Research on decadal to centennial scales into the dynamics of many of China's mountain lakes has, to a large extent, been limited by the absence of analyses combining geomorphic interpretations with detailed investigations into lacustrine archives.

We have sought to address this shortcoming and present herein a continuous sediment core recovered from Lake Mengda, a small mountain lake on the north-eastern margin of the Tibetan Plateau. We address the triggers, processes, and timing of the formation of Lake Mengda, together with the subsequent evolution of the lake, on the basis of geomorphological evidence and the chronological and sedimentary proxies from within the lake sediments.

8.2 Study area

Lake Mengda (35.79 °N, 102.67 °E; 2515 m a.s.l.) is located on the boundary between Qinghai and Gansu provinces, close to the upper reaches of the Yellow River that drain the north-eastern margin of the Tibetan Plateau (Figure 8-1A). The lake is about 700 m long and 250 m wide, covering an area of about 0.175 km^2. Steep mountain ranges that reach up to 2700 m a.s.l. dominate the north-western and south-eastern sides of lake. The lake has a water depth of about 20 m, as determined from field measurements (Figure 8-1B). Most of the inflow derives from precipitation during the East Asian Summer Monsoon and a number of small streams. According to the meteorological station at Xunhua, the mean annual temperature in the area is 4.4 °C, with the lowest monthly mean of -8.8 °C occurring in January and the highest monthly mean of 15.6 °C occurring in July; the mean annual precipitation is around 623 mm (Qinghai Forestry Bureau, 1990).

The mountainous regions surrounding the lake are mainly covered in coniferous forests consisting of *Abies fargesii* Franch, *Larix potaninii* Batal, *Picea crassifolia* Kom, *Pinus armandii* Frahch and *Juniperus formosana* Hayata, together with patches of scrub, e.g., *Salix sclerophylla* scrub, *S. ortitrepha* scrub and *Dasiphora fruticosa* scrub (Hou, 2001; Lu and Si, 2005).

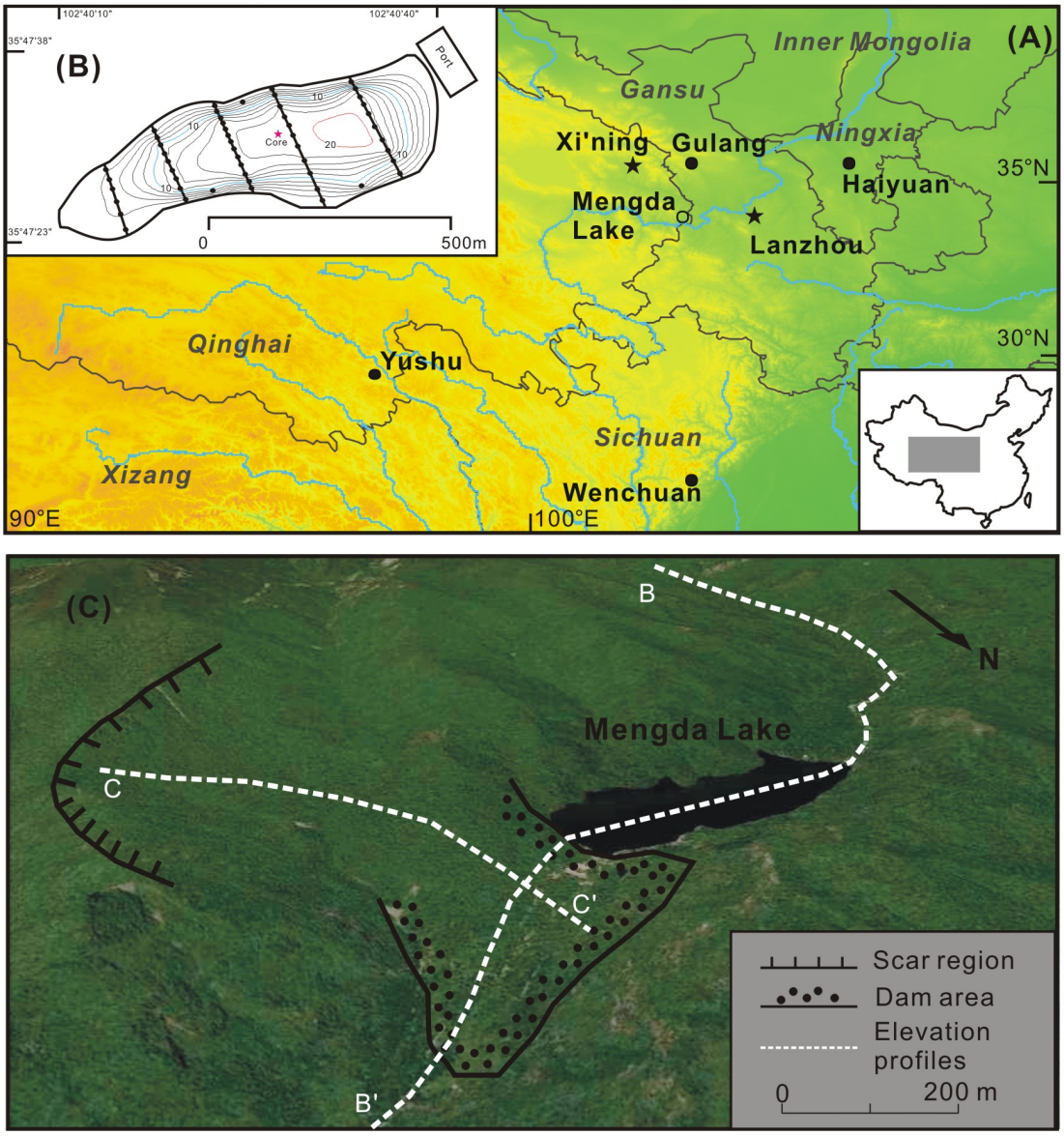

Figure 8-1 A. Overview of the study area and locations mentioned in the text. Stars: major cities; closed circles: recorded earthquakes; open circle: location of Lake Mengda; blue lines: major rivers; gray lines and gray text: province boundaries and names. B. Bathymetry of Lake Mengda: black dots indicate the locations of measurements and the red star the location of the core. C. Sketch map showing the geomorphologic setting surrounding the lake: the possible landslide scar, the dam, and the tracks of the elevation profiles (B–B' and C–C').

8.3 Materials and methods

8.3.1 Fieldwork

An expedition was carried out in autumn 2008, during which the water depth of the lake was measured with an SM-5 Depthmate Portable Sounder. Two continuous sediment cores (Core A and Core B) were collected from the central part of the lake beneath about 18 m of water

using the UWITEC platform and coring system (see location in Figure 8-1B). Large pieces of wood were recovered from the bottom of both cores.

8.3.2 Laboratory analyses

The overlap between the core segments was identified using scanning magnetic susceptibility data, resulting in ~400 cm (Core A) and 430 cm composite length (Core B). The longer Core B was selected for subsequent analyses.

Ten samples including six total organic carbon (TOC) samples and four macrofossil samples consisting of wood fragments were selected for AMS ^{14}C dating at the Leibniz-Laboratory for Radiometric Dating and Stable Isotope Research, University of Kiel. Both the humin and humic fractions were extracted and dated from the TOC samples.

Before splitting the core the major element distributions along the core segments were evaluated by X-Ray Fluorescence (XRF) analysis using the Avatec XRF/Color Core Scanner at AWI-Bremerhaven. The semi-quantitative XRF analyses were measured using voltages of 10 and 30 keV and a current ranging from 700 to 1000 mA, at 1 cm intervals. Elemental XRF peak area intensities were measured in total counts per second (cps). More detailed descriptions of the procedure can be found in Pompilio et al. (2007). High resolution color indices were also extracted, at 0.16 mm intervals.

The core segments were divided into 5 mm intervals and freeze-dried for further analyses. Magnetic susceptibilities (MS) were measured on the dried material using a Bartington MS2 System. Measurements of the total organic carbon content (TOC), the organic carbon isotope ratio $\delta^{13}C$, and the total organic nitrogen content (TN) were performed on powdered samples after first removing the carbonates, using a Vario EL III Element Analyzer (Elementar Analysensysteme GmbH, Hanau, Germany). For grain size analyses, the sediment samples were first treated with H_2O_2 (35%) to remove any organic matter and HCl (10%) to remove the carbonate, and then measured using a Laser Diffraction Particle Analyzer (Coulter LS 200).

8.3.3 Data analysis

We chose the End-Member Modeling Algorithm (EMMA) developed by Weltje (1997), which can convert measured grain-size distributions into proportional contributions of an optimal set of end members (Weltje and Prins, 2003; 2007), and evaluated the end members (EMs) from the total set of grain size measurements. The cumulative explained variance in grain size was used to determine the number of end members. All calculations were carried out using Matlab software. A detailed description on the EMMA method can be found in Dietz et al. (2011).

In order to characterize the geomorphic setting of the lake catchment we obtained topographic profiles along the valley in which Lake Mengda is located and a transverse profile past the downstream end of the lake using ESRI ArcMap 9.2 and ASTER GDEM data with a nominal resolution of 30 m. The hydrology analysis method within the Spatial Analyst tool package was applied to identify the track of the elevation profiles, while the 3D Analyst package

helped to construct the elevation profiles.

8.4 Results

8.4.1 Radiocarbon dating

The TOC samples yielded ages ranging between 400 and 1100 a BP. Consistently younger ages were obtained from the humic fractions than from the humin fractions (Table 8-1, Figure 8-2B). The ages were found to be distinctly out of stratigraphic order. Except for one relatively old age (670±20 a BP) from a large piece of wood at the bottom of the core, much younger ages were deduced from the three other wood fragment samples than from the TOC samples, i.e. 175±25, 140±20, and 85±25 a BP (Table 8-1, Figure 8-2B).

Table 8-1 AMS ^{14}C dating results for sediment core from Lake Mengda

Sample	Depth (cm)	Lab. Code	Material	AMS ^{14}C (a BP)
MD002	1	KIA39502	TOC Humic	435±25
MD002	1	KIA39502	TOC Humin	700±25
MD050	25	KIA39503	TOC Humic	715±25
MD050	25	KIA39503	TOC Humin	960±25
MD209	*105*	*KIA39508*	*Wood pieces*	*175±25*
MD355	178	KIA39504	TOC Humic	840±25
MD355	178	KIA39504	TOC Humin	1105±25
MD562	239	KIA39505	TOC Humic	630±20
MD562	239	KIA39505	TOC Humin	905±25
MD562	*239*	*KIA39509*	*Wood pieces*	*140±20*
MD718	267	KIA39506	TOC Humic	520±25
MD718	267	KIA39506	TOC Humin	840±20
MD930	382	KIA39507	TOC Humic	515±20
MD930	382	KIA39507	TOC Humin	825±40
MD1001	*418*	*KIA39510*	*Wood pieces*	*85±25*
MD1037	436	KIA39511	Wood pieces*	670±20

8.4.2 Grain size distributions and end member analysis

According to the accumulative explained variances of grain size by EMs, a two-member model was selected that explained up to 94% of the total variance (Figure 8-3A). The first end member (EM1) shows a unimodal pattern with a median grain size of ~70 μm and a slight skew to the coarse fraction (Figure 8-3B). In contrast, the second end-member (EM2) reveals a finer grained pattern with two main fine-sized fractions at about 4 and 20 μm, as well as a minor contribution from a coarse fraction greater than 100 μm (Figure 8-3B).

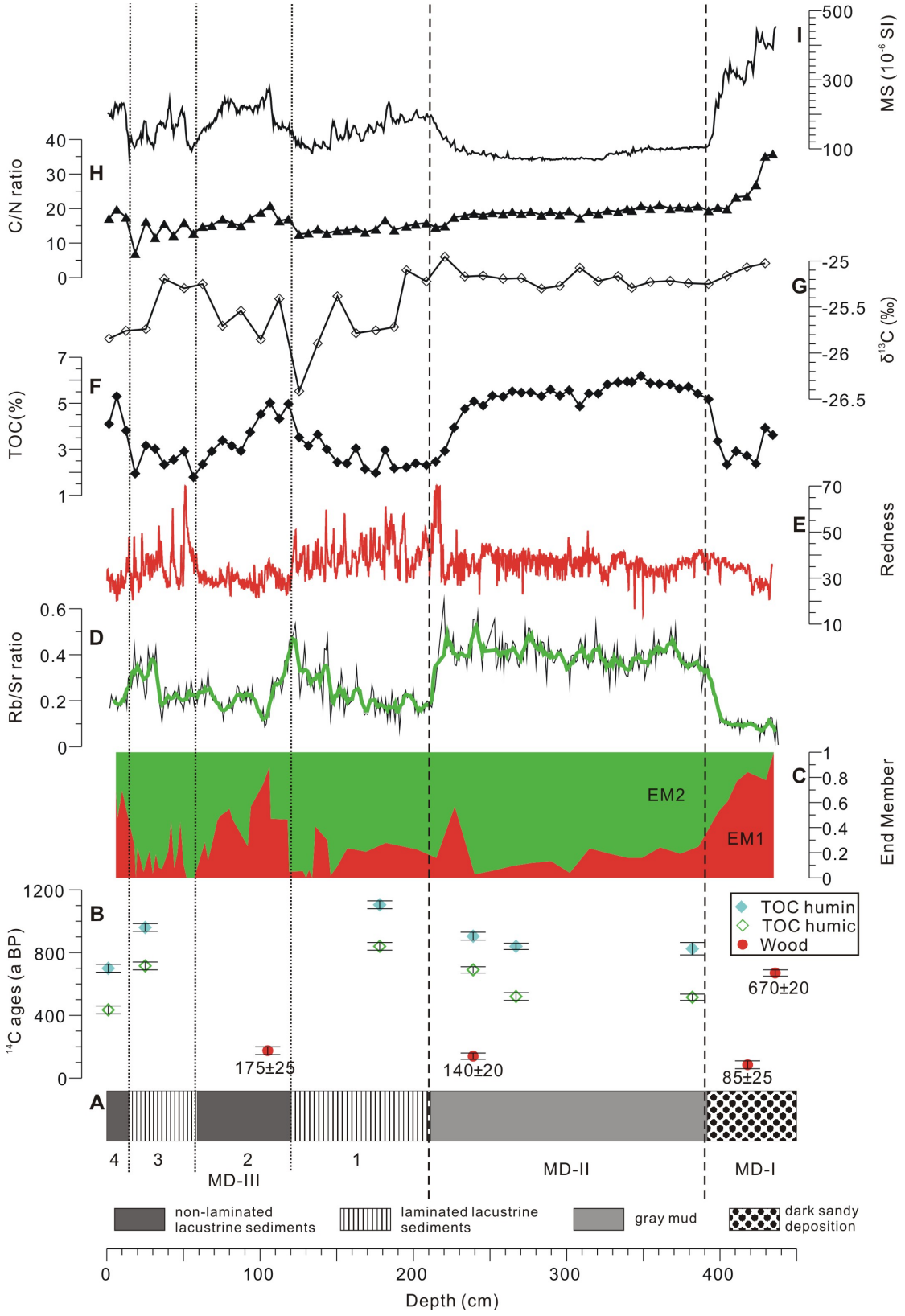

Figure 8-2 Results of core analyses. A: Lithology and sedimentary units. B: Radiocarbon dating. C: End Member analysis. D: Rb/Sr ratios. E: Redness. F: Total organic carbon content. G: Organic carbon isotope H: C/N ratios. I: Magnetic susceptibility. Vertical dashed and dotted lines indicate the boundaries between sedimentary units.

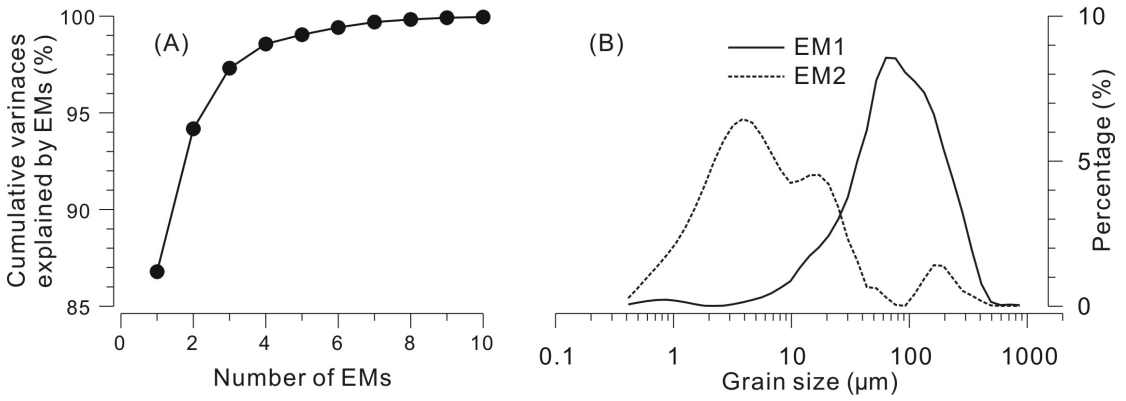

Figure 8–3 A. Cumulative variances explained by end members (EMs) plotted against the number of EMs. B. Grain size distributions for two end members, EM1 (solid line) and EM2 (dashed line).

8.4.3 Lithologic and sedimentary proxies

The core sequence was divided into three major sedimentary units (Figure 8-2) on the basis of lithology and the results from sedimentary proxies:

Unit MD-I (below 390 cm core depth) is characterized by coarse, dark sediments, as indicated by the predominance of EM1 (up to 80%) and low redness values of ~30. The TOC content is generally low (~2%), the C/N ratios are high (up to 35), and the $\delta^{13}C$ values are around -25‰. The rubidium strontium (Rb/Sr) ratios are very low at ~0.1. The unit is characterized by extremely high MS values (up to 5×10^{-4} SI).

Unit MD-II (390-210 cm core depth) consists of unlaminated gray mud with a grain-size distribution that is dominated by EM2 (>80%). The redness values are relatively stable at around 35, with only minor fluctuations. The TOC content is dramatically higher than in the underlying unit and includes the maximum for the entire sequence (~6%). The C/N ratios are stable at ~20, as are the $\delta^{13}C$ values at about -25.2‰. The Rb/Sr ratios are high (around 0.4, with minor variations). The unit also features the lowest MS values determined, at around 1×10^{-4} SI.

Unit MD-III (0-210 cm core depth) is characterized by distinct laminations and can be further divided in to four subunits. MD-III-1 (210-120 cm) and MD-III-3 (60-15 cm) are characterized by alternating light and dark laminations typical of lacustrine deposits, which correspond with marked fluctuations in redness values. The number of laminations counted was 47 in MD-III-1 and 17 in MD-III-3, which also correlates with the high resolution redness data. The upper 15 cm of the core (MD-III-4) and the section between 60 and 120 cm (MD-III-2) show no laminations and have coarser grain sizes, as indicated by the high EM1 contributions (up to 60%). These two unlaminated sections also show identical TOC contents to MD-II (over 5%), compared to ~2% for the laminated sections for which slightly lower C/N ratios were also determined. The $\delta^{13}C$ values fluctuate between -25‰ and -26‰. The sections with no laminations show slightly higher MS values (~2×10^{-4} SI) than the laminated sections (1-1.5×10^{-4} SI).

8.4.4 Elevation profile analyses

Figure 8-4 (a, b) shows an 11 km long elevation profile that reveals a generally smooth slope both upslope and down slope from Lake Mengda between 3200 and 2000 m a.s.l. The profile shows a conspicuous rise at 2550 m a.s.l. to about 20 m above the current lake level, and the transverse profile immediately downstream from the lake has a distinctly asymmetric shape (Figure 8-4c).

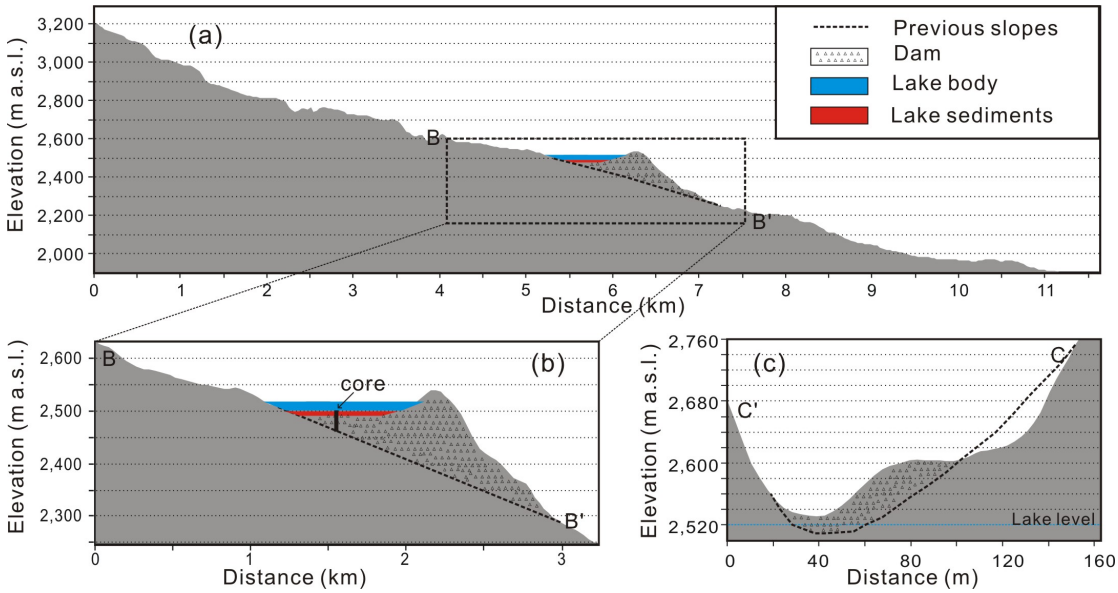

Figure 8-4 Elevation profiles for (a) the whole valley, (b) the valley section close the lake, and (c), transverse profile across the dam and scar. See the tracks marked "B'-B" and "C'-C" in Figure 8-1C.

8.5 Discussions

8.5.1 Explanation potential of sedimentary proxies

The C/N ratio can serve as an indicator for the source of organic materials in lacustrine sediments, owing to distinguishable characteristics between algae and vascular plants (Meyers and Lallier-Verges, 1999). The high cellulose and low protein content in vascular land plants leads to a higher C/N ratio (C/N>20) than in algae (4<C/N<10) (Meyers and Lallier-Verges, 1999). The low organic carbon isotope $\delta^{13}C$ values suggest that the organic material in Lake Mengda was mainly derived from C3 land plants (Meyers and Lallier-Verges, 1999). This is consistent with the fact that the lake catchment is partly covered by coniferous forests (Hou, 2001; Lu and Si, 2005). On the other hand, the marked variations in $\delta^{13}C$ values within the MD-III unit, together with the slightly lower C/N ratios in the laminated sections, may indicate a contribution from lake primary producers such as algae to the total organic carbon.

The Rb/Sr ratio was originally recognized as an indicator of the degree of pedogenesis for loess-paleosol sequences, due to the preferential solution of Sr relative to Rb (Goldstein, 1988;

Chen et al., 1999). This ratio has subsequently been applied to lacustrine sediments in order to quantify the degree of weathering within lake catchments on the Tibetan Plateau (Jin et al., 2005), and northern China (Jin et al., 2006). The low Rb/Sr ratios in the sandy MD-I unit may therefore indicate the deposition of largely unweathered material. In contrast, the higher Rb/Sr ratios for the generally fine-grained sediments in MD-II suggest that they may have been derived from material containing a high proportion of soil-forming minerals. Those sections with a higher degree of weathering in the MD-III unit that interrupt the relatively un-weathered lacustrine sediments are likely to be indicative of an increased contribution from terrestrial erosion during the deposition of the unlaminated sub-units.

The two end members represent distinctly different patterns in the grain size distributions, suggesting different possible sources for the sediments (Weltje and Prins, 2003; 2007). The EM1 end member represents the grain-size distribution of the uniformly sandy sediments at the base of the core. These can be interpreted as being due to sedimentation in a fluvial backwater or to fine-grained slopewash deposits. In contrast, EM2 represents patterns of bi-modal or tri-modal lacustrine sediments dominated by fine clay and silt fractions. We suspect that the higher proportions of EM1 probably indicate larger contributions of fluvial or slope deposits to the sediments.

The magnetic susceptibility (MS) of sediments may indicate the relative proportion of magnetic minerals in of the sediments. The bedrock surrounding the lake consists mainly of granodiorite, which is the likely source of magnetic minerals in the sediments. At the base of the core (unit MD-I), the high proportions of largely unweathered minerals are responsible for the extremely high MS values. The high MS values in the unlaminated sections of MD-III may possibly indicate further pulses contributing fresh, unweathered minerals, while the moderate MS values in the laminated sections suggest a reduced supply of such minerals. The extremely low MS values in MD-II may therefore indicate a very limited supply of unweathered minerals.

8.5.2 Formation and evolution of Lake Mengda

The ages obtained from the TOC samples show identical ranges to those obtained from the large wood fragments (670±20 a BP) at the base of the core (Figure 8-2B). This suggests that the TOC-based dating results may largely reflect the age of small pieces of wood embedded in the sediments. The predominance of organic material of terrestrial origin is confirmed by the high C/N ratios for the TOC. The slow rate of decomposition of wood in soils may contribute to these old ages. The three younger ages obtained from wood fragments (175±25, 140±20, and 85±25 a BP) may indicate a more recent source that is different from the older wood fragments that dominate the TOC. The youngest age from the base of the core indicates that the lake is most probably no more than 100 years old.

Our interpretation of the stratigraphically inconsistent AMS chronology data is supported by the number of laminations in the sediment core. Apart from the variations in sediment color, the grain-size distributions also shows distinctly different patterns between light and dark layers, with a slightly higher proportion of coarse material in the darker layers. Available

climate data (Qinghai Forestry Bureau, 1990) indicates that the entire lake surface is frozen during the winter and early spring, thus preventing the deposition of any coarse, dark materials and resulting in the formation of the fine-grained and relatively light colored layers. After the lake ice thaws in spring the coarse materials previously stored above or in the ice, together with aeolian deposits and those from surface runoff, begin to settle in the lake, forming the coarse-grained, darker layers. In other words, we interpret the laminations to represent buffered seasonal variations in sediment supply. This age model would sufficiently explain the ^{14}C ages as being artifacts of old wood fragments transported with incoming sediment. We therefore propose a tentative lake history based on this age model. The total count of 64 laminations preserved in the upper part of the core indicates that the lake is less than 100 years old, and is generally consistent with the radiocarbon dating results, taking into account the possible errors in identifying laminations and the sedimentation that occurred during periods when no laminations were formed.

The results of both radiocarbon dating and lamination counting indicate that the Lake Mengda system may have formed in the early part of the 20th century. The geomorphic evidence of a large triangular detachment zone above the downstream end of the lake, together with an asymmetric hump at the lower edn of the lake, points to lake formation behind a large, potentially catastrophic, landslide. In this scenario, hillslope material from about 1 km to the east of the lake would have slid down and abruptly dammed the valley. The existence of a dam-like structure can be clearly identified from the elevation profiles (Figure 8-4 a, b) as well as the asymmetric pattern of the transverse profile (Figure 8-4 c). River-blocking landslides of this size can be triggered by either heavy rains or earthquakes. Historical seismic records indicate that the 1927 Gulang Earthquake (M=8.0) had its epicenter some 100 km to the north of Lake Mengda (Lanzhou Earthquake Administration, 1991; Figure 8-1A). This earthquake caused severe damage in Lanzhou city, and was large enough to have caused numerous landslides (Keefer 2002). The larger of these landslides could easily have dammed river valleys, and one such natural blockage may have led to the formation of Lake Mengda. Observations following similar large earthquakes in western China, such as the Wenchuan Earthquake (M=8.0; 12th, May, 2008) (Ou and Li, 2011; He et al., 2011a, 2011b), and the Yushu Earthquake (M=7.1; 14th, April, 2010) (Xu et al., 2011) confirm that several hundred landslide-dammed lakes may form as a result of such regional-scale disturbances.

The base of the core (Unit MD-I) is distinctly different from the remainder of the sedimentary column. Its high content of large wood fragments suggests that it may have been a former ground surface, and may therefore represent part of the original valley floor, dominated by a sand fraction (EM1). Large proportions of unweathered minerals have produced high MS values and low Rb/Sr ratios, as well as an extremely low TOC content. If the 1927 earthquake did indeed trigger the landslide, large volumes of soil may have been transported into the area from the north-western slope, thus damming the valley. The rather stable sedimentary proxies in the MD-II unit indicate a uniform source of sediments. The extremely high TOC content, high degree of weathering (or pedogenesis), fine grain size, and low MS all indicate a unique source that is different from the other parts of the sequence, and probably of soil origin. A lake system had formed by the beginning of the MD-III unit, as indicated by the typical lacustrine laminations. The large fluctuations in organic carbon isotope levels and relatively low C/N

ratios in the laminated sections may be indicative of contributions from lake primary producers such as algae. The lacustrine sedimentation process was interrupted between depths of 60 and 120 cm, which would translate to a period ending some 20 years ago since 17 laminations were counted between 15 and 60 cm core depth. A nature reserve station was set up in the Lake Mengda catchment area during the 1980s, and the associated construction work may have disturbed the natural sediment input, possibly resulting in the sub-units with no laminations. A similar situation may also have occurred during the last few years, when construction work for a nature park was underway, resulting in the absence of laminations in the uppermost 15 cm of the sediments.

8.6 Conclusions

In this paper we have demonstrated the limitations of relying on a standard AMS ^{14}C dating approach to reveal the history of a small mountain lake in the headwaters of the Yellow River, China. Counting annual laminations has instead helped constrain an age for the lake's formation. The lake is characterized by very high average sedimentation rates (>4.8 mm yr^{-1}), most likely due to sudden inputs of material as a result of natural disturbances such sediment pulses following earthquakes or heavy rains, or of anthropogenic construction work. In this and other tectonically active regions, earthquake-triggered landslides have episodically dammed valleys to form lakes (Korup, 2004; Xu et al., 2009; Yin et al., 2009), some of which may contain high-resolution evidence of environmental change that is largely under-used to date. Sedimentological evidence, in particular lacustrine laminations, and absolute age constraints indicate that Lake Mengda formed in the early 20th century, and was possibly caused by a landslide event associated with the 1927 earthquake - a theory that is supported by the geomorphological investigations presented herein. Small lakes such as this could easily be affected by sudden natural events and may even be sensitive to relatively minor climatic or environmental changes. Our research has indicated that:

1) The sediments of Lake Mengda preserve a high-resolution archive of the 20th century. The extraction a climatic signal from these sediments, together with precise dating control is of great importance but presents many challenges due to the complexity of the depositional processes.

2) An understanding of the depositional processes during the sort of sudden events that led to the formation of this lake would provide valuable knowledge on landscape formation as well as on organic carbon storage related to the burial of former vegetation.

3) Such an understanding could improve the evaluation of potential natural hazards, thus contributing to urban planning and land management. In the particular case of Lake Mengda, the present nature reserve station can now be seen to have been built on the dam itself, which may have implications regarding future risks.

Acknowledgement

The authors would like to thank Bo Yang (Institute of Salt Lakes, CAS) for his help during the

fieldwork. Special thanks go to Elisabeth Dietze and Kai Hartmann (Free University Berlin) for providing us with the unpublished End-Member Modeling script. Benjamin Bekeschus, Christiane Funk, Janina Staple and Liv Heinecke (AWI-Potsdam & University Potsdam) are also acknowledged for their assistances with the laboratory analyses. We are grateful to Jan Blöthe (University Potsdam) for his guidance in extracting the elevation profiles. Y. Wang's doctoral research is funded by the "Helmholtz - China Scholarship Council (CSC) Young Scientist Fellowship" (No. 2008491101). The research was financially supported by the German Research Foundation (Deutsche Forschungsgemeinschaft DFG).

References

Aichner, B., Herzschuh, U., Wilkes, H., 2010a. Influence of aquatic macrophytes on the stable carbon isotopic signatures of sedimentary organic matter in lakes on the Tibetan Plateau. Organic Geochemistry 41, 706-718.

Aichner, B., Herzschuh, U., Wilkes, H., Vieth, A., Böhner, J., 2010b. δD values of n-alkanes in Tibetan lake sediments and aquatic macrophytes – a surface sediment study and an application in a palaeorecord from Lake Koucha. Organic Geochemistry 41, 779-790.

Aldenderfer, M.S., 2007. Modeling the Neolithic on the Tibetan Plateau. Developments in Quaternary Sciences 9, 151-165.

An, Z.S., Porter, S.C., Kutzbach, J.E., Wu, X.H., Wang S.M., Liu, X.D., Li, X.Q., Zhou, W.J., 2000. Asynchronous Holocene optimum of the East Asian monsoon. Quaternary Science Reviews 19, 743-762.

Andersen, S.T., 1970. The Relative Pollen Productivity and Pollen Representation of North European Trees, and Correction Factors for Tree Pollen Spectra. Danmarks Geologiske Undersbgelser vol. 96. Copenhagen.

Beer, R., Heiri, O., Tinner, W., 2007. Vegetation history, fire history and lake development recorded for 6300 years by pollen, charcoal, loss on ignition and chironomids at a small lake in southern Kyrgyzstan (Alay Range, Central Asia). The Holocene 17, 977-985.

Berman, F., Chien, A., Cooper, K., Dongarra, J., Foster, L., Gannon, D., Johnsson, L., Kennedy, K., Kesselman, C., Mellor-Crumme, J., Reed, D., Torczon, L., Wolski, R., 2001. The GrADS Project: Software Support for High-Level Grid Application Development. International Journal of High Performance Computing Applications 15, 327-344.

Besag, J. and Clifford, P., 1989. Generalized Monte Carlo significance tests. Biometrika 76, 633-642.

Beug, H.J., 2004. Leitfaden der Pollenbestimmung für Mitteleuropa und angrenzende Gebiete. Verlag Dr. Friedrich Pfeil, München (Germany).

Birks, H.J.B., 1981. The use of pollen analysis in the reconstruction of past climates: a review. In: Wigley, T.M.L., Ingram, M.J., Farmer, G. (EDs.), Climate and History, Cambridge University Press, Cambridge, pp. 111-138.

Birks, H.J.B., 2003. Quantitative palaeoenvironmental reconstructions from Holocene biological data. In: Mackay, A.W., Battarbee, R.W., Birks, H.J.B., Oldfield, F., (Eds.), Global Change in the Holocene. Arnold London, pp. 342-357.

Birks, H.J.B., 2007. Estimating the amount of compositional change in late-Quaternary pollen-stratigraphical data. Vegetation History and Archaeobotany 16, 197-202.

Birks, H.J.B. and Seppä, H., 2004. Pollen-based reconstructions of late-Quaternary climate in

Europe – progress, problems, and pitfalls. Acta Palaeobotanica 44, 317-334.

Birks, H.J.B., Heiri, O., Seppä, H., Bjune, A.E., 2010. Strengths and weaknesses of quantitative climate reconstructions based on Late-Quaternary biological proxies. The Open Ecology Journal 3, 68-110.

Böhner, J., 2005. Advancements and new approaches in climate spatial prediction and environmental modeling. Arbeitsberichte des Geographischen Institutes der Humboldt–Universität zu Berlin 109, 49-90.

Böhner, J., 2006. General climatic controls and topoclimatic variations in Central and High Asia. Boreas 35, 279-295.

Böhner, J. and Antonic, O., 2008. Land-Surface Parameters Specific to Topo-Climatology. In: Hengl, T. and Reuter, H.I. (Eds.), Geomorphometry: Concepts, Software, Applications. Elsevier, Amsterdam, pp. 195-226.

Bond, G., Kromer, B., Beer, J., Muscheler, R., Evans, M.N., Showers, W., Hoffmann, S., Lotti-Bond, R., Hajdas, I., Bonani, G., 2001. Persistent solar influence on North Atlantic climate during the Holocene. Science 294, 2130-2136.

Bonny, A.P., 1978. The effect of pollen recruitment processes on pollen distribution over the sediment surface of a small lake n Cumbria. Journal of Ecoloy 66, 385-416.

Broström, A., Sugita, S., Gaillard, M.J., Pilesjö, P., 2005. Estimating spatial scale of pollen dispersal in the cultural landscape of southern Sweden. Holocene 15, 252–262.

Borström, A., Nielsen, A.B., Gaillard, M.J., Hjelle, K., Mazier, F., Binney, H., Bunting, J., Fyfe, R., Meltsov, V., Poska, A., Räsänen, S., Soepboer, W., Stedingk, H., Suutari, H., Sugita, S., 2008. Pollen productivity estimates of key European plant taxa for quantitative reconstruction of past vegetation: A review. Vegetation History and Archaeobotany 17, 461-478.

Broecker, W., Bond, G., Klas, M., Clark, E., McManus, J., 1992. Origin of the northern Atlantic Heinrich events. Climate Dynamics 6, 265-273.

Bronk Ramsey, C., 2009. Bayesian analysis of radiocarbon dates. Radiocarbon 51, 337-360.

Bunting, M.J. and Middleton, R., 2005. Modelling pollen dispersal and deposition using HUMPOL software: simulating wind roses and irregular lakes. Review of Palaeobotany and Palynology 134, 185-196.

Bunting, M.J. and Hjelle, K.L., 2010. Effect of vegetation data collection strategies on estimates of relevant source area of pollen (RSAP) and relative pollen productivity estimates (relative PPE) for non-arboreal taxa. Vegetation History and Archaeobotany 19, 365-374.

Bunting, M.J., Gaillard, M.J., Sugita, S., Middleton, R., Broström, A., 2004. Vegetation structure and pollen source area. Holocene 14, 651–660.

Bush, A.B.G., 2001. Pacific Sea Surface Temperature forcing dominates orbital forcing of the early Holocene monsoon. Quaternary Research 55, 25-32.

Bush, A.B.G., 2005. CO_2/H_2O and orbitally driven climate variability over central Asia through the

Holocene. Quaternary International 136, 15-23.

Calcote, R., 1995. Pollen source area and pollen productivity: evidence from forest hollows. Journal of Ecology 83, 591–602.

Campbell, I.D., Last, W.D., Campbell, C., Clare, S., McAndrews, J.H., 2000. The late Holocene palaeohydrology of Pine Lake, Alberta: a multiproxy investigation. Journal of Paleolimnology 24, 427-441.

Campo, E.V., Cour, P., Hang, S.X., 1996. Holocene environmental changes in Bangong Co basin (Western Tibet). Part 2: The pollen record. Palaeogeography, Palaeoclimatology, Palaeoecology 120, 49-63.

Canfield, D.E. and Raiswell, R., 1991. Carbonate precipitation and dissolution: its relevance to fossil preservation. In: Allison PA and Briggs DE (eds) Taphonomy: releasing the data locked in the fossil record, Topic in Geobiology. Plenum Press, New York, pp 411-453.

Chai, H.J., Liu, H.C., Zhang, Z.Y., Xu, Z.W., 2000. The distribution, causes and effects of damming landslides in China. Journal of Chengdu University of Technology 27, 302-307.

Chang, C.P., Harr, P., Ju, J.H., 2000. Possible roles of Atlantic circulation on the weakening Indian Monsoon Rainfall-ENSO relationship. Journal of Climate 14, 2376-2380.

Chen, J., An, Z., Head, J., 1999. Variation of Rb/Sr ratios in the loess–paleosol sequences of Central China during the last 130,000 years and their implications for monsoon paleoclimatology. Quaternary Research 51, 215– 219.

Chen, F.H., Wu, W., Holmes, J.A., Madsen, D.B., Zhu, Y., Jin, M, Oviatt, C.G., 2003. A mid-Holocene drought interval as evidenced by lake desiccation in the Alashan Plateau, Inner Mongolia, China. Chinese Science Bulletin 48, 1401-1410.

Chen, F.H., Cheng, B., Zhao, Y., Zhu, Y., Madsen, D.B., 2006. Holocene environmental change inferred from a high-resolution pollen record, Lake Zhuyeze, arid China. The Holocene 16, 675-684.

Chen, F.H., Yu, Z.C., Yang, M.L., Ito, E., Wang, S.M., Madsen, D.B., Huang, X.Z., Zhao, Y., Sato, T., John, H., Birks, B., Boomer, I., Chen, J.H., An, C.B., Wünnemann, B., 2008. Holocene moisture evolution in arid central Asia and its out-of-phase relationship with Asian monsoon history. Quaternary Science Reviews 27, 351-364.

Christensen, J.H., Hewitson, B., Busuioc, A., Chen, A., Gao, X., Held, I., Jones, R., Kolli, R.K., Kwon, W.-T., Laprise, R., Magaña Rueda, V., Mearns, L., Menéndez, C.G., Räisänen, J., Rinke, A., Sarr, A., Whetton, P., 2007. Regional Climate Projections. In: “Climate Change 2007. The Physical Science Basis. Contribution of working group I to the fourth assessment report of the Intergovernmental Panel on Climate Change.” (Solomon, S., Qin, D., Manning, M., Chen, Z., Marquis, M., Averyt, K.B., Tignor M., Miller, H.L., Eds.), pp. 847- 940. Cambridge University Press, Cambridge and New York.

Chung, F.H., 1974. Quantitative interpretation of X-Ray diffraction patterns of mixture, II. Adiabatic principle of X-Ray diffraction analysis of mixture. Journal of Applied Crystallography 7, 526-531

Clift, P.D., Plumb, R.A., 2008. The Asian Monsoon: causes, history and effects. Cambridge University Press.

Cook, C.G., Jones, R.T., Langdon, P.G., Leng, M.J., Zhang, E.L., 2011. New insights on Late Quaternary Asian palaeomonsoon variability and the timing of the Last Glacial Maximum in southwestern China. Quaternary Science Reviews 30, 808-820.

Cosford, J., Qing, H.R., Eglington, B., Mattey, D., Yuan, D.X., Zhang, M.L., Cheng, H., 2008. East Asian monsoon variability since the mid-Holocene recorded in a high resolution absolute-dated aragonite speleothem from eastern China. Earth and Planetary Science Letters 275, 296-307.

Cour, P., Zheng, Z., Duzer, D., Calleja, M., Yao, Z., 1999. Vegetational and climatic significance of modern pollen rain in northwestern Tibet. Review of Palaeobotany and Palynology 104, 183-204.

Cowling, S.A. and Sykes, M.T., 1999. Physiological significance of low atmosphere CO_2 for plant –climate interactions. Quaternary Research 52, 237-242.

Dallmeyer, A., Claussen, M., Herzschuh, U., Fischer, N., 2011. Holocene vegetation and biomass changes on the Tibetan Plateau – a model-pollen data comparison. Climate of the Past 7, 881-901.

Dansgaard, W., White, J.W.C., Johnsen, S.J., 1989. The abrupt termination of the Younger Dryas climate event. Nature 339, 532-534.

Dansgaard, W., Johnsen, S.J., Clausen, H.B., Dahl-Jensen, D., Gundestrup, N.S., Hammer, C.U., Hvidgerg, C.S., Steffensen, J.P., Sveinbjornsdottir, A.E., Jouzel, J., Bond, G., 1993. Evidence for general instability of past climate from a 250-kyr ice-core record. Nature 364, 218-220.

Davidson, T.A., Sayer, C.D., Langdon, P.G., Burgess, A., Jackson, M., 2010a. Inferring past zooplanktivorous fish and macrophyte density: Application of a new regression tree model. Freshwater Biology 55, 584-599.

Davidson, T.A., Sayer, C.D., Perrow, M., Bramm, M., Jeppesen, E., 2010b. The simultaneous inference of zooplanktivorous fish and macrophyte density from sub-fossil cladoceran assemblages: A multivariate regression tree approach. Freshwater Biology 55, 546-564.

Davis, M.B., 1963. On the theory of pollen analysis. American Journal of Science 261, 897–912.

Dearing, J.A., Jones, R.T., Shen, J., Yang, X., Boyle, J.F., Foster, G.C., Crook, D.S. Elvin, M.J.D., 2008. Using multiple archives to understand past and present climate-human-environment interactions: the lake Erhai catchment, Yunnan Province, China. Journal of Paleolimnology 40, 3-31.

De'ath, G., 2002. Multivariate regression trees: A new technique for modeling species -environment relationships. Ecology 83, 1105-1117.

Debusk, G.H., 1997. The distribution of pollen in the surface sediments of Lake Malaŵi, Africa, and the transport of pollen in large lakes. Review of Palaeobotany and Palynology 97, 123-153.

Demske, D., Tarasov, P.E., Wünnemann, B., Riedel, F., 2009. Late glacial and Holocene vegetation, Indian monsoon and westerly circulation in the Trans-Himalaya recorded in the lacustrine pollen sequence from Tso Kar, Ladakh, NW India. Palaeogeography, Palaeoclimatology, Palaeoecology 279, 172-185.

Dietze, E., Wünnemann, B., Diekmann, B., Aichner, B., Hartmann, K., Herzschuh, U., Ijmker, J., Jin, H., Kopsch, C., Lehmkuhl, F., Li, S.J., Mischke, S., Niessen, F., Opitz, S., Stauch, G., Yang, S., 2010. Basin morphology and seismic stratigraphy of Lake Donggi Cona, north-eastern Tibetan Plateau, China. Quaternary International 218, 131-142.

Dietze, E., Hartmann, K., Diekmann, B., IJmker, J., Lehmkuhl, F., Opitz, S., Stauch, G., Wünnemann, B., Borchers, A., 2011. An end-member algorithm for deciphering modern detrital processes from lake sediments of Lake Donggi Cona, NE Tibetan Plateau, China. Sedimentary Geology, In press. DIO: 10.1016/j.sedgeo.2011.09.014

Dorofeyuk, N.I. and Tarasov, P.E., 1998. Vegetation and lake levels in northern Mongolia in the last 12,500 years as indicated by data of pollen and diatom analyses. Stratigraphy and Geological Correlations 6, 70-83.

Dykoski, C.A., Edwards, R.L., Cheng, H., Yuan, D.X., Cai, Y.J., Zhang, M.L., Lin, Y.S., Qing, J.M., An, Z.S., Revenaugh, J., 2005. A high-resolution, absolute-dated Holocene and deglacial Asian monsoon record from Dongge Cave, China. Earth Planetary Science Letters 233, 71-86.

Duffin, K. and Bunting, M.J., 2008. Relative pollen productivity and fall speed estimates for southern African savanna taxa. Vegetation History and Archaeobotany 17, 507–525.

Enzel, Y., Ely, L.L., Mishra, S., Ramesh, R., Amit, R., Lazar, B., Rajagure, S.N., Baker, V.R., Sandler, A., 1999. High-resolution Holocene environmental changes in the Thar Desert, northwestern India. Science 284, 125-128.

Fægri, K. and Iversen, J., 1989. Textbook of Pollen Analysis, 4th edition. The Blackwell Press, New Jersey, pp.69-89.

Feng, Z.D., Wang, W.G., Guo, L.L., Khosbayar, P., Narantsetseg, T., Jull, A.J.T., An, C.B., Li, X.Q., Ma, Y.Z., 2005. Lacustrine and eolian records of Holocene climate changes in the Mongolian Plateau: preliminary results. Quaternary International 136, 25-32.

Fleitmann, D., Burns, S.J., Mudelsee, M., Neff, U., Kramers, J., Mangini, A., Matter, A., 2003. Holocene forcing of the Indian Monsoon recorded in a stalagmite from southern Oman. Science 300, 1737-1939.

Fleitmann, D., Burns, S.J., Mangini, A., Mudelsee, M., Kramers, J., Villa, I., Neff, U., Al-Subbary, A.A., Buettner, A., Hippler, D., Matter, A., 2007. Holocene ITCZ and Indian monsoon dynamics recorded in stalagmites from Oman and Yemen (Socotra). Quaternary Science Reviews 26, 170-188.

Fontes, J.C., Gasse, F., Gibert, E., 1996. Holocene environmental changes in Lake Bangong basin (Western Tibet). Part 1: Chronology and stable isotopes of carbonates of a Holocene lacustrine core. Palaeogeography, Palaeoclimatology, Palaeoecology 120, 25-47.

Fowell, S.J., Hansen, B.C.S., Peck, J.A., Khosbayar, P., Ganbold, E., 2003. Mid to late Holocene climate evolution of the Lake Telmen Basin, north central Mongolia, based on palynological data. Quaternary Research 59, 353-363.

Fujiki, T. and Yasuda, Y., 2004. Vegetation history during the Holocene from Lake Hyangho. Quaternary International 123-125, 63-69.

Garrels RM and Thompson ME (1962) A chemical model for sea water at 25℃ and one atmosphere total pressure. American Journal of Science 260,57-66.

Gasse, F., Arnold, M., Fontes, J.C., Fort, M., Gibert, E., Huc, A., Li, B.Y., Li, Y.F., Liu, Q., Melieres, M., Campo, E.V., Wang, F.B., Zhang, Q.S., 1991. A 13000-year climate record from western Tibet. Nature 353, 742-745.

Gibbs, R.J., 1967. The geochemistry of the Amazon River system: part I, the factors that control the salinity and composition and concentration of the suspended solids. Geological Society of America Bulletin 78, 1203-1232.

Goldstein, S.L., 1988. Decoupled evolution of Nd and Sr isotopes in the continental crust and the mantle. Nature 336, 733–738.

Goring, S., Lacourse, T., Pellatt, M.G., Walker, I.R., Mathewes, R.W., 2010. Are pollen-based climate models improved by combining surface samples from soil and lacustrine substrates? Review of Paleobotany and Palynology 162, 203-212.

Goswami, B.N., Krishnamurthy, V., Annamalai, H., 1999. A broad-scale circulation index for the interannual variability of the Indian summer monsoon. The Quaternary Journal of Royal Meteorological Society 125, 611-633.

Goto, A., Arakawa, H., Morinage, H., Sakiyama, T., 2003. The occurrence of hydromagnesite in bottom sediments from Lake Siling, central Tibet: implications for the correction among $\delta^{18}O$, $\delta^{13}C$ and particle density. Journal of Asian Earth Science 21, 979-988.

Gregory, P.H., 1973. The Microbiology of the Atmosphere, 2nd edition. Leonard Hill, Aylesbury.

Grimm, E.C., 1991. TILIA and TILIAGRAPH Software. Illinois State Museum, Springfield.

Grootes, P.M., Stuiver, M., White, J.W.C., Johnsen, S., Jouzel, J., 1993. Comparison of oxygen isotope records from the GISP2 and GRIP Greenland ice cores. Nature 366, 552-554.

Guo, S., Savolainen, P., Su, J., Zhang, Q., Qi, D., Zhou, J., Zhong, Y., Zhao, X., Liu, J., 2006. Origin of mitochondrial DNA diversity of domestic yaks. BMC Evolutionary Biology 6, 73.

Gupta, A.K., Anderson, D.M., Overpeck, J.T., 2003. Abrupt changes in the Asian southwest monsoon during the Holocene and their links to the North Atlantic Ocean. Nature 421, 354-357.

Hardie, L.A., and Eugster, H.P., 1980. Evaporation of seawater: calculated mineral sequences. Science 208, 498-500.

He, Y., Theakstone, W.H., Zhang, Z.L., Zhang, D., Yao, T.D., Chen, T., Shen, Y.P., Pan, H.X., 2004. Asynchronous Holocene climate change across China. Quaternary Research 61, 52-63.

He, C.R., Zhang, R., Chen, Q., Han, S.L., 2011a. Earthquake characteristics and building damage in high-intensity areas of Wenchuan Earthquake I: Yingxiu Town. Natural Hazards 57, 435-451.

He, C.R., Chen, Q., Han, S.L., Zhang, R., 2011b. Earthquake characteristics and building damage in high-intensity areas of Wenchuan Earthquake II: Dujiangyan and Pengzhou City. Natural Hazards 57, 279-292.

Hellman, S., Gaillard, M.-J., Broström, A., Sugita, S., 2008a. The REVEALS model, a new tool to estimate past regional plant abundance from pollen data in large lakes: validation in southern Sweden. Journal of Quaternary Science 23, 21–42.

Hellman, S.E.V., Gaillard, M.-J., Broström, A., Sugita, S., 2008b. Effects of the sampling design and selection of parameter values on pollen-based quantitative reconstructions of regional vegetation: a case study in southern Sweden using the REVEALS model. Vegetation History and Archaeobotany 17, 445–459.

Henderson, A.C.G., Holmes, J.A.m Zhang, J.W., Leng, M.J., Carvalho, L.R., 2003. A carbon- and oxygen-isotope record of recent environmental change from Qinghai Lake, NE Tibetan Plateau. Chinese Science Bulletin 48, 1463-1468.

Henderson, A.C.G., Holmes, J.A., Leng, M.J., 2010. Late Holocene isotope hydrology of Lake Qinghai, NE Tibetan Plateau: Effective moisture variability and atmospheric circulation changes. Quaternary Science Reviews 29, 2215-2223.

Herzschuh, U., 2006. Palaeo-moisture evolution in monsoonal Central Asia during the last 50,000 years. Quaternary Science Reviews 25, 163-178.

Herzschuh, U., 2007. Reliability of pollen ratios for environmental reconstructions on the Tibetan Plateau. Journal of Biogeography 34, 1265-1273.

Herzschuh, U., Kürschner, H., Ma, Y.Z., 2003. The surface pollen and relative pollen production of the desert vegetation of the Alashan Plateau, western InnerMongolia. Chinese Science Bulletin 48, 1488-1493.

Herzschuh, U., Tarasov, P., Wu¨ nnemann, B., Hartmann, K., 2004. Holocene vegetation and climate of the Alashan Plateau, NW China, reconstructed from pollen data. Palaeogeography, Palaeoclimatology, Palaeoecology 211, 1–17.

Herzschuh, U., Winter, K., Wünnemann, B., Li, S.J., 2006a. A general cooling trend on the central Tibetan Plateau throughout the Holocene recorded by the Lake Zigetang pollen spectra. Quaternary International 154-155, 113-121.

Herzschuh, U., Kürschner, H., Battarbee, R., Holmes, J., 2006b. Desert plant pollen production and a 160-year record of vegetation and climate change on the Alashan Plateau, NW China. Vegetation History and Archaeobotany 15, 181-190.

Herzschuh, U., Kramer, A., Mischke, S., Zhang, C.J., 2009. Quantitative climate and vegetation trends since the late glacial on the northeastern Tibetan Plateau deduced from Koucha Lake pollen record. Quaternary Research 71, 162-171.

Herzschuh, U., Birks, H.J.B., Mischke, S., Zhang, C., and Böhner, J., 2010a. A modern pollen-climate calibration set based on lake sediments from the Tibetan Plateau and its application to a Late Quaternary pollen record from the Qilian Mountains. Journal of Biogeography 37, 752-766.

Herzschuh, U., Birks, H.J.B., Ni, J., Zhao, Y., Liu, H.Y., Liu, X.Q., Grosse, G., 2010b. Holocene land-cover changes on the Tibetan Plateau. The Holocene 20, 91-104.

Herzschuh, U., Ni, J., Birks, H.J.B., Böhner, J., 2011. Driving forces of mid-Holocene vegetation shifts on the upper Tibetan Plateau, with emphasis on changes in atmospheric CO_2 concentrations. Quaternary Science Reviews, 30, 1907-1917.

Hill, M.O. and Gauch, H.G., 1980. Detrended correspondence analysis: An improved ordination technique. Vegetatio 42, 41–58.

Hodell, D.A., Brenner, M., Kanfoush, S.L., Curtis, J.H., Stoner, J.S., Song, X.L., Wu, Y., 1999. Paleoclimate of southwestern China for the past 50,000 yr inferred from lake sediment records. Quaternary Research 52, 369-380.

Hong, Y.T., Hong, B., Lin, Q.H., Shibata, Y., Hirota, M., Zhu, Y.X., Leng, X.T., Wang, Y., Wang, H., and Yi, L., 2005. Inverse phase oscillations between the East Asian and Indian Ocean summer monsoons during the last 12000 years and paleo-El Nino. Earth and Planetary Science Letters 231, 337-346.

Hou, X., chief editor, 2001. Vegetation atlas of China. Science Press, Beijing.

Hu, C.Y., Henderson, G.M., Huang, J.H., Xie, S.C., Sun, Y., Johnson, K.R., 2008. Quantification of Holocene Asian monsoon rainfall from spatially separated cave records. Earth and Planetary Science Letters 266, 221-232.

Huang, G., 2004. An index measuring the interannual variability of the East Asian Summer Monsoon – the EAP Index. Advances in Atmospheric Sciences 20, 41-52.

Huang, C.C., Pang, J.L., Zhou, Q.Y., Chen, S.E., 2004. Holocene pedogenic changes and the emergence and decline of rain-fed cereal agriculture on the Chinese Loess Plateau. Quaternary Science Reviews 23, 2525-2535.

Huang, X.Z., Zhao, Y., Cheng, B., Chen, F.H., Xu, J.R., 2004. Modern pollen analysis of the surface sediments from the Bosten Lake, Xinjiang, China. Journal of Glaciology and Geocryology 26, 602-609 (in Chinese with English abstract).

Huang, X.Z., Chen, F.H., Fan, Y.X., Yang, M.L., 2009. Dry late-glacial and early Holocene climate in arid central Asia indicated by lithological and palynological evidence from Bosten Lake, China. Quaternary International 194, 19-27.

Huss, M., Bauder, A., Werder, M., Funk, M., Hock, R., 2007. Glacier-dammed lake outburst events of Gernersee, Switzerland. Journal of Glaciology 53, 189-200.

IGSNRR, Institute of Geographic Sciences and Natural Resources Research, CAS (ed), 1990. Geological maps of Tibetan Plateau. Science Publisher, Beijing. (In Chinese)

Jackson, D.A., 1995. PROTEST: A PROcrustean Randomization TEST of community environment concordance. Ecoscience 2, 297-303.

Jackson, S.T. and Kearsley, J.B., 1998. Quantitative representation of local forest composition in forest-floor pollen assemblages. Journal of Ecology 86, 474-490.

Jackson, S.T. and Lyford, M.E., 1999. Pollen dispersal models in Quaternary plant ecology: assumptions, parameters, and prescriptions. Botanical Review 65, 39-75.

Jackson, S.T., Webb III, T., Prentice, I.C., and Hansen, J.E., 1995. Exploration and calibration of pollen/vegetation relationships: a PC program for the extended R-value models. Review of Palaeobotany and Palynology 84, 365-374.

Jackson, S.T., Williams, J.W., 2004. Modern analogs in Quaternary paleoecology: Here today, gone yesterday, gone tomorrow? Annual Review of Earth and Planetary Sciences 32, 495-537.

Jarvis, D.I., 1993. Pollen evidence of changing Holocene monsoon climate in Sichuan province, China. Quaternary Research 39, 325-337.

Ji, J.F., Shen, J., Balsam, W., Chen, J., Liu, L.W., Liu, X.Q., 2005. Asian monsoon oscillations in the northeastern Qinghai-Tibet Plateau since the late glacial as interpreted from visible reflectance of Qinghai Lake sediments. Earth Planetary Science Letters 233, 61-70.

Ji, J.F., Balsam, W., Shen, J., Wang, M., Wang, H.T., Chen, J., 2009. Centennial blooming of anoxygenic phototrophic bacteria in Qinghai Lake linked to solar and monsoon activities during the last 18,000 years. Quaternary Science Reviews 28, 1304-1308.

Jian, Z.M., Wang, P.X., Saito, Y., Wang, J.L., Pflaumann, U., Oba, T., Cheng, X.R., 2000. Holocene variability of Kuroshio Current in the Okinawa Trough, northwestern Pacific Ocean. Earth and Planetary Science Letters 184, 305-319.

Jiang, W.Y., Guo, Z.T., Sun, X.J., Wu, H.B., Chu, G.Q., Yuan, B.Y., Hatte, C., Guiot, J., 2006. Reconstruction of climate and vegetation changes of Lake Bayanchagan (Inner Mongolia): Holocene variability of the East Asian monsoon. Quaternary Research 65, 411-420.

Jiang, Q.F., Shen, J., Liu, X.Q., Zhang, E.L., 2008. Holocene climate reconstructions of Ulungur Lake (Xinjiang, China) inferred from ostracod species assemblages and stable isotopes. Frontiers of Earth Science in China 2, 31-40.

Jin, Z.D., Wu, Y.H., Zhang, X.H., Wang, S.M., 2005. Role of late glacial to mid-Holocene climate in catchment weathering in the central Tibetan Plateau. Quaternary Research 63,161-170.

Jin, Z.D., Cao, J.J., Wu, J.L., Wang, S.M., 2006. A Rb/Sr record of catchment weathering response to Holocene climate change in Inner Mongolia. Earth Surface Process and Landforms 31, 285-291.

Johnston, K., Verhoef, J.M., Krivoruchko, K., Lucas, N., 2001. Using ArcGIS^{TM} Geostatistical Analyst. Redlands, California, 49pp.

Joseph, P.V., 1978. Subtropical westerlies in relation to large scale failure of Indian summer

monsoon. Indian Journal of Meteorology, Hydrology and Geophysics 29, 412-418.

Juggins, S., 2003. User guide C2 – a program for analysing and visualising palaeoenvironmental data. Department of Geography, University of Newcastle, UK.

Kalnay, E., Kanamitsu, M., Kistler, R., Collins, W., Deaven, D., Gandin, L., Iredell, M., Saha, S., White, G., Wollen, J., Zhu, Y., Leetmaa, A., Reynolds, R., Chelliah, M., Ebisuzaki, W., Higgins, W., Janowiak, J., Mo, K.C., Ropelewskim C., Wang, J., 1996. The NCEP/NCAR 40-year reanalysis project. Bulletin of the American Meteorological Society 77, 437-471.

Keefer, D.K., 2002. Investigating landslides caused by earthquakes – a historical review. Surveys in Geophysics 23, 473-510.

Kistler, R., Kalnay, E., Collins, W., Saha, S., White, G., Woollen, J., Chelliah, M., Ebisuzaki, W., Kanamitsu, M., Kousky, V., van den Dool, H., Jenne, R., Fiorino, M., 2001. The NCEP/ NCAR 50-year reanalysis. Bulletin of the American Meteorological Society 82, 247-267.

Korup, O., 2004. Geomorphometric characteristics of New Zealand landslide dams. Engineering Geology 73, 13-35.

Korup, O. and Tweed, F., 2007. Ice, moraine, and landslide dams in mountainous terrain. Quaternary Science Reviews 26, 3406-3422.

Kramer, A., Herzschuh, U., Mischke, S., and Zhang, C.J., 2010a. Late glacial vegetation and climate oscillations on the southeastern Tibetan Plateau inferred from the Lake Naleng pollen profile. Quaternary Research 73, 324-335.

Kramer, A., Herzschuh, U., Mischke, S., and Zhang, C., 2010b. Holocene tree-line shifts and monsoon variability in the Hengduan Mountains (southeastern Tibetan Plateau) implications from palynological investigations. Palaeogeography, Palaeoclimatology, Palaeoecology 286, 23-41.

Kürschner, H., Herzschuh, U., and Wagner, D., 2005. Phytosociological studies in the north-eastern Tibetan Plateau (NW China) — A first contribution to the subalpine scrub and alpine meadow vegetation. Botanische Jahrbücher der Systematik 126, 273-315.

Kutzbach, J., Prell, W., and Ruddiman, W.F., 1993. Sensitivity of Eurasian Climate to Surface Uplift of the Tibetan Plateau. The Journal of Geology 101, 177-190.

Lanzhou Earthquake Administration, 1991. Lanzhou Earthquakes. Lanzhou University Press.

Large, D.J., Spiro, B., Ferrat, M., Shopland, M., Kylander, M., Gallagher, K., Li, X.D., Shen, C.D., Possnert, G., Zhang, G., Darling, W.G., Weiss, D., 2009. The influence of climate, hydrology and permafrost on Holocene peat accumulation at 3500 m on the eastern Qinghai-Tibetan Plateau. Quaternary Science Reviews 28, 3303-3314.

Laskar, J., Robutel, P., Joutel, F., Gastineau, M., Correia, A.C.M., Levrard, B., 2004. A long term numerical solution for the insolation quantities of the earth. Astronomy and Astrophysics 428, 261-285.

Last, W.M., 1982. Holocene carbonate sedimentation in Lake Manitoba, Canada. International

Association of Sedimentologists, 691-704.

Last, W.M., 2001. Mineralogical analysis of lake sediments. In: Last, W.M., Smol, J.P. (eds) Tracing environmental change using lake sediments. Volume 2: Physical and geochemical methods. Kluwer Academic Publishers, Dordrecht, the Netherlands, pp 143-187.

Last, W.M.and Smol, J.P. (chief ed), 2001. Tracking environmental change using lake sediments. Volume 1: basin analysis, coring, and chronological techniques. Kluwer Academic Publishers, Dordrecht.

Li, B.Y., 1996. Environment of Kekexili area, Qinghai Province. Science Press, Beijing (in Chinese).

Li, B.H., Jian, Z.M., Wang, P.X., 1997. *Pulleniatina obliquiloculata* as a paleoceanographic indicator in the southern Okinawa Trough during the last 20,000 years. Marine Micropaleontology 32, 59-69.

Li, Q., Lu, H.Y., Zhu, L.P., Wu, N.Q., Wang, J.B., Lu, X.M., 2011a. Pollen-inferred climate changes and vertical shifts of alpine vegetation belts on the northern slope of the Nyainqentanglha Mountains (central Tibetan Plateau) since 8.4 kyr BP. Holocene, DOI: 10.1177/0959683611400218.

Li, Y.C., Bunting, M.J., Xu, Q.H., Jiang, S.X., Ding, W., Hun, L.Y., 2011b. Pollen-vegetation-climate relationships in some desert and desert-steppe communities in northern China. Holocene, DOI: 10.1177/0959683611400202.

Li, X.Q., Zhou, W.J., An, Z.S., Dodson, J., The vegetation and monsoon variations at the desert-loess transition belt at Midiwan in northern China for the last 13 ka. The Holocene 13, 779-784.

Linsely, B.K., 1996. Oxygen-isotope record of sea level and climate variations in the Sulu Sea over the past 150,000 years. Nature 380, 234-237.

Lister, G.S., Kelts, K., Chen, K.Z., Yu, J.Q., Niessen, F., 1991. Lake Qinghai, China: closed-basin lake levels and the oxygen isotope record for ostracoda sin the latest Pleistocene. Palaeogeography, Palaeoclimatology, Palaeoecology 84, 141-162.

Liu, K.B., Yao, Z.J., Thompson, L.G., 1998. A pollen record of Holocene climatic changes from the Dunde ice cap, Qinghai-Tibetan Plateau. Geology 26, 135-138.

Liu, H.P., Tang, X.C., Sun, D.H., Wang, K.F., 2001. Palynofloras of the Dajiuhu Basin in Shennongjia Mountains during the last 12.5 ka. Acta Mircropalaeontologica Sinica 18, 101-109. (in Chinese with English Abstract)

Liu, H.Y., Xu, L.H., Cai, H.T., 2002a. Holocene history of desertification along the woodland -steppe border in northern China. Quaternary Research 57, 259-270.

Liu, X.Q., Shen, J., Wang, S.M., Yang, X.D., Tong, G.B., Zhang, E.L., 2002b. A 16000-year pollen record of Qinghai Lake and its paleoclimate and paleoenvironment. Chinese Science Bulletin 47, 1931-1936.

Liu, X., Kutzbach, J., Liu, Z., An, Z., and Li, L., 2003a. The Tibetan Plateau as amplifier of orbitalscale variability of the East Asian monsoon. Geophysical Research Letters 30, 1839.

Liu, X.Q., Shen, J., Wang, S.M., Zhang, E.L., Cai, Y.F., 2003b. A 16000 year paleoclimatic record derived from authigenic carbonate of lacustrine sediment in Qinghai Lake. Geological Journal of China Universities 9, 38-46 (in Chinese with English abstract).

Liu, X.Q., Cai, K.Q., Yu, S.H., 2004. Geochemical simulation of the formation of brine and salt minerals based on Pitzer model in Caka Salt Lake. Science in China Series D 4, 720-726.

Liu, X.Q., Shen, J., Wang, S.M., Wang, Y.B., Liu, W.G., 2007. Southwest monsoon changes indicated by oxygen isotope of ostracode shells from sediments in Qinghai Lake since the late Glacial. Chinese Science Bulletin 52, 539-544.

Liu, X.Q., Dong, H.L., Rech, J.A., Matsumoto, R., Yang, B., Wang, Y.B., 2008a. Evolution of Chaka Salt Lake in NW China in response to climatic change during the latest Pleistocene -Holocene. Quaternary Science Reviews 27, 867-879.

Liu, X.Q., Herzschuh, U., Shen, J., Jiang, Q.F., Xiao, X.Y., 2008b. Holocene environmental and climatic changes inferred from Wulungu Lake in northern Xinjiang, China. Quaternary Research 70, 412-425.

Liu, X.Q., Dong, H.L., Yang, X.D., Herzschuh, U., Zheng, E.L., Stuut, J.W., and Wang, Y.B., 2009. Late Holocene forcing of the Asian winter and summer monsoon as evidenced by proxy records from the northern Qinghai–Tibetan Plateau. Earth and Planetary Science Letters 280, 276-284.

Lu, S.J. and Si, J.H., 2005. Investigation of arbors in Mengda nature reserve. Journal of Qinghai University (Nature Sciece) 23,70-72 (in Chinese with English abstract).

Lu, X.M., Herrmann, M., Mosbrugger, V., Yao, T.D., Zhu, L.P., 2010. Airborne pollen in the Nam Co Basin and its implication for palaeoenvironmental reconstruction. Review of Palaeobotany and Palynology 163, 104-112.

Lu, H.Y., Wu, N.Q., Liu, K.B., Zhu, L.P., Yang, X.D., Yao, T.D., Wang, L., Li, Q., Liu, X.Q., Shen, C.M., Li, X.Q., Tong, G.B., Jiang, H., 2011. Modern pollen distributions in Qinghai-Tibetan Plateau and the development of transfer functions for reconstructing Holocene environmental changes. Quaternary Science Reviews 30, 947-966.

Ludwig, J.A., Wilcox, B.P., Breshears, D.D., Tongway, D.J., Imeson, A.C., 2005. Vegetation patches and runoff-erosion as interacting ecohydrological processes in seimiarid landscapes. Ecology 86, 288-297.

Luly, J.G., 1997. Modern pollen dynamics and surficial sedimentary processes at Lake Tyrrell, semi-arid northwestern Victoria, Australia. Review of Palaeobotany and Palynology 97, 301-318.

Ma, Y.Z., Zhang, H.C., Pachur, H.J., Wünnemann, B., Li, J.J., Feng, Z.D., 2004a. Modern pollen-based interpretations of mid-Holocene palaeoclimate (8500 to 3000 cal. BP) at the southern margin of the Tengger Desert, northwestern China. The Holocene 14, 841-850.

Ma, D.T., Tu, J.J., Cui, P., Lu, R.R., 2004b. Approach to mountain hazards in Tibet, China. Journal of Mountain Science 1, 143-154.

Maher, B.A. and Hu, M.Y., 2006. A high-resolution record of Holocene rainfall variations from the western Chinese Loess Plateau: antiphase behaviour of the African/Indian and East Asian summer monsoons. The Holocene 16, 309-320.

Mangerud, J., Astakhov, V., Murray, A., Svendsen, J.I., 2001. The choronology of large ice-dammed lake and the Barents-Kara Ice Sheet advances, Northern Russia. Global and Planetary Change 31, 321-336.

Mardia, K.V., Kent, J.T., Bibby, J.M., 1979. Multivariate Analysis, Academic Press, London, 521pp.

Mazier, F., Brostöm, A., Sugita, S.,Vittoz, P.,Gaillard,M.-J., Buttler,A., 2008. Pollen productivity estimates and relevant source area for selected plant taxa in a pasture woodland of Jura Mountains (Switzerland). Vegetation History and Archaeobotany 17, 479–496.

McCune, B., Grace, J.B., 2002. Analysis of ecological communities. MjM Software Design, Glenden Beach, OR, USA.

Meehl, G.A. and Arblaster, J.M., 1998. The Asian-Australian Monsoon and El Niño – Southern Oscillation in the NCAR Climate System Model. Journal of Climate 11, 1356-1385.

Meyers, P.A., Lallier-Verges, E., 1999. Lacustrine sedimentary organic matter records of Late Quaternary paleoclimates. Journal of Paleolimnology 21, 345-372.

Meyer, M.C., Hofmann, Ch.-Ch., Gemmell, A.M.D., Haslinger, E., Häusler, H., Wangda, D., 2009. Holocene glacier fluctuations and migration of Neolithic yak pastoralists into the high valleys of northwest Bhutan. Quaternary Science Reviews 28, 1217-1237.

Miehe, G., Miehe, S., Kaiser, K., Liu, J., Zhao, X., 2008. Status and dynamics of the *Kobresia* pygmaea ecosystem on the Tibetan Plateau. Ambio 37, 272-279.

Miehe, G., Miehe, S., Kaiser, K., Reudenbach, C., Behrendes, L., Duo, L., Schlütz, F., 2009. How old is pastoralism in Tibet? An ecological approach to the making of a Tibetan landscape. Palaeogeography, Palaeoclimatology, Palaeoecology 276, 130-147.

Miehe, G., Miehe, S., Bach, K., Kluge, J., Wesche, K., Yang, Y.P., Liu, J.Q., 2011. Ecological stability during the LGM and the mid-Holocene in the Alpine Steppes of Tibet? Quaternary Resarch 76, 243-252.

Millero, F.J. and Pierrot, D., 1998 A chemical equilibrium model for natural water. Aquat Geochem 4, 153-199.

Mischke, S. and Wünennmann, B., 2006. The Holocene salinity history of Bosten Lake (Xinjiang, China) inferred from ostracod species assemblages and shell chemistry: Possible palaeoclimatic implications. Quaternary International 154-155, 100-112.

Mischke, S. and Zhang, C.J., 2011. Ostracod distribution in Ulungur Lake (Xinjiang, China) and a reassessed Holocene record. Ecol. Res. 26, 133-145.

Mischke, S., Demske, D., Wünennmann, B., Schudack, M.E., 2005. Groundwater discharge to a Gobi desert lake during Mid and Late Holocene dry periods. Palaeogeography, Palaeoclimatology, Palaeoecology, 225: 157-172.

Mischke, S., Herzschuh, U., Massmann, G., Zhang, C.J., 2007. An ostracod-conductivity transfer function for Tibetan lakes. Journal of Paleolimnology 38, 509-524.

Mischke, S., Kramer, M., Zhang, C., Shang, H., Herzschuh, U., Erzinger, J., 2008. Reduced early Holocene moisture availability in the Bayan Har Mountains, northeastern Tibetan Plateau, inferred from a multi-proxy lake record. Palaeogeography, Palaeoclimatology, Palaeoecology 267, 59-76.

Mischke, S., Zhang, C., Börner, A., and Herzschuh, U., 2009. Lateglacial and Holocene variation in aeolian sediment flux over the northeastern Tibetan Plateau recorded by laminated sediments of a saline meromictic lake. Journal of Quaternary Science 25, 162-177.

Mischke, S., Bößneck, U., Diekmann, B., Herzschuh, U., Jin, H.J., Kramer, A., Wünnemann, B., and Zhang, C.J., 2010a. Quantitative relationship between water-depth and sub-fossil ostracod assemblages in Lake Donggi Cona, Qinghai Province, China. Journal of Paleolimnolgy 32, 589-608.

Mischke, S., Aichner, B., Diekmann, B., Herzschuh, U., Plessen, B., Wünnemann, B., and Zhang, C.J., 2010b. Ostracods and stable isotopes of a late glacial and Holocene lake record from the NE Tibetan Plateau. Chemical Geology 276, 95-103.

Mitas, C.M. and Clement, A., 2006. Recent behavior of the Hadley cell and tropical thermo -dynamics in climate models and reanalyses. Geophysical Research Letters 33, L01810, DOI: 10.1029/2005GL024406.

Moore, P.D., Webb, J.A., and Collinson, M.E., 1991. Pollen Analysis, 2nd edition. Blackwell Science, Oxford.

Morinaga, H., Itota, C., Isezaki, N., Goto, H., Yaskawa, K., Kusakabe, M., 1993. Oxygen-18 and carbon-13 records for the last 14,000 years from lacustrine carbonates of Siling-Co (Lake) in the Qinghai-Tibetan Plateau. Geophysical Research Letters 20, 2909-2912.

Morrill, C., Overpeck, J.T., and Cole, J.E., 2003. A synthesis of abrupt changes in the Asian summer monsoon since the last deglaciation. The Holocene 13, 465-467.

Morrill, C., Overpeck, J.T., Cole, J.E., Liu, K.B., Shen, C.M., and Tang, L.Y., 2006. Holocene variations in the Asian monsoon inferred from the geochemistry of lake sediments in central Tibet. Quaternary Research 65, 232-243.

Mullins, H.T., 1998. Environmental change controls of lacustrine carbonate, Cayuga Lake, New York. Geology 26, 443-446.

Müller, G., Irion, G., Förstner, U., 1972. Formation and diagenesis of inorganic Ca-Mg carbonates in the lacustrine environment. Naturwissenschaften 59, 158-164.

Murakami, T., Katsuta, N., Yamamoto, K., Takamatsu, N., Takano, M., Oda, T., Matsumoto, G.I., Horiuchi, K., Kawai, T., 2009. A 27-kyr record of environmental change in central Asia

inferred from the sediment record of Lake Hovsgol, northwest Mongolia. Journal of Paleolimnology, DOI 10.1007/s10933-009-9336-5.

Nahm, W.H., Kim, J.K., Yang, D.Y., Kim, J.Y., Yi, S., Yu, K.M., 2006. Holocene paleosols of the Upo wetland, Korea: their implications for wetland formation. Quaternary International 144, 53-60.

Nielsen, A.B.and Sugita, S., 2005. Estimating relevant source area of pollen for small Danish lakes around AD 1800. Holocene 15, 1006–1020.

Nielsen, A.B. and Odgaard, B.V., 2010. Quantitative landscape dynamics in Denmark through the last three millennia based on the Landscape Reconstruction Algorithm approach. Vegetation History and Archaeobotany 19, 375-387.

O'Connor, J.E. and Costa, J.E., 2004. The world's largest floods, past and present - their causes and magnitudes. U.S. Geological Survey Circular 1254.

Oksanen, J., Kindt, R., Legendre, P., O'Hara, B., Simpson, G.L., Solymos, P., Stevens, M.H.H., and Wagner, H., 2008. Vegan: community ecology package. R package version1.15-1.

Oort, A.H. and Yienger, J.J., 1996. Observed interannual variability in the Hadley circulation and its connection to ENSO. Journal of Climate 9, 2751-2767.

Oppo, D.W., Linsley, B.K., Rosenthal, Y., Dannenmann, S., Beaufort, L., 2003. Orbital and suborbital climate variability in the Sulu Sea, western tropical Pacific. Geochemistry, Geophysics, Geosystems 4, 1003-1022.

Ou, J.P.and Li, H., 2011. The regional engineering damage and reconstruction strategy in Wenchuan Earthquake of China. Journal of Earthquake and Tsunami 5, 189-216.

Overpeck, J., Anderson, D., Trumbore, S., and Prell, W., 1996. The southwest Indian Monsoon over the last 18000 years. Climate Dynamics 12, 213-225.

Paillard, D., Labeyrie, L., and Yiou, P., 1996. Macintosh program performs time-series analysis. EOS Transactions AGU 77, 379.

Parsons, R.W. and Prentice, I.C., 1981. Statistical approaches to Rvalues and pollen-vegetation relationship. Review of Palaeobotany and Palynology 32, 127–152.

Peck, J.A., Khosbayar, P., Fowell, S.J., Pearce, R.B., Ariunbileg, S., Hansen, B.C.S., Soninkhishig, N., 2002. Mid to late Holocene climate change in north central Mongolia as recorded in the sediments of Lake Telmen. Palaeogeography, Palaeoclimatology, Palaeoecology 183, 135-153.

Pennington, W., 1979. The origin of pollen in lake sediments: an enclosed lake compared with one receiving inflow streams. New Phytologist 83, 189-213.

Peres-Neto, P. and Jackson, D., 2001. How well do multivariate data sets match? The advantages of a Procrustean superimposition approach over the Mantel test. Oecologia 129, 169-178.

Petit, J.R., Jouzel, J., Raynaud, D., Barkov, N.I., Barnola, J.-M., Basile, I., Bender, M., Chappellaz, J., Davis, M., Delaygue, G., Delmotte, M., Kotlyakov, V.M., Legrand, M., Lipenkov, V.Y.,

Lorius, C., Pepin, L., Ritz, C., Saltzman, E., Stievenard, M., 1999. Climate and atmospheric history of the past 420,000 years from the Vostok ice core, Antarctica. Nature 399, 429-436.

Phadtare, N.R., 2000. Sharp decrease in summer monsoon strength 4000-3500 cal. yr B.P. in the central higher Himalaya of India based on pollen evidence from Alpine peat. Quaternary Research 53, 122-129.

Pitzer, K.S., 1973. Thermodynamics of electrolytes.1.Theroretical basis and general equations. J Physical Chemistry 77, 268–277.

Pompilio, M., Dunbar, N., Gebhardt, A.C., Helling, D., Kuhn, G., Kyle, P., McKay, R., Talarico, F., Tulaczyk, F., Vogel, S., Wilch, T., 2007. Petrology and geochemistry on the AND-1B core, ANDRILL McMurdo Ice Shelf Project, Antarctica. Terra Antartica 15, 147-192.

Porter, S.C. and An, Z.S., 1995. Correlation between climate events in the north Atlantic and China during the last glaciation. Nature 375, 305-308.

Potter, P.E., Heling, D., Shimp, N.F., van Wie, W., 1975. Clay mineralogy of modern alluvial muds of the Mississippi River basin. Bull. Center Reche. Pau-SNPA 2, 353-389.

Prell, W. and Kutzbach, J.E., 1992. Sensitivity of the Indian Monsoon to forcing parameters and implcations for its evolution. Nature 360, 647-652.

Prentice, I.C., 1985. Pollen representation, source area, and basin size: toward a unified theory of pollen analysis. Quaternary Research 23, 76-86.

Prentice, I.C., 1987. Quantitative forest-composition sensing characteristics of pollen samples from Swedish lakes. Boreas 16, 43-54.

Prentice, I.C. and Parsons, R.W., 1983. Maximum likelihood linear calibration of pollen spectra in terms of forest composition. Biometrics 3, 1051–1057.

Qian, W.H., Quan, L.S., Shi, S.Y., 2002. Variations of dust storm in China and its climatic control. Journal of Climate 15, 1216-1229.

Qiang, M.R., Chen, F.H., Zhang, J.W., Zu, R.P., Jing, M., Zhou, A.F., Xiao, S., 2007a. Grain size in sediments from Lake Sugan: a possible linkage to dust storm events at the northern margin of the Qinghai–Tibetan Plateau. Environ. Geol. 51, 1229-1238.

Qiang, M.R., Chen, F.H., Zhou, A.F., Xiao, S., Zhang, J.W., Wang, Z.T., 2007b. Impacts of wind velocity on sand and dust deposition during dust storm as inferred from a series of observations in the northeastern Qinghai–Tibetan Plateau, China. Powder Technology 175, 82-89.

Qinghai Forestry Bureau, 1990). Mengda Natural Reserve in Qinghai. Qinghai People's Publishing House, Xi’ning.

R Development Core Team, 2008. R: A Language and Environment for Statistical Computing. R Foundation for Statistical Computing, Vienna, Austria.

Reimer, P.J., Baillie, M.G.L., Bard, E., Bayliss, A., Beck, J.W., Blackwell, P.G., Bronk Ramsey, C., Buck, C.E., Burr, G.S., Edwards, R.L., Friedrich, M., Grootes, P.M., Guilderson, T.P., Hajdas,

I., Heaton, T.J., Hogg, A.G., Hughen, K.A., Kaiser, K.F., Kromer, B., McCormac, F.G., Manning, S.W., Reimer, R.W., Richards, D.A., Southon, J.R., Talamo, S., Turney, C.S.M., van der Plicht, J., and Weyhenmeyer, C.E., 2009. IntCal09 and Marine09 radiocarbon age calibration curves, 0–50,000 years cal BP. Radiocarbon 51, 1111–1150.

Rhodes, T.E., Gasse, F., Lin, R.F., Fontes, J.C., Wei, K.Q., Bertrand, P., Gibert, E., Melieres, F., Tucholka, P., Wang, Z.X., Chen, Z.Y., 1996. A Late Pleistocene-Holocene lacustrine record from Lake Manas, Zunggar (northern Xinjiang, western China). Palaeogeography, Palaeoclimatology, Palaeoecology 120, 105-121.

Ricketts, R.D., Johnson, T.C., Brown, E.T., Rasmussen, K.A., Romanovsky, V.V., 2001. The Holocene paleolimnology of Lake Issyk-Kul, Kyrgyzstan: trace element and stable isotope composition of ostracodes. Palaeogeography, Palaeoclimatology, Palaeoecology 176, 207-227.

Rudaya, N., Tarasov, P., Dorofeyuk, N., Solovieva, N., Kalugin, I., Andreev, A., Darvin, A., Diekmann, B., Riedel, F., Tserendash, N., Wagner, M., 2009. Holocene environments and climate in the Mongolian Altai reconstructed from the Hoton-Nur pollen and diatom records: a step towards better understanding climate dynamics in Central Asia. Quaternary Science Reviews 28, 540-554.

Ruddiman, W.F., Kutzbach, J.E., 1989. Forcing of the Cenozoic northern hemisphere climate by plateau uplift in southern Asia and the American west. Journal of Geophysical Research 94, 18409-18427.

Sato, T., 2009. Influences of subtropical jet and Tibetan Plateau on precipitation pattern in Asia: insights from regional climate modeling. Quaternary International 194, 148-158.

Schettler, G., Liu, Q., Mingram, J., Stebich, M., Dulski, P., 2006. East-Asian monsoon variability between 15,000 and 2000 cal. yr BP recorded in varved sediments of Lake Sihailongwan (northeastern China, Long Gang volcanic field). The Holocene 16, 1043-1057.

Schlütz, F. and Lehmkuhl, F., 2009. Holocene climatic change and the nomadic Anthropocene in Eastern Tibet: palynological and geomorphological results from the Nianbaoyeze Mountains. Quaternary Science Reviews 28, 1449-1471.

Schöne, B.R., Oschmann, W., Tanabe, K., Dettman, D., Fiebig, J., Houk, S.D., Kanie, Y., 2004. Holocene seasonal environmental trends at Tokyo Bay, Japan, reconstructed from bivalve mollusk shells – implications for changes in the East Asian monsoon and latitudinal shifts of the Polar Front. Quaternary Science Reviews 23, 1137-1150.

Schultz, L.G., 1964. Quantitative interpretation of mineralogical composition from X-Ray and chemical data for the Pierre Shale. US Geological Survey, Professional Paper 391-C, p.31.

Schulz, M. and Mudelsse, M., 2002. REDEFIT: estimation red-noise spectra directly from unevenly spaced paleoclimatic time series. Computer Geoscience 28, 421–426.

Seppa, H. and Bennett, K.D., 2003. Quaternary pollen analysis: recent progress in palaeoecology and palaeolimatology. Progress in Physical Geography 27, 548-579.

Soepboer, W., Vervoort, J.M., Sugita, S., Lotter, A.F., 2008. Evaluating Swiss pollen productivity estimates using a simulation approach. Vegetation History and Archaeobotany 17, 497–506.

Soepboer, W., Sugita, S., Lotter, A.F., 2010. Regional vegetation-cover changes on the Swiss Plateau during the past two millennia: a pollen-based reconstrcution using the REVEALS model. Quaternary Science Reviews 29, 472–483.

Shao, X.M., Huang, L., Liu, H.B., Liang, E.Y., Fang, X.Q., Wang, L.L., 2005. Reconstruction of precipitation variation from tree ring in recent 1000 years in Delingha, Qinghai. Science in China Series D 48, 939-949.

Shao, X.H., Wang, Y.J., Cheng, H., Kong, X.G., Wu, J.Y., Lawrence, E.R., 2006. Long-term trend and abrupt events of the Holocene Asian monsoon inferred from a stalagmite $\delta^{18}O$ record from Shennongjia in Central China. Chinese Science Bulletin 51, 221-228.

Shen, C.M., 2003. Millennial-scale variations and centennial-scale events in the Southwest Asian Monsoon: Pollen evidence from Tibet. PhD Dissertation, Lousiana State University.

Shen, J., Liu, X.Q., Wang, S.M., and Matsumoto, R., 2005. Palaeoclimatic changes in the Qinghai Lake area during the last 18,000 years. Quaternary International 136, 131-140.

Shen, C.M., Liu, K.B., Tang, L.Y., Overpeck, J.T., 2006a. Quantitative relationships between modern pollen rain and climate in the Tibetan Plateau. Review of Palaeobotany and Palynology 140, 61-77.

Shen, J., Jones, R.T., Yang, X.D., Dearing, J.A., Wang, S.M., 2006b. The Holocene vegetation history of Lake Erhai, Yunnan province southwestern China: the role of climate and human forcings. The Holocene 16, 265-277.

Shen, C.M., Liu, K.-B., Morrill, C., Overpeck, J.T., Peng, J.L., Tang, L.Y., 2008. Ecotone shift and major droughts during the mid-late Holocene in the central Tibetan Plateau. Ecology 89, 1079-1088.

Shi, P.J. and Song, C.Q., 2003. Palynological records of environmental changes in the middle part of Inner Mongolia, China. Chinese Science Bulletin 48, 1433-1438.

Singh, G., Wasson, R.J., Agrawal, D.P., 1990. Vegetational and seasonal climatic changes since the last full glacial in the Thar Desert, northwestern India. Review of Palaeobotany and Palynology 64, 351-358.

Shukla, J. and Paolino, D.A., 1983. The Southern Oscillation and long range forecasting of the Summer Monsoon Rainfall over India. Monthly Weather Review 11, 1830-1837.

Sirocko, F., Sarnthein, M., Erlenkeuser, H., Lange, H., Arnold, M., Duplessy, J.C., 1993. Century -scale events in monsoonal climate over the past 24,000 years. Nature 364, 322-324.

Sonzogni, C., Bard, E., Rostek, F., 1998. Tropical Sea-Surface Temperatures during the last glacial period: a view based on alkenones in Indian Ocean sediments. Quaternary Science Reviews 17, 1185-1201.

Sowers, T., Bender, M., Labeyrie, L., Martinson, D., Jouzel, J., Rynaud, D., Korotkevich, Y.S., 1993. A 135,000-year Vostok-SPECMAP common temporal framework. Paleoceanography 8, 737-766.

Steinke, S., Kienast, M., Pflaumann, U., Weinelt, M., Stattegger, K., 2001. A high-resolution Sea-Surface Temperature record from the tropical South China Sea (16,500-3000 yr B.P.). Quaternary Research 55, 352-362.

Stott, L., Cannariato, K., Thunell, R., Haug, G.H., Koutavas, A., Lund, S., 2004. Decline of surface temperature and salinity in the western tropical Pacific Ocean in the Holocene epoch. Nature 431, 56-59.

Stuvier, M., Grootes, P.M., Braziunas, T.F., 1995. The GISP2 $\delta^{18}O$ climate record of the past 16,500 years and the role of the Sun, Ocean and Volcanoes. Quaternary Research 44, 341-354.

Sugita, S., 1993. A model of pollen source area for an entire lake surface. Quaternary Research 39, 239-244.

Sugita, S., 1994. Pollen representation of vegetation in Quaternary sediments: Theory and method in patchy vegetation. Journal of Ecology 82, 881-897.

Sugita, S., Gaillard, M.-J., Broström, A., 1999. Landscape openness and pollen records: a simulation approach. Holocene 9, 409-21.

Sugita, S., 2007a. Theory of quantitative reconstruction of vegetation. I: pollen from large sites REVEALS regional vegetation. Holocene 17, 229–241.

Sugita, S., 2007b. Theory of quantitative reconstruction of vegetation. II: all you need is LOVE. Holocene 17, 243–257.

Sugita, S., Gaillard, M.-J., Broström, A., 1999. Landscape openness and pollen records: a simulation approach. Holocene 9, 409–421.

Sugita, S., Parshall, T., Calcote, R., Walker, K., 2010. Testing the Landscape Reconstruction Algorithm for spatially explicit reconstruction of vegetation in northern Michigan and Wisconsin. Quaternary Research 74, 289-300.

Sun, H., chief editor, 1999. The national physical atlas of China. China Cartographic Publishing House, Beijing.

Sun, X.J. and Wu, Y.S., 1987. Distribution and quantity of sporopollen and algae in surface sediments of the Dianchi Lake, Yunnan Province. Marine Geology and Quaternary Geology 17, 81-92 (in Chinese with English abstract).

Sun, X.J. and Chen Y.S., 1991. Palynological records of the last 11,000 years in China. Quaternary Science Reviews 10, 537-544.

Tan, L.C., Cai, Y.J., Li, L., An, Z.S., Ai, L., 2008. Precipitation variations of Longxi, northeast margin of Tibetan Plateau since AD 960 and their relationship with solar activity. Climate of the Past 4, 19-28.

Tanaka, H.L., Ishizaki, N., Kitoh, A., 2004. Trend and interannual variability of Walker, monsoon and Hadley circulations defined by velocity potential in the upper troposphere. Tellus 56A, 250-269.

Tang, L.Y., Shen, C.M., Liu, K.B., Overpeck, J.T., 2000. Changes in south Asian monsoon: new high-resolution paleoclimatic records from Tibet, China. Chinese Science Bulletin. 45, 87-90.

Tang, L.Y., Shen, C.M., Liu, K.B., Yu, S.Y., and Li, C.H., 2004. Climatic changes in southeast Tibet since LGM: Evidences from Pollen records. Science in China Series D: Earth Sciences 34, 436-442 (in Chinese).

Tang, L.Y., Shen, C.M., Li, C.H., Peng, J.L., Liu, H., Liu, K.B., Morrill, C., Overpeck, J.T., Cole, J.E., Yang, B., 2009. Pollen-inferred vegetation and environmental changes in the central Tibetan Plateau since 8200 yr BP. Science in China Series D 52, 1104-1114.

ter Braak, C.J.F., 1986. Canonical correspondence analysis: a new eigenvector technique for multivariate direct gradient analysis. Ecology 67, 1167–1179.

ter Braak, C.J.F. and Šmilauer, P., 2002. Canoco for Windows 4.5. Biometrics, the Netherlands.

Thompson, L.G., Mosley-Thompson, E., Davis, M.E., Bolzan, J.F., Dai, J., Klein, L., Gundestrup, N., Yao, T.D., Wu, X., Xie, Z., 1990. Glacial stage ice-core records from the subtropical Dunde Ice Cap, China. Annuals of Glaciology 14, 288-297.

Thompson, L.G., Yao, T.D., Davis, M.E., Henderson, K.A., Mosley-Thompson, E., Lin, P.N., Beer, J., Synal, H.A., Cole-Dai, J., and Bolzan, J.F., 1997. Tropical climate instability: the last glacial cycle from a Qinghai-Tibetan Ice Core. Science 276, 1821-1825.

Vandenberghe, J., Renssen, H., Huissteden, K., Nugteren, G., Konert, M., Lu, H.Y., Dodonov, A., and Buylaert, J.-P., 2006. Penetration of Atlantic westerly winds into Central and East Asia. Quaternary Science Reviews 25, 2380-2389.

Velland, M., 2001. Do commonly used indices of –diversity measure species turnover? Journal of Vegetation Science 57, 545-552.

Wang, B., 2006. The Asian Monsoon. Springer, Chichester, 685pp.

Wang Y.B., 2008. A 4000-year climatic change inferred from Kusai lake of HohXil Region in the Nortern Tibetan Plateau. Master thesis, Nanjing Institute of Geography and Limnology, Chinese Academy of Sciences (in Chinese with English abstract).

Wang, S.M. and Dou, H.S. (chief eds), 1998. Lakes in China. Science Press, Beijing.

Wang, B. and Fan, Z., 1999. Choice of south Asian Summer Monsoon indices. Bulletin of American Meteorological Society 80, 629-638.

Wang, Y.B. and Herzschuh, U., 2011. Reassess the Holocene vegetation change on the upper Tibetan Plateau using the pollen-based REVEALS model. Review of Palaeobotany and Palynology 168, 31-40.

Wang, Y., Song, C.Q., Sun, X.J., 1997. Palynological record of paleovegetation change during Holocene at north Tumote Plain in Inner Mongolia, China. Acta Geographica Sinica 52,

430-438. (in Chinese with English Abstract)

Wang, F.X., Chen, N., Zhang, Y., and Yang, H., 1997. Pollen flora of China. Science Press, Beijing (in Chinese).

Wang, L.J., Sarnthein, M., Erlenkeuser, H., Grootes, P.M., Grimalt, J.O., Pelejero, C., Linck, G., 1999. Holocene variations in Asian Monsoon moisture: a bidecadal sediment record from the South China Sea. Geophysical Research letters 26, 2889-2892.

Wang, Y.J., Cheng, H., Edwards, R.L., An, Z.S., Wu, J.Y., Shen, C.C., Dorale, J.A., 2001a. A high resolution absolute-dated late Pleistocene monsoon record from Hulu Cave, China. Science 294, 2345-2348.

Wang, B., Wu, R.G., Lau, K.M., 2001b. Interannual variability of the Asian Summer Monsoon: contrasts between the Indian and Western North Pacific-East Asian Monsoon. Journal of Climate 14, 4073-4090.

Wang, H.Y., Liu, H.Y., Cui, H.T., Abrahamsen, N., 2001c. Terminal Pleistocene/Holocene palaeo -environmental changes revealed by mineral-magnetism measurements of lake sediments for Dali Nor area, southeastern Inner Mongolia Plateau, China. Palaeogeography, Palaeo -climatology, Palaeoecology 170, 115-132.

Wang, R.L., Scarpitta, S.C., Zhang, S.C., Zheng, M.P., 2002. Later Pleistocene/Holocene climate conditions of Qinghai-Xizhang Plateau (Tibet) based on carbon and oxygen stable isotopes of Zabuye Lake sediments. Earth Planetary Science Letters 203. 461-477.

Wang, H., Hong, Y.T., Zhu, Y.X., Hong, B., Lin, Q.H., Xu, H., Leng, X.T., Mao, X.M., 2004a, Humification degrees of peat in Qinghai-Xizang Plateau and palaeoclimate change. Chinese Science Bulletin 49, 514-519.

Wang, X.M., Dong, Z.B., Zhang, J.W., Liu, L.C., 2004b. Modern dust storms in China: an overview. Journal of Arid Envrionment 58, 559-574.

Wang, G.X., Yao, J.Z., Guo, Z.G., Wu, Q.B., Wang, Y.B., 2004c. Changes in permafrost ecosystem under the influences of human engineering activities and its enlightenments to railway construction. Chinese Science Bulletin. 49, 1741-1750.

Wang, Y.J., Cheng, H., Edwards, R.L., He, Y.Q., Kong, X.G., An, Z.S., Wu, J.Y., Kelly, M.J., Dykoski, C.A., and Li, X.D., 2005a. The Holocene Asian Monsoon links to Solar changes and North Atlantic Climate. Science 308, 854-857.

Wang, P.X., Clemens, S., Beaufort, L., Braconnot, P., Ganssen, G., Jian, Z.M., Kershaw, P., Sarnthein, M., 2005b. Evolution and variability of the Asian monsoon system: state of the art and outstanding issues. Quaternary Science Reviews 24, 595-629.

Wang, W.Y., Wang, Q.J., Li, S.X., and Wang, G., 2006. Distribution and species diversity of plant communities along transect on the northeastern Tibetan Plateau. Biodiversity and Conservation 15, 1811-1828.

Wang, X., Huang, J.P., Ji, M.X., Higuchi, K., 2008a. Variability of East Asia dust events and their long-term trend. Atmospheric Environment 42, 3156-3165.

Wang, Y.B., Liu, X.Q., Yang, X.D., Zhang, E.L., Matsumoto, R., 2008b. A 4000-year moisture evolution recorded by sediments of Lake Kusai in the Hoh Xil area, northern Tibetan Plateau. Journal of Lake Sciences 20, 605-612. (in Chinese with English Abstract)

Wang, Y.B., Liu, X.Q., Yang, X.D., Zhang, E.L., Yao, B., 2009. Dust storm events in Kekexili area, northern Tibetan Plateau during the past 4000 years: evidence from grain size analysis of lacustrine sediments in Kusai Lake. Acta Sedmentologica Sinca 27, 691-696 (in Chinese with English abstract).

Wang, Y.B., Liu, X.Q., and Herzschuh, U., 2010. Asynchronous evolution of the Indian and East Asian Summer Monsoon indicated by Holocene moisture patterns in monsoonal central Asia. Earth-Science Reviews 103, 135-153.

Wang, Y.B., Shumilovskikh, L., Mischke, S., Birks, H.J.B., Wischnewski, J., Böhner, J., Schlütz, F., Lehmkuhl, F., Diekmann, B., Herzschuh, U., 2011. Quantitative precipitation change on the NE Tibetan Plateau since the Last Glacial Maximum - extending the concept of pollen source area to pollen-based climate reconstructions from large lakes. Quaternary Science Reviews under review.

Wang, Y.B., Liu, X.Q., Mischke, S., Herzschuh, U., 2012. Environmental constraints on lake sediment mineral compositions from the Tibetan Plateau and implications for paleoenvironment reconstruction. Journal of Paleolimnology 47, 71-85.

Weaver, A.J., Saenko, O.A., Clark, P.U., Mitrovica, J.X., 2003. Melt water pulse 1A from Antarctica as a trigger of the Bølling-Allerød warm interval. Science 299, 1709-1713.

Webster, P.J. and Yang, S., 1992. Monsoon and ENSO: selectively interactive systems. The Quaternary Journal of Royal Meteorological Society 118, 877-926.

Webster, P.J., Magana, V.O., Palmer, T.N., Shukla, J., Tomas, R.A., Yanai, M., Yasunari., T., 1998. Monsoons: processes, predictability, and the prospects for prediction. Journal of Geophysical Research 103, 14451-1451.

Webster, P.J., Toma, V.E., Kim, H.M., 2010. Were the 2010 Pakistan floods predictable? Geophysical Research Letters 38, DOI:10.1209/2010GL046346.

Wei, H.C., Ma, H.Z., Zheng, Z., Pan, A.D., Huang, K.Y., 2011. Modern pollen assemblages of surface samples and their relationships to vegetation and climate in the northeastern Qinghai-Tibetan Plateau, China. Review of Palaeobotany and Palynology 163, 237-246.

Weltje, G., 1997. End-member modelling of compositional data: Numerical–statistical algorithms for solving the explicit mixing problem. Journal of Mathmatical Geology 29, 503–549.

Weltje, G.J. and Prins, M.A., 2003. Muddled or mixed? Inferring palaeoclimate from size distributions of deep-sea clastics. Sedimentary Geology 162, 39–62.

Weltje, G.J. and Prins, M.A., 2007. Genetically meaningful decomposition of grain-size distributions. Sedimentary Geology 202, 409–424.

Wischnewski, J., Mischke, S., Wang, Y.B., Herzschuh, U., 2011. Reconstructing climate variability on the northeastern Tibetan Plateau since the last Late glacial – a multi-proxy, dual-site

approach comparing terrestrial and aquatic signals. Quaternary Science Reviews 30, 82-97.

Wolfe, S.A. and Nickling, W.G., 1993. The protective role of sparse vegetation in wind erosion. Progress in Physical Geography 17, 50-68.

Wu, Z.Y., chief editor, 1995. The vegetation of China. Science Press, Beijing. (in Chinese)

Wu, B.Y. and Wang, J., 2002a. Winter Arctic Oscillation, Siberia High and East Asian Winter Monsoon. Geophysical Research Letters 29, 1897-1990.

Wu, B.Y. and Wang, J., 2002b. Possible impacts of winter Arctic Oscillation on Siberian high, the East Asian winter monsoon and sea–ice extent. Advances in Atmospheric Sciences 19, 297-320.

Wu, G.J., Pan, B.T., Guan, Q.Y., Wang, J.M., Zhao, Z.J., 1998. Climatic Changes in the North Piedmont of Eastern Qilian Mountains since 10 Ka B.P. Journal of Desert Research 18, 193-200. (in Chinese with English Abstract)

Wu, H., Guiot, J., Brewer, S., Cuo, Z., 2007. Climate changes in Eurasia and Africa at the last glacial maximum and mid-Holocene: reconstruction from pollen data using inverse vegetation modeling. Climate Dynamics 29, 211-229.

Wu, G.X., Liu, Y., Zhu, X., Li, W., Ren, R., Duan, A., Liang, X., 2009a. Multi-scale forcing and the formation of subtropical desert and monsoon. Annales Geophysiae 27, 3631-3644.

Wu, H.N., Ma, Y.Z., Feng, Z.D., Sun, A.Z., Zhang, C.J., Li, F., Kuang, J., 2009b. A high resolution record of vegetation and environmental variation through the last ~25,000 years in the western of Chinese Loess Plateau. Palaeogeography, Palaeoclimatology, Palaeoecology 273, 191-199.

Wu, Y.H., Lücke, A., Jin, Z.D., Wang, S.M., Schleser, G., Battarbee, R.W., Xia, W.L., 2006. Holocene climate development on the central Tibetan Plateau: A sedimentary record from Cuoe Lake. Palaeogeography, Palaeoclimatology, Palaeoecology 234, 328-340.

Wu, Y.H., Lücke, A., Wünnemann, B., Li, S.J., Wang, S.M., 2007. Holocene climate change in the central Tibetan Plateau inferred by lacustrine sediment geochemical records. Science in China Series D: Earth Sciences 50, 1548-1555.

Xiao, J.L., Nakamura, T., Lu, H.Y., Zhang, G.Y., 2002. Holocene climate changes over the desert/loess transition of north-central China. Earth Planetary Science Letters 197, 11-18.

Xiao, J.L., Xu, Q.H., Nakamura, T., Yang, X.L., Liang, W.D., Inouchi, Y., 2004. Holocene vegetation variation in the Daihai Lake region of north-central China: a direct indication of the Asian monsoon climatic history. Quaternary Science Reviews 23, 1669-1679.

Xiao, J.L., Wu, J.T., Si, B., Liang, W.D., Nakamura, T., Liu, B.L., Inouchi, Y., 2006. Holocene climate changes in the monsoon/arid transition reflected by carbon concentration in Daihai Lake of Inner Mongolia. Holocene 16, 551-560.

Xiao, J.L., Si, B., Zhai, D.Y., Itoh, S., Lomtatidze, Z., 2008. Partitioning of the grain-size components of Dali Lake core sediments: evidence for lake-level changes during the

Holocene. Journal of Paleolimnology 40, 519-528.

Xu, Q.H., Li, Y.C., Yang. X.L., Xiao, J.L., Liang, W.D., and Peng, Y.J., 2005. Source and distribution of pollen in the surface sediment of Daihai Lake, inner Mongolia. Quaternary International 136, 33-45.

Xu, Q., Fan, X.M., Huang, R.Q., Westen, C.V., 2009. Landslide dams triggered by the Wenchuan Earthquake, Sichuan Province, south west China. Bulletin of Engineering Geology and the Environment 68, 373-386.

Xu, Q.H., Xiao, J.L., Li, Y.C., Tian, F., and Nakagawa, T., 2010a. Pollen-based quantitative reconstruction of Holocene climate changes in the Daihai Lake area, inner Mongolia, China. Journal of Climate 23, 2856-2868.

Xu, Q.H., Li, Y.C., Bunting, M.J., Tian, F., Liu, J.S., 2010b. The effects of training set selection on the relationship between pollen assemblages and climate parameters: Implications for reconstructing past climate. Palaeogeography Palaeoclimatology Palaeoecology 289, 123-133.

Xu, Y., Zhang, J.W., Su, Y.J., 2011. Imaging the rupture of 14 April, 2010 Yushu earthquake using back-projection of global subarray P-waves. Chinese Journal of Geophysics-Chinese Edition 54, 1243-1250.

Xue, B., Qu, W.C., Wang, S.M., Ma, Y., Dickman, M.D., 2003. Lake level changes documented by sediment properties and diatom of Hulun Lake, China since the late Glacial. Hydrobiologia 498, 133-141.

Xue, J.B., Zhong, W., Zhao, Y.J., Peng, X.Y., 2008. Holocene Abrupt Climate Shifts and Mid-Holocene Drought Intervals Recorded in Barkol Lake of Northern Xinjiang of China. Chinese Geographical Science 18, 54-61.

Yan, G., Wang, F.B., Shi, G.R., and Li, S.F., 1999. Palynological and stable isotopic study of palaeo -environmental changes on the northeastern Tibetan plateau in the last 30,000 years. Palaeogeography, Palaeoclimatology, Palaeoecology 153, 147-159.

Yao, T.D. and Thompson L.G., 1992. Trends and features of climatic changes in the past 5000 years recorded by the Dunde ice core. Annals of Glaciology 16, 21-24.

Yao, B., Liu, X.Q., Wang, Y.B., Yang, B., 2011. Late Holocene climatic changes revealed by mineralogy records from lacustrine core KS-2006 from Lake Kusai in the Kekexili area, northern Tibetan Plateau. Journal of Lake Science, in press (in Chinese with English abstract).

Yasunari, T., 2006. Land-atmosphere interaction. In: Wang B. (Ed), The Asian Monsoon. Springer, Berlin, pp. 459-478.

Yancheva, G., Nowaczyk, N.R., Mingram, J., Dulski, P., Schettler, G., Negendank, J.F.W., Liu, J., Sigman, D.M., Peterson, L.C., Haug, G.H., 2007. Influence of the intertropical convergence zone on the East Asian monsoon. Nature 445, 74-77.

Yin, Y.P., Wang, F.W., Sun, P., 2009. Landslide hazards triggered by the 2009 Wenchuan

earthquake, Sichuan, China. Landslides 6, 139-151.

Yu, J.Q. and Kelts, K.R., 2002. Abrupt changes in climatic conditions across the late-glacial / Holocene transition on the N.E. Tibet-Qinghai Plateau: evidence from Lake Qinghai, China. Journal of Paleolimnology 28, 195-206.

Yu, G., Prentice, I.C., Harrison, S.P., Sun, X.J., 1998. Pollen-based biome reconstructions for China at 0 and 6000 years. Journal of Biogeography 25, 1055-1069.

Yuan, D.X., Cheng, H., Edwards, R.L., Dykoski, C.A., Kelly, M.J., Zhang, M.L., Qing, J.M., Lin, Y.S., Wang, Y.J., Wu, J.Y., Dorale, J.A., An, Z.S., Cai, Y.J., 2004 Timing, duration, and transitions of the last Interglacial Asian monsoon. Science 204, 575-578.

Zhang, K.J., 2000. Cretaceous palaeogeography of Tibet and adjacent areas (China): tectonic implications. Cretaceous Research 21, 23-33.

Zhang, C.J. and Mischke, S., 2009. A Late glacial and Holocene lake record from the Nianbaoyeze Mountains and inferences of lake, glacier and climate evolution on the eastern Tibetan Plateau. Quaternary Science Reviews 28, 1970-1983.

Zhang, M.L., Yuan, D.X., Lin, Y.S., Qin, J.M., Li, B., Cheng, H., Edwards, R.L., 2004. A 6000 -year high-resolution climatic record from a stalagmite in Xiangshui Cave, Guilin, China, The Holocene 14, 697-702.

Zhang, X.Y., Gong, S.L., Zhao, T.L., Arimoto, R., Wang, Y.Q., Zhou, Z.J., 2003. Sources of Asian dust and role of climate change versus desertification in Asian dust emission. Geophysical Research Letters 30, 2272-2275.

Zhang, P.Z., Cheng, H., Edwards, R.L., Chen, F.H., Wang, Y.J., Yang, X.L., Liu, J., Tan, M., Wang, X.F., Liu, J.H., An, C.L., Dai, Z.B., Zhou, J., Zhang, D.Z., Jia, J.H., Jin, L.Y., Johnson, K.R., 2008. A Test of Climate, Sun, and Culture Relationships from an 1810-Year Chinese Cave Record. Science 322, 940-942.

Zhao, H., Chen, F.H., Li, S.H., Wintle, A.G., Fan, Y.X., Xia, D.S., 2007. A record of Holocene climate change in the Guangzhong Basin, China, based on optical dating of a loess-palaeosol sequence. The Holocene 17, 1015-1022.

Zhao, Q., Wang, N.A., Cheng, H.Y., Kan, Y.S., Guo, J.Y., 2003. Grain-size characteristics of Qingtu Lake sediments and its paleaoenvironment explanation. Arid Land Geography 26, 1-5. (in Chinese with English Abstract)

Zhao, Y. and Herzschuh, U., 2009. Modern pollen representation of source vegetation in the Qaidam Basin and surrounding mountains, north-eastern Tibetan Plateau. Vegetation History and Archaeobotany 18, 245-260.

Zhao, Y., Yu, Z.C., Chen, F.H., Ito, M., Zhao, C., 2007. Holocene vegetation and climate history at Hurleg Lake in the Qaidam Basin, northwest China. Review of Palaeobotany and Palynology 145, 275-288.

Zhao, Y., Yu, Z.C., Chen, F.H., Zhang, J.W., and Yang, B., 2009a. Vegetation response to Holocene climate change in monsoon-influenced region of China. Earth-Science Reviews 97, 242-256.

Zhao, Y., Xu, Q.H., Huang, X.Z., Guo, X.L., and Tao, S.C., 2009b. Differences of modern pollen assemblages from lake sediments and surface soils in arid and semi-arid China and their significance for pollen-based quantitative climate reconstruction. Review of Palaeobotany and Palynology 156, 519-524.

Zhao, Y., Yu, Z.C., Liu, X.J., Zhao, C., Chen, F.H., Zhang, K., 2010. Late Holocene vegetation and climate oscillations in the Qaidam Basin of the northeastern Tibetan Plateau. Quaternary Research 73, 59-69.

Zhao, Y., Yu, Z.C., Zhao, W.W., 2011. Holocene vegetation and climate histories in the eastern Tibetan Plateau: controls by insolation-driven temperature or monsoon-derived precipitation changes? Quaternary Science Reviews 30, 1173-1184.

Zhou, X.M., Wang, Z.B., Du, Q., editor, 1986. Vegetation of Qinghai. People's Press of Qinghai, Xi'ning. (in Chinese)

Zhou, W.J., Donahue, D.J., Porter, S.C., Jull, T.A., Li, X.Q., Stuiver, M., An, Z.S., Matsumoto, E., Dong, G.R., 1996. Variability of monsoon climate in east Asia at the end of the last Glaciation. Quaternary Research 46, 219-229.

Zhou, W.J., Head, M.J., Lin, D., 2001. Climate changes in northern China since the late Pleistocene and its response to global change. Quaternary International 83-85, 285-292.

Zhou, W.J., Lu, X.F., Wu, Z.K., Deng, L., Jull, A.J.T., Donahue, D., Beck, W., 2002. Chinese Science Bulletin 47, 66-70.

Zhu, Y., Chen, F.H., and Madsen, D., 2002. The environmental signal of an early Holocene pollen record from the Shiyang River basin lake sediments, NW China. Chinese Science Bulletin 47, 267-273.

Zhu, L.P., Wu, Y.H., Wang, J.B., Lin, X., Ju, J.T., Xie, M.P., Li, M.R., Mäusbacher, R., Schwalb, A., Daut, G., 2008. Environmental changes since 8.4 ka reflected in the lacustrine core sediments from Nam Co, central Tibetan Plateau, China. The Holocene 18, 831-839.

Zhu, L.P., Zhen, X.L., Wang, J.B., Lv, H.Y., Xie, M.P., Kitagawa, H., Possnert, G., 2009. A ~30,000-year record of environmental changes inferred from Lake Chen Co, southern Tibet. Journal of Paleolimnology 42, 343-358.

Zisheng, A., Clemens, S.C., Shen, J., Qiang, X.K., Jin, Z.D., Sun, Y.B., Prell, W.L., Luo, J.J., Wang, S.M., Xu, H., Cai, Y.J., Zhou, W.J., Liu, X.D., Liu, W.G., Shi, Z.G., Yan, L.B., Xiao, X.Y., Chang, H., Wu, F., Ai, L., Lu, F.Y., 2011. Glacial-Interglacial Indian Summer Monsoon Dynamics. Science 333, 719-724.

Zuur, A.F., Leno, E.N., and Smith, G.M., 2009. Analysing Ecological Data. Springer, New York.

Zveryaev, I.I. and Aleksandrova, M.P., 2004. Differences in rainfall variability in the south and Southeast Asian summer monsoons. International Journal of Climatology 24, 1091-1107